Diffusive transport: theory and application

Remus Laurentiu Stana

University of Leeds

School of Mathematics

Submitted in accordance with the requirements for the degree of

Doctor of Philosophy

2020

The candidate confirms that the work submitted is his own and that appropriate credit has been given where reference has been made to the work of others.

This copy has been supplied on the understanding that it is copyright material and that no quotation from the thesis may be published without proper acknowledgement.

This thesis is dedicated to every important person in my life.

Joint Publications

The work in Chapter 2 has been submitted for preparation:

- **Stana R**, Lythe G, Molina-París C. Diffusive transport in two dimensions. *SIAM Journal on Applied Mathematics, submitted.*

Acknowledgements

This research has been funded by the Engineering and Physical Sciences Research Council Doctoral Training Grant CASE Studentship and has been jointly provided by the University of Leeds and the Defence Science and Technology Laboratory (Dstl).

My thanks goes to the following people who have helped me with my thesis: Sandro Azaele, John Kent, Gerasim Kokarev, Martín López-García, Mauro Mobilia, Jitse Niesen, Daniel Read, Martin Speight, Jonathan Ward, John Paul Gosling.

Additionally, I would like to thank my supervisors Carmen Molina-París and Grant Lythe for offering guidance during the past 5 years.

From Dstl, I would like to thank Joseph Gillard for the help offered during my studies.

Finally, I would like to thank my family for supporting me.

Abstract

In this thesis we investigate the behaviour of diffusing particles in a variety of scenarios. We are primarily interested in the case of molecules diffusing inside a cell in the context of biological processes where the mechanism by which a cell responds to an event occurring on its surface may involve the transport of molecular complexes from the cellular surface to the nucleus, and the transport of synthesised molecules from the nuclear surface to the cellular surface.

We find the Green's functions for diffusions in two and three dimensions, respectively, on a domain bounded by non-concentric surfaces, one absorbing and one reflecting. Exact expressions are also found for mean hitting times and hitting densities. Our motivation is diffusive transport from a nuclear surface, to a cellular surface and back. Hence, we consider cases where the initial condition is uniformly distributed on the nuclear or cellular surface, and where the hitting density of the outward leg is the density of initial conditions for the return leg. Mean times are calculated by integrating the Green's functions over the domain.

Additionally, we create a mathematical model for a specific type of assay experiments where *Coxiella burnetii* bacteria are placed inside a well and are allowed to be phagocytosed by a monolayer of monocytes on the bottom of the well. We obtain an expression for the intracellular bacterial load at any point during the experiment.

Symbols and abbreviations

Symbols

Symbol	Meaning	Dimensions
a	normalised radius of nucleus	non-dimensional
b	radius of assay well	length
c	normalised nuclear displacement	non-dimensional
R_n	radius of nucleus	length
R	radius of cell	length
r_c	nuclear displacement	length
k_B	Boltzmann's constant	$\frac{\text{mass}\times\text{length}^2\times\text{time}^2}{\text{temperature}}$
T_e	temperature	temperature
D	diffusion coefficient	$\text{length}^2\times\text{time}^{-1}$
N_0	number of monocytes	non-dimensional
σ	surface coverage of monocytes	non-dimensional
κ	trapping rate	$\text{length}\times\text{time}^{-1}$
k_{SM}	transport rate constant per cell	$\text{length}^3\times\text{time}^{-1}$
k_{disk}	rate constant of a perfectly absorbing disk	$\text{length}^3\times\text{time}^{-1}$
C	intracellular domain	non-dimensional
∂C_1	nuclear surface	non-dimensional
∂C_2	cellular surface	non-dimensional
$\mathbf{x}_c$	position of the cellular centre	non-dimensional
$\mathbf{x}_n$	position of the nuclear centre	non-dimensional
θ_1	angle defining $\mathbf{x} \in \partial C_1$	non-dimensional
θ_2	angle defining $\mathbf{x} \in \partial C_2$	non-dimensional

Functions

Function	Meaning	Dimensions
$t_1^{(2)}(\mathbf{x}_0)$	time to absorption by cellular surface in two dimensions	time
$t_2^{(2)}(\mathbf{x}_0)$	time to absorption by nuclear surface in two dimensions	time
$t_1^{(3)}(\mathbf{x}_0)$	time to absorption by cellular surface in three dimensions	time
$t_2^{(3)}(\mathbf{x}_0)$	time to absorption by nuclear surface in three dimensions	time
$H_2^{(2)}(\mathbf{x}_0, \mathbf{x})$	pseudo-Green's function in two dimensions	time$\times$length^{-2}
$H_2^{(3)}(\mathbf{x}_0, \mathbf{x})$	pseudo-Green's function in three dimensions	time$\times$length^{-2}
$G_1^{(2)}(\mathbf{x}_0, \mathbf{x})$	Green's function with absorbing cellular surface in two dimensions	time$\times$length^{-2}
$G_2^{(2)}(\mathbf{x}_0, \mathbf{x})$	Green's function with absorbing nuclear surface in two dimensions	time$\times$length^{-2}
$G_1^{(3)}(\mathbf{x}_0, \mathbf{x})$	Green's function with absorbing cellular surface in three dimensions	time$\times$length^{-2}
$G_2^{(3)}(\mathbf{x}_0, \mathbf{x})$	Green's function with absorbing nuclear surface in three dimensions	time$\times$length^{-2}
$\varepsilon_0^{(2)}(\theta_2)$	hitting density on the cellular surface in two dimensions with no target	non-dimensional
$\varepsilon^{(2)}(\theta_2)$	hitting density on the cellular surface in two dimensions	non-dimensional
$\varepsilon^{(3)}(\theta_2)$	hitting density on the cellular surface in three dimensions	non-dimensional

Function	**Meaning**	**Dimensions**
$T_1^{(2)}(\theta_1, a, c)$	mean time for absorption by cellular surface in two dimensions	time
$T_2^{(2)}(\theta_2, a, c)$	mean time for absorption by nuclear surface in two dimensions	time
$T_1^{(3)}(\theta_1, a, c)$	mean time for absorption by cellular surface in three dimensions	time
$T_2^{(3)}(\theta_2, a, c)$	mean time for absorption by nuclear surface in three dimensions	time
$\bar{T}_1^{(2)}(a, c)$	average mean time for absorption by cellular surface in two dimensions	time
$\bar{T}_2^{(2)}(a, c)$	average mean time for absorption by nuclear surface in three dimensions	time
$\bar{T}_1^{(3)}(a, c)$	average mean time for absorption by cellular surface in two dimensions	time
$\bar{T}_2^{(3)}(a, c)$	average mean time for absorption by nuclear surface in three dimensions	time
$\bar{\bar{T}}_1^{(2)}(a)$	global mean time for absorption by cellular surface in two dimensions	time
$\bar{\bar{T}}_2^{(2)}(a)$	global mean time for absorption by nuclear surface in two dimensions	time

Abbreviations

MOI	multiplicity of infection
FPT	first passage time
NEP	narrow escape problem
MFPT	mean first passage time
Dstl	Defence Science and Technology Laboratory
CDC	Centers for Disease Control and Prevention
GMSV	generalized method of separation of variables
ISLAE	infinite system of linear algebraic equations

Contents

List of Figures

Chapter 1

Introduction

1.1 Brownian motion

The botanist Robert Brown discovered in 1827 that particles of sufficiently small size are in a constant state of random motion called Brownian motion or diffusion. The average kinetic energy of a particle at absolute temperature T_e is equal to $kT_e/2$ along the axis of motion, where k is the Boltzmann constant. A particle of mass m and velocity v_x has kinetic energy $mv_x^2/2$ and, as a result, the root-mean-square velocity is deduced to be:

$$\langle v_x^2 \rangle^{\frac{1}{2}} = \sqrt{\frac{kT_e}{m}},$$

where $\langle\,\rangle$ is the average over an ensemble of similar particles.

Particles of small size such as molecules, organelles and cells can be described as undergoing Brownian motion. Berg (1993) gives the following example to illustrate this point: lysozymes are proteins with molecular weight (mass of one mole of a substance, or 6×10^{23} molecules) of $1.4 \times 10^4 g$ and so the mass of one molecule is $m = 2.3 \times 10^{-20} g$. Given the value of kT_e at 300 K (27 °C) is 4.14×10^{-14} $g\,cm^2/s^2$ the root-mean-square velocity is $\langle v_x^2 \rangle^{\frac{1}{2}} = 1.2 \times 10^3 cm/s$. Without any obstruction, this particle would travel the length of an average classroom in approximately one second. However the particle is confined in an aqueous medium and it cannot travel too far before hitting other water molecules. As a consequence, the particle is forced to wander in the medium executing a random walk.

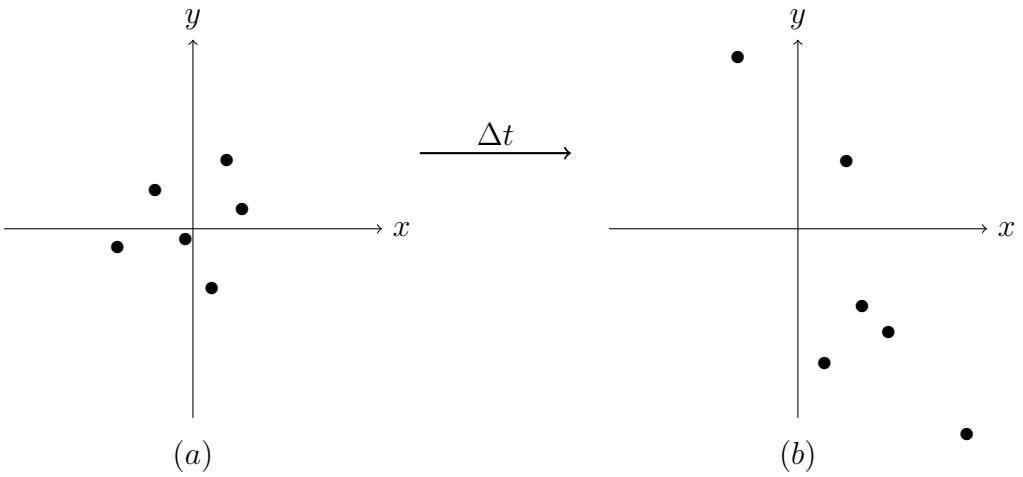

Figure 1.1: Particles which are confined initially in a small space (a) will diffuse outwardly (b).

If a region contains a number of diffusing particles as shown in Figure 1.1(a) then, if a period of time Δt has passed, the particles will have dispersed in all directions as shown in Figure 1.1(b).
In the following sections, dealing with Brownian motion, we will be following the work of Berg (1993).

1.1.1 One dimensional random walk

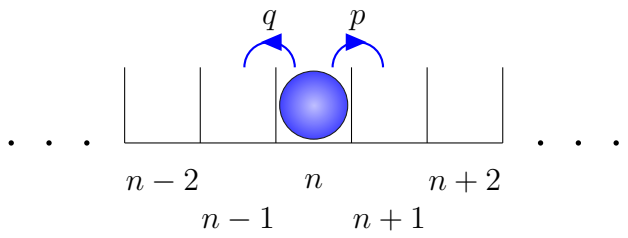

Figure 1.2: Random walk of particle located at $x = n$ which can move to the left with probability $p = 1/2$ and to the right with probability $q = 1/2$ (where $p + q = 1$).

In order to better understand diffusion, let us focus on the movement of particles

along a single axis. We assume that the particles start at position $x = 0$ at time $t = 0$ and they move according to the following rules (see Figure 1.2):

1. Every particle takes a step to either the left or the right every τ seconds moving with velocity $\pm v_x$ a distance of $\delta = \pm v_x \tau$. We will assume, for simplicity, that τ and δ are constant although, in reality, they will depend on the size of the particle, properties of the liquid and the absolute temperature T.

2. Each particle is equally likely to move to the right or to the left with probability 1/2. This is due to the water molecules which interact with the particles causing them to lose any knowledge of the previous step. As a result, the walk is not biased.

3. Particles move independently of each other because they do not interact. In reality, this is true if the suspension of particles is reasonably dilute.

Two consequences of these three rules are that:

(a) the mean position of the particles does not change with time and remains $x = 0$;

(b) the root-mean-square displacement is proportional to the square root of time, but not time.

These propositions will be proved bellow using an iterative procedure. We will consider a group of N particles and let $x_i(n)$ be the position of the $i-$th particle after the n-th step. From rule 1 we know that the position of a particle after the n-th step is different by $\pm\delta$ from its position after the $(n-1)$-th step:

$$x_i(n) = x_i(n-1) \pm \delta. \tag{1.1}$$

From rules 2 and 3, we know that roughly half the particles will move by $+\delta$ and the other half by $-\delta$. The mean displacement of the particles after the $n-$th step is calculated by summing the positions of the particles and dividing by N:

$$\langle x(n) \rangle = \frac{1}{N} \sum_{i=1}^{N} x_i(n). \tag{1.2}$$

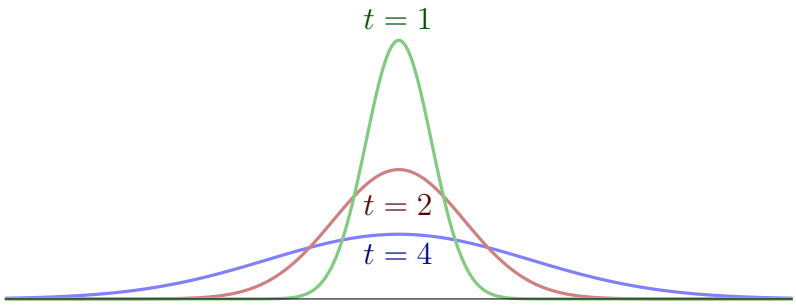

Figure 1.3: The probability of finding the particles at position x and times $t = 1, 2$ and 4 given that the particles start at $x = 0$ at $t = 0$.

Using (1.1) in (1.2) we obtain:

$$\langle x(n)\rangle = \frac{1}{N}\sum_{i=1}^{N}\left[x_i(n-1) \pm \delta\right] = \frac{1}{N}\sum_{i=1}^{N} x_i(n-1) = \langle x(n-1)\rangle. \tag{1.3}$$

The second term in the brackets averages to zero given that the plus sign is present in half the cases and the minus is present in the other half. As a result, equation (1.3) tells us that the mean position of the particles does not change with time and given that all the particles start at $x = 0$ then their mean position remains zero. The spread of the particles is symmetric about the origin as seen in Figure 1.3.

An adequate measure of particle spread is the root-mean-square displacement $\langle x^2(n)\rangle^{1/2}$ Berg (1993). This is because the square of a number is always non-negative and so summing over their square roots cannot give zero. We take the square of $x_i(n)$ in (1.1):

$$x_i^2(n) = x_i^2(n-1) \pm 2\delta x_i(n-1) + \delta^2.$$

Then the mean is:

$$\langle x^2(n)\rangle = \frac{1}{N}\sum_{i=1}^{N} x_i^2(n),$$

which is:

$$\langle x^2(n)\rangle = \frac{1}{N}\sum_{i=1}^{N}\left[x_i^2(n-1) \pm 2\delta x_i(n-1) + \delta^2\right] = \langle x^2(n-1)\rangle + \delta^2. \tag{1.4}$$

Here, the second term in brackets averages to zero again given that half the terms are negative and half are positive. Since $\langle x^2(0)\rangle = 0$ we deduce from (1.4) that $\langle x^2(1)\rangle = \delta^2$, $\langle x^2(2)\rangle = 2\delta^2$ and $\langle x^2(n)\rangle = n\delta^2$. As a result, the mean-square displacement is proportional to the number of steps n while the root-mean-square-displacement is proportional to the square root of n. From rule 1 we know that $t = n\tau$ is the time the particles need to execute n steps. It follows that the mean-square displacement and root-mean-square displacement are proportional to t and square-root of t, respectively. This proved the second proposition (b).
Writing $n = t/\delta$ then the mean-square-displacement becomes

$$\langle x^2(t)\rangle = \frac{t}{\tau}\delta^2 = 2Dt,$$

where

$$D = \frac{\delta^2}{2\tau}, \tag{1.5}$$

is the diffusion coefficient which characterises the movement of particles of a given type in a given medium at a specific temperature. As a result, the root-mean-square displacement is:

$$\langle x^2(t)\rangle^{1/2} = \sqrt{2Dt}.$$

1.1.2 Random walks in two and three dimensions

We can apply rules 1 to 3 for every dimension and we assume that motion in each direction is statistically independent then

$$\langle r^2\rangle = 4Dt,$$

in, two dimensions, and

$$\langle r^2\rangle = 6Dt,$$

in three dimensions. Here $r^2 = x^2 + y^2$, in two dimensions, and $r^2 = x^2 + y^2 + z^2$, in three dimensions, is the distance from the origin to (x, y) and (x, y, z), respectively.
We simulate a random walk and plot it in Figure 1.4 where movement in the x and y directions happen simultaneously so that motion is diagonal. We observe that since exploration over short distances takes significantly less time than exploration

Figure 1.4: An plot of a two dimensional random walk of 10^4 steps with diffusion coefficient $D = 0.5$.

over long distances then the random walk will explore a region of space throughly. However, a random walk is not biased toward regions of space it has explored neither toward those it has not explored Berg (1993).

1.1.3 Fick's equations

When discussing diffusion, a starting point is represented by Fick's equations which are differential equations that describe the spatial and temporal variation of nonuniform distributions of particles Berg (1993). We will derive these equations starting from the random walk model. Suppose we know the number of particles at each point x at time t (see Figure 1.5). We want to know how many particles will move across the unit area in unit time from point x to point $x + \delta$, and subsequently, what is the net flux J_x in the x direction. At time τ, after one step, half the particles, located initially at point x, will have moved to the right across the dashed line and half the particles located initially at $x + \delta$ will have moved to the left across the dashed line. The net number of particles crossing the dashed

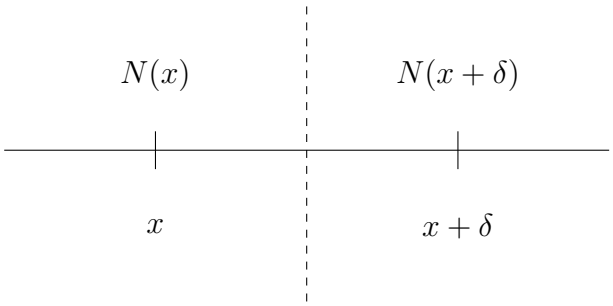

Figure 1.5: At time t, there are $N(x)$ and $N(x+\delta)$ at position x and $(x+\delta)$, respectively. At time $t+\tau$, half of the particles at each point will have moved to the right and half to the left.

line from the left to right is:

$$-\frac{1}{2}\left[N(x+\delta)-N(x)\right].$$

To obtain the net flux we divide the above expressing by the area normal to the x axis, A, and by the time interval τ:

$$J_x = -\frac{1}{2}\frac{\left[N(x+\delta)-N(x)\right]}{A\tau}.$$

Multiplying by δ^2/δ^2 and rearranging we obtain:

$$J_x = -\frac{\delta^2}{2\tau}\frac{1}{\delta}\left[\frac{N(x+\delta)}{A\delta}-\frac{N(x)}{A\delta}\right].$$

The quantity $\delta^2/2\tau$ is the diffusion coefficient D defined in (1.5). The number of particles per unit volume at point $x+\delta$ is $N(x+\delta)/A\delta$ which we denote as the concentration $C(x+\delta)$. Similarly $N(x)/A\delta$ is the concentration $C(x)$. As a result, we have:

$$J_x = -D\frac{1}{\delta}\left[C(x+\delta)-C(x)\right].$$

Taking $\delta \to 0$, and using the definition of partial derivatives, we obtain:

$$J_x = -D\frac{\partial C}{\partial x}. \tag{1.6}$$

This is Fick's first equation which states that the net flux at x ant t is proportional to the slope of the concentration at x and t where the constant of proportionality

is $-D$. We observe that when we defined $D = \delta^2/2\tau$ in (1.5) the reason for the factor $1/2$ was to make Fick's first equation more tidy Berg (1993).
Fick's second equation is derived from the first with the condition that total number of particles is constant (no particles are destroyed or created). Consider a box as the one shown in Figure 1.6, then in the time interval $[0, \tau]$, a number of $J_x(x)A\tau$ particles will enter from the left and a number of $J_x(x+\delta)A\tau$ will leave from the right. Given that the volume of the box is $A\delta$, the number of particles per unit volume in the box change at the rate:

$$\begin{aligned}\frac{1}{\tau}\left[C(t+\tau) - C(t)\right] &= -\frac{1}{\tau}\frac{\left[J_x(x+\delta) - J_x(x)\right]A\tau}{A\delta} \\ &= -\frac{1}{\delta}\left[J_x(x+\delta) - J_x(x)\right].\end{aligned}$$

Taking the limit $\tau \to 0$ and $\delta \to 0$ we obtain:

$$\frac{\partial C}{\partial t} = -\frac{\partial J_x}{\partial x}.$$

This, when combined with (1.6), gives:

$$\frac{\partial C}{\partial t} = D\frac{\partial^2 C}{\partial x^2}, \tag{1.7}$$

which is Fick's second equation, or the heat or diffusion equation. It states that the rate of change in time of the concentration at x and t is proportional to the curvature of the concentration at x and t where the constant of proportionality is D.

1.2 Mean time to capture

If a diffusing particle starts at $x = x_1$ in a one dimensional domain $[0, x_2]$ as indicated in Figure 1.7, where $0 \leq x_1 \leq x_2$, what is the mean time $T(x_1)$ for the particle to reach one of the absorbing boundaries at $x = 0$ or $x = x_2$? In order to answer this question, we will make use of random walks. A particle starts at position x at time t and it can move to the right or to the left, with equal probability, a distance of δ every τ seconds. As a result, at time τ the particle will be at position $x + \delta$, with probability $1/2$, or at position $x - \delta$ with probability

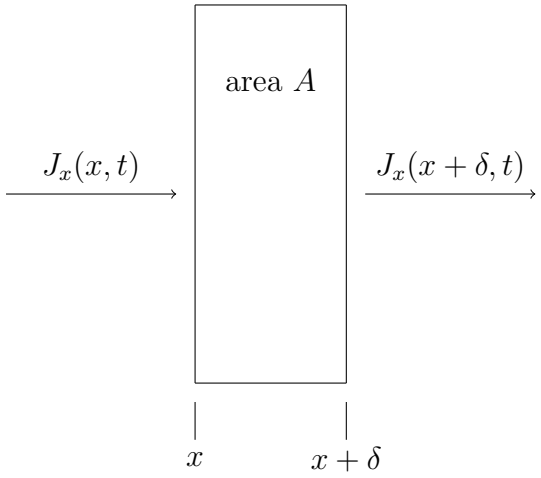

Figure 1.6: Fluxes through the faces of a thin box which extends from x to $x+\delta$ and has area, normal to the x axis, A.

1/2. The mean time to hit the absorbing boundaries from these positions are $T(x+\delta)$ and $T(x-\delta)$, respectively. As a result, we have:

$$T(x) = \tau + \frac{1}{2}\left[T(x+\delta) + T(x-\delta)\right].$$

Rearranging terms and diving the expression by $2/\delta$ we obtain:

$$\frac{1}{\delta}\left[T(x+\delta) - T(x)\right] - \frac{1}{\delta}\left[T(x) + T(x-\delta)\right] + \frac{2\tau}{\delta} = 0.$$

Taking the limit $\delta \to 0$ we get:

$$\left.\frac{\mathrm{d}T}{\mathrm{d}x}\right|_x - \left.\frac{\mathrm{d}T}{\mathrm{d}x}\right|_{x-\delta} + \frac{2\tau}{\delta} = 0.$$

Finally, we divide by δ and taking $\delta \to 0$ in the above expression:

$$\frac{\mathrm{d}^2T}{\mathrm{d}x^2} = -\frac{1}{D},$$

where we made use of the definition of the diffusion coefficient D.
This differential equation for the mean time $T(x)$ can be solved given appropriate boundary conditions. If the particle is at the absorbing boundary, the mean time to capture is zero. If the particle is at the reflecting boundary, the mean time to capture does not change with x, *i.e.* $dT/dx = 0$ at the boundary.

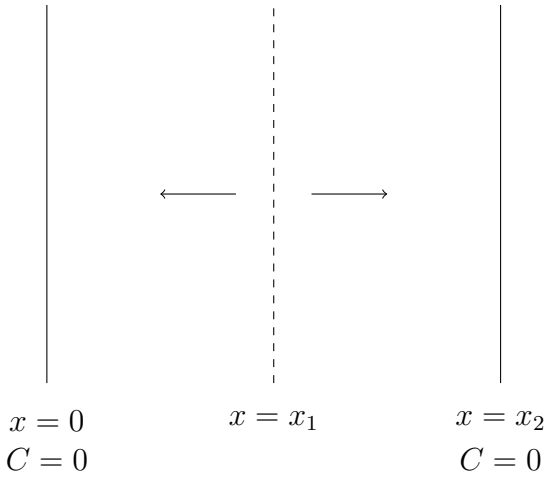

Figure 1.7: Fluxes through the faces of a thin box which extends from x to $x + \delta$ and has area, normal to the x axis, A.

If the boundaries at $x = 0$ and $x = x_2$ are absorbing then the mean time for a particle starting at x is:

$$T(x) = \frac{1}{2D}\left(x_2 x - x^2\right).$$

For the two and three dimensional cases the mean time T satisfies the following equation:

$$\nabla^2_{\mathbf{x}} T(\mathbf{x}) = -\frac{1}{D}, \tag{1.8}$$

where $\nabla^2_{\mathbf{x}}$ is the Laplacian in two and three dimensions, respectively.

1.2.1 From nuclear surface to cellular surface

If a particle diffuses in a two dimensional concentric annular region, as shown in Figure 1.8, we want to know what is the mean time to absorption under different boundary and initial conditions. For the following calculations we define R_n to be the radius of the inner circle and R to be the radius of the outer circle.
We define the following mean time:

$$T_1^{(2)}(r) = \text{mean time for a particle starting at } r \text{ to hit } r' = R,$$

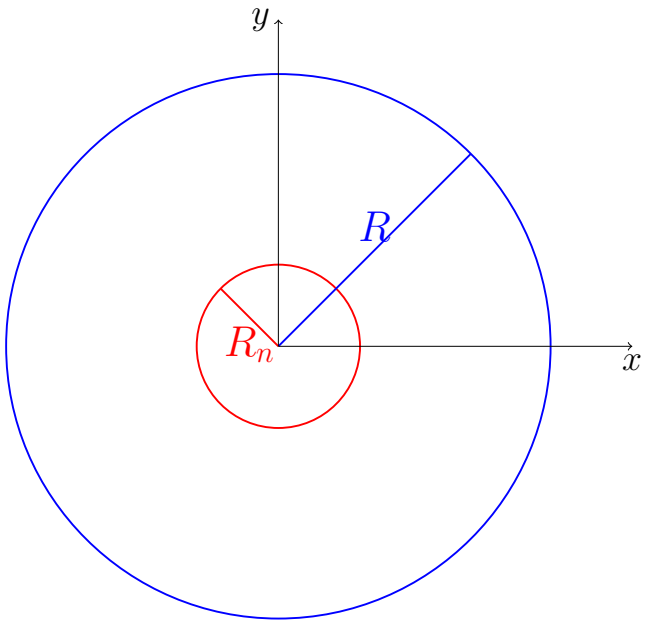

Figure 1.8: Plot of concentric annular region.

which satisfies:

$$\frac{1}{r}\frac{\mathrm{d}}{\mathrm{d}r}\left(r\frac{\mathrm{d}}{\mathrm{d}r}T_1^{(2)}(r)\right) = -\frac{1}{D}, \tag{1.9}$$

coupled with appropriate boundary conditions:

$$T_1^{(2)}(R) = 0, \tag{1.10}$$

$$\frac{\mathrm{d}}{\mathrm{d}r}T_1^{(2)}(r)\bigg|_{r=R_n} = 0. \tag{1.11}$$

Multiplying (1.9) by r and then integrating twice with respect to r we obtain:

$$T_1^{(2)}(r) = -\frac{r^2}{4D} + A\log r + B.$$

From the boundary conditions we deduce:

$$\frac{\mathrm{d}}{\mathrm{d}r}T_1^{(2)}(r)\bigg|_{r=R_n} = 0 \Rightarrow -\frac{R_n}{2D} + \frac{A}{R_n} = 0 \Rightarrow A = \frac{R_n^2}{2D},$$

$$T_1^{(2)}(R) = 0 \Rightarrow -\frac{R^2}{4D} + A\log R + B = 0 \Rightarrow B = \frac{R^2}{4D} - \frac{R_n^2}{2D}\log R.$$

As a result we obtain the mean time to absorption starting at r:

$$T_1^{(2)}(r) = \frac{R^2 - r^2}{4D} + \frac{R_n^2}{2D}\log\frac{r}{R}. \tag{1.12}$$

1.2.2 From cellular surface to nuclear surface

If instead of (1.10) and (1.11) we have:

$$T_2^{(2)}(R_n) = 0, \tag{1.13}$$

$$\frac{\mathrm{d}}{\mathrm{d}r} T_2^{(2)}(r)\Big|_{r=R} = 0. \tag{1.14}$$

Then we want to know the following mean time:

$$T_2^{(2)}(r) = \text{mean time for a particle starting at } r \text{ to hit } r' = R_n,$$

which satisfies:

$$\frac{1}{r}\frac{\mathrm{d}}{\mathrm{d}r}\left(r\frac{\mathrm{d}}{\mathrm{d}r}T_2^{(2)}(r)\right) = -\frac{1}{D}. \tag{1.15}$$

Multiplying (1.15) by r and then integrating twice with respect to r we obtain:

$$T_2^{(2)}(r) = -\frac{r^2}{4D} + A\log r + B.$$

From the boundary conditions (1.13) and (1.14) we deduce:

$$\frac{\mathrm{d}}{\mathrm{d}r} T_2^{(2)}(r)\Big|_{r=R} = 0 \Rightarrow -\frac{R}{2D} + \frac{A}{R} = 0 \Rightarrow A = \frac{R^2}{2D},$$

$$T_2^{(2)}(R_n) = 0 \Rightarrow -\frac{R_n^2}{4D} + A\log R_n + B = 0 \Rightarrow B = \frac{R_n^2}{4D} - \frac{R^2}{2D}\log R_n.$$

As a result we obtain the mean time to absorption starting at r:

$$T_2^{(2)}(r) = -\frac{r^2 - R_n^2}{4D} + \frac{R^2}{2D}\log\frac{r}{R_n}. \tag{1.16}$$

1.2.3 Three dimensions

If, instead of a circular concentric domain, we wish to investigate the mean time in a spherical concentric domain, with the radius of the outer sphere equal to R and the radius of the inner sphere equal to R_n, we solve (1.8) in spherical coordinates, with appropriate boundary conditions, and obtain:

$$T_1^{(3)}(r) = \frac{R^2 - r^2}{6D} + \frac{R_n^3}{3D}\left(\frac{1}{R} - \frac{1}{r}\right), \tag{1.17}$$

and

$$T_2^{(3)}(r) = \frac{R_n^2 - r^2}{6D} + \frac{R^3}{3D}\left(\frac{1}{R_n} - \frac{1}{r}\right), \tag{1.18}$$

where

$$T_1^{(3)}(r) = \text{mean time for a particle starting at } r \text{ to hit } r' = R,$$

and

$$T_2^{(3)}(r) = \text{mean time for a particle starting at } r \text{ to hit } r' = R_n.$$

1.3 Absorption probability

Consider the situation discussed at the beginning of Section 1.2 but instead of the mean time to capture $T(x)$ we want to calculate the probability $P(x)$ of the particle being absorbed at $x = 0$ before $x = x_2$ given that it starts at point x_1. Making use of the random walk model and the arguments used for deriving $T(x)$ we obtain the following:

$$P(x) = \frac{1}{2}\left[P(x+\delta) + P(x-\delta)\right],$$

from which we deduce that:

$$\frac{\mathrm{d}^2}{\mathrm{d}x^2}P(x) = 0.$$

The boundary conditions for the capture of a particle at $x = 0$ rather than at $x = x_2$ are $P(0) = 1$ and $P(x_2) = 0$, respectively. As a result, the capture probability is:

$$P(x) = \frac{x_2 - x}{x_2}.$$

In two and three dimensions the absorption probability P satisfies Laplace's equation:

$$\nabla_{\mathbf{x}}^2 P(\mathbf{x}) = 0.$$

1.3.1 Hitting the nuclear surface

Turning again to the case of diffusion in a concentric two dimensional annulus we want to calculate the following probability in two dimensions:

$$P(r) = \text{Prob(a particle is eventually absorbed at } r' = R_n | \text{ starts at } r). \quad (1.19)$$

This probability satisfies the following differential equation:

$$\frac{1}{r}\frac{\mathrm{d}}{\mathrm{d}r}\left(r\frac{\mathrm{d}}{\mathrm{d}r}P(r)\right) = 0, \quad (1.20)$$

with boundary conditions:

$$P(R_n) = 1, \quad (1.21)$$

$$\frac{\mathrm{d}}{\mathrm{d}r}P(r)\bigg|_{r=R} = 0. \quad (1.22)$$

Multiplying (1.20) by r and then integrating twice with respect to r we obtain:

$$P(r) = A\log r + B,$$

where A and B are constants.
From (1.22) we deduce that $A = 0$ and (1.21) gives us that $B = 1$. This tells us that $P(r) = 1$, *i.e.* the particle will always be absorbed at the inner circle.

1.4 Survival function

A Brownian particle is defined to be "alive" at time t if it has not yet been absorbed. Knowing this, we define the following probability:

$$S(r,t) = \text{Prob(a particle is "alive" at } r \text{ at time } t),$$

which satisfies Fick's second equation (1.7):

$$\frac{\partial}{\partial t}S\left(r,t\right) = D\nabla^2 S\left(r,t\right), \quad (1.23)$$

where D is the diffusion coefficient.
We wish to calculate the probability that a Brownian particle is "alive" at time t while diffusing inside a concentric annular region (see Figure 1.8) with absorbing inner boundary and reflecting boundary.

1.4.1 Two dimensions

In two dimensions, the diffusion equation can be written as:

$$\frac{\partial}{\partial t}S\left(r,t\right)=\frac{D}{r}\frac{\partial}{\partial r}\left(r\frac{\partial}{\partial r}S\left(r,t\right)\right). \tag{1.24}$$

Our probability also satisfies the following boundary and initial conditions:

$$S(R_n,t)=0, \quad t\geq 0, \tag{1.25a}$$

$$\frac{\partial}{\partial r}S(r,t)\bigg|_{r=R}=0, \quad t\geq 0, \tag{1.25b}$$

$$S(r,0)=1, \quad 0<R_n<r\leq R. \tag{1.25c}$$

We observe from (1.25a) and (1.25b) that there is a discontinuity in S at $t=0$ as r tends to R_n from above. We look for a separable solution of (1.24) of the form $S(r,t)=\mathcal{R}(r)\mathcal{T}(t)$ and as a result the diffusion equation becomes after simplification:

$$\frac{\mathcal{R}}{D}\frac{\mathrm{d}\mathcal{T}}{\mathrm{d}t}=\mathcal{T}\frac{\mathrm{d}^2\mathcal{R}}{\mathrm{d}r^2}+\frac{1}{r}\mathcal{T}\frac{\mathrm{d}\mathcal{R}}{\mathrm{d}r}. \tag{1.26}$$

Multiplying equation (1.26) by $\frac{1}{\mathcal{R}\mathcal{T}}$ we obtain:

$$\frac{1}{D\mathcal{T}}\frac{\mathrm{d}\mathcal{T}}{\mathrm{d}t}=\frac{1}{\mathcal{R}}\frac{\mathrm{d}^2\mathcal{R}}{\mathrm{d}r^2}+\frac{1}{r\mathcal{R}}\frac{\mathrm{d}\mathcal{R}}{\mathrm{d}r}. \tag{1.27}$$

We observe that the left-hand side of (1.27) is a function of t while the right-hand side is a function of r and we deduce that:

$$\frac{1}{D\mathcal{T}}\frac{\mathrm{d}\mathcal{T}}{\mathrm{d}t}=\frac{1}{\mathcal{R}}\frac{\mathrm{d}^2\mathcal{R}}{\mathrm{d}r^2}+\frac{1}{r\mathcal{R}}\frac{\mathrm{d}\mathcal{R}}{\mathrm{d}r}=-\lambda^2,$$

where λ is a constant. Here we choose the constant to be $-\lambda^2$ in order to ensure that the time function does not grow exponentially, as a consequence the survival function $S(r,t)$ will be finite when $t\to+\infty$ (from Section 1.3 that particle will eventually be absorbed and as a result $S(r,t)\to 0$ when $t\to+\infty$).
The time equation is:

$$\frac{1}{\mathcal{T}}\frac{\mathrm{d}\mathcal{T}}{\mathrm{d}t}=-\lambda^2 D,$$

which has the solution:

$$\mathcal{T}(t)=C\mathrm{e}^{-\lambda^2 Dt},$$

where C is a constant.
The r equation is:

$$\frac{\mathrm{d}^2\mathcal{R}}{\mathrm{d}r^2} + \frac{1}{r}\frac{\mathrm{d}\mathcal{R}}{\mathrm{d}r} + \lambda^2\mathcal{R} = 0. \tag{1.28}$$

This is Bessel's equation and has solution Morse & Feshbach (1954):

$$\mathcal{R}(r) = AJ_0(\lambda r) + BY_0(\lambda r), \tag{1.29}$$

where A and B are constants. $J_0(x)$ and $Y_0(x)$ are Bessel functions of the first and second kind, respectively, of order 0. From the boundary conditions (1.25a) and (1.25b) we know that:

$$\begin{aligned} &S(R_n, t) = \mathcal{R}(R_n)\mathcal{T}(t) = 0, \forall t > 0 \Rightarrow \mathcal{R}(R_n) = 0, \\ &\frac{\partial}{\partial r}S(r,t)\bigg|_{r=R} = 0 = \frac{\mathrm{d}\mathcal{R}}{\mathrm{d}r}\bigg|_{r=R} \mathcal{T}(t) = 0, \forall t > 0 \Rightarrow \frac{\mathrm{d}\mathcal{R}}{\mathrm{d}r}\bigg|_{r=R} = 0. \end{aligned}$$

Using (1.29) these boundary conditions can be written as:

$$AJ_0(\lambda R_n) + BY_0(\lambda R_n) = 0, \tag{1.30}$$

$$AJ_0'(\lambda R) + BY_0'(\lambda R) = 0. \tag{1.31}$$

This system of linear equations can be expressed as:

$$\begin{pmatrix} J_0(\lambda R_n) & Y_0(\lambda R_n) \\ J_0'(\lambda R) & Y_0'(\lambda R) \end{pmatrix} \begin{pmatrix} A \\ B \end{pmatrix} = \begin{pmatrix} 0 \\ 0 \end{pmatrix},$$

and given that we require $A \neq 0 \neq B$ we impose that:

$$\begin{vmatrix} J_0(\lambda R_n) & Y_0(\lambda R_n) \\ J_0'(\lambda R) & Y_0'(\lambda R) \end{vmatrix} = J_0(\lambda R_n)Y_0'(\lambda R) - Y_0(\lambda R_n)J_0'(\lambda R) = 0.$$

As a result, the solution for (1.28) can be written as:

$$\mathcal{R}(r) = J_0(\lambda_n r) - \delta_n Y_0(\lambda_n r),$$

where

$$\delta_n = \frac{J_0(\lambda_n R_n)}{Y_0(\lambda_n R_n)} = \frac{J_1(\lambda_n R)}{Y_1(\lambda_n R)},$$

and λ_n is the *n-th* root of

$$J_0(\lambda R_n) - \frac{J_1(\lambda R)}{Y_1(\lambda R)}Y_0(\lambda R_n) = 0. \tag{1.32}$$

The solution of the diffusion equation is the linear combination:

$$S(r,t) = \sum_{n=0}^{+\infty} \left[A_n J_0(\lambda_n r) + B_n Y_0(\lambda_n r)\right] \mathrm{e}^{-\lambda_n^2 Dt}.$$

From (1.30) we can write $B = -A\frac{J_0(\lambda_n R_n)}{Y_0(\lambda_n R_n)}$ and our series solution becomes:

$$S(r,t) = \sum_{n=0}^{+\infty} A_n \left[J_0(\lambda_n r) - \delta_n Y_0(\lambda_n r)\right] \mathrm{e}^{-\lambda_n^2 Dt}. \tag{1.33}$$

Now we need to calculate the coefficients A_n and for this purpose we define:

$$\mathcal{R}_n(r) = J_0(\lambda_n r) - \delta_n Y_0(\lambda_n r).$$

which satisfy the following differential equations:

$$\frac{\mathrm{d}}{\mathrm{d}r}\left(r\frac{\mathrm{d}\mathcal{R}_m}{\mathrm{d}r}\right) + r\lambda_m^2 \mathcal{R}_m = 0, \tag{1.34a}$$

$$\frac{\mathrm{d}}{\mathrm{d}r}\left(r\frac{\mathrm{d}\mathcal{R}_n}{\mathrm{d}r}\right) + r\lambda_n^2 \mathcal{R}_n = 0. \tag{1.34b}$$

Taking the difference of $\mathcal{R}_n$ times (1.34a) and $\mathcal{R}_m$ times (1.34b) we get:

$$[r(\mathcal{R}_m'\mathcal{R}_n - \mathcal{R}_m\mathcal{R}_n')]' + (\lambda_m^2 - \lambda_n^2) r\mathcal{R}_m\mathcal{R}_n = 0.$$

Integrating over the interval $[R_n, R]$ we obtain:

$$(\lambda_m^2 - \lambda_n^2)\int_{R_n}^{R} r\mathcal{R}_m\mathcal{R}_n \,\mathrm{d}r = [r(\mathcal{R}_m\mathcal{R}_n' - \mathcal{R}_m'\mathcal{R}_n)]_{R_n}^{R}. \tag{1.35}$$

We observe that $\frac{\mathrm{d}\mathcal{R}_m}{\mathrm{d}r}\big|_{r=R} = \frac{\mathrm{d}\mathcal{R}_n}{\mathrm{d}r}\big|_{r=R} = \mathcal{R}_m(R_n) = \mathcal{R}_n(R_n) = 0$ and if $m \neq n$ then (1.35) becomes:

$$\int_{R_n}^{R} r\mathcal{R}_m\mathcal{R}_n \,\mathrm{d}r = 0. \tag{1.36}$$

As a result, $\mathcal{R}_m$ and $\mathcal{R}_n$ are orthogonal with weight r on $[R_n, R]$.
Using the initial condition (1.25c) we want to obtain the coefficients A_n:

$$1 = S(r,0) = \sum_{n=0}^{+\infty} A_n \left[J_0(\lambda_n r) - \delta_n Y_0(\lambda_n r)\right].$$

We multiply the above equation by $r\mathcal{R}_m(r)$ and we integrate it from R_n to R with respect to r:

$$\int_{R_n}^{R} r\mathcal{R}_m \,\mathrm{d}r = \sum_{n=0}^{+\infty} \left(A_n \int_{R_n}^{R} r\mathcal{R}_m\mathcal{R}_n \,\mathrm{d}r \right),$$

and using the orthogonality condition (1.36) we obtain:

$$\int_{R_n}^{R} r\mathcal{R}_m \,\mathrm{d}r = A_m \int_{R_n}^{R} r\mathcal{R}_m^2 \,\mathrm{d}r, \tag{1.37}$$

where

$$\begin{aligned}
\int_{R_n}^{R} r\mathcal{R}_m^2 \,\mathrm{d}r &= \int_{R_n}^{R} r[J_0(\lambda_m r) - \delta_m Y_0(\lambda_m r)]^2 \,\mathrm{d}r \\
&= \int_{R_n}^{R} r[J_0^2(\lambda_m r) - 2\delta_m J_0(\lambda_m r)Y_0(\lambda_m r) + \delta_m^2 Y_0^2(\lambda_m r)] \,\mathrm{d}r \\
&= \int_{R_n}^{R} r J_0^2(\lambda_m r) \,\mathrm{d}r - 2\delta_m \int_{R_n}^{R} r J_0(\lambda_m r)Y_0(\lambda_m r) \,\mathrm{d}r + \\
&+ \delta_m^2 \int_{R_n}^{R} r Y_0^2(\lambda_m r) \,\mathrm{d}r.
\end{aligned}$$

Next, we calculate each integral in the above sum:

$$\begin{aligned}
&\int_{R_n}^{R} r J_0(\lambda_m r)^2 \,\mathrm{d}r = \lim_{\lambda_m \to \lambda_n} \frac{[r(\lambda_n J_0(\lambda_m r)J_0'(\lambda_n r) - \lambda_m J_0'(\lambda_m r)J_0(\lambda_n r))]_{R_n}^{R}}{\lambda_m^2 - \lambda_n^2} \\
&= \lim_{\lambda_m \to \lambda_n} \frac{[r(r\lambda_n J_0'(\lambda_m r)J_0'(\lambda_n r) - (J_0'(\lambda_m r) + r\lambda_m J_0''(\lambda_m r))J_0(\lambda_n r))]_{R_n}^{R}}{2\lambda_m} \\
&= \frac{R^2}{2}\{J_0'(\lambda_n R)^2 - [J_0''(\lambda_n R) + \frac{1}{R\lambda_n} J_0'(\lambda_n R)]J_0(\lambda_n R)\} \\
&- \frac{R_n^2}{2}\{J_0'(\lambda_n R_n)^2 - [J_0''(\lambda_n R_n) + \frac{1}{R_n\lambda_n} J_0'(\lambda_n R_n)]J_0(\lambda_n R_n)\}.
\end{aligned} \tag{1.38}$$

We know that:

$$J_0''(\lambda_n R) + \frac{1}{R\lambda_n} J_0'(\lambda_n R) = -J_0(\lambda_n R),$$

and, consequently, equation (1.38) can be written as:

$$\int_{R_n}^{R} r J_0(\lambda_m r)^2 \,\mathrm{d}r = \frac{R^2}{2}(J_0'(\lambda_n R)^2 + J_0(\lambda_n R)^2) - \frac{R_n^2}{2}(J_0'(\lambda_n R_n)^2 + J_0(\lambda_n R_n)^2).$$

Analogously, we obtain:

$$\int_{R_n}^{R} rY_0(\lambda_m r)^2\,\mathrm{d}r = \frac{R^2}{2}(Y_0'(\lambda_n R)^2 + Y_0(\lambda_n R)^2) - \frac{R_n^2}{2}(Y_0'(\lambda_n R_n)^2 + Y_0(\lambda_n R_n)^2),$$

and

$$\begin{aligned}\int_{R_n}^{R} rY_0(\lambda_m r)J_0(\lambda_m r)\,\mathrm{d}r = &\frac{R^2}{2}(Y_0'(\lambda_n R)J_0'(\lambda_n R) + Y_0(\lambda_n R)J_0(\lambda_n R)) \\ &- \frac{R_n^2}{2}(Y_0'(\lambda_n R_n)Y_0'(\lambda_n R_n) + Y_0(\lambda_n R_n)Y_0(\lambda_n R_n)).\end{aligned}$$

As a result:

$$\int_{R_n}^{R} r\mathcal{R}_m^2\,\mathrm{d}r = \frac{R^2}{2}[J_0(\lambda_n R) - \delta_n Y_0(\lambda_n R)]^2 - \frac{R_n^2}{2}[J_1(\lambda_n R_n) - \delta_n Y_1(\lambda_n R_n)]^2. \quad (1.39)$$

In order to simplify the above equation we use the following properties (Levine, 1997, p.626):

$$\begin{vmatrix} J_\nu(x) & Y_\nu(x) \\ \frac{\mathrm{d}}{\mathrm{d}x}J_\nu(x) & \frac{\mathrm{d}}{\mathrm{d}x}Y_\nu(x) \end{vmatrix} = \frac{2}{\pi x}, \quad (1.40)$$

and

$$\frac{\mathrm{d}}{\mathrm{d}x}T_0(x) = -T_1(x). \quad (1.41)$$

where $\nu \in \mathbb{C}$ and $T = J$ (Bessel function of the first kind) or $T = Y$ (Bessel function of the second kind).

Let $x = \lambda_n R_n$ and $x = \lambda_n R$ in (1.40), respectively, and we obtain:

$$J_1(\lambda_n R_n) - \delta_n Y_1(\lambda_n R_n) = \frac{2}{\lambda_n \pi R_n Y_0(\lambda_n R_n)}, \quad (1.42a)$$

$$J_0(\lambda_n R) - \delta_n Y_0(\lambda_n R) = -\frac{2}{\lambda_n \pi R Y_1(\lambda_n R)}. \quad (1.42b)$$

Using (1.42) in (1.39) we arrive at the following:

$$\begin{aligned}\int_{R_n}^{R} r\mathcal{R}_m^2\,\mathrm{d}r &= \frac{2}{\lambda_n^2\pi^2 Y_1(\lambda_n R)^2} - \frac{2}{\lambda_n^2\pi^2 Y_0(\lambda_n R_n)^2} \\ &= \frac{2}{\lambda_n^2\pi^2}\left(\frac{1}{Y_1(\lambda_n R)^2} - \frac{1}{Y_0(\lambda_n R_n)^2}\right). \quad (1.43)\end{aligned}$$

Additionally we need to calculate the left-hand side of (1.37) in order to obtain the coefficient A_n:

$$\int_{R_n}^{R} r\mathcal{R}_m\,\mathrm{d}r = \int_{R_n}^{R} r(J_0(\lambda_m r) - \delta_m Y_0(\lambda_m r))\,\mathrm{d}r$$

$$
\begin{aligned}
&= \int_{R_n}^{R} rJ_0(\lambda_m r)\,\mathrm{d}r - \delta_m \int_{R_n}^{R} rY_0(\lambda_m r)\,\mathrm{d}r \\
&= \frac{1}{\lambda_m^2}\left(\int_{R_n\lambda_m}^{R\lambda_m} \frac{\mathrm{d}}{\mathrm{d}x}(xJ_1(x))\,\mathrm{d}x - \delta_m \int_{R_n\lambda_m}^{R\lambda_m} \frac{\mathrm{d}}{\mathrm{d}x}(xY_1(x))\,\mathrm{d}x\right) \\
&= \frac{1}{\lambda_m}\left(RJ_1(\lambda_m R) - R_n J_1(\lambda_m R_n) - \delta_m(RY_1(\lambda_m R) - R_n Y_1(\lambda_m R_n))\right) \\
&= \frac{1}{\lambda_m}\left(R(J_1(\lambda_m R) - \delta_m Y_1(\lambda_m R)) - R_n(J_1(\lambda_m R_n) - \delta_m Y_1(\lambda_m R_n))\right) \\
&= -\frac{R_n}{\lambda_m}(J_1(\lambda_m R_n) - \delta_m Y_1(\lambda_m R_n)) \\
&= -\frac{2}{\pi\lambda_m^2 Y_0(\lambda_m R_n)}. \qquad (1.44)
\end{aligned}
$$

As a result, using (1.43) and (1.44) we obtain:

$$
\begin{aligned}
A_m = \frac{\int_{R_n}^{R} r\mathcal{R}_m\,\mathrm{d}r}{\int_{R_n}^{R} r\mathcal{R}_m^2\,\mathrm{d}r} &= \frac{-\frac{2}{\pi\lambda_m^2 Y_0(\lambda_m R_n)}}{\frac{2}{\lambda_m^2\pi^2}\left(\frac{1}{Y_1(\lambda_m R)^2} - \frac{1}{Y_0(\lambda_m R_n)^2}\right)} \\
&= \frac{\pi Y_1(\lambda_m R)^2 Y_0(\lambda_m R_n)}{Y_1(\lambda_m R)^2 - Y_0(\lambda_m R_n)^2}, \quad m \in \mathbb{N}\cup\{0\}, \qquad (1.45)
\end{aligned}
$$

Our series solution (1.33) becomes:

$$
S(r,t) = \sum_{n=0}^{+\infty} \frac{\pi Y_1(\lambda_n R)^2 Y_0(\lambda_n R_n)}{Y_1(\lambda_n R)^2 - Y_0(\lambda_n R_n)^2}\left[J_0(\lambda_n r) - \delta_n Y_0(\lambda_n r)\right]\mathrm{e}^{-\lambda_n^2 Dt}.
$$

Another quantity of great importance is the survival function averaged over the annular region which we normalise in order to obtain:

$$
\begin{aligned}
s(t) &= \frac{1}{\pi(R^2 - R_n^2)}\int_0^{2\pi}\int_{R_n}^{R} rS(r,t)\,\mathrm{d}r\mathrm{d}\theta \\
&= \frac{2}{(R^2 - R_n^2)}\sum_{n=0}^{+\infty}\frac{\pi Y_1(\lambda_n R)^2 Y_0(\lambda_n R_n)}{Y_1(\lambda_n R)^2 - Y_0(\lambda_n R_n)^2}\mathrm{e}^{-\lambda_n^2 Dt} \\
&\times \int_{R_n}^{R} r\left[J_0(\lambda_n r) - \delta_n Y_0(\lambda_n r)\right]\,\mathrm{d}r. \qquad (1.46)
\end{aligned}
$$

We know from (1.44) that:

$$
\int_{R_n}^{R} r\left[J_0(\lambda_m r) - \delta_0 Y_0(\lambda_m r)\right]\,\mathrm{d}r = -\frac{2}{\pi\lambda_m^2 Y_0(\lambda_m R_n)}.
$$

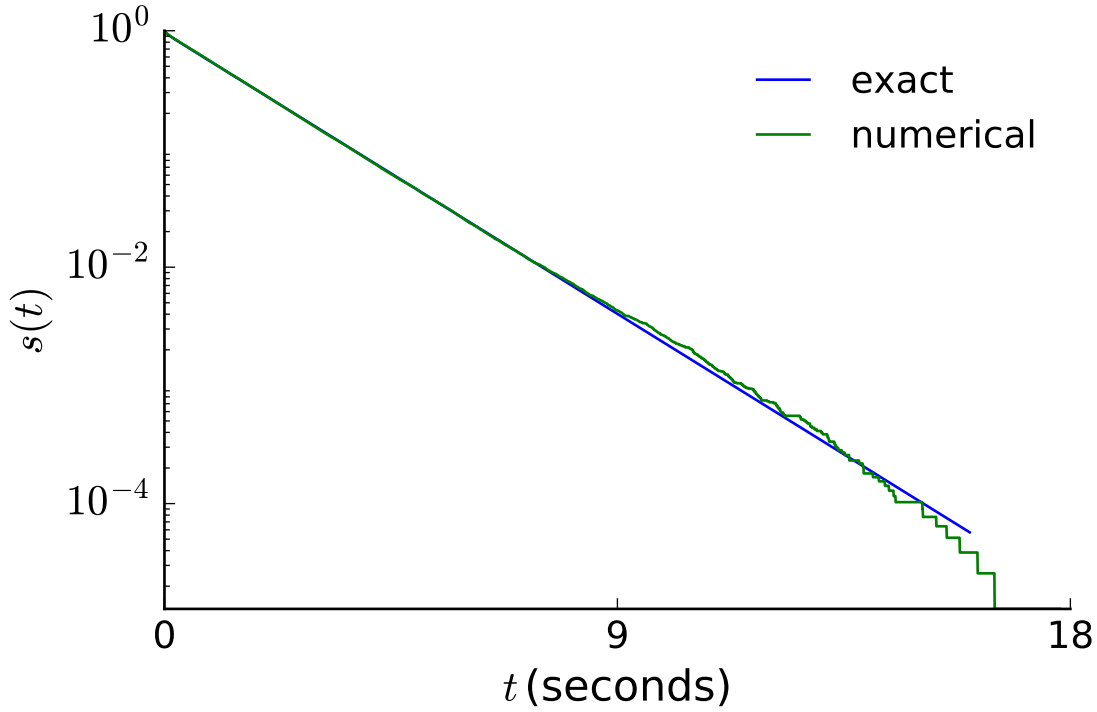

Figure 1.9: Plot of the survival function averaged over all starting points of a Brownian particle diffusing in a concentric annular region, as shown in Figure 1.8 as a function of time time t. The blue line represents the analytic formula (1.47) and the green line represents numerical simulations. For the numerical simulations we have used G.4.1 and this plot has been obtained using G.4.2 with 5 terms in the sum of the survival probability. Oscillation appear in the numerical simulations for large values of t because the number of Brownian particles is significantly smaller at those times. For this figure we have used the following parameters: $R = 1\,\mathrm{cm}, R_n = 0.1\,\mathrm{cm}, D = 0.5\,\mathrm{cm}^2\,\mathrm{s}^{-1}$.

and as a result (1.46) can be written as:

$$s(t) = \frac{4}{(R^2 - R_n^2)} \sum_{n=0}^{+\infty} \frac{1}{\lambda_n^2} \frac{Y_1(\lambda_n R)^2}{Y_0(\lambda_n R_n)^2 - Y_1(\lambda_n R)^2} \mathrm{e}^{-\lambda_n^2 D t}. \tag{1.47}$$

We plot (1.47) in Figure 1.9 and compare with numerical simulations.

1.4.2 Three dimensions

As in the two dimensional case a particle is "alive" at time t if it has not yet been absorbed at the interior barrier and the survival probability is defined as:

$$S(r,t) = \text{Prob(a particle is "alive" at } r \text{ at time } t),$$

which satisfies the differential equation:

$$\frac{\partial}{\partial t}S\left(r,t\right) = \nabla^2 S(r,t) \Rightarrow \frac{\partial}{\partial t}S\left(r,t\right) = \frac{D}{r^2}\frac{\partial}{\partial r}\left(r^2\frac{\partial}{\partial r}S\left(r,t\right)\right), \tag{1.48}$$

and the same boundary and initial conditions as the two dimensional case:

$$S(R_n,t) = 0, \quad t \geq 0, \tag{1.49}$$

$$\frac{\partial}{\partial r}S(r,t)\Big|_{r=R} = 0, \quad t \geq 0, \tag{1.50}$$

$$S(r,0) = 1, \quad 0 < R_n < r \leq R. \tag{1.51}$$

We look for a solution that is separable, of the form $S(r,t) = \mathcal{R}(r)\mathcal{T}(t)$ in order to solve (1.48) and after simplification we obtain:

$$\frac{\mathcal{R}}{D}\frac{\mathrm{d}\mathcal{T}}{\mathrm{d}t} = \mathcal{T}\frac{\mathrm{d}^2\mathcal{R}}{\mathrm{d}r^2} + \frac{2\mathcal{T}}{r}\frac{\mathrm{d}\mathcal{R}}{\mathrm{d}r}. \tag{1.52}$$

Multiplying equation (1.52) by $\frac{1}{\mathcal{R}\mathcal{T}}$ we obtain:

$$\frac{1}{D\mathcal{T}}\frac{\mathrm{d}\mathcal{T}}{\mathrm{d}t} = \frac{1}{\mathcal{R}}\frac{\mathrm{d}^2\mathcal{R}}{\mathrm{d}r^2} + \frac{2}{r\mathcal{R}}\frac{\mathrm{d}\mathcal{R}}{\mathrm{d}r}. \tag{1.53}$$

We observe that the left-hand side of (1.53) is a function of t while the right-hand side is a function of r and we deduce that:

$$\frac{1}{D\mathcal{T}}\frac{\mathrm{d}\mathcal{T}}{\mathrm{d}t} = \frac{1}{\mathcal{R}}\frac{\mathrm{d}^2\mathcal{R}}{\mathrm{d}r^2} + \frac{2}{r\mathcal{R}}\frac{\mathrm{d}\mathcal{R}}{\mathrm{d}r} = -\lambda^2,$$

where λ is a constant. Here we again choose the constant to be $-\lambda^2$ in order to ensure that the time function does not grow exponentially and as a consequence the survival function $S(r,t)$ will be finite when $t \to +\infty$.
The time equation is:

$$\frac{1}{\mathcal{T}}\frac{\mathrm{d}\mathcal{T}}{\mathrm{d}t} = -\lambda^2 D,$$

which has the solution:

$$\mathcal{T}(t) = C\mathrm{e}^{-\lambda^2 Dt},$$

where C is a constant.

The r-equation is:

$$\frac{\mathrm{d}^2\mathcal{R}}{\mathrm{d}r^2} + \frac{2}{r}\frac{\mathrm{d}\mathcal{R}}{\mathrm{d}r} + \lambda^2\mathcal{R} = 0.$$

which we can rewrite as:

$$\frac{\mathrm{d}^2}{\mathrm{d}r^2}(r\mathcal{R}) + \lambda^2 r\mathcal{R} = 0.$$

Let $g(r) = r\mathcal{R}$ in the above equation and we obtain:

$$\frac{\mathrm{d}^2 g}{\mathrm{d}r^2} + \lambda^2 g = 0.$$

We use the Ansatz $g = \mathrm{e}^{mr}$ and we get $m = \pm i\lambda$. As a result, we have:

$$g(r) = A\sin(\lambda r) + B\cos(\lambda r) \Rightarrow R(r) = \frac{A}{r}\sin(\lambda r) + \frac{B}{r}\cos(\lambda r).$$

We deduce from the boundary conditions:

$$\begin{aligned} &S(R_n, t) = \mathcal{R}(R_n)\mathcal{T}(t) = 0, \forall t > 0 \Rightarrow \mathcal{R}(R_n) = 0, \\ &\frac{\partial}{\partial r}S(R, t) = 0 = \left.\frac{\mathrm{d}\mathcal{R}}{\mathrm{d}r}\right|_{r=R} \mathcal{T}(t) = 0, \forall t > 0 \Rightarrow \left.\frac{\mathrm{d}\mathcal{R}}{\mathrm{d}r}\right|_{r=R} = 0. \end{aligned}$$

and as a result we obtain:

$$A\sin(\lambda R_n) + B\cos(\lambda R_n) = 0, \tag{1.54a}$$

$$\left(-\frac{A}{R^2} - \frac{B\lambda}{R}\right)\sin(\lambda R) + \left(\frac{A\lambda}{R} - \frac{B}{R^2}\right)\cos(\lambda R) = 0. \tag{1.54b}$$

From (1.54a) we obtain:

$$A = -B\frac{\cos(\lambda R_n)}{\sin(\lambda R_n)},$$

and, as a result, (1.54b) can be written as:

$$B\left[\left(\frac{\cot(\lambda R_n) - R\lambda}{R^2}\right)\sin(\lambda R) - \left(\frac{R\lambda\cot\lambda R_n + 1}{R^2}\right)\cos(\lambda R)\right] = 0.$$

Accordingly, the solution to can be written as:

$$\mathcal{R}(r) = \frac{1}{r}\left[\cos(\lambda r) - \delta_n\sin(\lambda r)\right],$$

where

$$\delta_n = \frac{\cos(\lambda_n R_n)}{\sin(\lambda_n R_n)},$$

and λ_n is the n-th root of

$$\left[\left(\frac{\cot(\lambda R_n) - R\lambda}{R^2}\right)\sin(\lambda R) - \left(\frac{R\lambda\cot(\lambda R_n) + 1}{R^2}\right)\cos(\lambda R)\right] = 0. \tag{1.55}$$

The solution of the diffusion equation is the linear combination:

$$S(r,t) = \sum_{n=0}^{+\infty} \frac{A_n}{r}\left[\cos(\lambda_n r) - \delta_n \sin(\lambda_n r)\right] \mathrm{e}^{-\lambda_n^2 D t}.$$

Now we need to calculate the coefficients A_n and for this purpose we define:

$$\mathcal{R}_n(r) = \frac{1}{r}\left[\cos(\lambda_n r) - \delta_n \sin(\lambda_n r)\right].$$

which satisfy the following differential equations:

$$\frac{\mathrm{d}}{\mathrm{d}r}\left(r^2 \frac{d\mathcal{R}_m}{dr}\right) + r^2\lambda_m^2 \mathcal{R}_m = 0, \tag{1.56a}$$

$$\frac{\mathrm{d}}{\mathrm{d}r}\left(r^2 \frac{d\mathcal{R}_n}{dr}\right) + r^2\lambda_n^2 \mathcal{R}_n = 0. \tag{1.56b}$$

Taking the difference of $\mathcal{R}_n$ times (1.56a) and $\mathcal{R}_m$ times (1.56b) we get:

$$\frac{\mathrm{d}}{\mathrm{d}r}\left[r^2\left(\frac{\mathrm{d}\mathcal{R}_m}{\mathrm{d}r}\mathcal{R}_n - \mathcal{R}_m\frac{\mathrm{d}\mathcal{R}_n}{\mathrm{d}r}\right)\right] + (\lambda_m^2 - \lambda_n^2) r^2 \mathcal{R}_m \mathcal{R}_n = 0.$$

Integrating over the interval $[R_n, R]$ we obtain:

$$(\lambda_m^2 - \lambda_n^2)\int_{R_n}^{R} r^2 \mathcal{R}_m \mathcal{R}_n \,\mathrm{d}r = \left[r^2\left(\frac{\mathrm{d}\mathcal{R}_m}{\mathrm{d}r}\mathcal{R}_n - \mathcal{R}_m\frac{\mathrm{d}\mathcal{R}_n}{\mathrm{d}r}\right)\right]_{R_n}^{R}. \tag{1.57}$$

We observe that $\frac{\mathrm{d}\mathcal{R}_m}{\mathrm{d}r}\big|_{r=R} = \frac{\mathrm{d}\mathcal{R}_n}{\mathrm{d}r}\big|_{r=R} = \mathcal{R}_m(R_n) = \mathcal{R}_n(R_n) = 0$ and if $m \neq n$ then (1.57) becomes:

$$\int_{R_n}^{R} r^2 \mathcal{R}_m \mathcal{R}_n \,\mathrm{d}r = 0. \tag{1.58}$$

As a result, $\mathcal{R}_m$ and $\mathcal{R}_n$ are orthogonal with weight r^2 on $[R_n, R]$.
Using the initial condition (1.51) we want to obtain the coefficients A_n:

$$1 = S(r,0) = \sum_{n=0}^{+\infty} \frac{A_n}{r}\left[\cos(\lambda_n r) - \delta_n \sin(\lambda_n r)\right].$$

We multiply the above equation by $r^2\mathcal{R}_m(r)$ and we integrate it from R_n to R with respect to r:

$$\int_{R_n}^{R} r^2\mathcal{R}_m \,\mathrm{d}r = \sum_{n=0}^{+\infty}\left(A_n \int_{R_n}^{R} r^2\mathcal{R}_m\mathcal{R}_n \,\mathrm{d}r\right),$$

and using the orthogonality condition (1.58) we obtain:

$$\int_{R_n}^{R} r^2\mathcal{R}_m \,\mathrm{d}r = A_m \int_{R_n}^{R} r^2\mathcal{R}_m^2 \,\mathrm{d}r,$$

where

$$\begin{aligned}
\int_{R_n}^{R} r^2\mathcal{R}_m^2 \,\mathrm{d}r &= \int_{R_n}^{R} [\cos(\lambda_m r) - \delta_n \sin(\lambda_m r)]^2 \,\mathrm{d}r \\
&= \int_{R_n}^{R} [\cos^2(\lambda_m r) - 2\delta_m \cos(\lambda_m r)\sin(\lambda_m r) + \delta_m^2 \sin^2(\lambda_m r)] \,\mathrm{d}r \\
&= \int_{R_n}^{R} \cos^2(\lambda_m r) \,\mathrm{d}r - 2\delta_m \int_{R_n}^{R} \cos(\lambda_m r)\sin(\lambda_m r) \,\mathrm{d}r + \\
&+ \delta_m^2 \int_{R_n}^{R} \sin^2(\lambda_m r) \,\mathrm{d}r.
\end{aligned}$$

and

$$\begin{aligned}
\int_{R_n}^{R} r^2\mathcal{R}_m \,\mathrm{d}r &= \int_{R_n}^{R} r[\cos(\lambda_m r) - \delta_n \sin(\lambda_m r)] \,\mathrm{d}r \\
&= \int_{R_n}^{R} r\cos(\lambda_m r) \,\mathrm{d}r - \delta_n \int_{R_n}^{R} r\sin(\lambda_m r) \,\mathrm{d}r.
\end{aligned}$$

Next, we calculate the following integrals:

$$\begin{aligned}
\int_{R_n}^{R} \cos^2(\lambda_m r) \,\mathrm{d}r &= \int_{R_n}^{R} \frac{1+\cos(2\lambda_m r)}{2} \,\mathrm{d}r \\
&= \frac{R-R_n}{2} + \frac{1}{4\lambda_m}\left[\sin(2\lambda_m R_n) - \sin(2\lambda_m R)\right], \\
\int_{R_n}^{R} \sin(\lambda_m r)\cos(\lambda_m r) \,\mathrm{d}r &= \frac{1}{2}\int_{R_n}^{R} \sin(2\lambda_m r) \,\mathrm{d}r \\
&= -\frac{1}{4\lambda_m}\left[\cos(2\lambda_m R) - \cos(2\lambda_m R_n)\right], \\
\int_{R_n}^{R} \sin^2(\lambda_m r) \,\mathrm{d}r &= \int_{R_n}^{R} \frac{1-\cos(2\lambda_m r)}{2} \,\mathrm{d}r
\end{aligned}$$

$$= \frac{R - R_n}{2} - \frac{1}{4\lambda_m} \left[\sin(2\lambda_m R) - \sin(2\lambda_m R_n)\right],$$

and

$$\int_{R_n}^{R} r\cos(\lambda_m r)\,\mathrm{d}r = \frac{1}{\lambda_m}\left[r\sin(\lambda_m r)\right]_{R_n}^{R} + \frac{1}{\lambda_m^2}\left[\cos(\lambda_m r)\right]_{R_n}^{R},$$
$$\int_{R_n}^{R} r\sin(\lambda_m r)\,\mathrm{d}r = -\frac{1}{\lambda_m}\left[r\cos(\lambda_m r)\right]_{R_n}^{R} + \frac{1}{\lambda_m^2}\left[\sin(\lambda_m r)\right]_{R_n}^{R}.$$

As a result we have:

$$\begin{aligned}\int_{R_n}^{R} r^2\mathcal{R}_m^2\,\mathrm{d}r &= \frac{R - R_n}{2}\left(1 + \delta_m^2\right) + \frac{1}{4\lambda_m}\left[\sin(2\lambda_m R) - \sin(2\lambda_m R_n)\right]\left(1 - \delta_m^2\right) \\ &\quad + \frac{\delta_m}{2\lambda_m}\left[\cos(2\lambda_m R) - \cos(2\lambda_m R_n)\right] \\ &\equiv O_s\left(\lambda_m\right), \end{aligned} \tag{1.59}$$

and

$$\begin{aligned}\int_{R_n}^{R} r^2\mathcal{R}_m\,\mathrm{d}r &= \frac{1}{\lambda_m}\left(R\sin(\lambda_m R) - R_n\sin(\lambda_m R_n)\right) + \frac{1}{\lambda_m^2}\left(\cos(\lambda_m R) - \cos(\lambda_m R_n)\right) \\ &\quad + \frac{\delta_m}{\lambda_m}\left(R\cos(\lambda_m R) - R_n\cos(\lambda_m R_n)\right) - \frac{\delta_m}{\lambda_m^2}\left(\sin(\lambda_m R) - \sin(\lambda_m R_n)\right) \\ &= \frac{1}{\lambda_m}\frac{R\cos(\lambda_m(R - R_n)) - R_n}{\sin(\lambda_m R_n)} + \frac{1}{\lambda_m^2}\frac{\sin(\lambda_m(R_n - R))}{\sin(\lambda_m R_n)} \\ &\equiv W_s\left(\lambda_m\right). \end{aligned} \tag{1.60}$$

From (1.59) and (1.60) we arrive at the following formula for the coefficient A_n:

$$A_m = \frac{\int_{R_n}^{R} r^2\mathcal{R}_m\,\mathrm{d}r}{\int_{R_n}^{R} r^2\mathcal{R}_m^2\,\mathrm{d}r} = \frac{W_s\left(\lambda_m\right)}{O_s\left(\lambda_m\right)}, \quad m \in \mathbb{N} \cup \{0\},$$

We again calculate the normalised survival function averaged over the spherical annular region:

$$\begin{aligned} s(t) &= \frac{3}{4\pi(R^3 - R_n^3)}\int_{-\pi}^{\pi}\int_{0}^{2\pi}\int_{R_n}^{R} r^2 S(r,t)\sin\varphi\,\mathrm{d}r\mathrm{d}\theta d\varphi \\ &= \frac{3}{(R^3 - R_n^3)}\sum_{n=0}^{+\infty} A_n \mathrm{e}^{-\lambda_n^2 Dt}\int_{R_n}^{R} r\left[\cos(\lambda_n r) - \delta_n\sin(\lambda_n r)\right]\,\mathrm{d}r. \end{aligned} \tag{1.61}$$

We know from (1.60) that:

$$\int_{R_n}^{R} r\left[\cos(\lambda_n r) - \delta_n \sin(\lambda_n r)\right] \mathrm{d}r = \frac{1}{\lambda_m}\frac{R\cos(\lambda_m(R-R_n)) - R_n}{\sin(\lambda_m R_n)} + \frac{1}{\lambda_m^2}\frac{\sin(\lambda_m(R_n - R))}{\sin(\lambda_m R_n)}, \tag{1.62}$$

and as a result (1.61) can be written as:

$$s(t) = \frac{3}{(R^3 - R_n^3)}\sum_{n=0}^{+\infty} A_n' \mathrm{e}^{-\lambda_n^2 Dt}. \tag{1.63}$$

where

$$A_n' = \frac{\left(W_s\left(\lambda_n\right)\right)^2}{O_s\left(\lambda_n\right)}, \quad n \in \mathbb{N} \cup \{0\},$$

We plot (1.63) in Figure 1.10 and compare with numerical simulations.

1.5 The Green's function method

Suppose we have a differential operator L and we want to find a function $u(\mathbf{x})$ which satisfies:

$$\begin{aligned} Lu(\mathbf{x}) &= f(\mathbf{x}), \quad \mathbf{x} \in C, \\ D\partial_{\mathbf{n}} u(\mathbf{x}) &= \kappa u(\mathbf{x}), \quad \mathbf{x} \in \partial C, \end{aligned}$$

where $f(\mathbf{x})$ is an arbitrary function, $\mathbf{n}$ is the normal vector to ∂C and D and κ are constants. For this purpose we define the Green's function $G\left(\mathbf{x}, \mathbf{s}\right)$:

$$\begin{aligned} LG(\mathbf{x}, \mathbf{s}) &= -\delta(\mathbf{x} - \mathbf{s}) \quad \text{if} \quad \mathbf{x}, \mathbf{s} \in C, \\ D\partial_{\mathbf{n}} G(\mathbf{x}, \mathbf{s}) &= \kappa G(\mathbf{x}, \mathbf{s}) \quad \text{if} \quad \mathbf{x} \in \partial C, \end{aligned}$$

where δ is the Dirac delta function. We obtain $u(\mathbf{x})$ as follows:

$$u(\mathbf{x}) = -\int G(\mathbf{x}, \mathbf{s}) f(\mathbf{s})\, \mathrm{d}\mathbf{s}.$$

We observe that:

$$Lu(\mathbf{x}) = -\int LG(\mathbf{x}, \mathbf{s}) f(\mathbf{s})\, \mathrm{d}\mathbf{s} = \int \delta(\mathbf{x} - \mathbf{s}) f(\mathbf{s})\, \mathrm{d}\mathbf{s} = f(\mathbf{x}),$$

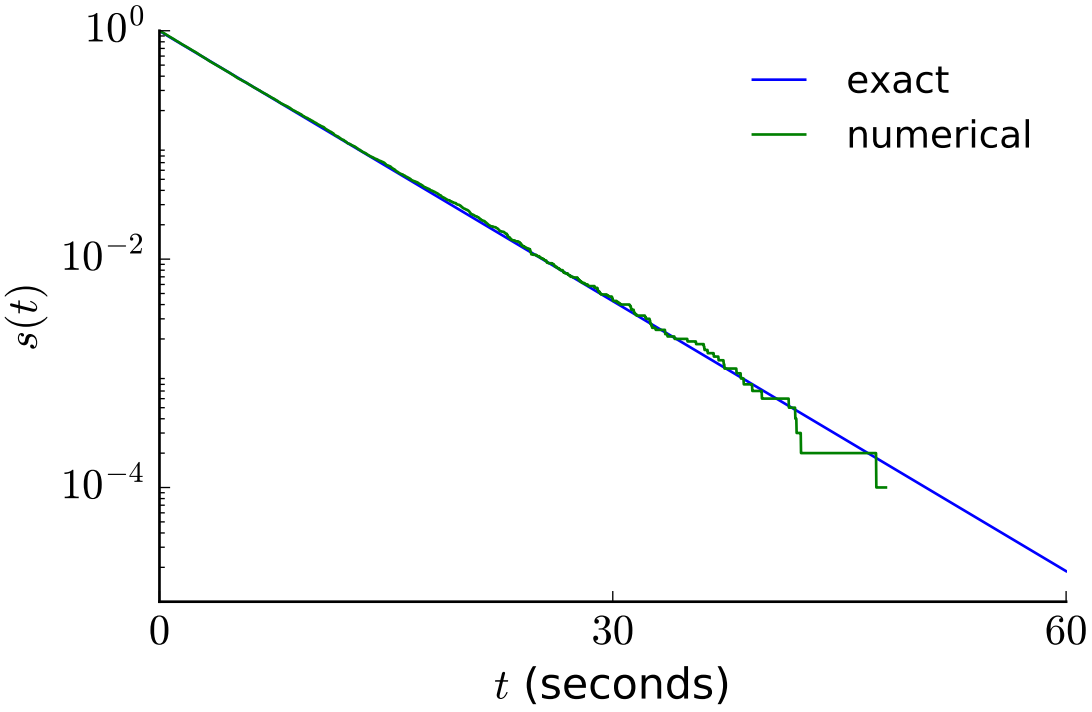

Figure 1.10: Plot of the survival function averaged over all starting points of a Brownian particle diffusing in a concentric annular region, as shown in Figure 1.8. The blue line represents the analytic formula (1.63) and the green line represents numerical simulations. For this plot we have used 5 terms in the sum of the survival probability. Oscillation appear in the numerical simulations for large values of t because the number of Brownian particles is significantly smaller at those times. For this figure we have used the following parameters: $R = 1\,\text{cm}$, $R_n = 0.1\,\text{cm}$, $D = 0.5\,\text{cm}^2\,\text{s}^{-1}$.

and

$$D\partial_{\mathbf{n}}u(\mathbf{x}) = -\int D\partial_{\mathbf{n}}G(\mathbf{x},\mathbf{s})f(\mathbf{s})\,\mathrm{d}\mathbf{s} = -\int \kappa G(\mathbf{x},\mathbf{s})f(\mathbf{s})\,\mathrm{d}\mathbf{s} = \kappa u(\mathbf{x}).$$

An important use of the Green's function method is in the calculation of first passage properties of diffusion. As such, the next section is a review of Condamin *et al.* (2007) which makes use of the Green's function method to determine the first passage properties of diffusion to the interior trap, in an eccentric annular

region, and which will be the benchmark of comparison for our exact formulas from Chapter 2 and 3 for the two dimensional case and the three dimensional case, respectively.

1.6 Rescaling of coordinate system

We represent a cell as a circle or as a sphere with radius R, containing a nucleus (or other intracellular compartment) with radius R_n. The center of the nucleus is displaced from that of the cell by a distance r_c.
We rescale lengths so that the radius of the cell is equal to 1. We shall calculate the Green's functions and mean times using the following dimensionless quantities:

$$a = \frac{R_n}{R} \qquad \text{and} \qquad c = \frac{r_c}{R}.$$

Note that $0 \leq c \leq 1-a$, and a^2 is the fraction of the cell occupied by the nucleus in two dimension, and a^3 in three dimensions.

1.7 Condamin *et al.* (2007) review

The time required for a Brownian particle to go from a starting position to a target site is called the first passage time (FPT) and it is found in a wide range of problems, such as diffusion limited reactions Rice (1985) or animal food searches Bénichou *et al.* (2005), which are called first passage problems.
The FPT depends on a multitude of factors, primary among them being geometry. For example, the mean first passage time (MFPT) for a two dimensional random walker is infinite if the walk is not bounded. However, in the case of a bounded walk the MFPT is finite and depends on the confining surface. Unfortunately, this dependency is difficult to explicitly determine but for the most simple geometries (*i.e.* one dimensional or spherically symmetric problems Redner (2001)) but which are not biologically realistic.
Previously to Condamin *et al.* (2007) this family of problems has received considerable attention. In particular, in the case of discrete random walks, an expression for the MFPT between two nodes of a general network has been derived Noh &

Rieger (2004). Furthermore, the MFPT of a continuous Brownian motion at a small absorbing window on a otherwise reflecting boundary has been studied Grigoriev *et al.* (2002); Singer *et al.* (2006b). When the window is a small sphere within the domain, the behavior of the MFPT has been given but it does not show the dependence of the MFPT on the initial position Pinsky (2003)(see Appendix A.3 for a review of this result).

Transitioning from discrete to continuous case, Condamin *et al.* (2007) investigate how much time does it take a Brownian particle with diffusion coefficient D to reach a target of radius a. They consider an n-sphere (where $n = 1, 2$) target of radius a centered at $\mathbf{x}_n$. The Brownian motion starts at $\mathbf{x}_0$ and is restricted to a domain C with volume/area of V/A.

1.7.1 The Green's function approximation

The continuous mean first passage time (MFPT) $\langle T(\mathbf{x}_0)\rangle$ is derived using the Green's function method:

$$\langle T(\mathbf{x}_0)\rangle = R^2 \int_C G(\mathbf{x}_0, \mathbf{x})\, \mathrm{d}\mathbf{x} \approx R^2 \int_{C^*} G(\mathbf{x}_0, \mathbf{x})\, \mathrm{d}\mathbf{r},$$

where the Green's function $G(\mathbf{x}_0, \mathbf{x})$ can be interpreted as the stationary distribution of particles in the domain C^* (where C^* is the domain C without the absorbing target) if there is a unit flux of particles incoming at $\mathbf{x}_0$, and the diffusion coefficient is D. The Green's function $G(\mathbf{x}, \mathbf{x}_0)$ is defined by:

$$D\Delta_{\mathbf{r}} G(\mathbf{x}_0, \mathbf{x}) = -\delta(\mathbf{x} - \mathbf{x}_0) \quad \text{if} \quad \mathbf{x} \in C^*, \tag{1.65a}$$

$$G(\mathbf{x}_0, \mathbf{x}) = 0 \quad \text{if} \quad \mathbf{x} \in \partial C_1, \tag{1.65b}$$

$$\partial_{\mathbf{n}} G(\mathbf{x}_0, \mathbf{x}) = 0 \quad \text{if} \quad \mathbf{x} \in \partial C_2, \tag{1.65c}$$

where $\mathbf{n}$ is the normal unit vector to ∂C_2. Condamin *et al.* (2007) produce the following approximation for the Green's function:

$$G(\mathbf{x}_0, \mathbf{x}) \approx G_0(a) + H^*(\mathbf{x}_n|\mathbf{x}_n) - H(\mathbf{x}_n|\mathbf{x}_0) + H(\mathbf{x}|\mathbf{x}_0) - H(\mathbf{x}|\mathbf{x}_n), \tag{1.66}$$

where $H(\mathbf{x}|\mathbf{x}_0)$ is the pseudo Green's function satisfying:

$$D\Delta_{\mathbf{x}} H(\mathbf{x}|\mathbf{x}_0) = -\delta(\mathbf{x} - \mathbf{x}_0) + \frac{1}{V} \quad \text{if} \quad \mathbf{x} \in C^*, \tag{1.67a}$$

$$\partial_{\mathbf{n}} H(\mathbf{x}|\mathbf{x}_0) = 0 \quad \text{if} \quad \mathbf{x} \in \partial C_2, \tag{1.67b}$$

$G_0(r)$ is the free Green's function defined as:

$$DG_0(r) = \begin{cases} \frac{1}{4\pi r}, & \text{in three dimensions,} \\ \frac{1}{2\pi} \log r, & \text{in two dimensions.} \end{cases} \tag{1.68}$$

$H^*(\mathbf{x}|\mathbf{x}_0)$ is the regular part of $H(\mathbf{r}|\mathbf{r}')$ defined as:

$$H^*(\mathbf{x}|\mathbf{x}_0) = H(\mathbf{x}|\mathbf{x}_0) - G_0\left(|\mathbf{x} - \mathbf{x}_0|\right).$$

We observe that (1.66) satisfies (1.65a) and (1.65b) exactly, however the absorbing boundary condition (1.65c) is satisfied only approximately (Condamin *et al.*, 2007, p.021111).
As a result, the MFPT becomes Condamin *et al.* (2007):

$$\langle T(\mathbf{x}_0)\rangle = \frac{V}{D}\left[G_0(a) + H^*(\mathbf{x}_n|\mathbf{x}_n) - H(\mathbf{x}_n|\mathbf{x}_0)\right] + \mathcal{O}\left(\frac{a^l G_0(a)}{D}\right),$$

where l is the distance between the target and the boundary. When the target is near the boundary this formula has deviations of scale a/l in two dimension and a/l^2 in three dimensions from the true MFPT. The boundary correction for $G(\mathbf{x}, \mathbf{x}_0)$ is derived to be:

$$\begin{aligned} G(\mathbf{x}, \mathbf{x}_0) = G_0(a) + H^*(\mathbf{x}_n|\mathbf{x}_n) - H(\mathbf{x}|\mathbf{x}_n) + q(\mathbf{x}_0)\left[H(\mathbf{x}|\mathbf{i}(\mathbf{x}_0)) - H(\mathbf{x}|\mathbf{x}_n)\right. \\ \left. + H^*(\mathbf{i}(\mathbf{x}_0)|\mathbf{x}_n) - H^*(\mathbf{x}_n|\mathbf{x}_n)\right], \end{aligned}$$

where $q(\mathbf{x}_0)$ is the image charge:

$$q(\mathbf{x}_0) = \begin{cases} -\frac{a}{|\mathbf{x}_0 - \mathbf{x}_n|}, & \text{in three dimensions,} \\ -1, & \text{in two dimensions,} \end{cases}$$

placed on $\mathbf{i}(\mathbf{x}_0)$ which is the image point of $\mathbf{x}_0$ reflected off the surface of the target. As a result, the boundary corrected MFPT is given by:

$$\langle T(\mathbf{x}_0)\rangle = \frac{V}{D}\left[G_0(a) - H(\mathbf{x}_n|\mathbf{x}_0) + H^*(\mathbf{x}_n|\mathbf{x}_n) - K(\mathbf{x}_0) - K(\mathbf{s}(\mathbf{x}_0)) + K(\mathbf{s}(\mathbf{x}_n))\right],$$

where

$$K(\mathbf{x}) = q(\mathbf{x})\left[H^*(\mathbf{i}(\mathbf{x})|\mathbf{x}_n) - H^*(\mathbf{x}_n|\mathbf{x}_n)\right],$$

and $\mathbf{s}(\mathbf{x})$ is the image point of $\mathbf{x}$ reflected off the surface of the domain C. Condamin *et al.* (2007) also calculated the n-th moments of the FPT in three dimensional case:

$$\langle T^n(\mathbf{x}_0)\rangle = \frac{n\,!V^n}{D^n}\left\{\left[G_0(a)+H^*(\mathbf{x}_n|\mathbf{x}_n)-H(\mathbf{x}_n|\mathbf{x}_0)\right]\left[G_0(a)+H^*(\mathbf{x}_n|\mathbf{x}_n)-\bar{H}\right]^{n-1} + \mathcal{O}\left(nV^{-\frac{2}{3}}a^{2-n}\right)\right\}, \tag{1.69}$$

where

$$\bar{H} = \frac{1}{V}\int_C H\left(\mathbf{x}_0|\mathbf{x}\right)\,\mathrm{d}\mathbf{x}_0.$$

We define $p(t)$ be the probability density function of the absorption time $T(\mathbf{x}_0)$ which is deduced from (1.69) by ignoring the $\mathcal{O}\left(nV^{-\frac{2}{3}}a^{2-n}\right)$ term:

$$p(t) = \frac{D}{V}\frac{G_0(a)+H^*(\mathbf{x}_n|\mathbf{x}_n)-H(\mathbf{x}_n|\mathbf{x}_0)}{\left(G_0(a)+H^*(\mathbf{x}_n|\mathbf{x}_n)-\bar{H}\right)^2}\exp\left(\frac{-Dt}{V\left[G_0(a)+H^*(\mathbf{x}_n|\mathbf{x}_n)-\bar{H}\right]}\right) + \frac{H(\mathbf{x}_n|\mathbf{x}_0)-\bar{H}}{G_0(a)+H^*(\mathbf{x}_n|\mathbf{x}_n)-\bar{H}}\delta(t),$$

In order to prove the above statement we notice that the exponential distribution:

$$f(x;\lambda) = \lambda\exp(-\lambda x), \quad x \geq 0,$$

has moments

$$\mu_n = \frac{n!}{\lambda^n},$$

If we let $\lambda = \frac{D}{V\left[G_0(a)+H^*(\mathbf{x}_n|\mathbf{x}_n)-\bar{H}\right]}$ then $\frac{G_0(a)+H^*(\mathbf{x}_n|\mathbf{x}_n)-H(\mathbf{x}_n|\mathbf{x}_0)}{G_0(a)+H^*(\mathbf{x}_n|\mathbf{x}_n)-\bar{H}}f(t;\lambda)$ will have the moments (1.69) but this is not longer a probability density function. As a result, we need to add the correction term:

$$\frac{H(\mathbf{x}_n|\mathbf{x}_0)-\bar{H}}{G_0(a)+H^*(\mathbf{x}_n|\mathbf{x}_n)-\bar{H}}\delta(t),$$

and, as a result, we have

$$\int_0^{+\infty} f(t;\lambda)\,\mathrm{d}t = 1.$$

We notice that he correction term does not add to the moments since:

$$\int_0^{+\infty} x^n\delta(x)\,\mathrm{d}x = 0.$$

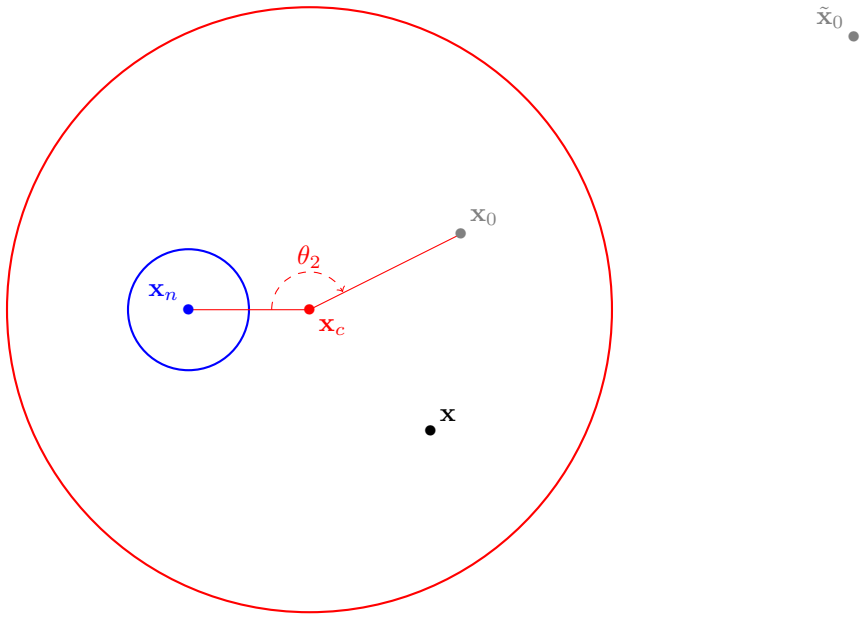

Figure 1.11: Plot of eccentric annular region where $\mathbf{x}_n$ is the centre of the interior boundary, $\mathbf{x}_0$ is the starting position of the Brownian particle, $\tilde{\mathbf{x}}_0$ is the image point of $\mathbf{x}_0$ such that $\mathbf{x}_0 \cdot \tilde{\mathbf{x}}_0 = 1$, and $\mathbf{x}_c$ is the centre of the exterior boundary. Here, θ_2 is the angle formed by $\mathbf{x}_n$ and $\mathbf{x}_0$. The point $\mathbf{x}$ represents the point at which the Green's function is evaluated.

Taking the limit $a \to 0$ and keeping $\mathbf{x}_0$ fixed then $H(\mathbf{x}_n|\mathbf{x}_n)$ is constant and $1/G_0(a)$ tends to zero. As a result, the probability density becomes exponential:

$$p(t) = \frac{4\pi aD}{V} \exp\left(-\frac{4\pi aDt}{V}\right),$$

where we have used (1.68) for the three dimensional case. However, in the same limit when R/a is held fixed then $H(\mathbf{x}_0|\mathbf{x}_n)$ can be approximated by $G_0(R)$ and the probability density becomes:

$$p(t) = \frac{4\pi Da}{V}\left(1 - \frac{a}{R}\right) \exp\left(-\frac{4\pi aDt}{V}\right) + \frac{a}{R}\delta(t),$$

where $\mathrm{R} = |\mathbf{x}_n - \mathbf{x}_0|$.

1.7.2 Two dimensional eccentric annular region

We are interested in particles diffusing in an eccentric annular region C as shown in Figure 1.11. We will use the Green's function method and the formula derived by Condamin *et al.* (2007) to obtain the mean time for a random walk to reach the absorbing target while starting at $\mathbf{x}_0$. Let $\mathbf{x}, \mathbf{x}_0, \mathbf{x}_n \in \mathbb{R}^2$, then the function $G_2^{(2)}(\mathbf{x}_0, \mathbf{x})$ we are looking for satisfies the following:

$$D\Delta_{\mathbf{z}} G_2^{(2)}(\mathbf{x}_0, \mathbf{x}) = -\delta(\mathbf{x} - \mathbf{x}_0) \quad \text{if} \quad \mathbf{x} \in C, \tag{1.70a}$$

$$G_2^{(2)}(\mathbf{x}_0, \mathbf{x}) = 0 \quad \text{if} \quad \mathbf{x} \in \partial C_1, \tag{1.70b}$$

$$\partial_{\mathbf{n}} G_2^{(2)}(\mathbf{x}_0, \mathbf{x}) = 0 \quad \text{if} \quad \mathbf{x} \in \partial C_2, \tag{1.70c}$$

where $\partial_{\mathbf{n}}$ is the normal derivative, ∂C_1 is the absorbing interior boundary centred at $\mathbf{x}_n$, ∂C_2 is the reflecting outer boundary (as shown in Figure 1.11) and $\mathbf{x}_0 \in C$ is the initial position of the point particle. $G_2^{(2)}(\mathbf{x}_0, \mathbf{x})$ is the occupation density of the time a particle spends at $\mathbf{x}$ given that it started at $\mathbf{x}_0$ and is diffusing in an annular region with reflecting outer boundary and absorbing interior boundary centred at $\mathbf{x}_n$.
In order to find $G_2^{(2)}(\mathbf{x}_0, \mathbf{x})$ we will need the pseudo-Green's function $H_2^{(2)}(\mathbf{x}|\mathbf{x}_0)$.

1.7.2.1 The pseudo-Green's function for a circular domain

The following function is known as a pseudo-Green function(Condamin *et al.*, 2007, p.021111-13):

$$H_2^{(2)}(\mathbf{x}|\mathbf{x}_0) = \frac{1}{2\pi D}\left(\log\frac{1}{x_0} + \log\frac{1}{\mathrm{R}\tilde{\mathrm{R}}} + \frac{x^2 + x_0^2}{2}\right), \tag{1.71}$$

and satisfies the following equations:

$$D\Delta H_2^{(2)}(\mathbf{x}|\mathbf{x}_0) = -\delta(\mathbf{x} - \mathbf{x}_0) + \frac{1}{\pi} \quad \text{if} \quad \mathbf{x} \in C^*,$$

$$\partial_{\mathbf{n}} H_2^{(2)}(\mathbf{x}, \mathbf{x}_0) = 0 \quad \text{if} \quad \mathbf{x} \in \partial C_2,$$

where $x = |\mathbf{x}|$, $x_0 = |\mathbf{x}_0|$, $\mathrm{R} = |\mathbf{x} - \mathbf{x}_0|$, $\tilde{\mathrm{R}} = |\mathbf{x} - \tilde{\mathbf{x}}_0|$ and $\tilde{\mathbf{x}}_0$ is defined such that $\mathbf{x}_0 \cdot \tilde{\mathbf{x}}_0 = 1$ where $\cdot$ is the scalar product of the position vectors of $\mathbf{x}_0$ and $\tilde{\mathbf{x}}_0$. $H_2^{(2)}$ is called the Neumann Green's function and is not unique, as it is defined only

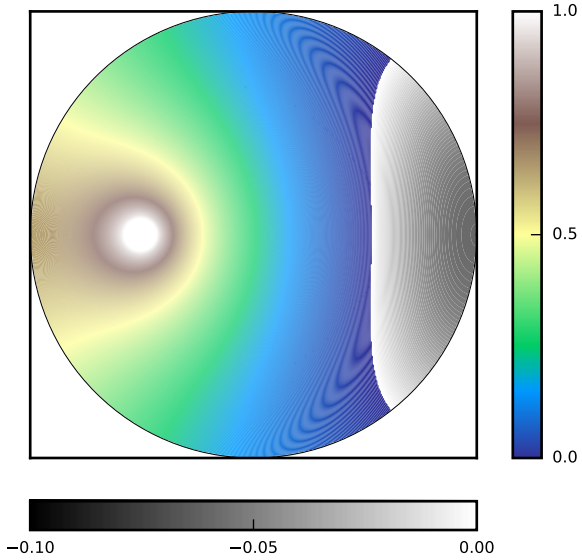

Figure 1.12: Plot of $H_2^{(2)}(\mathbf{x}|\mathbf{x}_0)$ from (1.71) with $\mathbf{x}_0 = (-0.5, 0)$.

up to an additive constant. We plot $H_2^{(2)}(\mathbf{x}|\mathbf{x}_0)$ in Figure 1.12 and we observe that it can take negative values.
It is helpful to define the regular part $H_{2*}^{(2)}(\mathbf{x}|\mathbf{x}_0)$ of $H_2^{(2)}(\mathbf{x}|\mathbf{x}_0)$ as:

$$H_2^{(2)}(\mathbf{x}|\mathbf{x}_0) = H_{2*}^{(2)}(\mathbf{x}|\mathbf{x}_0) + \frac{1}{2\pi D}\log\frac{1}{\mathrm{R}},$$

because $H_{2*}^{(2)}(\mathbf{x}|\mathbf{x}) \neq \infty$ and:

$$H_{2*}^{(2)}(\mathbf{x}|\mathbf{x}) = \frac{1}{2\pi D}\left(\log\frac{1}{1-x^2} + x^2\right).$$

Furthermore, we also notice the following property of $H_2^{(2)}$:

$$\int_{C^*} H_2^{(2)}(\mathbf{x}_0|\mathbf{x})\,\mathrm{d}\mathbf{x} = \frac{3}{8D} \quad \forall \mathbf{x}_0 \in C^*, \tag{1.72}$$

which is proved in Appendix A.1 and will be used in the next section to calculate the mean time.

1.7.2.2 Mean time to capture in two dimensional domain

We have defined $H_2^{(2)}(\mathbf{x}|\mathbf{x}_0)$ in the previous section in order to obtain the approximation of the desired Green's function for (1.70) derived by (Condamin *et al.*,

2007, p.021111-8):

$$G_2^{(2)}(\mathbf{x}_0,\mathbf{x}) \approx H_2^{(2)}(\mathbf{x}_0|\mathbf{x}) - H_2^{(2)}(\mathbf{x}_n|\mathbf{x}) + \frac{1}{2D\pi}\log\frac{1}{a} + H_{2*}^{(2)}(\mathbf{x}_n|\mathbf{x}_n) - H_2^{(2)}(\mathbf{x}_0|\mathbf{x}_n), \tag{1.73}$$

and will be used to calculate the mean of the following time to absorption:

$$t_2^{(2)}(\mathbf{x}_0) = \text{time for a particle starting at } \mathbf{x}_0 \text{ to hit } \partial C_1,$$

where $|\mathbf{y}| \leq 1$.
As a result we have:

$$\begin{aligned}
\mathbb{E}\left[t_2^{(2)}(\mathbf{x}_0)\right] &= \int_C G_2^{(2)}(\mathbf{x}_0,\mathbf{x})\,\mathrm{d}\mathbf{x} \\
&\approx \int_{C^*} G_2^{(2)}(\mathbf{x}_0,\mathbf{x})\,\mathrm{d}\mathbf{x} \\
&\approx \pi\left(\frac{1}{2\pi D}\log\frac{b}{a} + H_{2*}^{(2)}(\mathbf{x}_n,\mathbf{x}_n) - H_2^{(2)}(\mathbf{x}_0,\mathbf{x}_n)\right) \\
&= \frac{1}{2D}\left(\log\frac{|\mathbf{x}_0|}{a} + \log\frac{1}{1-|\mathbf{x}_n|^2} - \log\frac{1}{|\mathbf{x}_n-\mathbf{x}_0||\mathbf{x}_n-\tilde{\mathbf{y}}_0|}\right. \\
&\quad \left. + \frac{|\mathbf{x}_n|^2-|\mathbf{x}_0|^2}{2}\right).
\end{aligned} \tag{1.74}$$

where in the third line of the above equation we have used (1.72) and where C^* is the domain C without the absorbing target.
Setting $\mathbf{x}_n = (-c,0)$, where $0 \leq c \leq 1-a$, $\mathbf{x}_0 = (-\cos\theta_2, \sin\theta_2) \in \partial C_2$ in (1.74) and θ_2 is the angle between $\mathbf{x}_n$ and $\mathbf{x}_0$ as shown in Figure 1.11, we obtain $\mathbb{E}\left[t_2^{(2)}(\mathbf{x}_0)\right] = T_2^{(2)}(\theta_2,a,c)$:

$$\frac{2D}{R^2}T_2^{(2)}(\theta_2,a,c) = \log\frac{1}{a} + \log\frac{1}{1-c^2} - \log\frac{1}{(\cos\theta_2-c)^2+\sin^2\theta_2} + \frac{c^2-1}{2}. \tag{1.75}$$

This is plotted in Figure 1.13 as a function of θ_2, for $c = 0.45$ and $a = 0.1$, and compared with simulated data and the concentric case from Section 1.2.2 in rescaled coordinates.

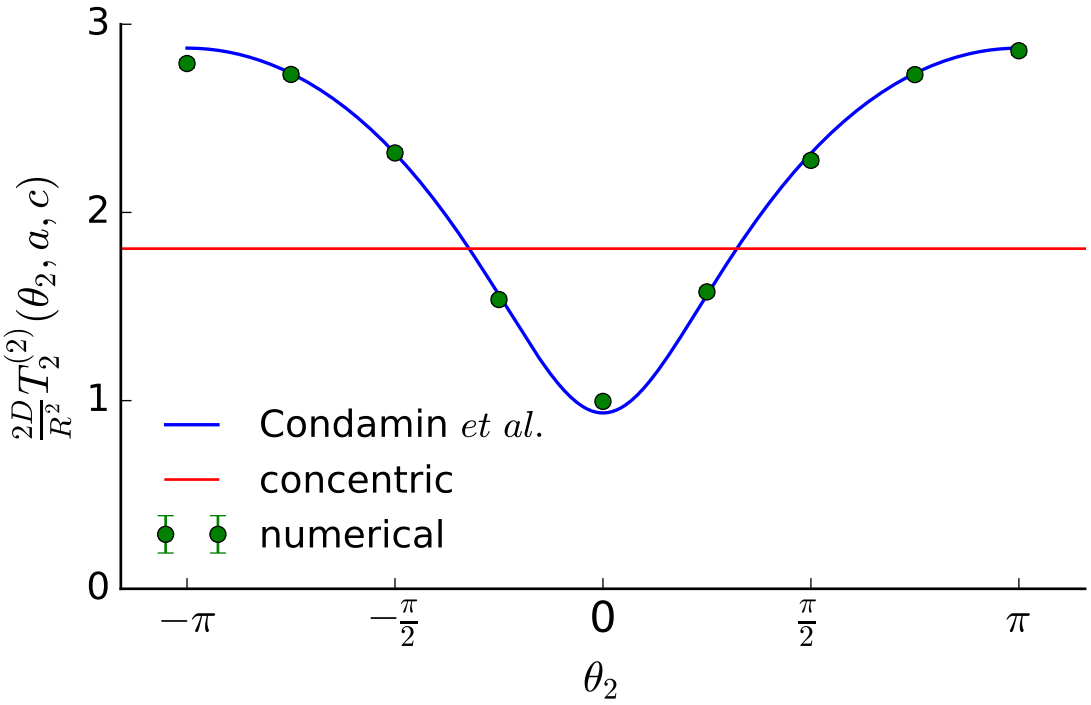

Figure 1.13: Plot of $T_2^{(2)}(\theta_2, a, c)$ comparing the numerical simulation with the analytic result obtained in (1.75) as a function of θ_2. Here we have chosen the following parameter values: $a = 0.1$ and $c = 0.45$.

1.7.2.3 Mean time averaged over the reflecting surface in two dimensions

We are interested in the mean time averaged over the reflecting boundary defined in the following way:

$$\bar{T}_2^{(2)}(a, c) = A \int_0^{2\pi} T_2^{(2)}(\theta_2, a, c)\, \mathrm{d}\theta_2, \tag{1.76}$$

where $A = 1/2\pi$ is the normalisation constant. If $\mathbf{x}_0 = (-\cos\theta_2, \sin\theta_2) \in \partial C_2$ we observe that $\mathbf{x}_0 = \tilde{\mathbf{x}}_0$ and using the following identity Barton (1989):

$$\log \frac{1}{|\mathbf{x}_n - \tilde{\mathbf{x}}_0|} = \log \frac{1}{|\mathbf{x}_n - \mathbf{x}_0|} = \sum_{m=1}^{+\infty} \frac{\cos(m\theta_2)}{m} c^m,$$

where $\mathbf{x}_n = (-c, 0)$ we derive that:

$$\begin{aligned}
&\int_0^{2\pi} \log \frac{1}{(\cos\theta_2 - c)^2 + \sin^2\theta_2}\, \mathrm{d}\theta_2 = \int_0^{2\pi} \log \frac{1}{|\mathbf{x}_n - \mathbf{x}_0||\mathbf{x}_n - \tilde{\mathbf{x}}_0|}\, \mathrm{d}\theta_2 \\
&= \int_0^{2\pi} \log\left(\frac{1}{|\mathbf{x}_n - \mathbf{x}_0|}\right) \mathrm{d}\theta_2 + \int_0^{2\pi} \log\left(\frac{1}{|\mathbf{x}_n - \tilde{\mathbf{x}}_0|}\right) \mathrm{d}\theta_2 \\
&= 2\int_0^{2\pi} \sum_{m=1}^{+\infty} \frac{\cos(m\theta_2)}{m} c^m\, \mathrm{d}\theta_2 = 0. \qquad (1.77)
\end{aligned}$$

As a result, using (1.77) and (1.75) in (1.76) we obtain the following:

$$\frac{2D}{R^2}\bar{T}_2^{(2)}(a, c) = \log\frac{1}{a} + \log\left(\frac{1}{1-c^2}\right) + \frac{c^2-1}{2}, \qquad (1.78)$$

which we plot in Figure 1.14 where we compare with numerical simulations.

1.7.3 Three dimensional eccentric annular region

We now turn to the case when our domain C is a three dimensional annular region bounded by non-concentric spheres. Analogous to Section 1.7.2 we want to find a Green's function $G_2^{(3)}(\mathbf{x}_0, \mathbf{x})$ which satisfies (1.70) and for that we need the pseudo-Green's function for a spherical domain.

1.7.3.1 The pseudo-Green's function for a spherical domain

The following function is known as a pseudo-Green function(Condamin *et al.*, 2007, p.021111-13):

$$H_2^{(3)}(\mathbf{x}|\mathbf{x}_0) = \frac{1}{4\pi D}\left(\frac{1}{\mathrm{R}} + \frac{1}{y\tilde{\mathrm{R}}} - \log\left(y\tilde{\mathrm{R}} + 1 - zy\mu\right) + \frac{z^2+y^2}{2}\right),$$

and satisfies the following equations:

$$\begin{aligned}
&D\Delta H_2^{(3)}(\mathbf{x}|\mathbf{x}_0) = -\delta(\mathbf{x} - \mathbf{x}_0) + \frac{3}{4\pi} \quad \text{if} \quad \mathbf{x} \in C^*, \\
&\partial_{\mathbf{n}} H_2^{(3)}(\mathbf{x}|\mathbf{x}_0) = 0 \quad \text{if} \quad \mathbf{x} \in \partial C_2,
\end{aligned}$$

where C^* is a sphere of radius 1, ∂C_2 is the reflecting outer boundary, $\mathbf{x}_0$ is the initial condition of the particle, $x = |\mathbf{x}|$, $x_0 = |\mathbf{x}_0|$, $\mathrm{R} = |\mathbf{x} - \mathbf{x}_0|$, $\tilde{\mathrm{R}} = |\mathbf{x} - \tilde{\mathbf{x}}_0|$ and

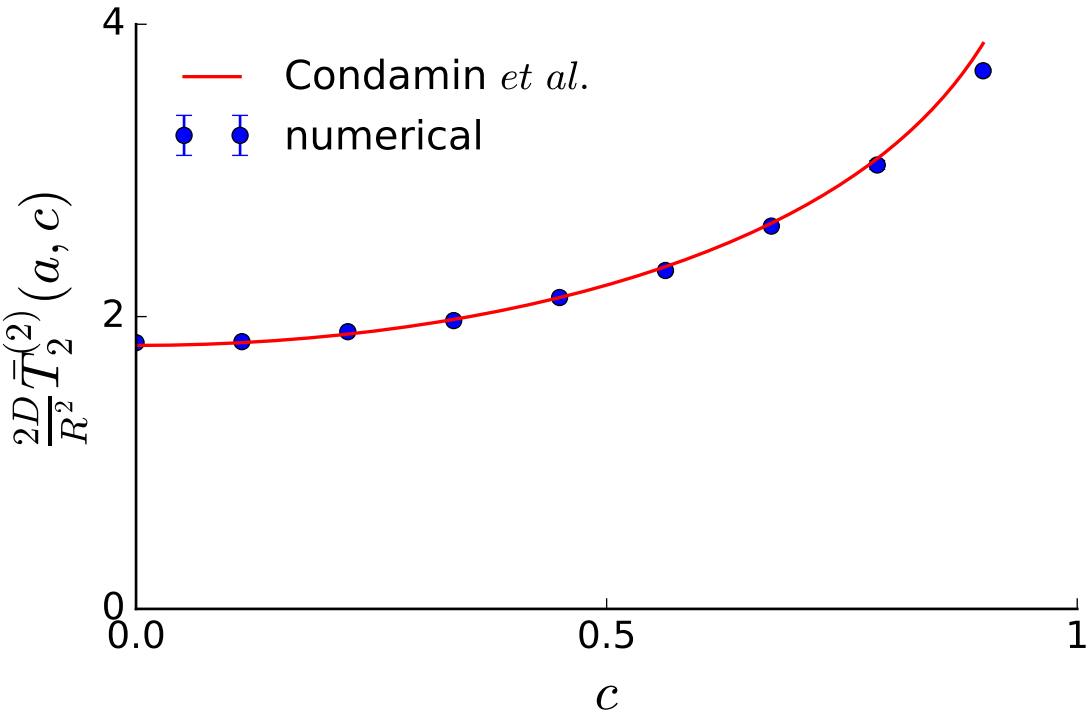

Figure 1.14: Plot of $\bar{T}_2^{(2)}(a,c)$ as a function of the nuclear displacement c. The red line is the approximation obtained in (1.78) and the blue dots are numerical simulations. Here we have chosen the following parameter values: $a = 0.1$.

$\tilde{\mathbf{x}}_0$ is defined such that $\mathbf{x}_0 \cdot \tilde{\mathbf{x}}_0 = 1$. Analogous to the two dimensional case, the Neumann Green's function $H^{(3)}$ is defined only up to an additive constant (for a derivation of $H_2^{(3)}$ see (Cheviakov & Ward, 2011, p.1408)).
It is helpful to define the regular part $H_{2*}^{(3)}(\mathbf{x}|\mathbf{x}_0)$ of $H_2^{(3)}(\mathbf{x}|\mathbf{x}_0)$ as:

$$H_2^{(3)}(\mathbf{x}|\mathbf{x}_0) = H_{2*}^{(3)}(\mathbf{x}|\mathbf{x}_0) + \frac{1}{4\pi D\mathrm{R}},$$

because $H_{2*}^{(3)}(\mathbf{x}|\mathbf{x}) \neq \infty$:

$$H_{2*}^{(3)}(\mathbf{x}|\mathbf{x}) = \frac{1}{4\pi D}\left(\frac{1}{1-x^2} + \log\frac{1}{2(1-x^2)} + x^2\right),$$

Furthermore, we also notice the following property of $H_2^{(3)}(\mathbf{x}|\mathbf{x}_0)$:

$$\int_{C^*} H_2^{(3)}(\mathbf{x}_0|\mathbf{x})\,\mathrm{d}\mathbf{x} = \frac{56}{60D} - \frac{1}{3D}\log 2, \quad \forall \mathbf{x} \in C^*, \tag{1.79}$$

which is proved in Appendix A.2 and we will use next to calculate the mean time.

1.7.3.2 Mean time to capture in three dimensions

We have defined $H_2^{(3)}(\mathbf{x}|\mathbf{x}_0)$ in the previous section in order to obtain the Condamin *et al.* (2007) Green's function approximation for (1.70):

$$G_2^{(3)}(\mathbf{x}_0,\mathbf{x}) \approx H_2^{(3)}(\mathbf{x}_0,\mathbf{x}) - H_2^{(3)}(\mathbf{x}_n,\mathbf{x}) + \frac{1}{4D\pi a} + H_{2*}^{(3)}(\mathbf{x}_n,\mathbf{x}_n) - H_2^{(3)}(\mathbf{x}_0,\mathbf{x}_n),$$

and will be used to calculate the mean of the following time to absorption:

$$t_2^{(3)}(\mathbf{x}_0) = \text{time for a particle starting at } \mathbf{x}_0 \text{ to hit } \partial C_2,$$

where $|\mathbf{y}| \leq 1$.

$$\begin{aligned}
\mathbb{E}\left[t_2^{(3)}(\mathbf{x}_0)\right] &= \int_C G_2^{(3)}(\mathbf{x}_0,\mathbf{x})\,\mathrm{d}\mathbf{x} \approx \int_{C^*} G_2^{(3)}(\mathbf{x}_0,\mathbf{x})\,\mathrm{d}\mathbf{z} \\
&\approx \frac{4\pi}{3}\left(\frac{1}{4D\pi a} + H_{2*}^{(3)}(\mathbf{x}_n,\mathbf{x}_n) - H_2^{(3)}(\mathbf{x}_0,\mathbf{x}_n)\right) \\
&= \frac{1}{3D}\left(\frac{1}{a} + \frac{1}{1-|\mathbf{x}_n|^2} + \log\frac{1}{2(1-|\mathbf{x}_n|^2)} - \frac{1}{|\mathbf{x}_n-\mathbf{x}_0|} - \frac{1}{|\mathbf{x}_0||\mathbf{x}_n-\tilde{\mathbf{x}}_0|}\right. \\
&\quad \left. + \log\left(|\mathbf{x}_0||\mathbf{x}_n-\tilde{\mathbf{x}}_0| + 1 - |\mathbf{x}_n||\mathbf{x}_0|\cos\theta_2\right) - \frac{|\mathbf{x}_n|^2-|\mathbf{x}_0|^2}{2}\right). \qquad (1.80)
\end{aligned}$$

where in the third line of the above equation we have used (1.79). Setting $\mathbf{x}_n = (0,0,-c)$, $\mathbf{x}_0 = (0,\sin\theta_2,-\cos\theta_2)$ in (1.80), where θ_2 is the angle between $\mathbf{x}_n$ and $\mathbf{x}_0$, we obtain $\mathbb{E}\left[t_2^{(3)}(\mathbf{x}_0)\right] = T_2^{(3)}(\theta_2,a,c)$:

$$\begin{aligned}
\frac{2D}{R^2}T_2^{(3)}(\theta_2,a,c) \approx \frac{2}{3a}\Bigg[1 + \frac{a}{1-c^2} + a\log\frac{1}{2(1-c^2)} - \frac{2a}{\sqrt{(\cos\theta_2-c)^2+\sin^2\theta_2}} \\
- a\log\left(\frac{1}{1-c\cos\theta_2+\sqrt{(\cos\theta_2-c)^2+\sin^2\theta_2}}\right) + a\frac{c^2-1}{2}\Bigg], \qquad (1.81)
\end{aligned}$$

which we plot in Figure 1.15 and compare with numerical simulations.

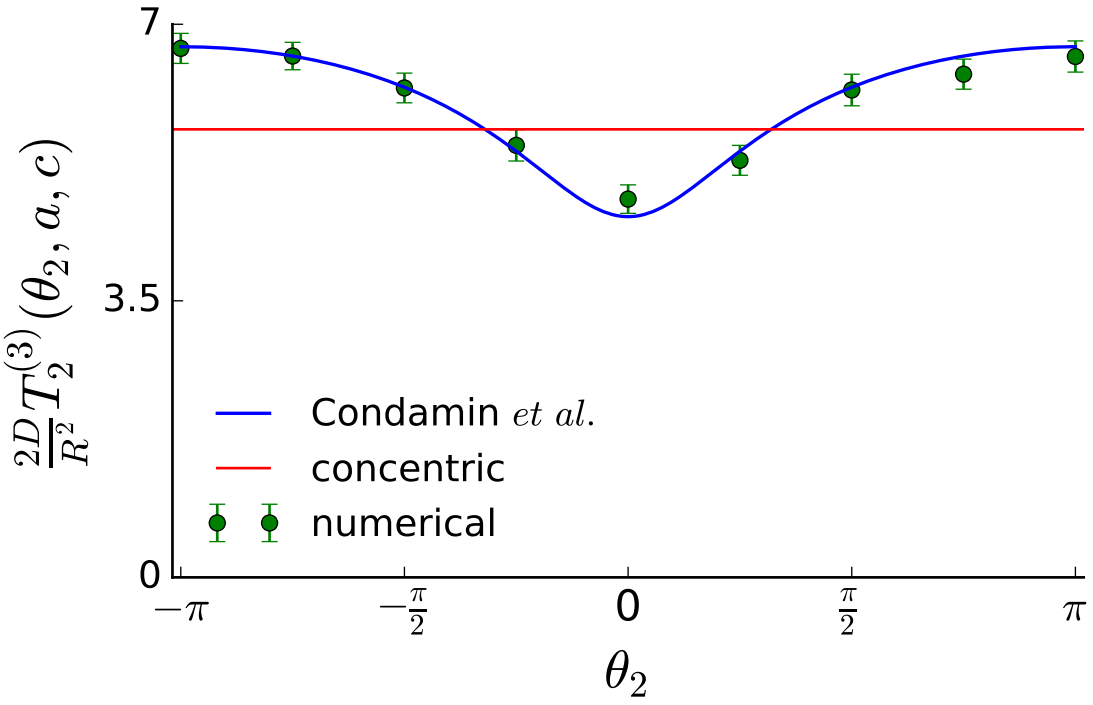

Figure 1.15: Plot of $T_2^{(3)}(\theta_2, a, c)$ comparing the numerical simulation obtained analytic result obtained in (1.81) as a function of θ_2. Here we have chosen the following parameter values: $a = 0.1$ and $c = 0.45$.

1.7.3.3 Mean time averaged over the reflecting surface in three dimensions

We are interested in the mean time averaged over the reflecting boundary defined in the following way:

$$\bar{T}_2^{(3)}(a, c) = A \int_0^{\pi} T_2^{(3)}(\theta_2, a, c) \sin\theta_2 \, \mathrm{d}\theta_2, \tag{1.82}$$

where $A = 1/4\pi$ is the normalisation constant. If $\mathbf{x}_0 = (0, \sin\theta_2, -\cos\theta_2)$ we observe that $\mathbf{x}_0 = \tilde{\mathbf{x}}_0$ and we know from Barton (1989) that:

$$\frac{1}{|\mathbf{x}_n - \tilde{\mathbf{x}}_0|} = \frac{1}{|\mathbf{x}_n - \mathbf{x}_0|} = \sum_{l=0}^{+\infty} P_l(\mu) c^l,$$

where $\mathbf{x}_n = (0, 0, -c)$, $\mu = \cos\theta_2$ and $P_n(x)$ is a Legendre polynomial of degree n, from which we deduce that:

$$\int_0^\pi \frac{\sin\theta_2}{|\mathbf{x}_n - \tilde{\mathbf{x}}_0|}\,\mathrm{d}\theta_2 = \int_0^\pi \frac{\sin\theta_2}{|\mathbf{x}_n - \mathbf{x}_0|}\,\mathrm{d}\theta_2 = \sum_{l=0}^{+\infty} \int_0^\pi P_l(\cos\theta_2)\sin\theta_2\,\mathrm{d}\theta_2 c^l = 2. \tag{1.83}$$

Furthermore, we know that Barton (1989):

$$\log\left(\frac{2}{|\mathbf{x}_0||\mathbf{x}_n - \tilde{\mathbf{x}}_0| + 1 - |\mathbf{x}_n||\mathbf{x}_0|\cos\theta_2}\right) = \sum_{l=1}^{+\infty} P_l(\mu)\frac{1}{l}\xi^l,$$

where

$$\xi = |\mathbf{x}_n||\mathbf{x}_0|,$$

from which we obtain that:

$$\int_0^\pi \left(\frac{2}{|\mathbf{x}_0||\mathbf{x}_n - \tilde{\mathbf{x}}_0| + 1 - |\mathbf{x}_n||\mathbf{x}_0|\cos\theta_2}\right)\sin\theta_2\,\mathrm{d}\theta_2 = \sum_{l=1}^{+\infty}\int_0^\pi P_l(\mu)\sin\theta_2\,\mathrm{d}\theta_2\frac{1}{l}\xi^l = 0,$$

and, consequently, that:

$$\int_0^\pi \log\left(|\mathbf{x}_0||\mathbf{x}_n - \tilde{\mathbf{x}}_0| + 1 - |\mathbf{x}_n||\mathbf{x}_0|\cos\theta_2\right)\sin\theta_2\,\mathrm{d}\theta_2 = 2\log 2. \tag{1.84}$$

As a result, using (1.83), (1.84) and (1.81) in (1.82) we have:

$$\frac{2D}{R^2}\bar{T}_2^{(3)}(a, c) \approx \frac{2}{3a}\left[1 + \frac{a}{1-c^2} + a\log\frac{1}{1-c^2} + a\frac{c^2-5}{2}\right], \tag{1.85}$$

which we plot in Figure 1.16 where we compare with numerical simulations.

1.8 Hitting density on the cellular surface

What is the probability of a Brownian particle starting at $\mathbf{x}_0$ to be absorbed at point $\mathbf{x}$ on the outer surface? In order to answer this question, we define θ_2 as the angle between $\mathbf{x}_0$ and $\mathbf{x}$ and we use the fact that the hitting density $\varepsilon_0^{(2)}(\theta_2)$ is the same as the electric field at the impact point $\mathbf{x}$ when at $\mathbf{x}_0$ there is point charge of magnitude $q = 1/(\Omega_n D)$, where n is the dimension and Ω_n is the area

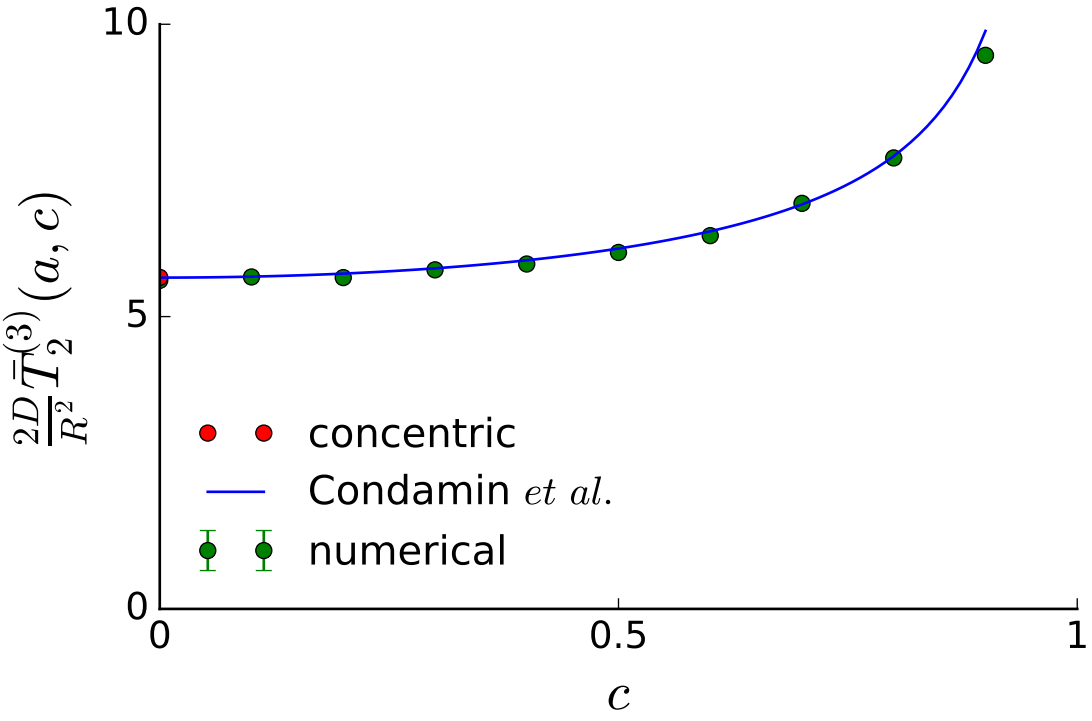

Figure 1.16: Plot of $\bar{T}_2^{(3)}(a,c)$ as a function of the nuclear displacement c. The blue line is the approximation obtained in (1.85), the green dots are numerical simulations and the red dot is the concentric case. Here we have chosen the following parameter values: $a = 0.1$.

or length of the cell (Redner, 2001, p.214). The electrostatic potential in two dimensions, with no internal target, at $\mathbf{x}$ is (Redner, 2001, p.215):

$$H_1^{(2)}(\mathbf{x}|\mathbf{x}_0) = \frac{q}{2}\log\left(\frac{x_0^2x^2 + 1 - 2xx_0\cos\theta_2}{x^2 + x_0^2 - 2xx_0\cos\theta_2}\right).$$

where $x = |\mathbf{x}|$ and $x_0 = |\mathbf{x}_0|$. Taking the x-derivative of $H_1^{(2)}(\mathbf{x}|\mathbf{x}_0)$:

$$\frac{\partial H_1^{(2)}}{\partial x}(x = 1|x_0 = c) = \frac{1}{4\pi D}\frac{2(c^4 - 1 - c^3\cos\theta_2) + 2c(2 - c^2)\cos\theta_2}{(c^2 + 1 - 2c\cos\theta_2)^2},$$

and multiplying by $-D$ we obtain the hitting probability:

$$\varepsilon_0^{(2)}(\theta_2) = \frac{1}{4\pi}\frac{1 - c^2}{1 - 2c\cos\theta_2 + c^2}, \tag{1.86}$$

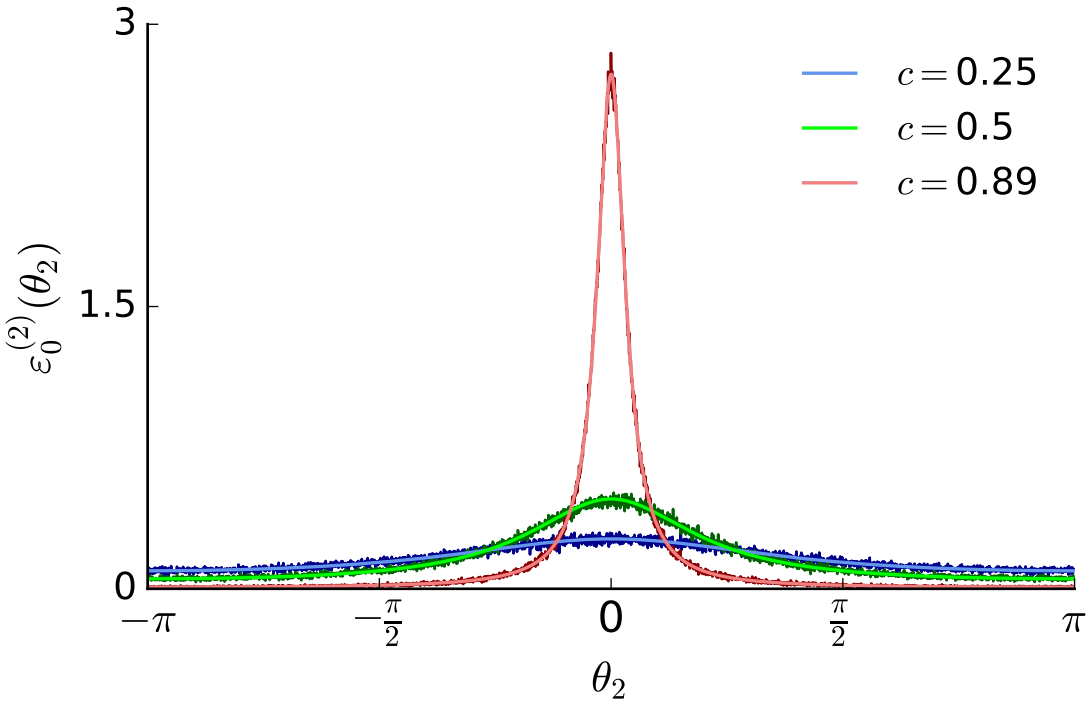

Figure 1.17: Plot of $\varepsilon_0^{(2)}(\theta_2)$ comparing the numerical simulation with the analytic result (thick lines) obtained in (1.86) as a function of θ_2 for values of $c = 0.25, 0.5$ and 0.89. The lighter colours represent the analytic result and the darker colours represent the numerical simulations. For the numerical simulations we have used G.7.1.1 and this plot has been obtained using G.7.1.2. For this figure we have used the following parameters: $a = 0.1$.

which we compare with in Figure 1.17 with simulated data.
We observe from Figure 1.17 that as the distance between the initial position and the absorbing boundary decreases the hitting density becomes centered at the angle of smallest distance. This is because the random walks are more likely to hit the surface at a point close to the initial position.

1.9 Discussion

In this chapter we have introduced the notion of Brownian motion and the first passage properties of diffusing particles. We begin with the one dimensional random walk model, expanding it to higher dimensions and present Fick's equations which govern the behaviour of random walks.
In Section 1.2 we use the one dimensional random walk model to define the mean time to capture on an absorbing target. Additionally, we calculated the mean time for a Brownian particle diffusing in a circular eccentric annular region to reach the inner boundary or the outer boundary in Section 1.2.2 and 1.2.1, respectively.
In Section 1.4 we define the survival probability of a diffusing particle in a concentric annular region which will be used in Chapter 4 to determine the intracellular distribution of absorbed *Coxiella burnetii* bacteria in a specific experiment.
We review Condamin *et al.* (2007) in Section 1.7 and construct their approximation for the Green's function for an eccentric annular region in two and three dimensions. From the Green's function we derive the mean first passage time and the mean first passage time averaged over the starting surface in Sections 1.7.2.2 and 1.7.2.3 for the two dimensional case, and Sections 1.7.3.2 and 1.7.3.3 for the three dimensional case, respectively. We will compute the analytic Green's function for circular and spherical eccentric annular regions in chapter 2 and 3, respectively, and compare with the results of Condamin *et al.* (2007).
We have validated our results by using numerical simulations displayed in Appendix G. In order to maintain the size of this thesis in reasonable bounds only certain representative Python scripts, which we have used to generate the figures, are shown in the remainder of this work.

Chapter 2

Diffusive transport in circular domains

2.1 Introduction

We consider diffusion of a particle, with diffusivity D, in a circular domain of radius R which contains an interior compartment of radius R_n and has displacement r_c from the centre of the domain (see Figure 2.1). If transport is simply diffusive, not accelerated by directed mechanisms or localised pathways, the basic timescale is R^2/D, where R is the radius of the domain and D is the diffusivity Amitai & Holcman (2017); Barkai *et al.* (2012); Bénichou *et al.* (2010); Bressloff & Newby (2013); Coombs *et al.* (2002, 2009); Wosniack *et al.* (2015). The mean time to find the internal compartment, thought of as a target within a larger domain, is a function of a and c, where a is the radius of the target, and c its distance from the centre of the domain, divided by R.

Living cells contain many proteins that constantly move about Lagache & Holcman (2008); Lagache *et al.* (2009); Mullineaux *et al.* (2006); cells interact with their surroundings by means of surface receptor molecules that bind ligands, either free or themselves on the surface of other cells. The mechanism by which a cell responds to an event occurring on its surface may involve the transport of molecular complexes from the cellular surface to the nucleus Imada & Leonard (2000); Lillemeier *et al.* (2001), and the transport of synthesised molecules from the nucleus to the cellular surface. With the motivation of cell biology in mind,

we refer to the boundary of the domain as the cellular surface and the interior compartment as the nucleus. We consider transport from a reflecting nuclear surface to an absorbing cellular surface, and the opposite case of diffusion from a reflecting cellular surface to an absorbing nuclear surface.
Using bipolar coordinates, we derive exact Green's functions. Hence, we derive exact expressions for arrival densities and mean arrival times. We also consider the mean arrival time, where the initial position is averaged over the surface of the nucleus or of the cell. The idea is that the point on the surface of a nucleus where a molecule emerges, or the point on the cellular surface where a molecular complex is internalised, is uniformly distributed on the surface of the nucleus or cell. We consider distributions of initial conditions that are (i) uniform on the nuclear surface, (ii) uniform on the cellular surface, or (iii) given by the hitting density of particles diffusing from the nuclear surface to the cellular surface. This hitting density is also obtained from the appropriate Green's function. Numerical simulations are used for comparison.

2.2 Literature review

Many intercellulater and intracellular process are diffusion limited and, as a result, the rates of many types of reactions can be calculated from the diffusion equation with appropriate boundary conditions Katja *et al.* (2019); Lauffenburger & Linderman (1993). Once the corresponding Green's function is calculated, quantities such as mean hitting times are obtained by standard integration, for any initial distribution of particles Prüstel & Meier-Schellersheim (2012, 2013); Prüstel & Tachiya (2013). Similar procedures are followed in discrete space Montroll & Weiss (1965). Approximating animal motion by Brownian motion, or diffusive motion with a directed component, the expected mean time for a predator to locate small patches of prey is a mean hitting time Kurella *et al.* (2015); McKenzie *et al.* (2009). Another context in which diffusion within a confined domain provides a timescale is the encounters, inside lymph nodes, of T cells and antigen-presenting cells Catron *et al.* (2004); Celli *et al.* (2012); Delgado *et al.* (2015); Garside *et al.* (1998); Krummel *et al.* (2016); Textor *et al.* (2014); Zinselmeyer *et al.* (2005).

As shown in Section 1.7 Condamin *et al.* (2007) derived an approximation of the Green's function for an eccentric annular region with an absorbing inner target and reflecting outer boundary. Using the Green's function method and pseudo-Green's functions they derive the first passage properties of diffusion in the eccentric annular region. In Section 1.7.2 we looked at the two dimensional case and the mean time for a Brownian particle to hit the inner circular boundary. The results were extended using pseudo-Green's function by Bénichou & Voituriez (2014); Chevalier *et al.* (2010) to determine the first passage properties of Brownian motion in a domain where the absorbing targets are on an otherwise reflecting surface.

Lindsay *et al.* (2016) derive a hybrid asymptotic-numerical approach to estimate the density of the first passage time of a random walker to multiple small traps located inside a bounded two dimensional domain with a reflecting boundary. They make use of the Laplace transform on the underlying diffusion equation in combination with the method of matched asymptotic expansions to obtain the short time solution. For large times, they used numerical evaluations to complete the derivation.

Grebenkov *et al.* (2017) calculated the MFPT of a Brownian particle, diffusing inside a finite length cylinder, to reach a reactive patch on the surface of an interior concentric cylinder by replacing the mixed boundary condition on the interior cylinder with a inhomogeneous Neumann boundary condition and solving the new problem using a separable solution. Additionally, asymptotic solutions are derived for different parameter scenarios from the results.

Tzou & Kolokolnikov (2015) compute the MFPT of a Brownian particle diffusing inside a two dimensional disk with reflecting boundary and an interior absorbing trap which is rotating at a constant angular velocity.

When the target is an absorbing arc located on an otherwise reflecting boundary, the problem can be classified as a narrow escape problem (NEP) and has been studied extensively Cheviakov *et al.* (2012); Grebenkov *et al.* (2020); Holcman & Schuss (2004, 2014, 2015); Marshall (2016); Pillay *et al.* (2010). When the absorbing arc shrinks to zero the mean time to absorption diverges to infinity and the narrow escape problem becomes a singular perturbation problem and is solved by using asymptotic expansions Schuss *et al.* (2007); Singer *et al.* (2006a,b).

Boundary homogenisation is used to solve problems where an otherwise reflecting boundary has absorbing traps located on it, making use of the fact that non-uniform boundaries affect a relatively small neighbourhood near the surface and, as a result, the memory about the local properties of the boundary declines as a function of distance from the boundary Berezhkovskii *et al.* (2004); Makhnovskii *et al.* (2005).

We represent a cell as a circle of radius R, containing a nucleus (or other intracellular compartment) of radius R_n. The centre of the nucleus is displaced from that of the cell by a distance r_c. Given that we are interested in eccentric annular regions like the one shown in Figure 2.1, the coordinate systems we have been using are not the best suited. Instead, in this section, we replace Cartesian coordinates (x, y) with bipolar coordinates (τ,σ).

2.3 Bipolar coordinates

Bipolar coordinates (τ, σ) are defined in terms of two foci whose separation is $2F$ (Figure 2.2) Heyda (1959); Kurella *et al.* (2015). Curves of constant τ are circles with radius r, centred at $x = \sqrt{r^2 + F^2}$ and $y = 0$, where $\tau = \log(F/r + \sqrt{1 + (F/r)^2})$. Similarly as we did is Section 1.6, we rescale lengths so that the radius of the cell is equal to 1. We shall calculate the Green's functions and mean times using the following dimensionless quantities:

$$a = \frac{R_n}{R}, \qquad c = \frac{r_c}{R} \qquad \text{and} \qquad d = \frac{F}{R}.$$

Note that $0 \leq c \leq 1 - a$, and a^2 is the fraction of the cell occupied by the nucleus. In order that the centres of the two circles of radii 1 and a be displaced by $c = \sqrt{1 + d^2} - \sqrt{a^2 + d^2}$, we must choose:

$$d = \frac{1}{2c}\sqrt{(1 + a^2 - c^2)^2 - 4a^2}. \tag{2.1}$$

Thus, the eccentric annular region C (grey in Figure 2.3) is represented by

$$\tau_2 < \tau < \tau_1 \qquad , \qquad 0 \leq \sigma < 2\pi,$$

where

$$\tau_1 = \log\left(d/a + \sqrt{1 + (d/a)^2}\right) \text{ (nuclear surface)} ,$$

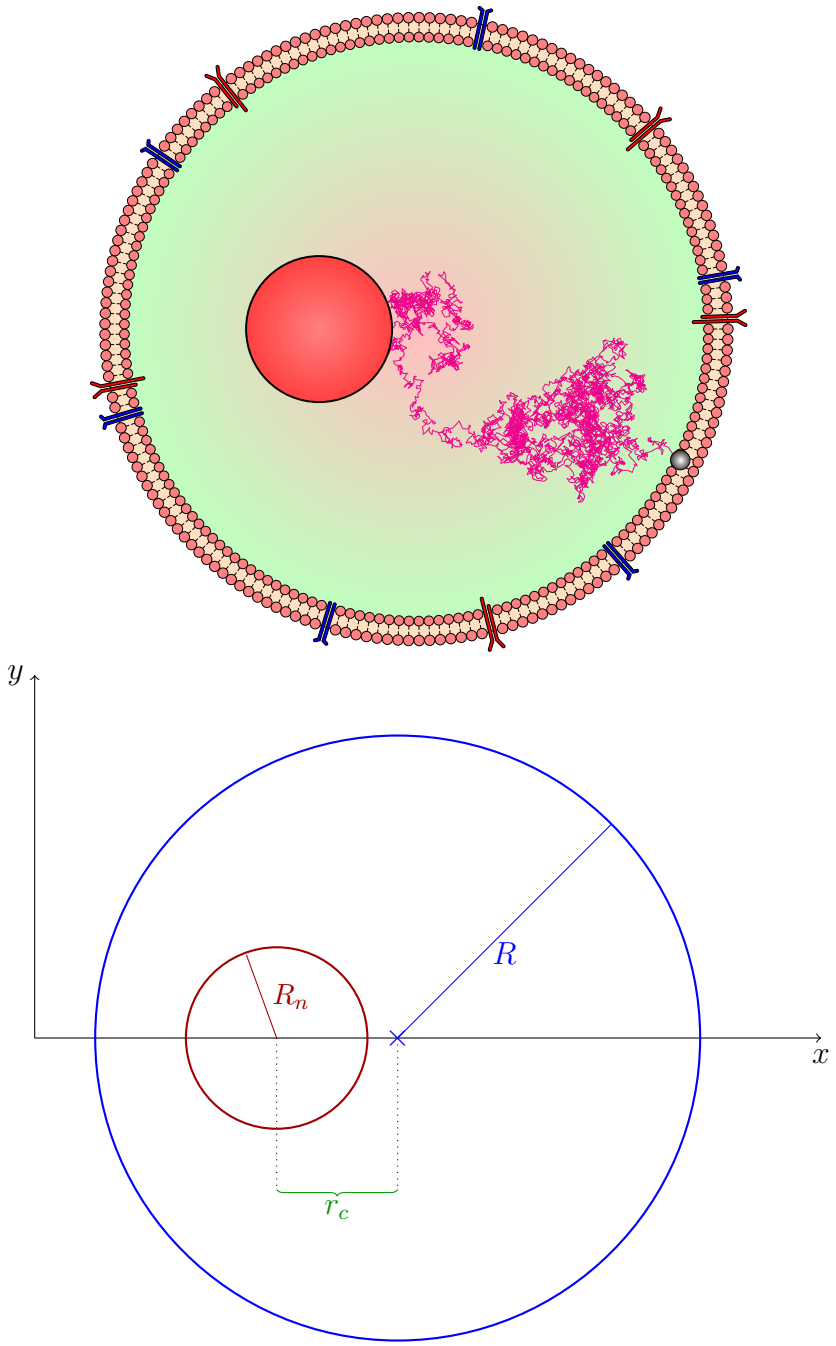

Figure 2.1: Intracellular geometry. We represent a cell as a circle of radius R, containing a nucleus (or other intracellular compartment) of radius R_n. The centre of the nucleus is displaced from that of the cell by a distance r_c.

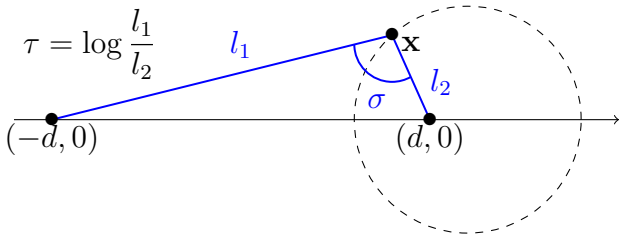

Figure 2.2: Graphical definition of the bipolar coordinates, τ and σ, of the point $\mathbf{x}$.

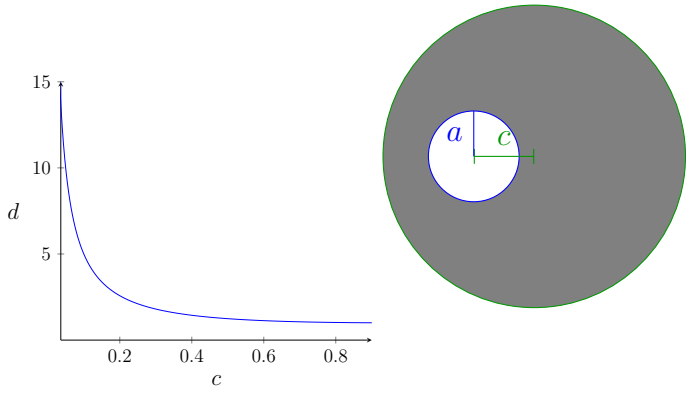

Figure 2.3: Left: the distance d used to define bipolar coordinates, as a function of c with $a = 0.1$. Right: the domain C is shown in grey.

and

$$\tau_2 = \log\left(d + \sqrt{1 + d^2}\right) \text{ (cellular surface).}$$

We denote the nuclear surface (a circle of radius a, blue in Figure 2.3) by ∂C_1 and the cellular surface (a circle of radius 1, green in Figure 2.3) by ∂C_2. We plot in Figure 2.4 a sampling of bipolar coordinates. Heyda (1959); Liemert (2014) calculate the Green's function for an eccentric circular annular domain, where both the inner and outer boundaries are absorbing, by using bipolar coordinates. Kurella *et al.* (2015) utilise bipolar coordinates to solve the Laplace equation for the following system: two circles with Dirichlet boundary conditions embedded in an infinite medium.

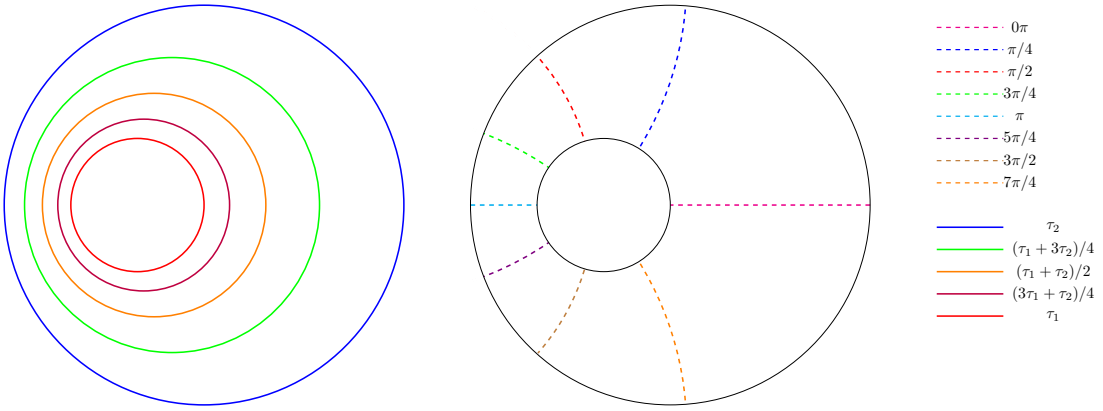

Figure 2.4: Bipolar coordinates τ (left) and σ (right) where τ_1 is the bipolar representation of the nuclear surface and τ_2 is the bipolar representation of the cellular surface.

2.4 Bipolar Green's function

The mean time to reach an absorbing boundary of C, starting from $\mathbf{x}_0 \in C$ can be written as

$$T(\mathbf{x}_0) = R^2 \int_C G(\mathbf{x}_0, \mathbf{x})\, \mathrm{d}\mathbf{x}, \tag{2.2}$$

using the Green's function $G(\mathbf{x}_0, \mathbf{x})$, which may thus be interpreted as an occupation density, satisfying

$$D\Delta_{\mathbf{x}} G(\mathbf{x}_0, \mathbf{x}) = -\delta(\mathbf{x} - \mathbf{x}_0) \qquad \mathbf{x} \in C, \tag{2.3}$$

with suitable boundary conditions. Green's function, $G(\mathbf{x}_0, \mathbf{x})$ can be constructed numerically by dividing the domain into small boxes and recording the mean amount spent in each, by paths starting at $\mathbf{x}_0$. Let (τ, σ) be the bipolar coordinates of $\mathbf{x}$ and (τ_0, σ_0) the bipolar coordinates of $\mathbf{x}_0$. Then $d^2\Delta_x = (\cosh\tau - \cos\sigma)^2 \left(\frac{\partial^2}{\partial\tau^2} + \frac{\partial^2}{\partial\sigma^2}\right)$ El-Saden (1961); Snyder & Goldstein (1965) and we can write:

$$T(\mathbf{x}_0) = R^2 \int_{\tau_2}^{\tau_1} \int_0^{2\pi} \frac{G(\mathbf{x}_0, \mathbf{x}) d^2}{(\cosh\tau - \cos\sigma)^2} \mathrm{d}\sigma \mathrm{d}\tau. \tag{2.4}$$

2.4.1 From nucleus to cellular surface

We begin with the case of diffusion with absorption on the cellular surface. The Green's function, denoted by $G_1^{(2)}(\mathbf{x}_0, \mathbf{x})$, satisfies (2.3), is equal to zero on the

cellular surface and has vanishing normal derivative on the nuclear surface. That is, we impose the following boundary conditions:

$$\begin{aligned} \frac{\partial G_1^{(2)}}{\partial \mathbf{n}_1}(\mathbf{x}_0, \mathbf{x}) = 0, \quad \mathbf{x} \in \partial C_1, \\ G_1^{(2)}(\mathbf{x}_0, \mathbf{x}) = 0, \quad \mathbf{x} \in \partial C_2. \end{aligned} \tag{2.5}$$

where $\mathbf{n}_1$ is the unit normal outward vector to ∂C_1.
We are looking for a solution to (2.3) of the form (Heyda, 1959, p.30):

$$G_1^{(2)}(\tau, \sigma; \tau_0, \sigma_0) = G_s^{(2)}(\tau, \sigma; \tau_0, \sigma_0) + G_r^{(2)}(\tau, \sigma; \tau_0, \sigma_0), \tag{2.6}$$

where $G_r^{(2)}$ is the non-singular component of the Green's function:

$$\begin{aligned} G_r^{(2)}(\tau, \sigma; \tau_0, \sigma_0) = A_0\tau + B_0 + \sum_{n=1}^{+\infty} \big((A_n \cos n\sigma + B_n \sin n\sigma)\mathrm{e}^{-n\tau} \\ + (C_n \cos n\sigma + D_n \sin n\sigma)\mathrm{e}^{n\tau} \big), \end{aligned}$$

and $G_s^{(2)}(\tau, \sigma; \tau_0, \sigma_0)$ is the singular part of $G_1^{(2)}$ (for a derivation of $G_s^{(2)}$ see (Heyda, 1959, p.29–30)):

$$G_s^{(2)}(\tau, \sigma; \tau_0, \sigma_0) = \frac{1}{2D\pi} \left[\tau_m - \log 2d + \sum_{n=1}^{+\infty} \frac{1}{n} H_n(\tau, \sigma; \tau_0, \sigma_0) \right],$$

where $\tau_m = \min(\tau, \tau_0)$ and

$$H_n(\tau, \sigma; \tau_0, \sigma_0) = \mathrm{e}^{-n|\tau - \tau_0|} \cos n(\sigma - \sigma_0) - \mathrm{e}^{-n\tau} \cos n\sigma - \mathrm{e}^{-n\tau_0} \cos n\sigma_0.$$

Given the boundary conditions (2.5) we translate them into bipolar coordinates (for the normal derivative in bipolar coordinates of a function on a circle of constant τ see Appendix B.1) and use (2.6):

$$\begin{aligned} \frac{\partial G_r^{(2)}}{\partial \tau}(\tau, \sigma; \tau_0, \sigma_0)\bigg|_{\tau=\tau_1} = -\frac{\partial G_s^{(2)}}{\partial \tau}(\tau, \sigma; \tau_0, \sigma_0)\bigg|_{\tau=\tau_1}, \\ G_r^{(2)}(\tau_2, \sigma; \tau_0, \sigma_0) = -G_s^{(2)}(\tau_2, \sigma; \tau_0, \sigma_0), \end{aligned}$$

which gives us:

$$A_0 + \sum_{n=1}^{+\infty} \left[-n(A_n \cos n\sigma + B_n \sin n\sigma)\mathrm{e}^{-n\tau_1} + n(C_n \cos n\sigma + D_n \sin n\sigma)\mathrm{e}^{n\tau_1} \right]$$

$$= \frac{1}{2D\pi} \sum_{n=1}^{+\infty} \left(\mathrm{e}^{-n(\tau_1-\tau_0)} \cos n(\sigma-\sigma_0) - \mathrm{e}^{-n\tau_1} \cos n\sigma \right), \tag{2.7}$$

and

$$\begin{aligned} &A_0\tau_2 + B_0 + \sum_{n=1}^{+\infty} \left[(A_n \cos n\sigma + B_n \sin n\sigma)\mathrm{e}^{-n\tau_2} + (C_n \cos n\sigma + D_n \sin n\sigma)\mathrm{e}^{n\tau_2} \right] \\ &= -\frac{1}{2D\pi} \left[\tau_2 - \log 2d + \sum_{n=1}^{+\infty} \frac{1}{n} \left(\mathrm{e}^{-n(\tau_0-\tau_2)} \cos n(\sigma-\sigma_0) \right.\right. \\ &\left.\left. -\mathrm{e}^{-n\tau_2} \cos n\sigma - \mathrm{e}^{-n\tau_0} \cos n\sigma_0 \right) \right]. \end{aligned} \tag{2.8}$$

We multiply both (2.7) and (2.8) by $\cos m\sigma$ and $\sin m\sigma$ and integrate from 0 to 2π with respect to σ to obtain:

$$A_m \mathrm{e}^{-m\tau_1} - C_m \mathrm{e}^{m\tau_1} = -\frac{1}{2D\pi m} \mathrm{e}^{-m(\tau_1-\tau_0)} \cos m\sigma_0 + \frac{1}{2D\pi m} \mathrm{e}^{-m\tau_1}, \tag{2.9a}$$

$$A_m \mathrm{e}^{-m\tau_2} + C_m \mathrm{e}^{m\tau_2} = -\frac{1}{2D\pi m} \mathrm{e}^{-m(\tau_0-\tau_2)} \cos m\sigma_0 + \frac{1}{2D\pi m} \mathrm{e}^{-m\tau_2}, \tag{2.9b}$$

and

$$B_m \mathrm{e}^{-m\tau_1} - D_m \mathrm{e}^{m\tau_1} = -\frac{1}{2D\pi m} \mathrm{e}^{-m(\tau_1-\tau_0)} \sin m\sigma_0, \tag{2.10a}$$

$$B_m \mathrm{e}^{-m\tau_2} + D_m \mathrm{e}^{m\tau_2} = -\frac{1}{2D\pi m} \mathrm{e}^{-m(\tau_0-\tau_2)} \sin m\sigma_0. \tag{2.10b}$$

Solving (2.9) and (2.10) we obtain the coefficients:

$$A_m = -\frac{1}{2D\pi m} \left(\mathrm{e}^{m\tau_2} \cos m\sigma_0 \frac{\cosh m(\tau_1-\tau_0)}{\cosh m(\tau_2-\tau_1)} - 1 \right), \tag{2.11a}$$

$$B_m = -\frac{1}{2D\pi m} \mathrm{e}^{m\tau_2} \sin m\sigma_0 \frac{\cosh m(\tau_1-\tau_0)}{\cosh m(\tau_2-\tau_1)}, \tag{2.11b}$$

$$C_m = -\frac{1}{2D\pi m} \mathrm{e}^{-m\tau_1} \cos m\sigma_0 \frac{\sinh m(\tau_2-\tau_0)}{\cosh m(\tau_2-\tau_1)}, \tag{2.11c}$$

$$D_m = -\frac{1}{2D\pi m} \mathrm{e}^{-m\tau_1} \sin m\sigma_0 \frac{\sinh m(\tau_2-\tau_0)}{\cosh m(\tau_2-\tau_1)}, \tag{2.11d}$$

where $m \in \mathbb{N}$. Integrating (2.7) and (2.8) with respect to σ from 0 to 2π we obtain:

$$2\pi A_0 = 0,$$

$$2D\pi A_0\tau_2 + 2D\pi B_0 = -\left(\tau_2 - \log 2d - \sum_{n=1}^{+\infty} \frac{\mathrm{e}^{-n\tau_0}\cos n\sigma_0}{n}\right),$$

from which we deduce that:

$$A_0 = 0, \tag{2.12a}$$

$$B_0 = -\frac{1}{2D\pi}\left(\tau_2 - \log 2d - \sum_{n=1}^{+\infty} \frac{\mathrm{e}^{-n\tau_0}\cos n\sigma_0}{n}\right). \tag{2.12b}$$

Using (2.11) and (2.12) in (2.6) we obtain the desired Green's function:

$$2D\pi G_1^{(2)}(\tau,\sigma;\tau_0,\sigma_0) = \tau_m - \tau_2 + \sum_{n=1}^{+\infty} \frac{\cos n\,(\sigma-\sigma_0)}{n}\left(\mathrm{e}^{-n|\tau-\tau_0|} - H(\tau,\tau_0;\tau_1,\tau_2)\right),$$

where

$$H(\tau,\tau_0;\tau_1,\tau_2) = \frac{\mathrm{e}^{n(\tau_2-\tau)}\cosh n(\tau_1-\tau_0) + \mathrm{e}^{n(\tau-\tau_1)}\sinh n(\tau_2-\tau_0)}{\cosh n(\tau_2-\tau_1)}.$$

Rearranging the coefficient of $\cos n(\sigma-\sigma_0)$ we notice:

$$\frac{\mathrm{e}^{-n|\tau-\tau_0|} - H(\tau,\tau_0;\tau_1,\tau_2)}{n} = \frac{2\sinh n(\tau_m-\tau_2)\cosh n(\tau_1-\tau_M)}{n\cosh n(\tau_2-\tau_1)},$$

where $\tau_M = \max\{\tau,\tau_0\}$.
Thus, $G_1^{(2)}(\mathbf{x}_0,\mathbf{x})$ can be written in the following compact and elegant form:

$$2\pi D G_1^{(2)}(\mathbf{x}_0,\mathbf{x}) = \tau_m - \tau_2 + \sum_{n=1}^{+\infty} \frac{2}{n}\cos n(\sigma-\sigma_0) K_{1,n}^{(2)}(\tau,\tau_0), \tag{2.13}$$

where $K_{1,n}^{(2)}(\tau,\tau_0) = \sinh n(\tau_m-\tau_2)\dfrac{\cosh n(\tau_1-\tau_M)}{\cosh n(\tau_1-\tau_2)}$, and $\tau_M = \max\{\tau,\tau_0\}$.
We plot $G_1^{(2)}(\mathbf{x}_0,\mathbf{x})$ in Figure 2.5 and compare with numerical simulation. Additionally, examples of $G_1^{(2)}(\mathbf{x}_0,\mathbf{x})$ are shown in Figure 2.6 for multiple combinations of a and $\mathbf{x}_0$.

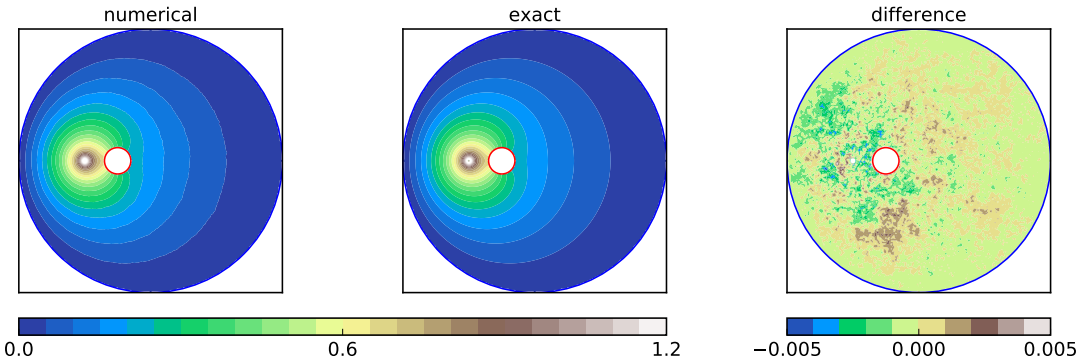

Figure 2.5: Plot of numerical simulation of $G_1^{(2)}(\mathbf{x}_0, \mathbf{x})$ (left), analytic formula (2.13) (centre) and difference (right). For the numerical simulations we have used G.5.1.1 and this plot has been obtained using G.5.1.2. The initial position is $\mathbf{x}_0 - \mathbf{x}_c = (-0.5, 0)$. Here $\mathbf{x}_c$ is the position vector of the cellular centre. For this figure we have used the following parameters: $a = 0.1$ and $c = 0.25$.

2.4.1.1 Comparison with interior Dirichlet Green's function

The interior Dirichlet Green's function satisfies the following equations:

$$\begin{aligned} D\Delta_{\mathbf{x}} G_0^{(2)}(\mathbf{x}_0, \mathbf{x}) &= -\delta(\mathbf{x} - \mathbf{x}_0) \quad \text{if} \quad \mathbf{x} \in C^*, \\ G_0^{(2)}(\mathbf{x}_0, \mathbf{x}) &= 0 \quad \text{if} \quad \mathbf{x} \in \partial C_2, \end{aligned} \tag{2.14}$$

where ∂C_2 is the absorbing cellular boundary, $\mathbf{x}_0 \in C^*$ is the initial position of the point particle and C^* is the disk of radius of 1. $G_0^{(2)}(\mathbf{x}_0, \mathbf{x})$ is the occupation density of the time a particle spends at $\mathbf{x}$ given that it started at $\mathbf{x}_0$ and is diffusing in a disk of radius 1 with absorbing boundary. The solution of (2.14) is given by Barton (1989) as:

$$G_0^{(2)}(\mathbf{x}_0, \mathbf{x}) = \frac{1}{2\pi D}\left(\log\frac{1}{\mathrm{R}} - \log\frac{1}{\tilde{\mathrm{R}}} + \log r_0\right), \tag{2.15}$$

where $\tilde{\mathbf{x}}_0$ is the image point of $\mathbf{x}_0$ such that the scalar product $\mathbf{x}_0 \cdot \tilde{\mathbf{x}}_0 = 1$ and

$$\mathrm{R} = |\mathbf{x} - \mathbf{x}_0|, \quad \tilde{\mathrm{R}} = |\mathbf{x} - \tilde{\mathbf{x}}_0| \quad \text{and} \quad r_0 = |\mathbf{x}_0|.$$

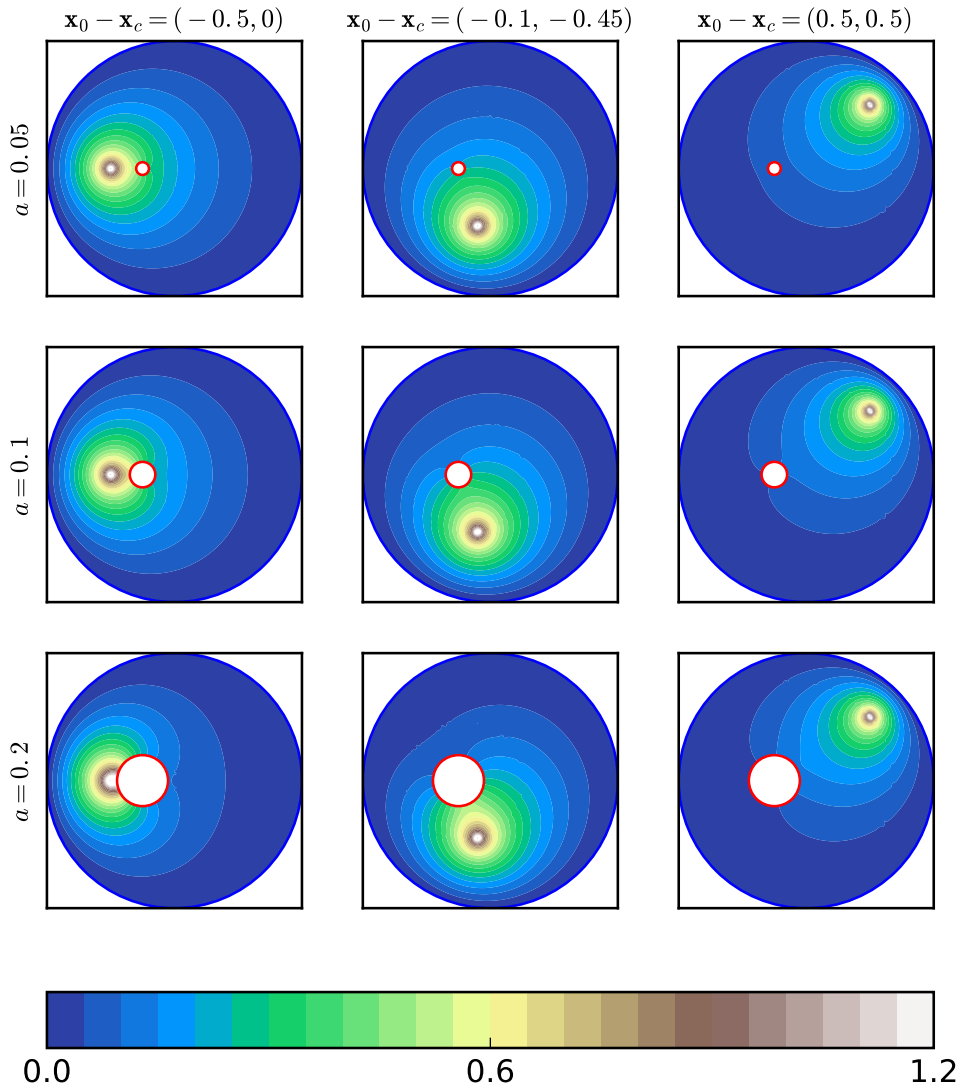

Figure 2.6: Green's function (2.13) with reflecting nuclear surface and absorbing cellular surface. Nine cases are shown: (i) $c = 0.25$, $a = 0.05$, $\mathbf{x}_0 - \mathbf{x}_c = (-0.5, 0)$ and $D = 0.5$. (ii) $c = 0.25$, $a = 0.05$, $\mathbf{x}_0 - \mathbf{x}_c = (-0.1, -0.45)$ and $D = 0.5$. (iii) $c = 0.25$, $a = 0.05$, $\mathbf{x}_0 - \mathbf{x}_c = (0.5, 0.5)$ and $D = 0.5$. (iv) $c = 0.25$, $a = 0.1$, $\mathbf{x}_0 - \mathbf{x}_c = (-0.5, 0)$ and $D = 0.5$. (v) $c = 0.25$, $a = 0.1$, $\mathbf{x}_0 - \mathbf{x}_c = (-0.1, -0.45)$ and $D = 0.5$. (vi) $c = 0.25$, $a = 0.1$, $\mathbf{x}_0 - \mathbf{x}_c = (0.5, 0.5)$ and $D = 0.5$. (vii) $c = 0.25$, $a = 0.2$, $\mathbf{x}_0 - \mathbf{x}_c = (-0.5, 0)$ and $D = 0.5$. (viii) $c = 0.25$, $a = 0.2$, $\mathbf{x}_0 - \mathbf{x}_c = (-0.1, -0.45)$ and $D = 0.5$. (ix) $c = 0.25$, $a = 0.2$, $\mathbf{x}_0 - \mathbf{x}_c = (0.5, 0.5)$ and $D = 0.5$. Here $\mathbf{x}_c$ is the position vector of the cellular centre.

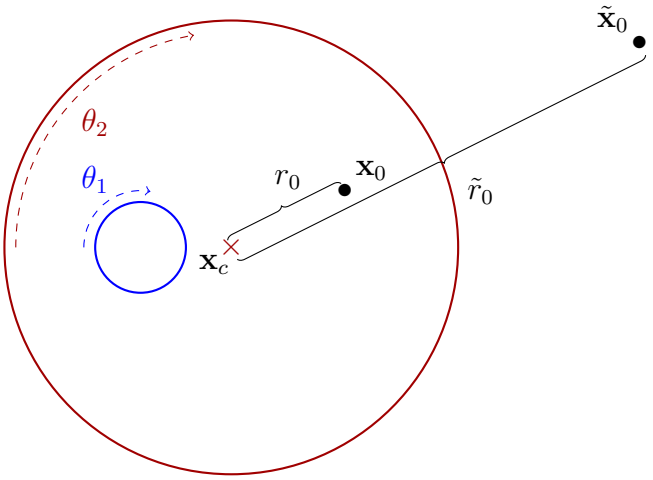

Figure 2.7: (i) The angles θ_1 and θ_2. (ii) Given $\mathbf{x}_0$, the image point $\tilde{\mathbf{x}}_0$ is defined such that $r_0\tilde{r}_0 = 1$, where $|\mathbf{x}_0| = r_0$ and $|\tilde{\mathbf{x}}_0| = \tilde{r}_0$. If the representation of $\tilde{\mathbf{x}}_0$ in bipolar coordinates is $(\tilde{\tau}_0, \tilde{\sigma}_0)$, then $\tau_0 + \tilde{\tau}_0 = 2\tau_2$. The centre of the cell is represented by $\mathbf{x}_c$.

Let $\mathbf{z}, \mathbf{z}_0$ be the complex representation of $\mathbf{x}$ and $\mathbf{x}_0$, respectively. Following (Heyda, 1959, p.29), we have:

$$\mathbf{z} - \mathbf{z}_0 = \frac{2d\left(\mathrm{e}^{u_0} - \mathrm{e}^{u}\right)}{\left(\mathrm{e}^{u} - 1\right)\left(\mathrm{e}^{u_0} - 1\right)} = \begin{cases} \frac{2d\mathrm{e}^{u}\left(1-\mathrm{e}^{-(u-u_0)}\right)}{(1-\mathrm{e}^{u})(1-\mathrm{e}^{u_0})}, & \text{if } \tau_0 \geq \tau, \\ -\frac{2d\mathrm{e}^{u_0}\left(1-\mathrm{e}^{-(u_0-u)}\right)}{(1-\mathrm{e}^{u})(1-\mathrm{e}^{u_0})}, & \text{if } \tau_0 \leq \tau, \end{cases}$$

where $u = -\tau + \mathbf{i}\sigma$ and (τ, σ) are the bipolar coordinates of $\mathbf{r}$. Taking the real part of $-\log(\mathbf{z} - \mathbf{z}_0)$ we obtain:

$$-\Re\left[\log\left(\mathbf{z} - \mathbf{z}_0\right)\right] = \max\{\tau, \tau_0\} - \log 2d + \sum_{n=1}^{+\infty} \frac{1}{n} H_n\left(\mathbf{x}_0, \mathbf{x}\right), \tag{2.16}$$

where

$$H_n\left(\mathbf{x}_0, \mathbf{x}\right) = \mathrm{e}^{-n|\tau-\tau_0|}\cos n(\sigma - \sigma_0) - \mathrm{e}^{-n\tau}\cos n\sigma - \mathrm{e}^{-n|\tau_0|}\cos n\sigma_0.$$

For the second term in (2.15) we have:

$$\mathbf{z} - \tilde{\mathbf{z}}_0 = \frac{2d\left(\mathrm{e}^{\tilde{u}_0} - \mathrm{e}^{u}\right)}{\left(\mathrm{e}^{u} - 1\right)\left(\mathrm{e}^{\tilde{u}_0} - 1\right)} = \begin{cases} -\frac{2d\mathrm{e}^{u}\left(1-\mathrm{e}^{-(u-\tilde{u}_0)}\right)}{\left(1-\mathrm{e}^{u}\right)\left(1-\mathrm{e}^{\tilde{u}_0}\right)}, & \text{if } \tilde{\tau}_0 \geq 0, \\ -\frac{2d\left(1-\mathrm{e}^{-(\tilde{u}_0-u)}\right)}{\left(1-\mathrm{e}^{u}\right)\left(1-\mathrm{e}^{-\tilde{u}_0}\right)}, & \text{if } \tilde{\tau}_0 \leq 0, \end{cases}$$

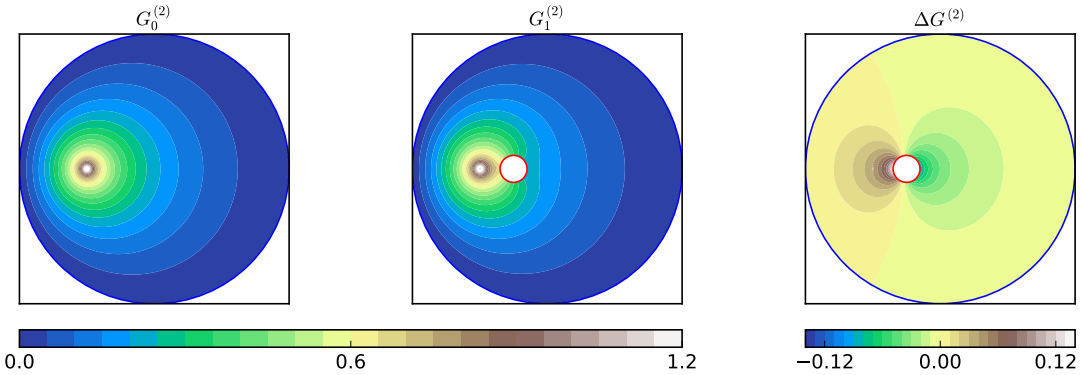

Figure 2.8: Plot of the Green's function $G_0^{(2)}(\mathbf{x}_0, \mathbf{x})$ formula (left, formula from (2.15)), Green's function $G_1^{(2)}(\mathbf{x}_0, \mathbf{x})$ (centre, formula from (2.13)) and difference (right). The initial condition is $\mathbf{x}_0 - \mathbf{x}_c = (-0.5, 0)$ and $a = 0.1, c = 0.5$. Here $\mathbf{x}_c$ is the position vector of the cellular centre.

and we deduce that:

$$\log(\mathbf{z} - \tilde{\mathbf{z}}_0) = \begin{cases} \mathbf{i}\pi + \log 2d + u - \sum_{n=1}^{+\infty} \frac{1}{n}\left[\mathrm{e}^{n(u-\tilde{u}_0)} - \left(\mathrm{e}^{nu} + \mathrm{e}^{n\tilde{u}_0}\right)\right], & \text{if } \tilde{\tau}_0 \geq 0, \\ \mathbf{i}\pi + \log 2d - \sum_{n=1}^{+\infty} \frac{1}{n}\left[\mathrm{e}^{-n(u-\tilde{u}_0)} - \left(\mathrm{e}^{nu} + \mathrm{e}^{-n\tilde{u}_0}\right)\right], & \text{if } \tilde{\tau}_0 \leq 0. \end{cases}$$

As a result, we have:

$$-\Re\left[\log(\mathbf{z} - \tilde{\mathbf{z}}_0)\right] = \max\{\tilde{\tau}, 0\} - \log 2d + \sum_{n=1}^{+\infty} \frac{1}{n} H_n(\tilde{\mathbf{x}}_0, \mathbf{x}), \tag{2.17}$$

where

$$H_n(\tilde{\mathbf{x}}_0, \mathbf{x}) = \mathrm{e}^{-n|\tau - \tilde{\tau}_0|} \cos n(\sigma - \tilde{\sigma}_0) - \mathrm{e}^{-n\tau} \cos n\sigma - \mathrm{e}^{-n|\tilde{\tau}_0|} \cos n\tilde{\sigma}_0.$$

The third term in (2.15) can be written as:

$$\log r_0 = \Re\left[\log(\mathbf{z_c} - \mathbf{z}_0)\right],$$

where $\mathbf{z}_c$ is the position of the centre of the cell, which can be written as $(\tau_c, \sigma_c) = (2\tau_2, 0)$ in bipolar coordinates (see Appendix B.7). As a result we have:

$$\mathbf{z_c} - \mathbf{z}_0 = \frac{2d(\mathrm{e}^{u_0} - \mathrm{e}^{u_c})}{(\mathrm{e}^{u_c} - 1)(\mathrm{e}^{u_0} - 1)} = \begin{cases} \frac{2d\mathrm{e}^{u_0}\left(1 - \mathrm{e}^{-(u_0 - u_c)}\right)}{\left(1 - \mathrm{e}^{u^c}\right)(1 - \mathrm{e}^{u_0})}, & \text{if } 2\tau_2 \leq \tau_0, \\ -\frac{2d\mathrm{e}^{u_c}\left(1 - \mathrm{e}^{-(u_c - u_0)}\right)}{\left(1 - \mathrm{e}^{u^c}\right)(1 - \mathrm{e}^{u_0})}, & \text{if } 2\tau_2 \geq \tau_0. \end{cases}$$

Taking the real part of $\log(\mathbf{z}_c - \mathbf{z}_0)$ we obtain:

$$\log r_0 = -\min\{2\tau_2, \tau_0\} + \log 2d - \sum_{n=1}^{+\infty} \frac{1}{n} H_n\left(\mathbf{x}_0, \mathbf{x}_c\right), \tag{2.18}$$

where

$$H_n\left(\mathbf{x}_0, \mathbf{x}_c\right) = \mathrm{e}^{-n|2\tau_2-\tau_0|}\cos n\sigma_0 - \mathrm{e}^{-2n\tau_2} - \mathrm{e}^{-n|\tau_0|}\cos n\sigma_0.$$

Using (2.16), (2.17) and (2.18) in (2.15) we obtain:

$$\begin{aligned}
2\pi D G_0^{(2)}(\mathbf{x}_0, \mathbf{x}) &= \log\frac{1}{R} - \log\frac{1}{\tilde{R}} + \log r_0 \\
&= \min\{\tau, \tau_0\} - \max\{\tilde{\tau}, 0\} - \min\{2\tau_2, \tau_0\} + \log 2d \\
&+ \sum_{n=1}^{+\infty} \frac{1}{n}\left(H_n\left(\mathbf{x}_0, \mathbf{x}\right) - H_n\left(\tilde{\mathbf{x}}_0, \mathbf{x}\right) - H_n\left(\mathbf{x}_0, \mathbf{x}_c\right)\right) \\
&= \min\{\tau, \tau_0\} - 2\tau_2 + \log 2d \\
&+ \sum_{n=1}^{+\infty} \frac{1}{n}\Big(\mathrm{e}^{-n|\tau-\tau_0|}\cos n(\sigma-\sigma_0) - \mathrm{e}^{-n\tau}\cos n\sigma - \mathrm{e}^{-n|\tau_0|}\cos n\sigma_0 \\
&- \mathrm{e}^{-n|\tau-\tilde{\tau}_0|}\cos n(\sigma-\tilde{\sigma}_0) + \mathrm{e}^{-n\tau}\cos n\sigma + \mathrm{e}^{-n|\tau_2-\tau_0|}\cos n\tilde{\sigma}_0 \\
&- \mathrm{e}^{-n|2\tau_2-\tau_0|}\cos n\sigma_0 + \mathrm{e}^{-2n\tau_2} + \mathrm{e}^{-n|\tau_0|}\cos n\sigma_0\Big) \\
&= \min\{\tau, \tau_0\} - 2\tau_2 + \log 2d + \sum_{n=1}^{+\infty} \frac{1}{n} e^{-2n\tau_2} \\
&+ \sum_{n=1}^{+\infty} \frac{1}{n}\left(\mathrm{e}^{-n|\tau-\tau_0|}\cos n(\sigma-\sigma_0) - \mathrm{e}^{-n(\tau-\tilde{\tau}_0)}\cos n(\sigma-\sigma_0)\right) \\
&= \min\{\tau, \tau_0\} - \tau_2 + \sum_{n=1}^{+\infty} \frac{\cos n(\sigma-\sigma_0)}{n}\left(\mathrm{e}^{-n|\tau-\tau_0|} - \mathrm{e}^{-n(\tau-\tilde{\tau}_0)}\right) \\
&= \min\{\tau, \tau_0\} - \tau_2 + \sum_{n=1}^{+\infty} \frac{2}{n}\cos n(\sigma-\sigma_0)\sinh n(\tau_m-\tau_2)\mathrm{e}^{-n(\tau_M-\tau_2)},
\end{aligned} \tag{2.19}$$

where $\tau_m = \min\{\tau, \tau_0\}$, $\tau_M = \max\{\tau, \tau_0\}$ and we have used appendix B.5 and C.2, respectively.

The difference of (2.13) and (2.19) can be written as:

$$2\pi D \Delta G_1^{(2)}(\mathbf{x}_0, \mathbf{x}) = 2\pi D\left(G_1^{(2)}(\mathbf{x}_0, \mathbf{x}) - G_0^{(2)}(\mathbf{x}_0, \mathbf{x})\right)$$

$$= 2\sum_{n=1}^{+\infty} \frac{\cos n(\sigma - \sigma_0)}{n} \Delta K^{(2)}_{1,n}(\tau, \tau_0), \tag{2.20}$$

where

$$\Delta K^{(2)}_{1,n}(\tau, \tau_0) = \mathrm{e}^{-n(\tau_1 - \tau_2)} \frac{\sinh n\left(\tau_M - \tau_2\right) \sinh n\left(\tau_m - \tau_2\right)}{\cosh n\left(\tau_1 - \tau_2\right)}. \tag{2.21}$$

We plot horizontal slices of $G^{(2)}_0(\mathbf{x}_0, \mathbf{x})$, $G^{(2)}_1(\mathbf{x}_0, \mathbf{x})$ and $\Delta G^{(2)}_1(\mathbf{x}_0, \mathbf{x})$ in Figure 2.9. We observe that while $G^{(2)}_0(\mathbf{x}_0, \mathbf{x})$ and $G^{(2)}_1(\mathbf{x}_0, \mathbf{x})$ have a singularity at $\mathbf{x} = \left(\frac{1}{2}, 0\right)$, their difference $\Delta G^{(2)}_1(\mathbf{x}_0, \mathbf{x})$ does not present any singularity.

We wish to expand $\Delta K^{(2)}_{1,n}(\tau, \tau_0)$ as a series in powers of a and we begin by making use of:

$$\tau_1 = \log\left(\frac{1 - c^2}{ac} - \frac{a}{c\left(1 - c^2\right)}\right) = \log\frac{1 - c^2}{c} - \log a + \mathcal{O}\left(a^2\right), \tag{2.22a}$$

$$\tau_2 = \log\left(\frac{1}{c} - \frac{a^2}{c\left(1 - c^2\right)}\right) = \log\frac{1}{c} + \mathcal{O}\left(a^2\right), \tag{2.22b}$$

$$\tau_1 - \tau_2 = \log(1 - c^2) - \log a + \mathcal{O}\left(a^2\right), \tag{2.22c}$$

to obtain the following:

$$\begin{aligned}
\mathrm{e}^{-n(\tau_1 - \tau_2)} &= \mathrm{e}^{-n\left(\log(1-c^2) - \log a + \mathcal{O}\left(a^2\right)\right)} \\
&= \mathrm{e}^{-n\log\left(1-c^2\right)} \mathrm{e}^{n\log a} \mathrm{e}^{\mathcal{O}\left(a^2\right)} \\
&= \frac{a^n}{\left(1 - c^2\right)^n} + \mathcal{O}\left(a^{n+1}\right), \\
\frac{1}{\cosh n\left(\tau_1 - \tau_2\right)} &= \frac{2}{\mathrm{e}^{n(\tau_1 - \tau_2)} + \mathrm{e}^{-n(\tau_1 - \tau_2)}} \\
&= \frac{2\mathrm{e}^{-n(\tau_1 - \tau_2)}}{1 + \mathrm{e}^{-2n(\tau_1 - \tau_2)}} \\
&= \frac{2\mathrm{e}^{-n\left(\log(1-c^2) - \log a + \mathcal{O}\left(a^2\right)\right)}}{1 + \mathrm{e}^{-2n(\log(1-c^2) - \log a + \mathcal{O}(a^2))}} \\
&= 2\frac{\frac{a^n}{(1-c^2)^n} + \mathcal{O}\left(a^{n+1}\right)}{1 + \frac{a^{2n}}{(1-c^2)^{2n}} + \mathcal{O}\left(a^{2n+1}\right)} \\
&= \frac{2a^n}{\left(1 - c^2\right)^n} + \mathcal{O}\left(a^{n+1}\right).
\end{aligned}$$

The τ-component can be expressed as follows:

$$\tau = \log\left(\frac{d}{r} + \sqrt{1 + \left(\frac{d}{r}\right)^2}\right),$$

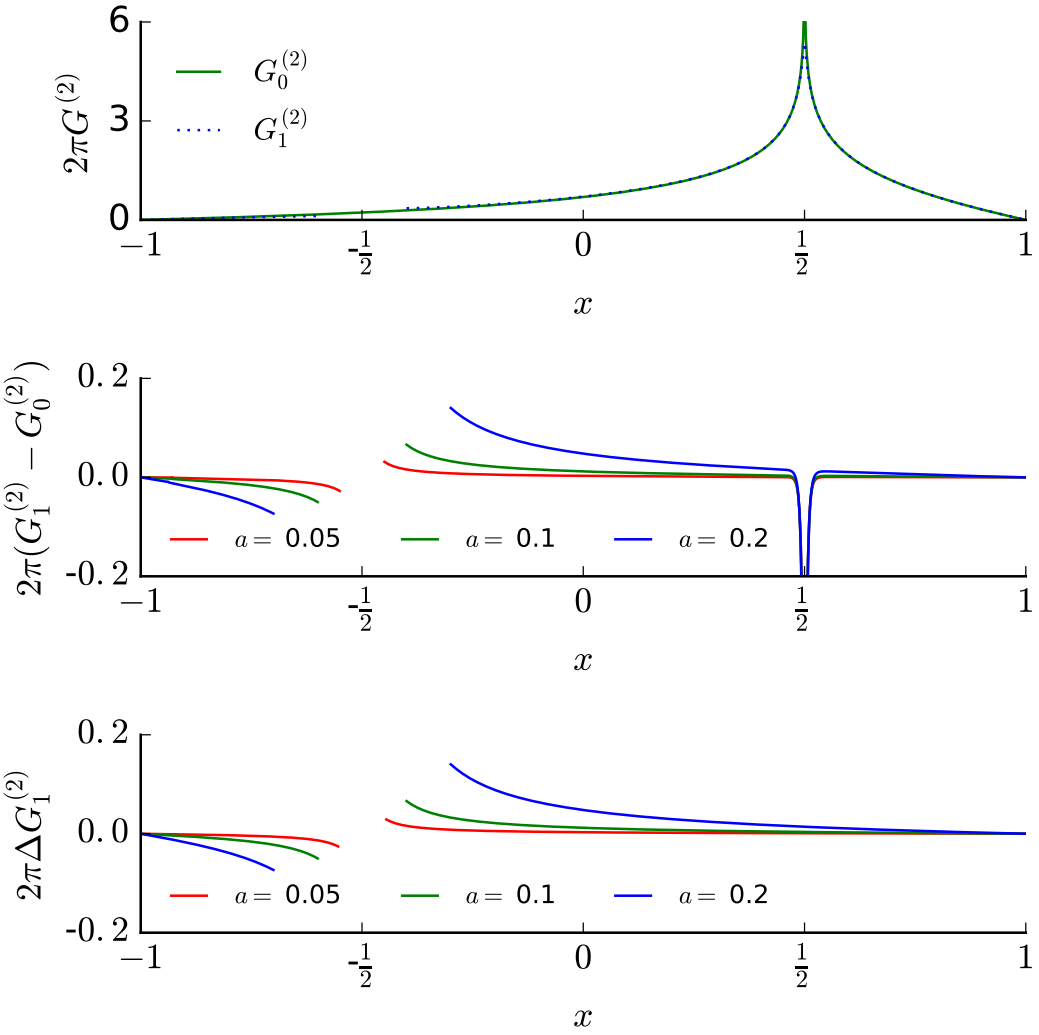

Figure 2.9: Top: plot of the Green's function $2\pi G_0^{(2)}(\mathbf{x}_0, \mathbf{x})$ from (2.15) and $2\pi G_1^{(2)}(\mathbf{x}_0, \mathbf{x})$ from (2.13) as a function of the horizontal distance x. Middle: plot of the difference between $G_1^{(2)}(\mathbf{x}_0, \mathbf{x})$ and $G_0^{(2)}(\mathbf{x}_0, \mathbf{x})$ as a function of the horizontal distance x for multiple values of a. Bottom: plot of the difference Green's function $\Delta G_1^{(2)}(\mathbf{x}_0, \mathbf{x})$ from (2.20) as a function of the horizontal distance x for multiple values of a.

where r is the radius of the circle defined by τ. Using the following expansion:

$$d = \frac{1 - c^2}{2c} - \frac{a^2}{2}\frac{1 + c^2}{1 - c^2} + \mathcal{O}\left(a^3\right),$$

$$1+\left(\frac{d}{r}\right)^2 = 1+\frac{\left(1-c^2\right)^2}{4c^2r^2} - a^2\frac{1+c^2}{2c^2r^2} + \mathcal{O}\left(a^3\right),$$

we obtain:

$$\begin{aligned}
&\frac{d}{r}+\sqrt{1+\left(\frac{d}{r}\right)^2} = \frac{\sqrt{4c^2r^2+(1-c^2)^2}+1-c^2}{2rc} \\
&-a^2\frac{1+c^2}{2rc}\left(\frac{1}{\sqrt{4c^2r^2+(1-c^2)^2}}+\frac{1}{1-c^2}\right)+\mathcal{O}\left(a^3\right) \\
&=\frac{\sqrt{4c^2r^2+(1-c^2)^2}+1-c^2}{2rc}\left[1-a^2\frac{1+c^2}{2c}\frac{\left(\frac{1}{\sqrt{4c^2r^2+(1-c^2)^2}}+\frac{1}{1-c^2}\right)}{\frac{\sqrt{4c^2r^2+(1-c^2)^2}+1-c^2}{2c}}+\mathcal{O}\left(a^3\right)\right].
\end{aligned}$$

As a result we have:

$$\begin{aligned}
\tau &= \log\left\{\frac{\sqrt{4c^2r^2+(1-c^2)^2}+1-c^2}{2rc}\left[1-a^2\alpha+\mathcal{O}\left(a^3\right)\right]\right\} \\
&= \log\left(\frac{\sqrt{4c^2r^2+(1-c^2)^2}+1-c^2}{2rc}\right)+\log\left(1-\alpha a^2+\mathcal{O}\left(a^3\right)\right) \\
&= \log\left(\frac{\sqrt{4c^2r^2+(1-c^2)^2}+1-c^2}{2rc}\right)+\mathcal{O}\left(a^2\right), \qquad (2.23)
\end{aligned}$$

where

$$\alpha = \frac{1+c^2}{2c}\frac{\left(\frac{1}{\sqrt{4c^2r^2+(1-c^2)^2}}+\frac{1}{1-c^2}\right)}{\frac{\sqrt{4c^2r^2+(1-c^2)^2}+1-c^2}{2c}}.$$

When $r=1$ we have:

$$\tau_2 = \log\left(\frac{1}{c}\right)+\mathcal{O}\left(a^2\right), \qquad (2.24)$$

which is consistent with our previous result (2.22b). From (2.23) and (2.24) we deduce that:

$$\tau-\tau_2 = \log\left(\frac{\sqrt{4c^2r^2+(1-c^2)^2}+1-c^2}{2r}\right)+\mathcal{O}\left(a^2\right).$$

As a result, we obtain:

$$\sinh n\left(\tau-\tau_2\right) =$$

$$\frac{\mathrm{e}^{n\left(\log\left(\frac{\sqrt{4c^2r^2+(1-c^2)^2}+1-c^2}{2r}\right)+\mathcal{O}\left(a^2\right)\right)}-\mathrm{e}^{-n\left(\log\left(\frac{\sqrt{4c^2r^2+(1-c^2)^2}+1-c^2}{2r}\right)+\mathcal{O}\left(a^2\right)\right)}}{2}$$
$$=\frac{\left(\frac{\sqrt{4c^2r^2+(1-c^2)^2}+1-c^2}{2r}\right)^n-\left(\frac{\sqrt{4c^2r^2+(1-c^2)^2}+1-c^2}{2r}\right)^{-n}}{2}+\mathcal{O}\left(a^2\right),$$

where in the above calculation we have used the following expansions:

$$\mathrm{e}^{\pm n\alpha a^2}=1\pm n\alpha a^2+\mathcal{O}\left(a^4\right).$$

Analogously, we obtain:

$$\sinh n\left(\tau_0-\tau_2\right)=\frac{\left(\frac{\sqrt{4c^2r_0^2+(1-c^2)^2}+1-c^2}{2r_0}\right)^n-\left(\frac{\sqrt{4c^2r_0^2+(1-c^2)^2}+1-c^2}{2r_0}\right)^{-n}}{2}+\mathcal{O}\left(a^2\right).$$

The difference term (2.21) can be written as:

$$\Delta K_{1,n}^{(2)}(\tau,\tau_0)=a^{2n}\frac{\left[\left(\frac{\sqrt{4c^2r^2+(1-c^2)^2}+1-c^2}{2r}\right)^n-\left(\frac{\sqrt{4c^2r^2+(1-c^2)^2}+1-c^2}{2r}\right)^{-n}\right]}{2\left(1-c^2\right)^{2n}}$$
$$\times\left[\left(\frac{\sqrt{4c^2r_0^2+(1-c^2)^2}+1-c^2}{2r_0}\right)^n-\left(\frac{\sqrt{4c^2r_0^2+(1-c^2)^2}+1-c^2}{2r_0}\right)^{-n}\right]$$
$$+\mathcal{O}\left(a^{2(n+1)}\right).$$

When $n=1$ we have:

$$\Delta K_{1,1}^{(2)}(\tau,\tau_0)=a^2\frac{\left[\left(\frac{\sqrt{4c^2r^2+(1-c^2)^2}+1-c^2}{2r}\right)-\left(\frac{\sqrt{4c^2r^2+(1-c^2)^2}+1-c^2}{2r}\right)^{-1}\right]}{2\left(1-c^2\right)^2}$$
$$\times\left[\left(\frac{\sqrt{4c^2r_0^2+(1-c^2)^2}+1-c^2}{2r_0}\right)-\left(\frac{\sqrt{4c^2r_0^2+(1-c^2)^2}+1-c^2}{2r_0}\right)^{-1}\right]$$
$$+\mathcal{O}\left(a^4\right),$$

from which we deduce that $G_1^{(2)}(\mathbf{x}_0,\mathbf{x})$ can be written as the sum of $G_0^{(2)}(\mathbf{x}_0,\mathbf{x})$ and corrections proportional to a^2. We observe that when $c\to 0^+$:

$$\Delta K_{1,1}^{(2)}(\tau,\tau_0)\to\frac{a^2}{2}\left(\frac{1}{r}-r\right)\left(\frac{1}{r_0}-r_0\right)+\mathcal{O}\left(a^4\right)$$

$$\rightarrow \frac{a^2}{2}\left(\frac{1}{r_M}-r_M\right)\left(\frac{1}{r_m}-r_m\right)+\mathcal{O}\left(a^4\right), \tag{2.25}$$

where $r_M=\max\{r,r_0\}$ and $r_m=\min\{r,r_0\}$.

2.4.1.2 Comparison with the concentric Green's function

When $c=0$ the Green's function $G_1^{(2)}$ can be written as:

$$\begin{aligned}2\pi D G_1^{(2)}(\mathbf{x}_0,\mathbf{x}) &= -\log r_M+\sum_{n=1}^{+\infty}\frac{\cos n\left(\theta-\theta_0\right)}{n}\\ &\times\frac{\left[(1/r_M)^n-r_M^n\right]\left[(r_m/a)^n+(a/r_m)^n\right]}{a^n+(1/a)^n},\end{aligned} \tag{2.26}$$

where $r_m=\min(r_0,r)$ and $r_M=\max\{r_0,r\}$. Here (r,θ) and (r_0,θ_0) are the polar coordinates of $\mathbf{x}$ and $\mathbf{x}_0$, respectively. We plot (2.26) in Figure 2.10.
In order to prove (2.26) we make use of appendix B.8 in (2.13). From (Barton, 1989, p. 414) we know that:

$$\begin{aligned}2\pi D G_0^{(2)}(\mathbf{x}_0,\mathbf{x}) &= -\log r_M+\sum_{n=1}^{+\infty}\frac{\cos n\left(\theta-\theta_0\right)}{n}\left[\left(\frac{r_m}{r_M}\right)^n-\left(r_m r_M\right)^n\right]\\ &= -\log r_M+\sum_{n=1}^{+\infty}\frac{\cos n\left(\theta-\theta_0\right)}{n}(r_m)^n\left[\left(\frac{1}{r_M}\right)^n-(r_M)^n\right],\end{aligned}$$

from which we deduce:

$$\begin{aligned}&2\pi D\left(G_1^{(2)}(\mathbf{x}_0,\mathbf{x})-G_0^{(2)}(\mathbf{x}_0,\mathbf{x})\right)\\ &=\sum_{n=1}^{+\infty}\frac{\cos n\left(\theta-\theta_0\right)}{n}\left[\left(\frac{1}{r_M}\right)^n-(r_M)^n\right]\left[\frac{(r_m)^{2n}+a^{2n}}{(r_m)^n(a^{2n}+1)}-(r_m)^n\right]\\ &=\sum_{n=1}^{+\infty}\frac{\cos n\left(\theta-\theta_0\right)}{n}\left[\left(\frac{1}{r_M}\right)^n-(r_M)^n\right]\frac{a^{2n}\left[(r_m)^{2n}-1\right]}{(r_m)^n\left(a^{2n}+1\right)}\\ &=\sum_{n=1}^{+\infty}\frac{\cos n\left(\theta-\theta_0\right)}{n}\left[\left(\frac{1}{r_M}\right)^n-(r_M)^n\right]\left[\left(\frac{1}{r_m}\right)^n-(r_m)^n\right]\frac{a^{2n}}{1+a^{2n}}\\ &=\sum_{n=1}^{+\infty}\frac{\cos n\left(\theta-\theta_0\right)}{n}\left[\left(\frac{1}{r_M}\right)^n-(r_M)^n\right]\left[\left(\frac{1}{r_m}\right)^n-(r_m)^n\right]a^{2n}\\ &\times\left(1-a^{2n}+a^{4n}-\cdots\right)\end{aligned}$$

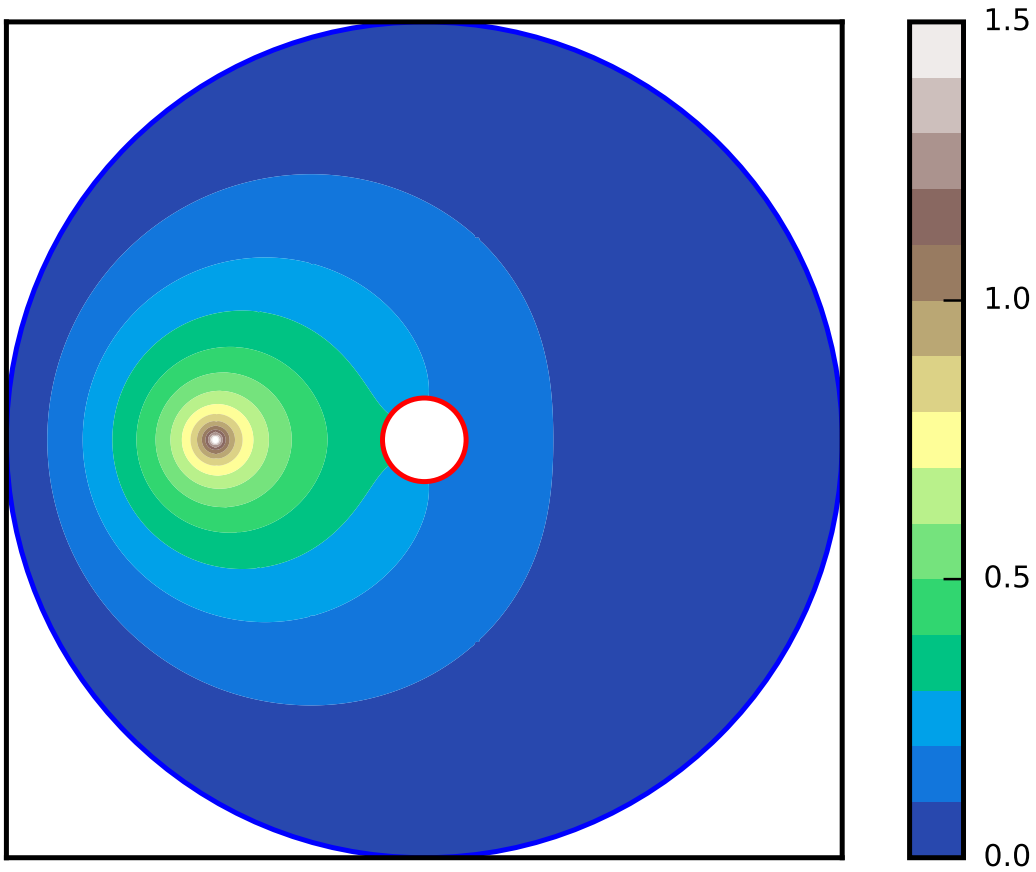

Figure 2.10: Plot of the Green's function $G_1^{(2)}(\mathbf{x}_0, \mathbf{x})$ for the concentric case (2.26).Here we have used $\mathbf{x}_0 = (-0.5, 0)\,, D = 0.5$.

$$= a^2 \cos(\theta - \theta_0) \left(\frac{1}{r_M} - r_M\right) \left(\frac{1}{r_m} - r_m\right) + \mathcal{O}\left(a^3\right). \tag{2.27}$$

We observe that the concentric case (2.27) is consistent with our previous calculations (2.25) for the concentric case.

2.4.2 From cellular surface to nucleus

We turn to the case of diffusion from the cellular surface to an absorbing nucleus, and denote the Green's function by $G_2^{(2)}(\mathbf{x}_0, \mathbf{x})$. It satisfies (2.3) with the

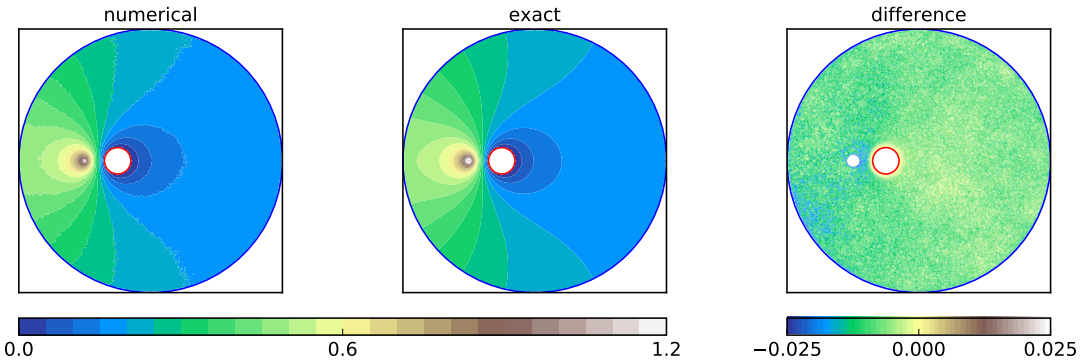

Figure 2.11: Plot of numerical simulation of $G_2^{(2)}(\mathbf{x}_0, \mathbf{x})$ (left), analytic formula (2.28) (centre) and difference (right). The initial condition is $\mathbf{x}_0 - \mathbf{x}_c = (-0.5, 0)$ and $a = 0.1, c = 0.25$. Here $\mathbf{x}_c$ is the position vector of the cellular centre.

conditions:

$$G_2^{(2)}(\mathbf{x}_0, \mathbf{x}) = 0, \quad \mathbf{x} \in \partial C_1,$$
$$\frac{\partial G_2}{\partial \mathbf{n}_2}(\mathbf{x}_0, \mathbf{x}) = 0, \quad \mathbf{x} \in \partial C_2,$$

where $\mathbf{n}_2$ is the unit normal outward vector to ∂C_2. Following the same methodology as used in Section 2.4.1 to derive $G_1^{(2)}(\mathbf{x}_0, \mathbf{x})$, we find

$$2\pi D G_2^{(2)}(\mathbf{x}_0, \mathbf{x}) = \tau_1 - \tau_M + \sum_{n=1}^{+\infty} \frac{2}{n} \cos n(\sigma - \sigma_0) K_{2,n}^{(2)}(\tau, \tau_0), \tag{2.28}$$

where $K_{2,n}^{(2)}(\tau, \tau_0) = \sinh n(\tau_1 - \tau_M) \dfrac{\cosh n(\tau_m - \tau_2)}{\cosh n(\tau_1 - \tau_2)}$. In Figure 2.13, the exact Green's function is compared with the approximation of Condamin *et al.* (2007), which was constructed as a sum of pseudo-Green functions (see (1.67) for a definition of pseudo-Green functions).
We plot $G_2^{(2)}(\mathbf{x}_0, \mathbf{x})$ in Figure 2.11 and compare with numerical simulation. Additionally, examples of $G_2^{(2)}(\mathbf{x}_0, \mathbf{x})$ are shown in Figure 2.12 for multiple combinations of a and $\mathbf{x}_0$.

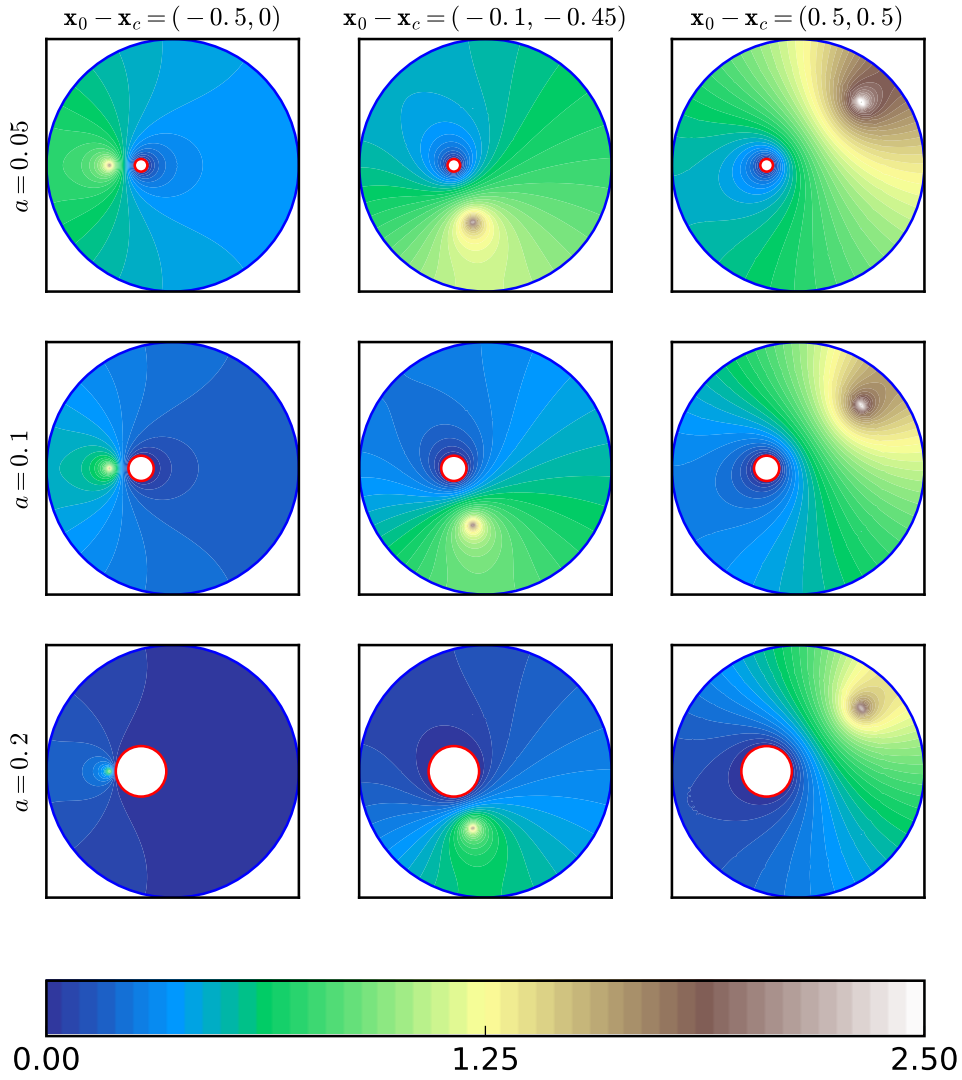

Figure 2.12: Green's function (2.28) with absorbing nuclear surface and reflecting cellular surface. Nine cases are shown: (i) $c = 0.25$, $a = 0.05$, $\mathbf{x}_0 - \mathbf{x}_c = (-0.5, 0)$ and $D = 0.5$. (ii) $c = 0.25$, $a = 0.05$, $\mathbf{x}_0 - \mathbf{x}_c = (-0.1, -0.45)$ and $D = 0.5$. (iii) $c = 0.25$, $a = 0.05$, $\mathbf{x}_0 - \mathbf{x}_c = (0.5, 0.5)$ and $D = 0.5$. (iv) $c = 0.25$, $a = 0.1$, $\mathbf{x}_0 - \mathbf{x}_c = (-0.5, 0)$ and $D = 0.5$. (v) $c = 0.25$, $a = 0.1$, $\mathbf{x}_0 - \mathbf{x}_c = (-0.1, -0.45)$ and $D = 0.5$. (vi) $c = 0.25$, $a = 0.1$, $\mathbf{x}_0 - \mathbf{x}_c = (0.5, 0.5)$ and $D = 0.5$. (vii) $c = 0.25$, $a = 0.2$, $\mathbf{x}_0 - \mathbf{x}_c = (-0.5, 0)$ and $D = 0.5$. (viii) $c = 0.25$, $a = 0.2$, $\mathbf{x}_0 - \mathbf{x}_c = (-0.1, -0.45)$ and $D = 0.5$. (ix) $c = 0.25$, $a = 0.2$, $\mathbf{x}_0 - \mathbf{x}_c = (0.5, 0.5)$ and $D = 0.5$. Here $\mathbf{x}_c$ is the position vector of the cellular centre.

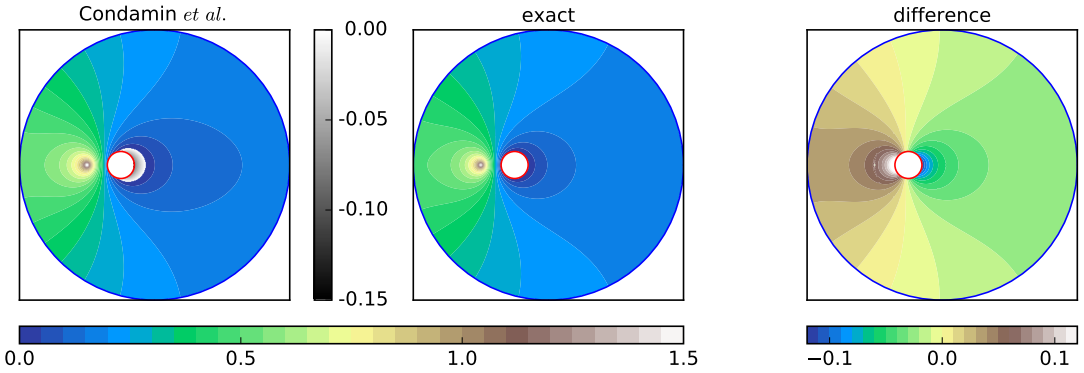

Figure 2.13: The approximation of Condamin *et al.* (2007), the exact Green's function (2.28), with reflecting cell surface and absorbing nuclear surface, which is negative on part of the domain, and the difference. Here we have chosen the following parameter values $c = 0.25$, $a = 0.1$, $\mathbf{x}_0 - \mathbf{x}_c = (-0.5, 0)$, where $\mathbf{x}_c$ is the position vector of the cellular centre.

2.4.2.1 Comparison with Condamin *et al.* (2007) formula

We wish to compare (2.28) with the result produced by Condamin *et al.* (2007) for the Green's function:

$$2\pi D G_c(\mathbf{x}_0, \mathbf{x}) = \log \frac{1}{a} + H(\mathbf{x}, \mathbf{x}_0) - H(\mathbf{x}, \mathbf{x}_n) + H^*(\mathbf{x}_n, \mathbf{x}_n) - H(\mathbf{x}_n, \mathbf{x}_0),$$

where

$$H(\mathbf{x}, \mathbf{y}) = \log \frac{1}{|\mathbf{x} - \mathbf{y}|} + \log \frac{1}{|\mathbf{x} - \tilde{\mathbf{y}}|} + \log \frac{1}{|\mathbf{y}|} + \frac{|\mathbf{x}|^2 + |\mathbf{y}|^2}{2},$$

and

$$H^*(\mathbf{x}, \mathbf{y}) = \log \frac{1}{|\mathbf{x} - \tilde{\mathbf{y}}|} + \log \frac{1}{|\mathbf{y}|} + \frac{|\mathbf{x}|^2 + |\mathbf{y}|^2}{2}.$$

As a result, we obtain:

$$2\pi D G_c(\mathbf{x}_0, \mathbf{x}) = \log \frac{1}{a} + \log \frac{1}{|\mathbf{x} - \mathbf{x}_0|} + \log \frac{1}{|\mathbf{x} - \tilde{\mathbf{x}}_0|} - \log \frac{1}{|\mathbf{x} - \mathbf{x}_n|} - \log \frac{1}{|\mathbf{x} - \tilde{\mathbf{x}}_n|} - \log \frac{1}{|\mathbf{x}_n - \mathbf{x}_0|} - \log \frac{1}{|\mathbf{x}_n - \tilde{\mathbf{x}}_0|} + \log \frac{1}{|\mathbf{x}_n - \tilde{\mathbf{x}}_n|},$$

where $\tilde{\mathbf{x}}$ is the image point of $\mathbf{x}$.

Using the following bipolar expansions Heyda (1959):

$$\log \frac{1}{|\mathbf{x} - \mathbf{y}|} = \min(\tau_x, \tau_y) - \log 2d$$

$$+\sum_{n=1}^{+\infty}\frac{1}{n}\left[\mathrm{e}^{-n|\tau_x-\tau_y|}\cos n(\sigma_x-\sigma_y)-\mathrm{e}^{-n|\tau_x|}\cos n\sigma_x-\mathrm{e}^{-n|\tau_y|}\cos n\sigma_y\right], \tag{2.29}$$

and

$$\log\frac{1}{|\mathbf{x}-\tilde{\mathbf{y}}|}=\max\{\tilde{\tau}_y,0\}-\log 2d +\sum_{n=1}^{+\infty}\frac{1}{n}\left[\mathrm{e}^{-n|\tau_x-\tilde{\tau}_y|}\cos n(\sigma_x-\sigma_y)-\mathrm{e}^{-n|\tau_x|}\cos n\sigma_x-\mathrm{e}^{-n|\tilde{\tau}_y|}\cos n\sigma_y\right], \tag{2.30}$$

we obtain, after simplification:

$$\begin{aligned}2\pi DG_c(\mathbf{x}_0,\mathbf{x})=\tau_1-\tau_M+\sum_{n=1}^{+\infty}\frac{1}{n}\Big[&\mathrm{e}^{-n|\tau-\tau_0|}\cos n(\sigma-\sigma_0)+\mathrm{e}^{-n|\tau-\tilde{\tau}_0|}\cos n(\sigma-\sigma_0)\\ &-\mathrm{e}^{-n|\tau-\tau_c|}\cos n\sigma-\mathrm{e}^{-n|\tau-\tilde{\tau}_c|}\cos n\sigma-\mathrm{e}^{-n|\tau_c-\tau_0|}\cos n\sigma_0-\mathrm{e}^{-n|\tau_c-\tilde{\tau}_0|}\cos n\sigma_0\\ &+\mathrm{e}^{-n|\tau_c-\tilde{\tau}_c|}+\mathrm{e}^{-n|\tau_c|}\Big].\end{aligned}$$

Using the fact that $\tau_c=2\tau_1$ (see appendix B.7) and $\tilde{\tau}=2\tau_2-\tau$ (see appendix C.2) we observe that:

$$\begin{aligned}2\pi DG_c(\mathbf{x}_0,\mathbf{x})&=\tau_1-\tau_M+\sum_{n=1}^{+\infty}\frac{1}{n}\Big[\mathrm{e}^{-n|\tau-\tau_0|}\cos n(\sigma-\sigma_0)+\mathrm{e}^{-n|\tau-2\tau_2+\tau_0|}\cos n(\sigma-\sigma_0)\\ &\quad-\mathrm{e}^{-n|\tau-2\tau_1|}\cos n\sigma-\mathrm{e}^{-n|\tau-2\tau_2+2\tau_1|}\cos n\sigma-\mathrm{e}^{-n|2\tau_1-\tau_0|}\cos n\sigma_0\\ &\quad-\mathrm{e}^{-n|2\tau_1-2\tau_2-\tau_0|}\cos n\sigma_0+\mathrm{e}^{-n|4\tau_1-2\tau_2|}+\mathrm{e}^{-n|2\tau_1|}\Big]\\ &=\tau_1-\tau_M+2\sum_{n=1}^{+\infty}\frac{1}{n}\Bigg[\mathrm{e}^{-n(\tau_M-\tau_2)}\cosh n\left(\tau_m-\tau_2\right)\cos n(\sigma-\sigma_0)\\ &\quad-\mathrm{e}^{-n(2\tau_1-\tau_2)}\cosh n\left(\tau-\tau_2\right)\cos n\sigma\\ &\quad-\mathrm{e}^{-n(2\tau_1-\tau_2)}\cosh n\left(\tau_0-\tau_2\right)\cos n\sigma_0+\frac{\mathrm{e}^{-n|4\tau_1-2\tau_2|}+\mathrm{e}^{-n|2\tau_1|}}{2}\Bigg],\end{aligned} \tag{2.31}$$

where we have used:

$$\begin{aligned}\left[\mathrm{e}^{-n|\tau-\tau_0|}+\mathrm{e}^{-n|\tau-2\tau_2+\tau_0|}\right]\cos n(\sigma-\sigma_0)&=2\mathrm{e}^{-n(\tau_M-\tau_2)}\cosh n\left(\tau_m-\tau_2\right)\cos n(\sigma-\sigma_0),\\ \left[\mathrm{e}^{-n|\tau-2\tau_1|}+\mathrm{e}^{-n|\tau-2\tau_2+2\tau_1|}\right]\cos n\sigma&=2\mathrm{e}^{-n(2\tau_1-\tau_2)}\cosh n\left(\tau-\tau_2\right)\cos n\sigma,\end{aligned}$$

$$\left[\mathrm{e}^{-n|\tau_0-2\tau_1|}+\mathrm{e}^{-n|\tau_0-2\tau_2+2\tau_1|}\right]\cos n\sigma_0 = 2\mathrm{e}^{-n(2\tau_1-\tau_2)}\cosh n\left(\tau_0-\tau_2\right)\cos n\sigma_0.$$

We want to calculate the following:

$$\begin{aligned}
&2\pi D\Delta G_2^{(2)}\left(\mathbf{x}_0,\mathbf{x}\right)\\
&=2\pi D\left(G_2^{(2)}\left(\mathbf{x}_0,\mathbf{x}\right)-G_c\left(\mathbf{x}_0,\mathbf{x}\right)\right)\\
&=2\sum_{n=1}^{+\infty}\frac{1}{n}\Bigg\{\left[\sinh n\left(\tau_1-\tau_M\right)\frac{\cosh n\left(\tau_m-\tau_2\right)}{\cosh n\left(\tau_1-\tau_2\right)}-\mathrm{e}^{-n(\tau_M-\tau_2)}\cosh n\left(\tau_m-\tau_2\right)\right]\\
&\times\cos n(\sigma-\sigma_0)+\mathrm{e}^{-n(2\tau_1-\tau_2)}\cosh n\left(\tau-\tau_2\right)\cos n\sigma\\
&+\mathrm{e}^{-n(2\tau_1-\tau_2)}\cosh n\left(\tau_0-\tau_2\right)\cos n\sigma_0-\frac{\mathrm{e}^{-n|4\tau_1-2\tau_2|}+\mathrm{e}^{-n|2\tau_1|}}{2}\Bigg\}\\
&=2\sum_{n=0}^{+\infty}\frac{1}{n}\Delta K_{2,n}^{(2)}(\mathbf{x}_0,\mathbf{x}).
\end{aligned}$$

We plot $\Delta G_2^{(2)}\left(\mathbf{x}_0,\mathbf{x}\right)$ in the left panel of Figure 2.14.
Using the fact that:

$$\begin{aligned}
\tau&=\log\left(\frac{\sqrt{4c^2r^2+\left(1-c^2\right)^2}+1-c^2}{2rc}\right)+\mathcal{O}\left(a^2\right),\\
\tau_1&=\log\frac{1-c^2}{c}-\log a+\mathcal{O}\left(a^2\right),\\
\tau_2&=\log\frac{1}{c}+\mathcal{O}\left(a^2\right),
\end{aligned}$$

we obtain:

$$\begin{aligned}
\tau_1-\tau&=\log\frac{1-c^2}{c}-\log a-\log\left(\frac{\sqrt{4c^2r^2+\left(1-c^2\right)^2}+1-c^2}{2rc}\right)+\mathcal{O}\left(a^2\right)\\
&=\log\left(\frac{1}{a}\underbrace{\frac{2r\left(1-c^2\right)}{\sqrt{4c^2r^2+\left(1-c^2\right)^2}+1-c^2}}_{f(r)}\right)+\mathcal{O}\left(a^2\right)\\
&=\log\frac{f(r)}{a}+\mathcal{O}\left(a^2\right),
\end{aligned}$$

$$\begin{aligned}\tau - \tau_2 &= \log\left(\underbrace{\frac{\sqrt{4c^2r^2 + \left(1-c^2\right)^2} + 1 - c^2}{2r}}_{g(r)}\right) + \mathcal{O}\left(a^2\right) \\ &= \log g(r) + \mathcal{O}\left(a^2\right),\end{aligned}$$

and, subsequently, that:

$$\begin{aligned}\cosh n\left(\tau - \tau_2\right) &= \frac{\mathrm{e}^{n\log g(r)} + \mathrm{e}^{-n\log g(r)}}{2} \\ &= \frac{g^n(r) + g^{-n}(r)}{2} + \mathcal{O}\left(a^2\right) \\ &= \frac{g^{2n}(r) + 1}{2g^n(r)} + \mathcal{O}\left(a^2\right).\end{aligned}$$

The first term in the sum of $\Delta K_{2,n}^{(2)}(\mathbf{x}_0, \mathbf{x})$ can be written as:

$$\begin{aligned}&\frac{\sinh n\left(\tau_1 - \tau_M\right)\cosh n\left(\tau_m - \tau_2\right)}{\cosh n\left(\tau_1 - \tau_2\right)} - \mathrm{e}^{-n(\tau_M - \tau_2)}\cosh n\left(\tau_m - \tau_2\right) \\ &= \cosh n\left(\tau_m - \tau_2\right)\frac{\sinh n\left(\tau_1 - \tau_M\right) - \mathrm{e}^{-n(\tau_M - \tau_2)}\cosh n\left(\tau_1 - \tau_2\right)}{\cosh n\left(\tau_1 - \tau_2\right)} \\ &= -\mathrm{e}^{-n(\tau_1 - \tau_2)}\frac{\cosh n\left(\tau_m - \tau_2\right)\cosh n\left(\tau_M - \tau_2\right)}{\cosh n\left(\tau_1 - \tau_2\right)} \\ &= -\frac{a^{2n}}{\left(1-c^2\right)^{2n}}\frac{\left[g^{2n}(r_m) + 1\right]\left[g^{2n}(r_M) + 1\right]}{2g^n(r_m)g^n(r_M)} + \mathcal{O}\left(a^{2(n+1)}\right).\end{aligned}$$

Furthermore, the second and third terms can be expanded as:

$$\begin{aligned}\mathrm{e}^{-n(2\tau_1 - \tau_2)}\cosh n\left(\tau_0 - \tau_2\right) &= \frac{a^{2n}c^n}{\left(1-c^2\right)^{2n}}\frac{g^{2n}(r_0) + 1}{g^n(r_0)} + \mathcal{O}\left(a^{2(n+1)}\right), \\ \mathrm{e}^{-n(2\tau_1 - \tau_2)}\cosh n\left(\tau - \tau_2\right) &= \frac{a^{2n}c^n}{\left(1-c^2\right)^{2n}}\frac{g^{2n}(r) + 1}{g^n(r)} + \mathcal{O}\left(a^{2(n+1)}\right),\end{aligned}$$

and the fourth term as:

$$\begin{aligned}\mathrm{e}^{-2n\tau_1} &= \frac{a^{2n}c^{2n}}{\left(1-c^2\right)^{2n}} + \mathcal{O}\left(a^{2(n+1)}\right), \\ \mathrm{e}^{-2n(2\tau_1 - \tau_2)} &= \frac{a^{4n}c^{2n}}{\left(1-c^2\right)^{4n}} + \mathcal{O}\left(a^{2(2n+1)}\right),\end{aligned}$$

where we have used the fact that:

$$\mathrm{e}^{-n(\tau_1 - \tau_2)} = \mathrm{e}^{-n\left(\log(1-c^2) - \log a + \mathcal{O}\left(a^2\right)\right)} = \mathrm{e}^{-n\log\left(1-c^2\right)}\mathrm{e}^{n\log a}\mathrm{e}^{\mathcal{O}\left(a^2\right)}$$

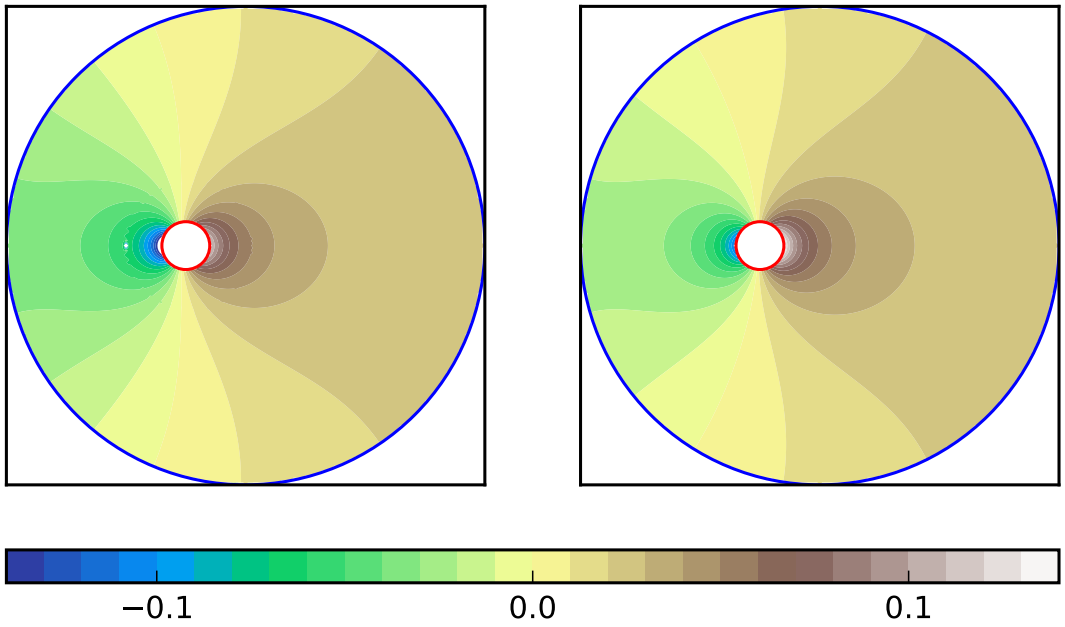

Figure 2.14: Left: difference between the Green's function $G_2^{(2)}(\mathbf{x}_0, \mathbf{x})$ obtained in (2.28) and $G_c(\mathbf{x}_0, \mathbf{x})$ from (2.31). Right: one term of the Green's function $\Delta G_2^{(2)}(\mathbf{x}_0, \mathbf{x})$ obtained in (2.32). For this figure we have used the following parameters: $a = 0.1$, $c = 0.25$ and $D = 0.5$.

$$
\begin{aligned}
&= \frac{a^n}{(1-c^2)^n} + \mathcal{O}\left(a^{n+1}\right), \\
\frac{1}{\cosh n\left(\tau_1 - \tau_2\right)} &= \frac{2}{\mathrm{e}^{n(\tau_1-\tau_2)} + \mathrm{e}^{-n(\tau_1-\tau_2)}} = \frac{2\mathrm{e}^{-n(\tau_1-\tau_2)}}{1 + \mathrm{e}^{-2n(\tau_1-\tau_2)}} \\
&= \frac{2\mathrm{e}^{-n\left(\log(1-c^2) - \log a + \mathcal{O}\left(a^2\right)\right)}}{1 + \mathrm{e}^{-2n(\log(1-c^2) - \log a + \mathcal{O}(a^2))}} = 2\frac{\frac{a^n}{(1-c^2)^n} + \mathcal{O}\left(a^{n+1}\right)}{1 + \frac{a^{2n}}{(1-c^2)^{2n}} + \mathcal{O}\left(a^{2n+1}\right)} \\
&= \frac{2a^n}{(1-c^2)^n} + \mathcal{O}\left(a^{n+1}\right).
\end{aligned}
$$

As a result, we obtain:

$$
\begin{aligned}
\Delta K_{2,n}^{(2)}(\mathbf{x}_0, \mathbf{x}) = \frac{a^{2n}}{2\left(1-c^2\right)^{2n}} \Bigg[&- \frac{\left[g^{2n}(r_m) + 1\right]\left[g^{2n}(r_M) + 1\right]}{g^n(r_m) g^n(r_M)} \cos n\left(\sigma - \sigma_0\right) \\
&+ c^n \left(\frac{g^{2n}(r_0) + 1}{g^n(r_0)} \cos n\sigma + \frac{g^{2n}(r) + 1}{g^n(r)} \cos n\sigma_0 \right) - c^{2n} \Bigg] + \mathcal{O}\left(a^{2(n+1)}\right).
\end{aligned}
$$

$$\Delta G_2^{(2)}(\mathbf{x}_0,\mathbf{x}) = \frac{a^2}{2\left(1-c^2\right)^2}\left[-\frac{\left[g^2(r_m)+1\right]\left[g^2(r_M)+1\right]}{g(r_m)g(r_M)}\cos\left(\sigma-\sigma_0\right)\right.$$
$$\left.+c\left(\frac{g^2(r_0)+1}{g(r_0)}\cos\sigma+\frac{g^2(r)+1}{g(r)}\cos\sigma_0\right)-c^2\right]+\mathcal{O}\left(a^4\right). \quad (2.32)$$

We plot (2.32) in the right panel of Figure 2.14. We observe that the approximation used by Condamin *et al.* (2007) for the absorbing boundary condition on ∂C_1 induces error proportional to a^2 when compared to analytic result derived in (2.28).

2.5 Hitting density on the cellular surface

We consider the scenario where molecules are produced in the nucleus, or other intracellular compartment, and may be released from it to diffuse until reaching the cellular surface. Given that the initial condition is uniformly distributed on ∂C_1, what is the density of the hitting (arrival) point on the cellular surface ∂C_2? Starting from Section 1.8 let us integrate $G_1^{(2)}(\mathbf{x}_0,\mathbf{x})$ over ∂C_1 to define

$$P^{(2)}(\mathbf{x}) = \frac{1}{2\pi a}\int_{\partial C_1} G_1^{(2)}(\mathbf{x}_0,\mathbf{x})\mathrm{d}\mathbf{x}_0,$$

to obtain the electrostatic potential of the cellular surface. The density of the hitting point on the cellular surface ∂C_2, is given as a function of the cartesian angle θ_2 (here θ_2 is the angle defined by $\mathbf{x}\in\partial C_2$, *i.e.* the angle $\angle\mathbf{O}\mathbf{x}_c\mathbf{x}$ where $\mathbf{x}_c$ is the centre of the cell and $\mathbf{O}$ is the origin of the coordinate system):

$$\varepsilon^{(2)}(\theta_2) = -D\left.\frac{\partial P^{(2)}(\mathbf{x})}{\partial \mathbf{n}_2}\right|_{\partial C_2},$$

where $\mathbf{n}_2$ is the unit normal outward vector to ∂C_2. Using the bipolar Green's function $G_1^{(2)}(\mathbf{x}_0,\mathbf{x})$ derived in Section 2.3 we can construct the hitting density in an eccentric annulus by first integrating over the inner boundary parametrised by $\tau=\tau_1$:

$$d\int_0^{2\pi}\frac{G_1^{(2)}(\tau,\sigma;\tau_1,\sigma_0)}{\cosh\tau_1-\cos\sigma_0}\mathrm{d}\sigma_0 = \frac{d}{D}\int_0^{2\pi}\left(\frac{\tau-\tau_2}{2\pi(\cosh\tau_1-\cos\sigma_0)}\right.$$
$$\left.+\sum_{n=1}^{+\infty}\frac{\sinh n(\tau-\tau_2)}{n\pi\cosh n(\tau_2-\tau_1)(\cosh\tau_1-\cos\sigma_0)}\cos n(\sigma-\sigma_0)\right)\mathrm{d}\sigma_0.$$

We know that:

$$\frac{1}{2\pi}\int_0^{2\pi}\frac{\tau-\tau_2}{\cosh\tau_1-\cos\sigma_0}\,\mathrm{d}\sigma_0=\frac{1}{2\pi}\frac{2\pi(\tau-\tau_2)}{\sqrt{\cosh^2\tau_1-1}}=\frac{\tau-\tau_2}{\sinh\tau_1}.$$

Using the integral formula (B.6) we obtain:

$$\frac{1}{\pi}\int_0^{2\pi}\frac{\cos n(\sigma-\sigma_0)}{\cosh\tau_1-\cos\sigma_0}\,\mathrm{d}\sigma_0=\frac{2\cos n\sigma}{\mathrm{e}^{n\tau_1}\sinh\tau_1}.$$

As a result, we have:

$$\begin{aligned}P^{(2)}(\mathbf{x})&=\frac{d}{2\pi a}\int_0^{2\pi}\frac{G_1^{(2)}(\tau,\sigma;\tau_0,\sigma_0)}{\cosh\tau_1-\cos\sigma_0}\,\mathrm{d}\sigma_0\\&=\frac{d}{2D\pi a}\int_0^{2\pi}\left(\frac{\tau-\tau_2}{2\pi\left(\cosh\tau_1-\cos\sigma_0\right)}\right.\\&\left.+\sum_{n=1}^{+\infty}\frac{\sinh n(\tau-\tau_2)}{n\pi\cosh n(\tau_2-\tau_1)\left(\cosh\tau_1-\cos\sigma_0\right)}\cos n(\sigma-\sigma_0)\right)\mathrm{d}\sigma_0\\&=\frac{d\left(\tau-\tau_2\right)}{2D\pi a\sinh\tau_1}+\frac{d}{D\pi a}\sum_{n=1}^{+\infty}\frac{\sinh n(\tau-\tau_2)\mathrm{e}^{-n\tau_1}}{n\sinh\tau_1\cosh n(\tau_2-\tau_1)}\cos n\sigma.\end{aligned}$$

Taking the $\tau-$derivative (see appendix B.1) evaluated at τ_2 and multiplying by $-D$ we obtain the hitting density:

$$\begin{aligned}\varepsilon^{(2)}(\theta_2)&=\frac{\cosh\tau_2-\cos\sigma_2}{2\pi a\sinh\tau_1}+\frac{\cosh\tau_2-\cos\sigma_2}{\pi a}\\&\times\sum_{n=1}^{+\infty}\frac{\mathrm{e}^{-n\tau_1}}{\sinh\tau_1\cosh n(\tau_2-\tau_1)}\cos n\sigma_2.\end{aligned}$$

As a result we have:

$$\varepsilon^{(2)}(\theta_2)=\frac{\cosh\tau_2-\cos\sigma_2}{2\pi a\sinh\tau_1}\left(1+\sum_{n=1}^{+\infty}\frac{2\mathrm{e}^{-n\tau_1}\cos n\sigma_2}{\cosh n(\tau_1-\tau_2)}\right),\tag{2.33}$$

where $\tan\sigma_2=\frac{d\sin\theta_2}{1+\sqrt{1+d^2}\cos\theta_2}$ and which we plot in Figure 2.15 in comparison to numerical simulations. Similarly to the case when there is no reflecting target, as seen in Figure 1.17, as the cellular displacement c increases the hitting density in increasingly centered at $\theta_2=0$.

However, we observe that as c increases, the density $\varepsilon^{(2)}(\theta_2)$ becomes bimodal, as opposed to unimodal in the case with no intracellular compartment (see Figure

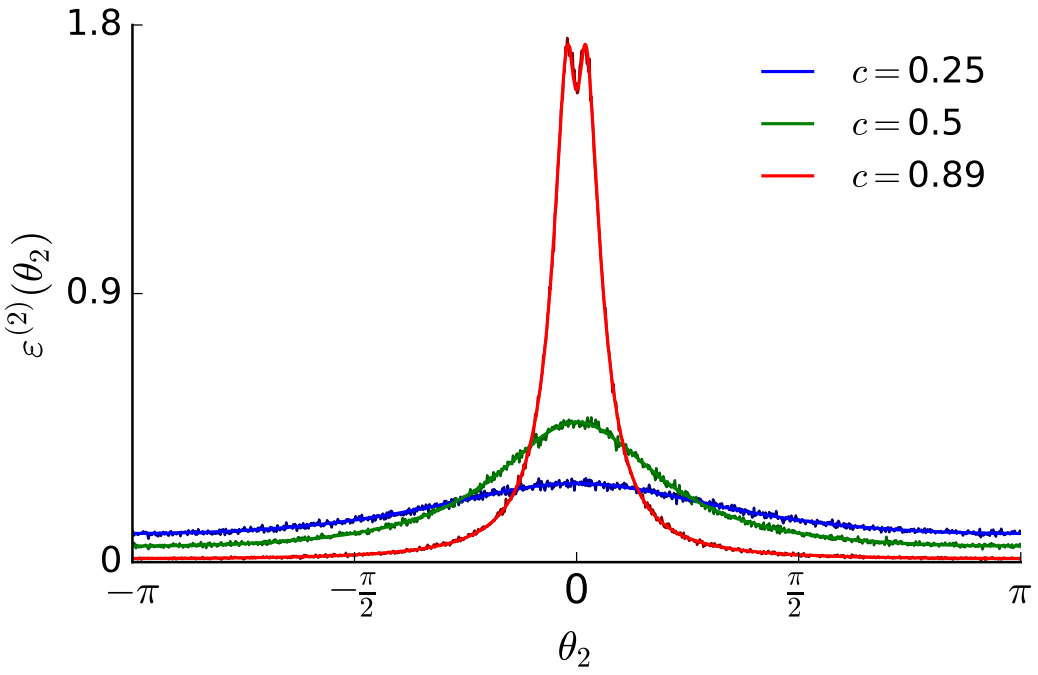

Figure 2.15: Plot of $\varepsilon^{(2)}(\theta_2)$ comparing the numerical simulation with the analytic result obtained in (2.33) as a function of θ_2 for $c = 0.25, 0.5$ and 0.89. The lighter colours represent the analytic result and the darker colours represent the numerical simulations. The numerical results have been obtained by having 10^5 particles uniformly distributed on the circle of radius a from Figure 2.1 and recording their endpoint. The lighter colours represent the analytic result and the darker colours represent the numerical simulations.

1.17), and we are interested in the bifurcation point c^* at which this occurs. In order to approximate it we use the truncated form of (2.33) with one term:

$$\varepsilon^{(2)}(\theta_2) \approx \frac{\cosh\tau_2 - \cos\sigma_2}{2\pi a \sinh\tau_1}\left(1 + \frac{2\mathrm{e}^{-\tau_1}\cos\sigma_2}{\cosh(\tau_1 - \tau_2)}\right), \tag{2.34}$$

and we want to find the coefficients of $(\sigma_2)^2$. As a result we have:

$$\left.\frac{d^2\varepsilon^{(2)}}{d\sigma^2}\right|_{\sigma_2=\pi} = \frac{1}{\pi a \sinh\tau_1}\left[1 - \frac{2\left(\cosh\tau_2 + 2\right)\mathrm{e}^{-\tau_1}}{\cosh\left(\tau_1 - \tau_2\right)}\right].$$

The bifurcation point c^* is the value of c such that $\frac{d^2\varepsilon^{(2)}}{d\sigma^2}\Big|_{\sigma_2=\pi} = 0$ which gives:

$$2\cosh\tau_2 + 4 = \cosh(\tau_1 - \tau_2)\,\mathrm{e}^{\tau_1}. \tag{2.35}$$

Using the following approximations:

$$\begin{aligned}\tau_1 &\approx \log(1-c^2) - \log a - \log c,\\ \tau_2 &\approx -\log c,\\ \tau_1 - \tau_2 &\approx \log(1-c^2) - \log a,\end{aligned}$$

equation (2.35) becomes the quartic equation:

$$c^4 - (2a^2+2)c^2 - 8a^2c - a^2 + 1 = 0, \tag{2.36}$$

the solution c^* of which we plot in Figure 2.16. We observe that the bifurcation point can be approximated by $c^* \approx 1-ka$, where k is a constant to be determined and $0 \le a < 1$. Using the binomial approximation:

$$(1-ka)^n = 1 - \binom{n}{1}ka + \binom{n}{2}k^2a^2 + \mathcal{O}\left(a^3\right),$$

gives us:

$$c^4 = (1-ka)^4 \approx 1 - 4ka + 6k^2a^2, \quad c^2 = (1-ka)^2 \approx 1 - 2ka + k^2a^2,$$

which we make use in (2.36):

$$1 - 4ka + 6k^2a^2 - \left(2a^2+2\right)\left(1 - 2ka + k^2a^2\right) - 8a^2(1-ka) - a^2 + 1 = 0.$$

Rearranging the above equation we obtain:

$$-2a^4k^2 + 12a^3k + \left(4k^2 - 11\right)a^2 = 0 \Rightarrow \left(4k^2-11\right) + \mathcal{O}(a^3) = 0. \tag{2.37}$$

The principle contribution to the left-hand side of (2.37) is given by terms of order a^2 from which we deduce:

$$\mathcal{O}\left(a^2\right): \qquad 4k^2 - 11 = 0 \Rightarrow k = \frac{\sqrt{11}}{2}, \tag{2.38}$$

which we plot as the aqua line in Figure 2.16.
We observe from Figure 2.16 that our approximation constitutes a lower bound for the bifurcation point c^*. An appropriate upper bound is represented by $c^* = 1-a$ (green line in Figure 2.16) given that the nucleus cannot escape the cell.

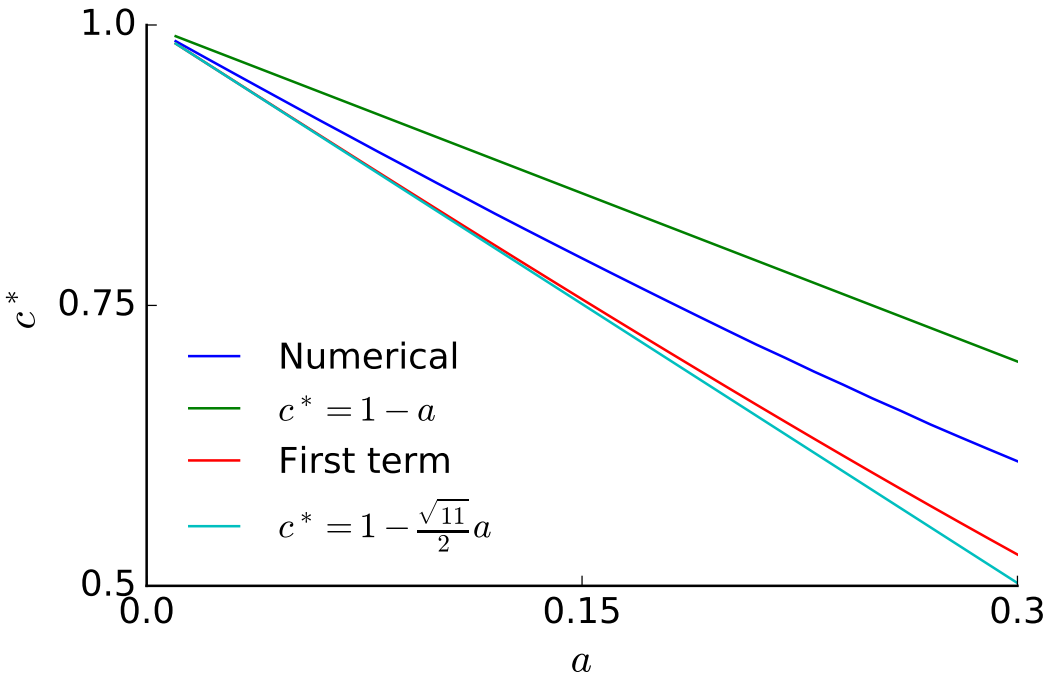

Figure 2.16: Plot of c^* comparing the numerical simulation (blue line) with the analytic result obtained in (2.36) as a function of a. The green line represents an upper bound for the bifurcation point. The aqua line represents the approximation $c^* = 1 - \frac{\sqrt{11}}{2}a$ from (2.38) and the red line represents the numerical estimation of c^* from the first term.

2.6 Mean transport times

We can now use the formula (3.4) to evaluate mean times by integrating the Green's functions over the domain C. We write

$$T_{1,2}^{(2)}(\theta_{1,2}, a, c) = R^2 d^2 \int_{\tau_2}^{\tau_1} \int_0^{2\pi} \frac{G_{1,2}^{(2)}(\mathbf{x}_0, \mathbf{x})}{(\cosh\tau - \cos\sigma)^2} \, \mathrm{d}\sigma \mathrm{d}\tau, \tag{2.39}$$

where

$$T_1^{(2)}(\theta_1, a, c) = E\left(t_1^{(2)}(\mathbf{x}_0)\right)$$
$$= \text{mean time for a particle starting at } \mathbf{x}_0 \in \partial C_1 \text{ to hit } \partial C_2,$$

and

$$T_2^{(2)}(\theta_2, a, c) = E\left(t_2^{(2)}(\mathbf{x}_0)\right)$$
$$= \text{mean time for a particle starting at } \mathbf{x}_0 \in \partial C_2 \text{ to hit } \partial C_1,$$

Here, $t_1^{(2)}(\mathbf{x}_0)$ and $t_2^{(2)}(\mathbf{x}_0)$ are the random variables defined as follows:

$t_1^{(2)}(\mathbf{x}_0)$ = time for a particle starting at $(\mathbf{x}_0)$ on the cellular nucleus to reach the cellular surface,

$t_2^{(2)}(\mathbf{x}_0)$ = time for a particle starting at $(\mathbf{x}_0)$ on the cellular surface to reach the nucleus.

We first consider the mean time to reach the cellular surface, starting on the nuclear surface. The initial point $\mathbf{x}_0 \in \partial C_1$ is specified by the angle θ_1 (here θ_1 is the angle defined by $\mathbf{x} \in \partial C_1$, *i.e.* the angle $\angle \mathbf{O}\mathbf{x}_n\mathbf{x}$ where $\mathbf{x}_n$ is the centre of the nucleus and $\mathbf{O}$ is the origin of the coordinate system):

$$\begin{aligned} T_1^{(2)}(\theta_1, a, c) &= \frac{R^2 d^2}{D} \int_{\tau_2}^{\tau_1} \int_0^{2\pi} \frac{G_1^{(2)}(\mathbf{x}_0, \mathbf{x})}{(\cosh\tau - \cos\sigma)^2} \,\mathrm{d}\sigma\mathrm{d}\tau \\ &= \frac{R^2 d^2}{D} \int_{\tau_2}^{\tau_1} \int_0^{2\pi} \left(\frac{\tau - \tau_2}{2\pi(\cosh\tau - \cos\sigma)^2} \right. \\ &\left. + \frac{1}{\pi} \sum_{n=1}^{+\infty} \frac{\cos n(\sigma - \sigma_1)}{n(\cosh\tau - \cos\sigma)^2} \frac{\sinh n(\tau - \tau_2)}{\cosh n(\tau_2 - \tau_1)} \right) \mathrm{d}\sigma\mathrm{d}\tau. \end{aligned} \tag{2.40}$$

and $\tan\sigma_1 = d\sin\theta_1/(a - \sqrt{a^2 + d^2}\cos\theta_1)$. From appendix B.3 we obtain:

$$\begin{aligned} \frac{1}{2\pi} \int_{\tau_2}^{\tau_1} \int_0^{2\pi} \frac{\tau - \tau_2}{(\cosh\tau - \cos\sigma)^2} \,\mathrm{d}\sigma\mathrm{d}\tau &= \int_{\tau_2}^{\tau_1} \frac{\cosh\tau}{\sinh^3\tau} (\tau - \tau_2) \,\mathrm{d}\tau \\ &= \frac{1}{2} \left(\frac{\tau_2 - \tau_1}{\sinh^2\tau_1} + \coth\tau_2 - \coth\tau_1 \right), \end{aligned} \tag{2.41}$$

and

$$\begin{aligned} &\frac{1}{\pi} \int_{\tau_2}^{\tau_1} \sinh n(\tau - \tau_2) \int_0^{2\pi} \frac{\cos n(\sigma - \sigma_1)}{(\cosh\tau - \cos\sigma)^2} \,\mathrm{d}\sigma\mathrm{d}\tau \\ &= \cos n\sigma_1 \int_{\tau_2}^{\tau_1} \sinh n(\tau - \tau_2) \mathrm{e}^{-n\tau} \frac{n\sinh\tau + \cosh\tau}{\sinh^3\tau} \,\mathrm{d}\tau \end{aligned}$$

$$= \left[\operatorname{csch}^2\tau_1 \mathrm{e}^{-n\tau_1}\sinh n(\tau_2-\tau_1) + n\operatorname{csch}\tau_1\operatorname{csch}\tau_2 \mathrm{e}^{-n\tau_2}\sinh(\tau_1-\tau_2)\right]\cos n\sigma_1. \tag{2.42}$$

As a result, using (2.41) and (2.42) in (2.40) we see that:

$$\frac{2D}{R^2}T_1^{(2)}(\theta_1,a,c) = d^2\left(\coth\tau_2-\coth\tau_1\right)+a^2(\tau_2-\tau_1)+2\sum_{n=1}^{+\infty}\frac{\cos n\sigma_1}{n\cosh n(\tau_2-\tau_1)} \times\left(a^2\mathrm{e}^{-n\tau_1}\sinh n(\tau_2-\tau_1)+na\mathrm{e}^{-n\tau_2}\sinh(\tau_1-\tau_2)\right). \tag{2.43}$$

Analogously

$$\frac{2D}{R^2}T_2^{(2)}(\theta_2,a,c) = d^2\left(\coth\tau_1-\coth\tau_2\right)+(\tau_1-\tau_2)+2\sum_{n=1}^{+\infty}\frac{d^2\cos n\sigma_2}{n\cosh n(\tau_2-\tau_1)} \times\left(\mathrm{e}^{-n\tau_2}\sinh n(\tau_1-\tau_2)-na\mathrm{e}^{-n\tau_1}\sinh(\tau_1-\tau_2)\right). \tag{2.44}$$

In the previous two results we made use of the following identities:

$$\frac{d}{\sinh\tau_1}=a,\quad \frac{d}{\sinh\tau_2}=1.$$

With the use of relationships $d^2\left(\coth\tau_2-\coth\tau_1\right)=dc$ and $a\sinh(\tau_1-\tau_2)=dc$, we find that (2.43) and (2.44) are simplified as:

$$\frac{2D}{R^2}T_1^{(2)}(\theta_1,a,c) = dc-a^2(\tau_1-\tau_2) + 4\sum_{n=1}^{+\infty}\frac{\cos n\sigma_1}{\mathrm{e}^{n\tau_1}}\left(\frac{dc}{1+\mathrm{e}^{-2n(\tau_1-\tau_2)}}-\frac{a^2}{2n}\tanh n\left(\tau_1-\tau_2\right)\right), \tag{2.45}$$

and

$$\frac{2D}{R^2}T_2^{(2)}(\theta_2,a,c) = \tau_1-\tau_2-dc - 4\sum_{n=1}^{+\infty}\frac{\cos n\sigma_2}{\mathrm{e}^{n\tau_2}}\left(\frac{dc}{1+\mathrm{e}^{2n(\tau_1-\tau_2)}}-\frac{1}{n}\tanh n\left(\tau_1-\tau_2\right)\right). \tag{2.46}$$

We plot $T_1^{(2)}\left(\theta_1,a,c\right)$ and $T_2^{(2)}\left(\theta_2,a,c\right)$ for $c=0.45$ in Figure 2.18 and we compare with numerical simulations. Additionally, we compare (2.46) with the formula we derived from Condamin *et al.* (2007) in (1.75) in Figure 2.17 for the case of $c=0.9$ and we observe that our formula is consistent with the numerical simulations, while the Condamin *et al.* (2007) mean time has large deviations at $\theta_2=0$ and $\theta_2=\pm\pi$.

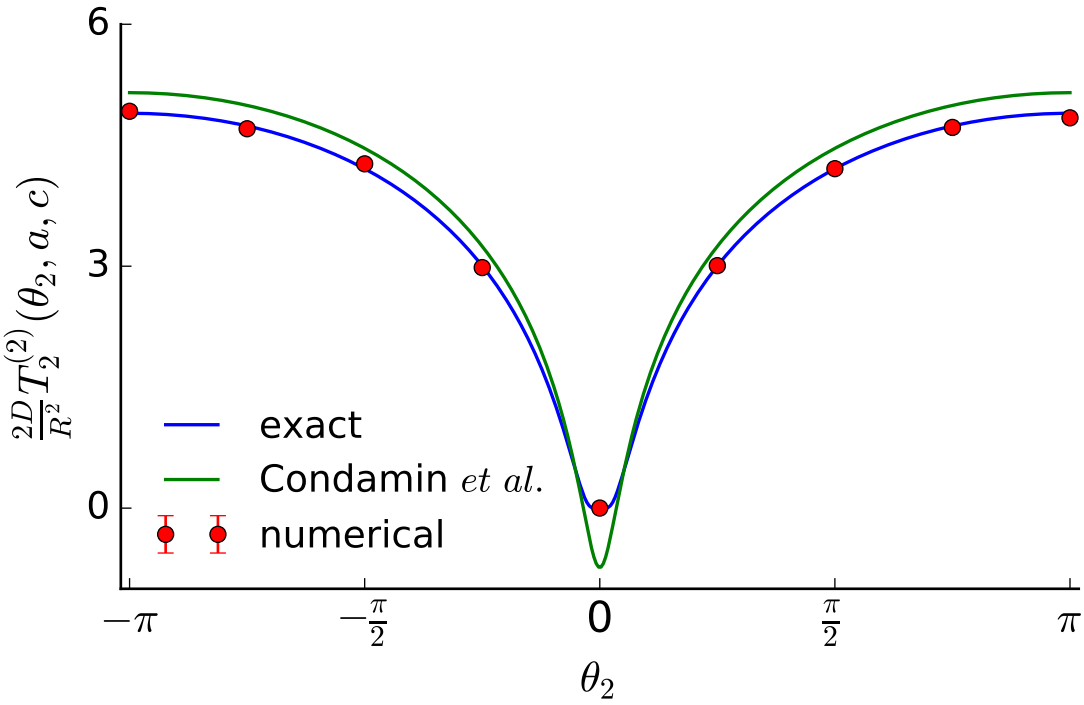

Figure 2.17: Plot of $T_2^{(2)}(\theta_2, a, c)$ as a function of θ_2. The blue line is the analytic series formula in (2.46), the green line is approximation derived from Condamin *et al.* (2007) in (1.75) and the red dots are numerical simulations. Here we have chosen the following parameter values: $a = 0.1, c = 0.9$.

2.6.1 Direct solution of Poisson's equation

An alternative way to find mean transport times, in bipolar coordinates but without first calculating Green's functions, is to solve the Poisson's equation El-Saden (1961); Snyder & Goldstein (1965)

$$\frac{D}{R^2}\Delta_{\mathbf{x}_0}T = -1.$$

We first consider the mean time $T_3(\tau_0, \sigma_0)$ to the cellular surface, starting from $\mathbf{x}_0 \in C$, where (τ_0, σ_0) are the bipolar coordinates of $\mathbf{x}_0$, and with the nucleus as an excluded region. The boundary conditions are

$$T_3(\tau_0, \sigma_0)|_{\tau_0=\tau_2} = 0, \tag{2.47a}$$

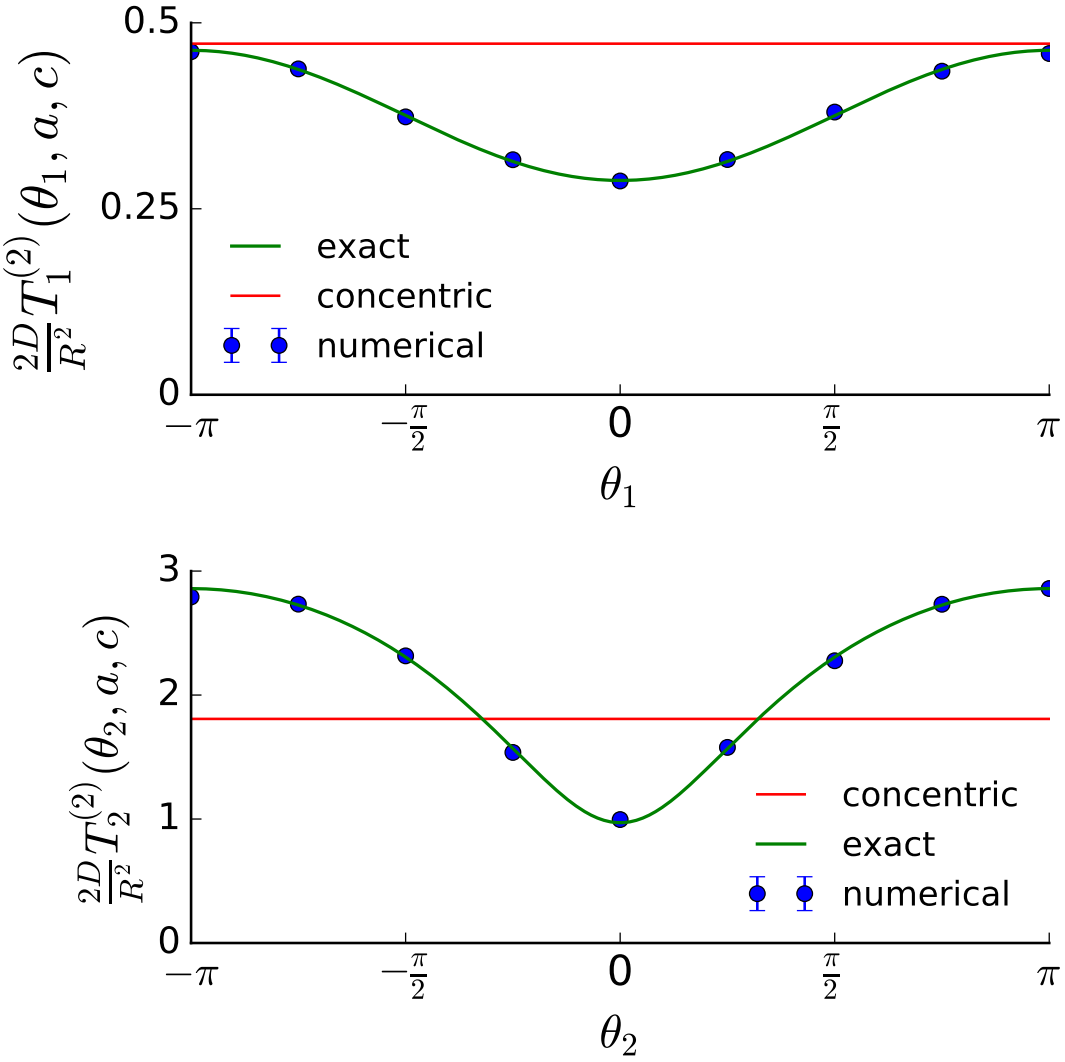

Figure 2.18: Plot of $T_1^{(2)}(\theta_1, a, c)$ shown in the upper plot as a function of θ_1 and of $T_2^{(2)}(\theta_2, a, c)$ shown in the lower plot as a function of θ_2. The green lines are the analytic series formulas obtained in (2.43) and (2.44), respectively. The blue dots are numerical simulations. The red lines are the concentric cases (1.12) and (1.16), respectively, with rescaled coordinates. Here we have chosen the following parameter values: $a = 0.1, c = 0.45$.

$$\frac{\partial}{\partial \tau} T_3(\tau_0, \sigma_0)\Big|_{\tau_0=\tau_1} = 0, \tag{2.47b}$$

$$\frac{\partial}{\partial\sigma}T_3(\tau_0,\sigma_0)\bigg|_{\sigma_0=0,\pi}=0. \tag{2.47c}$$

The last boundary condition is due to symmetry when $y=0,\sigma=0,\sigma=\pi$. Writing $T_3(\tau_0,\sigma_0)$ as the sum of the complementary function $T_c(\tau_0,\sigma_0)$ and a particular function $T_p(\tau_0,\sigma_0)$ where:

$$\begin{aligned}T_c(\tau_0,\sigma_0)&=A\tau_0+B+\left(Ce^{n\tau_0}+De^{-n\tau_0}\right)(E\cos n\sigma_0+F\sin n\sigma_0),\quad n\in\mathbb{N}\\ T_p(\tau_0,\sigma_0)&=-\frac{d^2R^2}{2D}\frac{\cosh\tau_0}{\cosh\tau_0-\cos\sigma_0},\end{aligned} \tag{2.48}$$

we obtain:

$$\begin{aligned}T_3(\tau_0,\sigma_0)=A\tau_0+B+\sum_{n=1}^{+\infty}\left(C_ne^{n\tau_0}+D_ne^{-n\tau_0}\right)(E_n\cos n\sigma_0+F_n\sin n\sigma_0)\\ -\frac{d^2R^2}{2D}\frac{\cosh\tau_0}{\cosh\tau_0-\cos\sigma_0}.\end{aligned}$$

Applying the boundary conditions (2.47c) the above equation reduces to:

$$T_3(\tau_0,\sigma_0)=A\tau_0+B+\sum_{n=1}^{+\infty}\left(C_ne^{n\tau_0}+D_ne^{-n\tau_0}\right)\cos n\sigma_0-\frac{d^2R^2}{2D}\frac{\cosh\tau_0}{\cosh\tau_0-\cos\sigma_0}.$$

Using the following identity (Morse & Feshbach, 2010, p.1215):

$$\frac{\cosh\tau_0}{\cosh\tau_0-\cos\sigma_0}=\coth\tau_0\left(1+2\sum_{n=1}^{+\infty}e^{-n\tau_0}\cos n\sigma_0\right),$$

we write:

$$\begin{aligned}T_3(\tau_0,\sigma_0)=A\tau_0+B+\sum_{n=1}^{+\infty}\left(C_ne^{n\tau_0}+D_ne^{-n\tau_0}\right)\cos n\sigma_0\\ -\frac{d^2R^2}{2D}\coth\tau_0\left(1+2\sum_{n=1}^{+\infty}e^{-n\tau_0}\cos n\sigma_0\right).\end{aligned}$$

From the boundary conditions (2.47a) and (2.47b) we deduce that:

$$\begin{aligned}A&=-\frac{d^2R^2}{2D}\frac{1}{\sinh^2\tau_1},\quad B=\frac{d^2R^2\tau_2}{2D\sinh^2\tau_1}+\frac{d^2}{2D}\coth\tau_2,\\ C_n&=-\frac{d^2R^2}{2D}\frac{e^{-n(\tau_1+\tau_2)}}{\cosh n(\tau_2-\tau_1)}\left(\frac{1}{n\sinh^2\tau_1}+\coth\tau_1\right)+\frac{d^2}{2D}\frac{e^{-n(\tau_1+\tau_2)}\coth\tau_2}{\cosh n(\tau_2-\tau_1)},\end{aligned}$$

$$D_n = \frac{d^2R^2}{2D}\frac{\mathrm{e}^{n(\tau_2-\tau_1)}}{\cosh n(\tau_2-\tau_1)}\left(\frac{1}{n\sinh^2\tau_1}+\coth\tau_1\right)-\frac{d^2}{2D}\frac{\mathrm{e}^{n(\tau_1-\tau_2)}\coth\tau_2}{\cosh n(\tau_2-\tau_1)},$$

where $n\in\mathbb{N}$, and as a result:

$$\begin{aligned}\frac{2D}{R^2}T_3(\tau_0,\sigma_0) = {} & d^2\left(\frac{\tau_2-\tau_0}{\sinh^2\tau_1}+\coth\tau_2-\coth\tau_0\right)\\ & +2d^2\sum_{n=1}^{+\infty}\left[\frac{\mathrm{e}^{-n\tau_1}\sinh n(\tau_2-\tau_0)}{\cosh n(\tau_2-\tau_1)}\left(\frac{1}{n\sinh^2\tau_1}+\coth\tau_1\right)\right.\\ & \left.+\frac{\coth\tau_2\mathrm{e}^{-n\tau_2}}{\cosh n(\tau_2-\tau_1)}\cosh n(\tau_1-\tau_0)-\coth\tau_0\mathrm{e}^{-n\tau_0}\right]\cos n\sigma_0. \qquad (2.49)\end{aligned}$$

Analogously

$$\begin{aligned}\frac{2D}{R^2}T_4(\tau_0,\sigma_0) = {} & d^2\left(\frac{\tau_1-\tau_0}{\sinh^2\tau_2}+\coth\tau_1-\coth\tau_0\right)\\ & +2d^2\sum_{n=1}^{+\infty}\left[\frac{\mathrm{e}^{-n\tau_2}\sinh n(\tau_1-\tau_0)}{\cosh n(\tau_2-\tau_1)}\left(\frac{1}{n\sinh^2\tau_2}+\coth\tau_2\right)\right.\\ & \left.+\frac{\coth\tau_1\mathrm{e}^{-n\tau_1}}{\cosh n(\tau_2-\tau_1)}\cosh n(\tau_2-\tau_0)-\coth\tau_0\mathrm{e}^{-n\tau_0}\right]\cos n\sigma_0, \qquad (2.50)\end{aligned}$$

where $T_4(\tau_0,\sigma_0)$ is the mean time to the nuclear surface, starting from $\mathbf{x}_0\in C$. We plot $T_3(\tau_0,\sigma_0)$ and $T_4(\tau_0,\sigma_0)$ in Figure 2.19.

2.6.2 Average mean time

We next obtain the average mean hitting times, $\bar{T}_1^{(2)}(a,c)$ and $\bar{T}_2^{(2)}(a,c)$, when the initial angles θ_1 and θ_2 are uniformly distributed. Firstly,

$$\bar{T}_1^{(2)}(a,c)=\int_0^{2\pi}\frac{T_1(\theta_1)}{2\pi a}\mathrm{d}\theta_1=\frac{d}{2\pi a}\int_0^{2\pi}\frac{T_1^{(2)}(\theta_1,a,c)}{\cosh\tau_1-\cos\sigma_1}\mathrm{d}\sigma_1. \qquad (2.51)$$

Using

$$\int_0^{2\pi}\frac{\cos n\sigma}{\cosh\tau-\cos\sigma}\mathrm{d}\sigma=\frac{2\pi}{\mathrm{e}^{n\tau}\sinh\tau},$$

we find

$$\frac{2D}{R^2}\bar{T}_1^{(2)}(a,c)=dc-a^2(\tau_1-\tau_2)$$

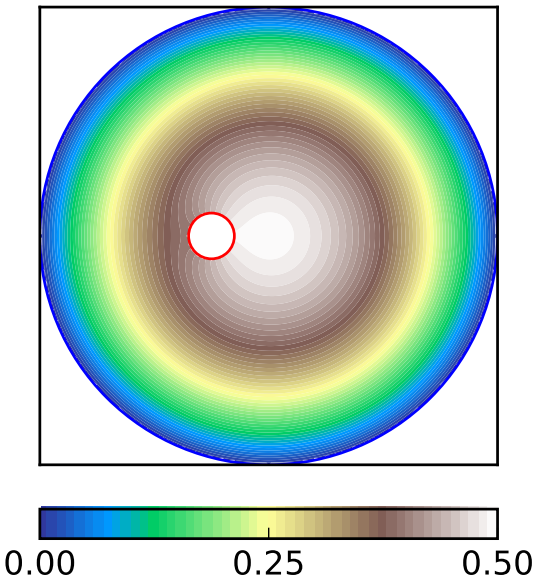

(a) $i = 1$

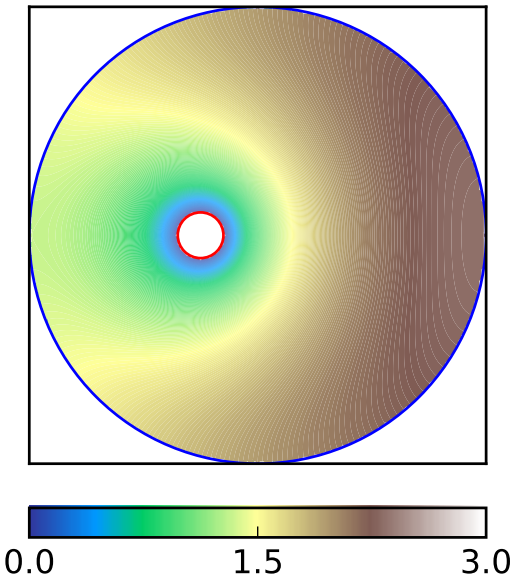

(b) $i = 2$

Figure 2.19: Plot of (2.49) shown in (a) and of (2.50) shown in (b). The values of the parameters for the above plots are $a = 0.1$ and $c = 0.25$.

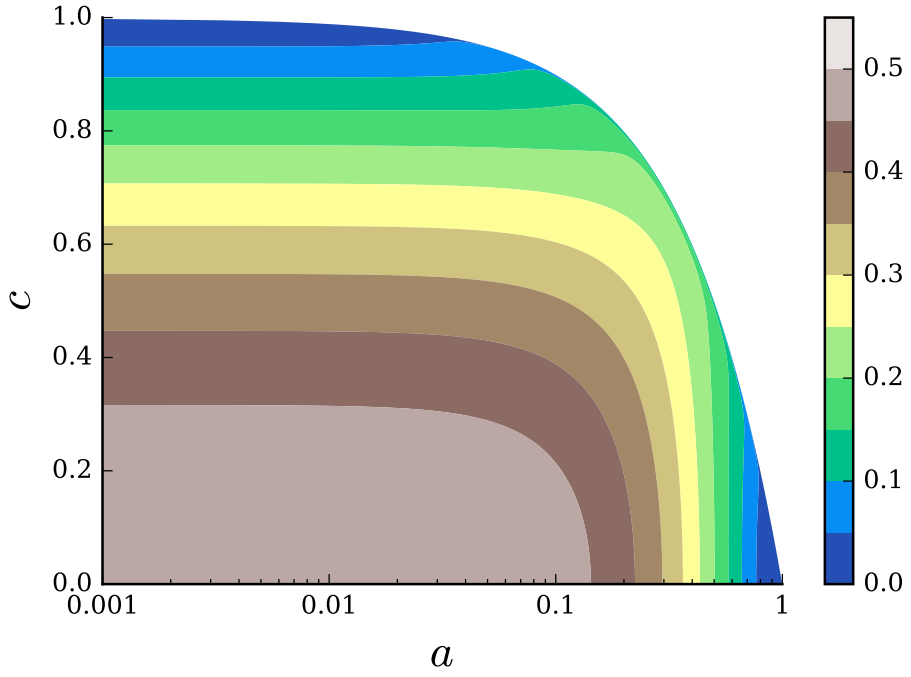

Figure 2.20: Contours of $\frac{2D}{R^2}\bar{T}_1^{(2)}(a,c)$ obtained in (2.52), the mean time for a particle, whose initial condition is uniformly distributed on the nuclear surface, to reach the cellular surface, as a function of the dimensionless parameters a and c.

$$+\,4\sum_{n=1}^{+\infty}\mathrm{e}^{-2n\tau_1}\left(\frac{dc}{1+\mathrm{e}^{-2n(\tau_1-\tau_2)}}-\frac{a^2}{2n}\tanh n\,(\tau_1-\tau_2)\right). \qquad (2.52)$$

The dependence on a and c is shown in Figure 2.20.
Similarly, the mean time for a particle, whose initial condition is uniformly distributed on the cellular surface, to reach the nucleus is given by

$$\begin{aligned}\frac{2D}{R^2}\bar{T}_2^{(2)}(a,c) =&\tau_1-\tau_2-dc\\ &+4\sum_{n=1}^{+\infty}\mathrm{e}^{-2n\tau_2}\left(\frac{1}{2n}\tanh n\,(\tau_1-\tau_2)-\frac{dc}{1+\mathrm{e}^{2n(\tau_1-\tau_2)}}\right). \qquad (2.53)\end{aligned}$$

The dependence on a and c is shown in Figure 2.21. Based on the results of Condamin *et al.* (2007) we have derived an approximation for $\bar{T}_2^{(2)}(a,c)$ in Cartesian

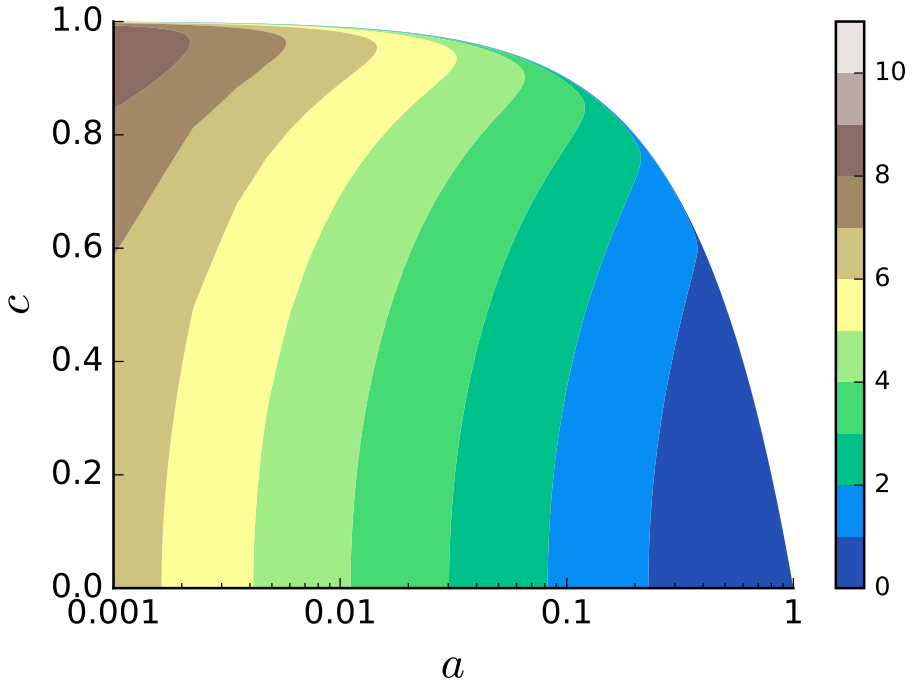

Figure 2.21: Contours of $\frac{2D}{R^2}\bar{T}_2^{(2)}(a,c)$ obtained in (2.53), the mean time for a particle, whose initial condition is uniformly distributed on the cellular surface, to reach the nuclear surface, as a function of the dimensionless parameters a and c.

coordinates (see equation (1.78)):

$$\frac{2D}{R^2}\bar{T}_2^{(2),C}(a,c) = \log\left(\frac{1}{a}\right) + \log\left(\frac{1}{1-c^2}\right) + \frac{c^2-1}{2}, \tag{2.54}$$

and we compare this result with our formula from (2.53) and numerical results in Figure 2.22.

2.6.3 Series expansion of mean times averaged over the reflecting surface

Given that $a < 1$ we will make use of the following expansions in powers of a:

$$d = \frac{1}{2c}\sqrt{(1^2+a^2-c^2)^2 - 4a^2b^2} = \frac{1-c^2}{2c}\sqrt{1 - \frac{2a^2(1+c^2)}{(1-c^2)^2} + \frac{a^4}{(1-c^2)^2}}$$

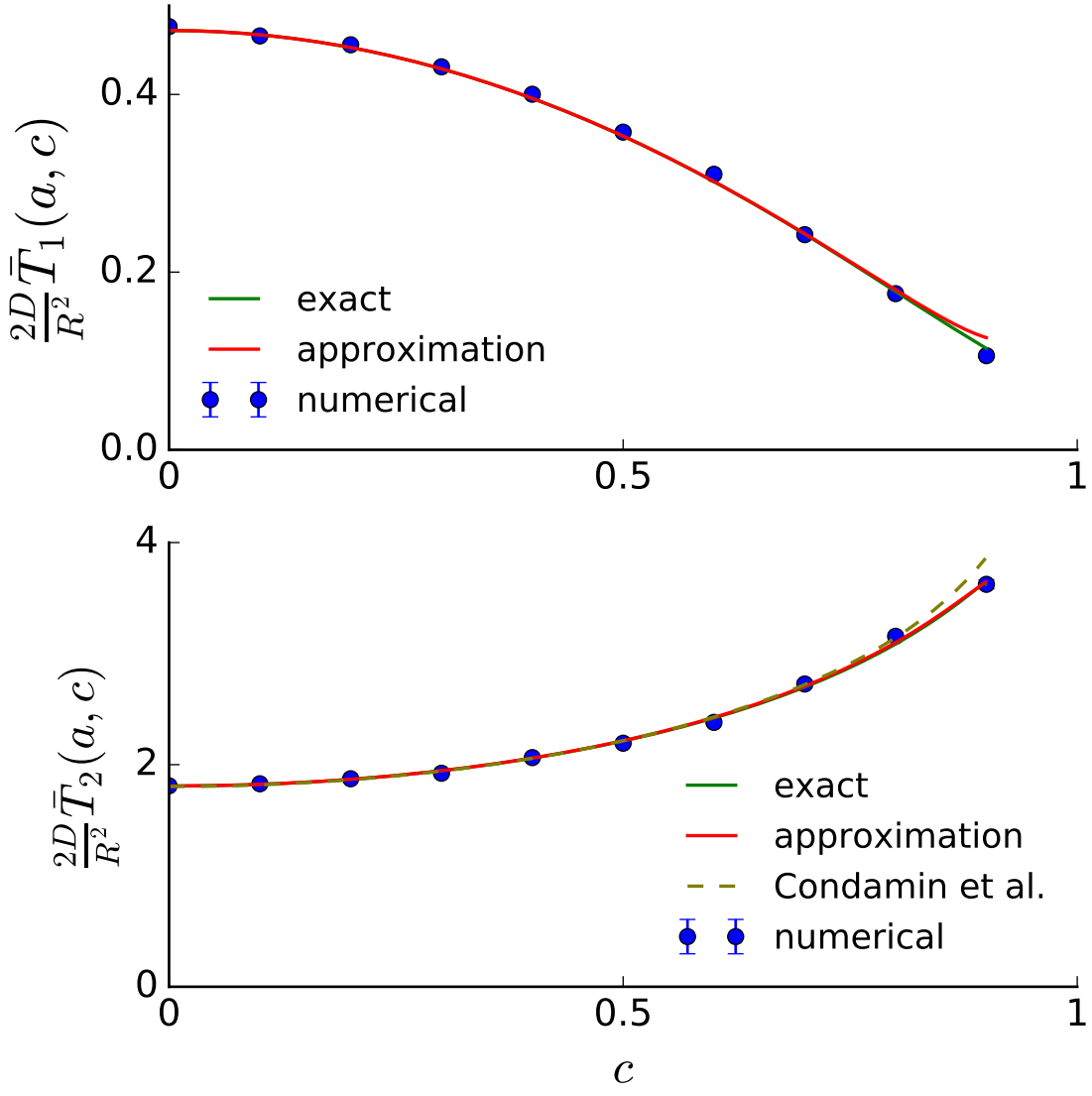

Figure 2.22: Plot of $\bar{T}_1^{(2)}(a,c)$ shown in the upper figure and of $\bar{T}_2^{(2)}(a,c)$ shown in the lower figure as a function of nuclear displacement c. The green lines are the analytic series formulas obtained in (2.52) and (2.53), respectively. The red lines are the approximations obtained in (2.57) and (2.60), respectively. The olive line in the lower plot represents the formula (2.61) obtained from Condamin *et al.* (2007). The blue dots are numerical simulations. For the numerical simulations we have used G.6.1.3 for $\bar{T}_1^{(2)}(a,c)$ and G.6.1.4 for $\bar{T}_2^{(2)}(a,c)$. This plot has been obtained using G.6.2.3. Here we have chosen the following parameter values: $a = 0.1$.

$$= \frac{1-c^2}{2c} - \frac{a^2(1+c^2)}{2c(1-c^2)} + \mathcal{O}(a^4),$$

$$\tau_1 = \log\left(\frac{d}{a} + \sqrt{1+\left(\frac{d}{a}\right)^2}\right) = \log\left(\frac{d}{a} + \frac{1-a^2-c^2}{2ac}\right)$$

$$= \log\left(\frac{1-c^2}{ac} - \frac{a}{c(1-c^2)} + \mathcal{O}(a^4)\right)$$

$$= \log\left(1-c^2\right) - \log a - \log c - \frac{a^2}{(1-c^2)^2} + \mathcal{O}(a^5),$$

$$\tau_2 = \log\left(d + \sqrt{1+d^2}\right) = \log\left(d + \frac{1-a^2+c^2}{2c}\right) = \log\left(\frac{1}{c} - \frac{a^2}{c(1-c^2)} + \mathcal{O}(a^4)\right)$$

$$= -\log c - \frac{a^2}{1-c^2} + \mathcal{O}(a^4),$$

to obtain a series expansion of:

$$\frac{2D}{R^2}\bar{T}_1^{(2)}(a,c) = dc - a^2(\tau_1 - \tau_2) + 4\sum_{n=1}^{+\infty} \mathrm{e}^{-2n\tau_1}\left(\frac{dc}{1+\mathrm{e}^{-2n(\tau_1-\tau_2)}} - \frac{a^2}{2n}\tanh n\,(\tau_1-\tau_2)\right), \tag{2.56}$$

in powers of a up to and including a^2. Making use of appendix B.4 and (2.55) we obtain:

$$\frac{2D}{R^2}\bar{T}_1^{(2)}(a,c) = \frac{1-c^2}{2} - \frac{a^2(1+c^2)}{2(1-c^2)} - a^2\left[\log\left(1-c^2\right) - \log a\right] + \mathcal{O}(a^4) + 4\sum_{n=1}^{+\infty}\left(\left(\frac{ac}{1-c^2}\right)^{2n} + \mathcal{O}(a^{(2+2n)})\right) \times \left[\frac{1-c^2}{2} + \mathcal{O}(a^{2n}) - \frac{a^2}{2n}\left(1 - 2\left(\frac{a}{1-c^2}\right)^{2n} + \mathcal{O}(a^{4n})\right)\right].$$

From which we deduce that:

$$\frac{2D}{R^2}\bar{T}_1^{(2)}(a,c) = \frac{1-c^2}{2} - a^2\log\frac{1}{a} - a^2\left[\log(1-c^2) + \frac{1-3c^2}{2(1-c^2)}\right] + \mathcal{O}(a^4), \tag{2.57}$$

which we plot in Figure 2.22 where we compare with numerical simulations and the analytic result (2.56). Analogously, we want to obtain a series expansion in powers of a for:

$$\frac{2D}{R^2}\bar{T}_2^{(2)}(a,c) = \tau_1 - \tau_2 - dc$$

$$+ 4 \sum_{n=1}^{+\infty} \mathrm{e}^{-2n\tau_2} \left(\frac{1}{2n} \tanh n \left(\tau_1 - \tau_2 \right) - \frac{dc}{1 + \mathrm{e}^{2n(\tau_1 - \tau_2)}} \right), \qquad (2.58)$$

and for that we will use:

$$\begin{aligned}
\mathrm{e}^{-2n\tau_2} &= \mathrm{e}^{-2n\left(-\log c - \frac{a^2}{1-c^2} + \mathcal{O}(a^4) \right)} = c^{2n} \left(1 + 2n \frac{a^2}{1-c^2} \right) + \mathcal{O}(a^4), \\
\frac{1}{1 + \mathrm{e}^{2n(\tau_1 - \tau_2)}} &= \frac{\mathrm{e}^{-2n(\tau_1 - \tau_2)}}{1 + \mathrm{e}^{-2n(\tau_1 - \tau_2)}} \\
&= \left[\left(\frac{a}{1-c^2} \right)^{2n} + \mathcal{O}(a^{(2+2n)}) \right] \left[1 - \left(\frac{a}{1-c^2} \right)^{2n} + \mathcal{O}(a^{(2+2n)}) \right] \\
&= \left(\frac{a}{1-c^2} \right)^{2n} + \mathcal{O}(a^{(2+2n)}).
\end{aligned}$$

As a result, we obtain:

$$\begin{aligned}
&\frac{2D}{R^2} \bar{T}_2^{(2)}(a, c) \\
&= \log\left(1 - c^2\right) - \log a - \frac{a^2}{(1-c^2)^2} + \frac{a^2}{1-c^2} - \frac{1-c^2}{2} + \frac{a^2(1+c^2)}{2(1-c^2)} + \mathcal{O}(a^4) \\
&+ 4 \sum_{n=1}^{+\infty} \left[c^{2n} \left(1 + 2n \frac{a^2}{1-c^2} \right) + \mathcal{O}(a^4) \right] \left[\frac{1}{2n} \left(1 - 2 \left(\frac{a}{1-c^2} \right)^{2n} + \mathcal{O}(a^{4n}) \right) \right. \\
&\left. - \left(\frac{1-c^2}{2} - \frac{a^2(1+c^2)}{2(1-c^2)} + \mathcal{O}(a^4) \right) \left(\left(\frac{a}{1-c^2} \right)^{2n} + \mathcal{O}(a^{(2+2n)}) \right) \right),
\end{aligned}$$

which, while keeping terms up to and including a^2, becomes:

$$\begin{aligned}
\frac{2D}{R^2} \bar{T}_2^{(2)}(a, c) = \log\left(1 - c^2\right) - \log a - \frac{a^2}{(1-c^2)^2} + \frac{a^2}{1-c^2} - \frac{1-c^2}{2} + \frac{a^2(1+c^2)}{2(1-c^2)} + \\
+ 4 \sum_{n=1}^{+\infty} \frac{1}{2n} \left[c^{2n} \left(1 + 2n \frac{a^2}{1-c^2} \right) \right] - \frac{4a^2c^2}{(1-c^2)^2} - \frac{2a^2c^2}{1-c^2} + \mathcal{O}(a^4).
\end{aligned} \qquad (2.59)$$

Making use of the following expansions:

$$\begin{aligned}
\sum_{n=1}^{+\infty} \frac{c^{2n}}{n} &= -\log\left(1 - c^2\right), \\
\sum_{n=1}^{+\infty} c^{2n} &= \sum_{n=0}^{+\infty} c^{2n} - 1 = \frac{1}{1-c^2} - 1 = \frac{c^2}{1-c^2},
\end{aligned}$$

we rewrite (2.59) as:

$$\begin{aligned}\frac{2D}{R^2}\bar{T}_2^{(2)}(a,c) &= \frac{c^2-1}{2} - \log\left(1-c^2\right) + \log\frac{1}{a} + a^2\left[\frac{1}{1-c^2} - \frac{1}{(1-c^2)^2}\right.\\ &= \left. +\frac{1+c^2}{2\left(1-c^2\right)} - \frac{4c^2}{\left(1-c^2\right)^2} - \frac{2c^2}{1-c^2} + \frac{4c^2}{\left(1-c^2\right)^2}\right] + \mathcal{O}(a^4),\end{aligned}$$

and, finally, as:

$$\frac{2D}{R^2}\bar{T}_2^{(2)}(a,c) = \frac{c^2-1}{2} - \log(1-c^2) + \log\frac{1}{a} + \frac{a^2}{2}\frac{1-4c^2+c^4}{(1-c^2)^2} + \mathcal{O}(a^4), \quad (2.60)$$

which we plot in Figure 2.22 where we compare with numerical simulations and the analytic result (2.58).

Using Condamin *et al.* (2007) we deduced the following approximation for $\bar{T}_2^{(2)}(a,c)$ in (1.78):

$$\frac{2D}{R^2}\bar{T}_2^{2,C}(a,c) = \log\left(\frac{1}{a}\right) + \log\left(\frac{1}{1-c^2}\right) - \frac{1-c^2}{2}, \quad (2.61)$$

and we observe that:

$$\frac{2D}{R^2}\bar{T}_2^{(2)}(a,c) = \frac{2D}{R^2}\bar{T}_2^{2,C}(a,c) + \frac{a^2}{4D}\frac{1-4c^2+c^4}{(1-c^2)^2} + \mathcal{O}(a^4).$$

2.6.4 Global mean first passage time

In order to obtain the global mean first passage time we integrate $\bar{T}_1^{(2)}(a,c)$ and $\bar{T}_2^{(2)}(a,c)$ over all possible positions of c:

$$\bar{\bar{T}}^{(2)}(a) = \frac{\int_0^{1-a} c\bar{T}^{(2)}(a,c)\,\mathrm{d}c}{\int_0^{1-a} c\,\mathrm{d}c},$$

to obtain:

$$\begin{aligned}\frac{2D}{R^2}\bar{\bar{T}}_1^{(2),1}(a) &= \frac{1+2a-3a^2}{4D} - a^2\log(2-a) + \mathcal{O}(a^3),\\ \frac{2D}{R^2}\bar{\bar{T}}_2^{(2),1}(a) &= \frac{3-2a+3a^2}{4D} + \log\frac{1}{a} + \frac{2a}{1-a}\log(2a-a^2) + \frac{a}{a-2} + \mathcal{O}(a^3),\end{aligned} \quad (2.62)$$

which we plot in Figure 2.23(a) and 2.23(b), respectively.

Using the following expansions:

$$\begin{aligned}\frac{a}{1-a} &= a + a^2 + \mathcal{O}(a^3),\\ \frac{a}{a-2} &= -\frac{a}{2} - \frac{a^2}{4} + \mathcal{O}(a^3),\\ \log(2-a) &= \log(2) - a/2 + \mathcal{O}(a^2),\end{aligned}$$

in (2.62) we obtain:

$$\begin{aligned}\frac{2D}{R^2}\bar{\bar{T}}_1^{(2),2}(a) &= \frac{1 + 2a - (3 + 4\log 2)\, a^2}{4} + \mathcal{O}(a^3),\\ \frac{2D}{R^2}\bar{\bar{T}}_2^{(2),2}(a) &= \frac{3 - (8\log 2 - 4)\, a + (8\log 2 - 2)\, a^2}{4}\\ &\quad + \left(2a^2 + 2a - 1\right)\log a + \mathcal{O}(a^3),\end{aligned} \tag{2.63}$$

which we plot in Figure 2.23(a) and 2.23(b), respectively, and compare with numerical simulations. We observe that for small values of a the global mean time $\bar{\bar{T}}_1^{(2)}(a)$ is an increasing function, reaching a maximum at $a \approx 0.173$, because the nucleus acts as a barrier for Brownian motion, at large values of c, and it takes longer to hit the cellular surface. As a increases the space that a Brownian motion can traverse decreases in such a way that the previously stated effect is cancelled and reversed. From 2.23(b) we observe that $\bar{\bar{T}}_2^{(2)}(a)$ is a decreasing function of a because of the fact that as a increases the path of a Brownian motion starting uniformly on the cellular surface decreases for the majority of values of c (see Figure 2.21).

2.6.5 Mean round-trip time

We want to calculate the average mean time for a particle to diffuse from the inner boundary to the outer boundary of an eccentric annulus and back. The end point of the outward path on the outer boundary is the starting point of the inward path. This affects the calculations for $\bar{T}_2^{(2)}(a, c)$ where we previously assumed that the particle starts uniformly on the outer boundary. To take this into account we will use the hitting density $\varepsilon^{(2)}(\theta_2)$, calculated in Section 2.5, as the initial density:

$$\bar{T}_2^{\varepsilon,2}(a, c) = \int_0^{2\pi} \varepsilon^{(2)}(\theta_2) T_2^{(2)}(\theta_2, a, c)\, \mathrm{d}\theta_2$$

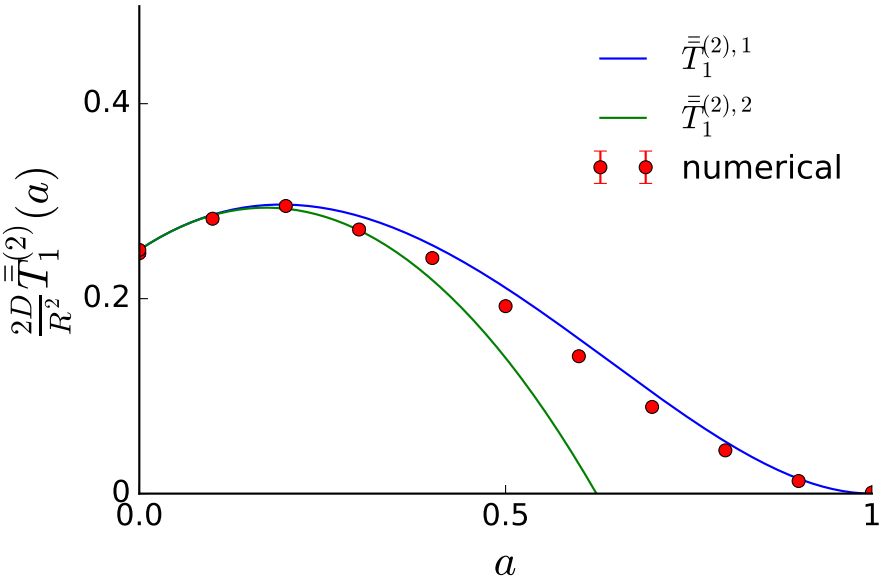

(a) $i = 1$

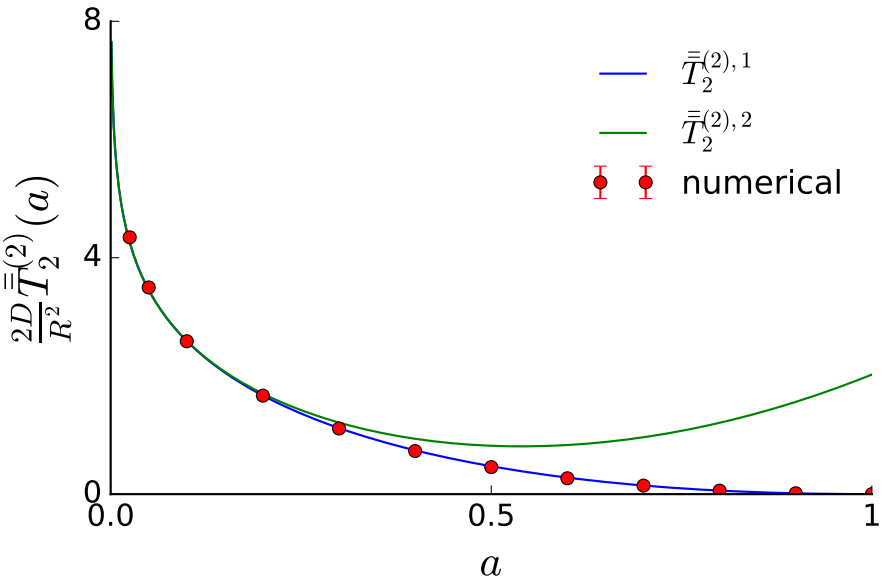

(b) $i = 2$

Figure 2.23: Plot of $\bar{\bar{T}}_1^{(2)}$ shown in (a) and of $\bar{\bar{T}}_2^{(2)}$ shown in (b). The blue lines are the expansion formulas obtained in (2.62), the green lines represent the expansion formulas obtained in (2.63), and the red dots are numerical simulations.

Using (2.33), (2.46) and Appendix B.2 (we can write $\varepsilon^{(2)}(\theta_2)$ and $T_2^{(2)}(\theta_2, a, c)$ as Fourier series) we write the integrand in the form:

$$\varepsilon^{(2)}(\theta_2)T_2^{(2)}(\theta_2, a, c) = \frac{R^2}{2D}\frac{1}{2\pi}\left(C_0/2 + \sum_{n=1}^{+\infty} C_n \cos n\sigma_0\right)$$

Then

$$\begin{aligned}\frac{2D}{R^2}\bar{T}_2^{\varepsilon,2}(a,c) &= \frac{d}{2\pi}\int_0^{2\pi} \frac{C_0/2 + \sum_{n=1}^{+\infty} C_n \cos n\sigma_0}{\cosh\tau_2 - \cos\sigma_0}\,\mathrm{d}\sigma_0 \\ &= \frac{C_0}{2} + \sum_{n=1}^{+\infty} \mathrm{e}^{-n\tau_2} C_n, \end{aligned} \tag{2.64}$$

where

$$C_n = \frac{1}{2}\sum_{k=-\infty}^{+\infty} A_{|n-k|}B_{|k|},$$

and

$$\begin{aligned} A_0 &= 2\left[(\tau_1 - \tau_2) - dc\right], \\ A_n &= 4\mathrm{e}^{-n\tau_2}\left(\frac{1}{2n}\tanh n(\tau_1 - \tau_2) - \frac{dc}{1 + \mathrm{e}^{2n(\tau_1 - \tau_2)}}\right), \quad n \in \mathbb{N} \end{aligned}$$

and

$$\begin{aligned} B_0 &= \frac{\cosh\tau_2}{d} - \frac{\mathrm{e}^{-\tau_1}}{d\cosh(\tau_2 - \tau_1)}, \\ B_n &= \frac{2\mathrm{e}^{-n\tau_1}\cosh\tau_2}{d\cosh n(\tau_2 - \tau_1)} \\ &\quad - \frac{1}{d}\left[\frac{\mathrm{e}^{-(n-1)\tau_1}}{\cosh[(n-1)(\tau_2 - \tau_1)]} + \frac{\mathrm{e}^{-(n+1)\tau_1}}{\cosh[(n+1)(\tau_2 - \tau_1)]}\right], \quad n \in \mathbb{N}. \end{aligned}$$

In (2.64) we used Appendix (B.6) to evaluate the integral:

$$\int_0^{2\pi} \frac{\cos n\sigma_0}{\cosh\tau_2 - \cos\sigma_0}\,\mathrm{d}\sigma_0 = \frac{2\pi\mathrm{e}^{-n\tau_2}}{\sinh\tau_2},$$

In Figure 2.24, we plot $\bar{T}_1(a,c) + \bar{T}_2^{\varepsilon,2}(a,c)$ (where $\bar{T}_1(a,c)$ is the mean time obtained in (2.52)) and compare with numerical simulations. We deduce from Figure 2.22 and 2.24 that, while $\bar{T}_2^{(2)}(a,c)$ is an increasing function of c, $\bar{T}_2^{\varepsilon,2}(a,c)$ is a decreasing function which is explained by the fact that the initial position of the Brownian particle, on the cellular surface, is concentrated at the point of shortest distance to the nuclear surface (see Figure 2.15).

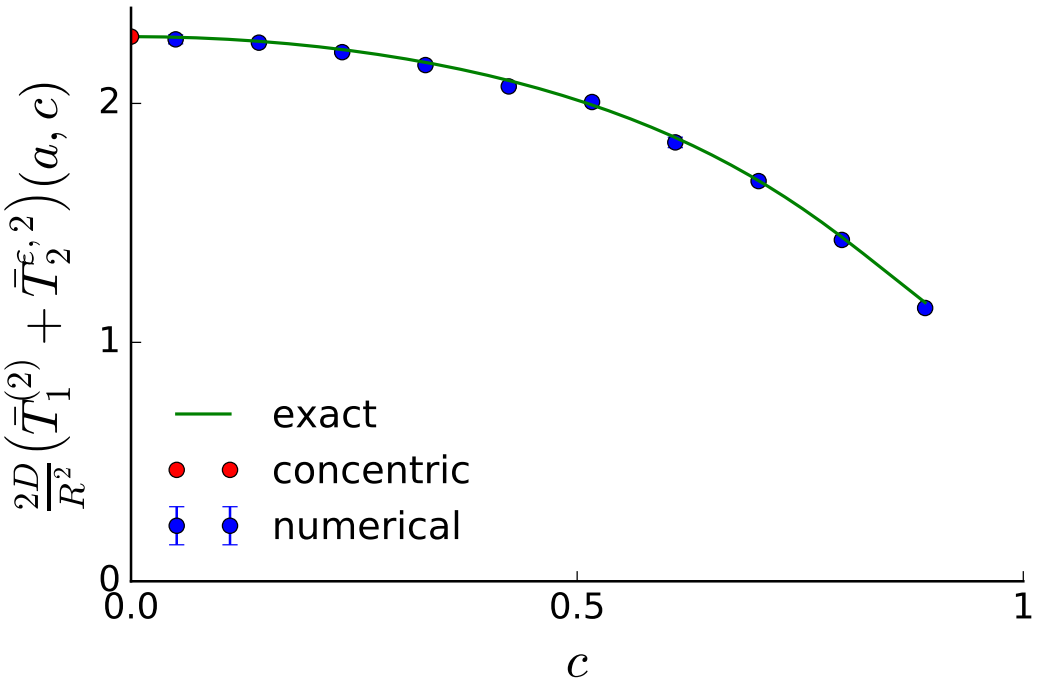

Figure 2.24: Mean round-trip time $\bar{T}_1 + \bar{T}_2^{\varepsilon,2}$ as a function of c. The green line is the sum of analytic results (2.52) and (2.64). The numerical results have been obtained by having 2×10^3 particles uniformly distributed on the circle of radius a from Figure 2.1 and recording the mean time for them to return given that they hit the outer circle. The blue dots are numerical simulations. The red dot at $c = 0$ is the sum of (1.12) and (1.16), with rescaled coordinates, the analytic formula derived by solving the time Poisson's equation for a concentric annulus (see Section 1.2). For the numerical simulations we have used G.6.1.2 and this plot has been obtained using G.6.2.2. For our simulations we have chosen the following parameter values: $a = 0.1$.

2.7 Higher moments of the first passage times

In the previous section we have calculated the mean time for a particle to diffuse from the nucleus to the cellular surface and vice versa. Subsequently, the question of higher order moments arises and we will investigate it in this section starting by defining $\mu_{n,i}^{(2)}(\mathbf{x}_0)$ to be the $n-$th moment of $t_i^{(2)}(\mathbf{x}_0)$, $i \in \{1,2\}$, which are

random variables defined as:

$$t_i^{(2)}(\mathbf{x}_0) = \text{time for a particle starting at } \mathbf{x}_0 \in \partial C_{3-i} \text{ to reach } \partial C_i.$$

The higher order moment satisfy the following system of equations(Condamin *et al.*, 2007, p. 021111):

$$\begin{aligned}
\frac{D}{R^2}\nabla^2 \mu_{n,i}^{(2)}(\mathbf{x}) &= -n\mu_{n-1,i}^{(2)}(\mathbf{x}), \quad \text{if } \mathbf{x} \in C, \\
\mu_{n,i}^{(2)}(\mathbf{x}) &= 0, \quad \text{if } \mathbf{x} \in \partial C_{3-i}, \\
\frac{\partial \mu_{n,i}^{(2)}}{\partial \mathbf{n}_i}(\mathbf{x}) &= 0, \quad \text{if } \mathbf{x} \in \partial C_i.
\end{aligned}$$

We know that the moments $\mu_{n,i}^{(2)}$ are given by (Condamin *et al.*, 2007, p. 021111):

$$\mu_{n,i}^{(2)}(\theta_i, a, c) = R^2 n \int_C G_i^{(2)}(\mathbf{x}_0, \mathbf{x}) \mu_{n-1,i}^{(2)}(\mathbf{x})\, \mathrm{d}\mathbf{x},$$

where $G_i^{(2)}$ is the Green's function obtained in (2.13) for $i = 1$ and in (2.28) for $i = 2$, respectively. Using the fact that $\mu_{1,1}^{(2)}(\mathbf{x}) = T_3(\tau, \sigma)$ and $\mu_{1,2}^{(2)}(\mathbf{x}) = T_4(\tau, \sigma)$ we deduce that:

$$\mu_{2,1}^{(2)}(\theta_1, a, c) = 2R^2 d^2 \int_{\tau_2}^{\tau_1} \int_0^{2\pi} \frac{G_1^{(2)}(\mathbf{x}_0, \mathbf{x}) T_3(\tau, \sigma)}{(\cosh\tau - \cos\sigma)^2}\, \mathrm{d}\sigma \mathrm{d}\tau,$$

$$\mu_{2,2}^{(2)}(\theta_2, a, c) = 2R^2 d^2 \int_{\tau_2}^{\tau_1} \int_0^{2\pi} \frac{G_2^{(2)}(\mathbf{x}_0, \mathbf{x}) T_4(\tau, \sigma)}{(\cosh\tau - \cos\sigma)^2}\, \mathrm{d}\sigma \mathrm{d}\tau,$$

where $T_3(\tau, \sigma)$ and $T_4(\tau, \sigma)$ are the mean times derived in (2.49) and (2.50), respectively.

From (2.49) we know that the mean time $T_3(\tau, \sigma)$ can we written as:

$$\begin{aligned}
T_3(\tau, \sigma) = {} & \frac{d^2 R^2}{2D}\left(\frac{\tau_2 - \tau}{\sinh^2 \tau_1} + \coth\tau_2 - \coth\tau\right) \\
& + \frac{d^2 R^2}{D} \sum_{n=1}^{+\infty} \left[\frac{\mathrm{e}^{-n\tau_1} \sinh n(\tau_2 - \tau)}{\cosh n(\tau_2 - \tau_1)} \left(\frac{1}{n \sinh^2 \tau_1} + \coth\tau_1\right)\right. \\
& \left. + \frac{\coth\tau_2 \mathrm{e}^{-n\tau_2}}{\cosh n(\tau_2 - \tau_1)} \cosh n(\tau_1 - \tau) - \coth\tau \mathrm{e}^{-n\tau}\right] \cos n\sigma, \\
\frac{2D}{R^2} T_3(\tau, \sigma) = {} & A^1(\tau) + \sum_{n=1}^{+\infty} B_n^1(\tau) \cos n\sigma,
\end{aligned}$$

where

$$
\begin{aligned}
A^1(\tau) &= d^2\left(\frac{\tau_2-\tau}{\sinh^2\tau_1}+\coth\tau_2-\coth\tau\right),\\
B_n^1(\tau) &= 2d^2\left[\frac{\mathrm{e}^{-n\tau_1}\sinh n(\tau_2-\tau)}{\cosh n(\tau_2-\tau_1)}\left(\frac{1}{n\sinh^2\tau_1}+\coth\tau_1\right)\right.\\
&\quad\left.+\frac{\coth\tau_2\mathrm{e}^{-n\tau_2}}{\cosh n(\tau_2-\tau_1)}\cosh n(\tau_1-\tau)-\coth\tau\mathrm{e}^{-n\tau}\right],
\end{aligned}
$$

Analogously, we know from (2.50) that:

$$
\begin{aligned}
T_4(\tau,\sigma) &= \frac{d^2R^2}{2D}\left(\frac{\tau_1-\tau}{\sinh^2\tau_2}+\coth\tau_1-\coth\tau\right)\\
&\quad+\frac{d^2R^2}{D}\sum_{n=1}^{+\infty}\left[\frac{\mathrm{e}^{-n\tau_2}\sinh n(\tau_1-\tau)}{\cosh n(\tau_2-\tau_1)}\left(\frac{1}{n\sinh^2\tau_2}+\coth\tau_2\right)\right.\\
&\quad\left.+\frac{\coth\tau_1\mathrm{e}^{-n\tau_1}}{\cosh n(\tau_2-\tau_1)}\cosh n(\tau_2-\tau)-\coth\tau\mathrm{e}^{-n\tau}\right]\cos n\sigma,\\
\frac{2D}{R^2}T_4(\tau,\sigma) &= A^2(\tau)+\sum_{n=1}^{+\infty}B_n^2(\tau)\cos n\sigma,
\end{aligned}
$$

where

$$
\begin{aligned}
A^2(\tau) &= d^2\left(\frac{\tau_1-\tau}{\sinh^2\tau_2}+\coth\tau_1-\coth\tau\right),\\
B_n^2(\tau) &= 2d^2\left[\frac{\mathrm{e}^{-n\tau_2}\sinh n(\tau_1-\tau)}{\cosh n(\tau_2-\tau_1)}\left(\frac{1}{n\sinh^2\tau_2}+\coth\tau_2\right)\right.\\
&\quad\left.+\frac{\coth\tau_1\mathrm{e}^{-n\tau_1}}{\cosh n(\tau_2-\tau_1)}\cosh n(\tau_2-\tau)-\coth\tau\mathrm{e}^{-n\tau}\right].
\end{aligned}
$$

From (2.13) and (2.28) we have the Green's functions:

$$
2DG_1^{(2)}(\mathbf{x}_0,\mathbf{x}) = \underbrace{\frac{\tau_m-\tau_2}{\pi}}_{Q_{1,0}(\tau,\tau_0)}+2\sum_{n=1}^{+\infty}\underbrace{\frac{K_{1,n}^{(2)}(\tau,\tau_0)}{n\pi}}_{Q_{1,n}(\tau,\tau_0)}\cos n(\sigma-\sigma_0),
$$

and

$$
2DG_2^{(2)}(\mathbf{x}_0,\mathbf{x}) = \underbrace{\frac{\tau_1-\tau_M}{\pi}}_{Q_{2,0}(\tau,\tau_0)}+2\sum_{n=1}^{+\infty}\underbrace{\frac{K_{2,n}^{(2)}(\tau,\tau_0)}{n\pi}}_{Q_{2,n}(\tau,\tau_0)}\cos n(\sigma-\sigma_0).
$$

We derive $\mu_{2,1}^{(2)}(\theta_1, a, c)$ and then proceed, by analogy, to obtain the second moment of $t_2^{(2)}(\mathbf{x}_0)$. We begin by evaluating the integral:

$$\begin{aligned}
&\int_0^{2\pi} \frac{G_1^{(2)}(\tau_0, \sigma_0, \tau, \sigma) T_3(\tau, \sigma)}{(\cosh\tau - \cos\sigma)^2} \, \mathrm{d}\sigma \\
&= \int_0^{2\pi} \frac{\left[Q_{1,0}(\tau) + \sum_{n=1}^{+\infty} Q_{1,n}(\tau) \cos n(\sigma - \sigma_0) \right] \left[A^1(\tau) + \sum_{n=1}^{+\infty} B_n^1(\tau) \cos n\sigma \right]}{(\cosh\tau - \cos\sigma)^2} \, \mathrm{d}\sigma \\
&= \int_0^{2\pi} \frac{Q_{1,0}(\tau) A^1(\tau)}{(\cosh\tau - \cos\sigma)^2} \, \mathrm{d}\sigma + \int_0^{2\pi} \frac{Q_{1,0}(\tau) \sum_{n=1}^{+\infty} B_n^1(\tau) \cos n\sigma}{(\cosh\tau - \cos\sigma)^2} \, \mathrm{d}\sigma \\
&+ \int_0^{2\pi} \frac{A^1(\tau) \sum_{n=1}^{+\infty} Q_{1,n}(\tau) \cos n(\sigma - \sigma_0)}{(\cosh\tau - \cos\sigma)^2} \, \mathrm{d}\sigma \\
&+ \int_0^{2\pi} \frac{\left[\sum_{n=1}^{+\infty} Q_{1,n}(\tau) \cos n(\sigma - \sigma_0) \right] \left[\sum_{n=1}^{+\infty} B_n^1(\tau) \cos n\sigma \right]}{(\cosh\tau - \cos\sigma)^2} \, \mathrm{d}\sigma. \qquad (2.65)
\end{aligned}$$

Using the fact that:

$$\left(\sum_{n=1}^{+\infty} a_n \right) \left(\sum_{m=1}^{+\infty} b_m \right) = \sum_{n=1}^{+\infty} \sum_{m=1}^{+\infty} a_n b_m,$$

and

$$\begin{aligned}
\cos m\sigma \cos n(\sigma - \sigma_0) &= \cos m\sigma \cos n\sigma \cos n\sigma_0 + \cos m\sigma \sin n\sigma \sin n\sigma_0 \\
&= \frac{1}{2} \{ [\cos(m-n)\sigma + \cos(m+n)\sigma] \cos n\sigma_0 \\
&+ [\sin(m+n)\sigma - \sin(m-n)\sigma] \sin n\sigma_0 \},
\end{aligned}$$

we rewrite

$$\begin{aligned}
&\left[\sum_{n=1}^{\infty} Q_{1,n}(\tau) \cos n(\sigma - \sigma_0) \right] \left[\sum_{n=1}^{+\infty} B_n^1(\tau) \cos n\sigma \right] \\
&= \sum_{n=1}^{+\infty} \sum_{m=1}^{+\infty} Q_{1,n}(\tau) B_m^1(\tau) \cos n(\sigma - \sigma_0) \cos m\sigma \\
&= \frac{1}{2} \sum_{n=1}^{+\infty} \sum_{m=1}^{+\infty} Q_{1,n}(\tau) B_m^1(\tau) \{ [\cos(m-n)\sigma + \cos(m+n)\sigma] \cos n\sigma_0
\end{aligned}$$

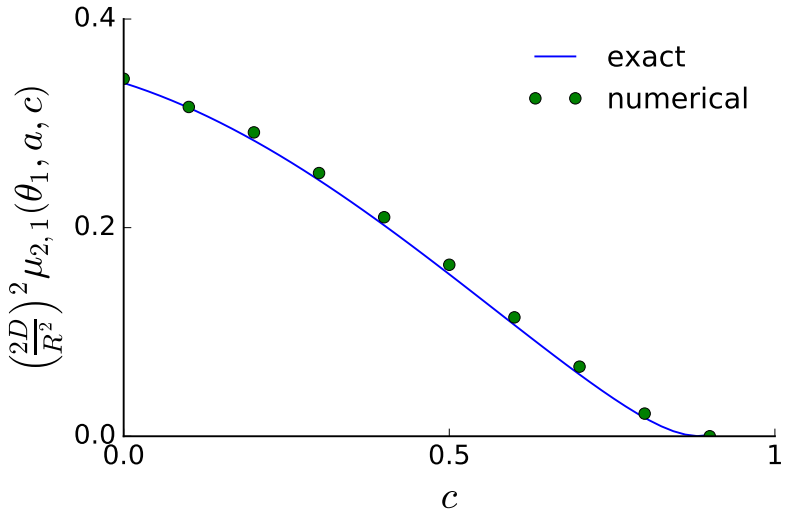

(a) $i = 1$

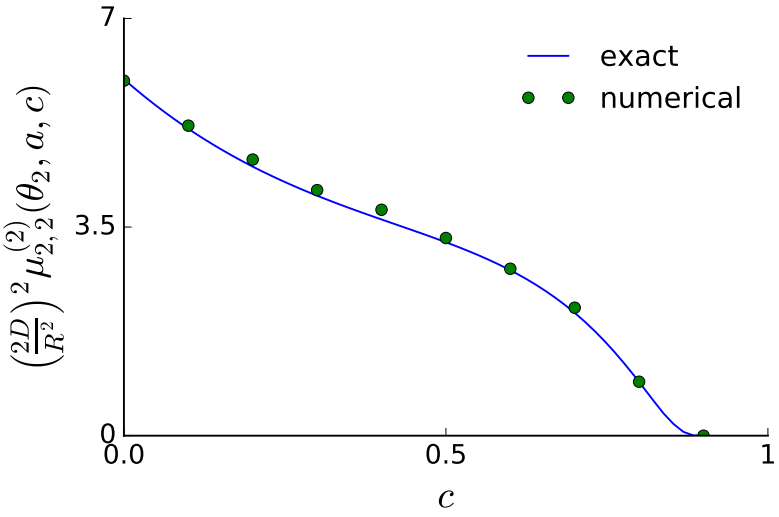

(b) $i = 2$

Figure 2.25: Second order moments of $t_1^{(2)}$ in 2.25(a) and of $t_2^{(2)}$ in 2.25(b), respectively. The green dots are numerical simulations and the blue lines are the analytic results obtained in (2.67) and (2.68), respectively. For our simulations we have chosen the following parameter values: $\mathbf{x}_0 - \mathbf{x}_c = (-1, 0), a = 0.1$ for $\mu^{(2)}_{2,2}$; $\mathbf{x}_0 - \mathbf{x}_c = (-a - c, 0), a = 0.1$ for $\mu^{(2)}_{2,1}$. Here $\mathbf{x}_c$ is the position vector of the cellular centre.

$$+\left[\sin\left(m+n\right)\sigma-\sin\left(m-n\right)\sigma\right]\sin n\sigma_0\big\}\,.$$

As a result, the last integral on the right-hand side of (2.65) becomes:

$$\int_0^{2\pi}\frac{\left[\sum_{n=1}^{+\infty}Q_{1,n}(\tau)\cos n(\sigma-\sigma_0)\right]\left[\sum_{n=1}^{+\infty}B_n^1(\tau)\cos n\sigma\right]}{(\cosh\tau-\cos\sigma)^2}\,\mathrm{d}\sigma=\pi\sum_{n=1}^{+\infty}\sum_{m=1}^{+\infty}Q_{1,n}(\tau)B_m^1(\tau)$$
$$\times\frac{\left(\mathrm{e}^{-|n-m|\tau}|n-m|+\mathrm{e}^{-|n+m|\tau}|n+m|\right)\sinh\tau+\left(\mathrm{e}^{-|n-m|\tau}+\mathrm{e}^{-|n+m|\tau}\right)\cosh\tau}{\sinh^3\tau}$$
$$\times\cos n\sigma_0, \tag{2.66}$$

where we have used the fact that:

$$\int_0^{2\pi}\frac{\sin n\sigma}{(\cosh\tau-\cos\sigma)^2}\mathrm{d}\sigma=0,\quad\forall n\in\mathbb{N}.$$

Using Appendix B.3 in (2.65) and (2.66) we obtain the first moment:

$$\left(\frac{2D}{R^2}\right)^2\mu_{2,1}^{(2)}(\theta_1,a,c)=2d^2\int_{\tau_2}^{\tau_1}\int_0^{2\pi}\frac{G_1^{(2)}(\tau_0,\sigma_0,\tau,\sigma)T_3(\tau,\sigma)}{(\cosh\tau-\cos\sigma)^2}\,\mathrm{d}\sigma\mathrm{d}\tau$$
$$=4\pi d^2\int_{\tau_2}^{\tau_1}Q_{1,0}(\tau)A^1(\tau)\frac{\cosh\tau}{\sinh^3\tau}\mathrm{d}\tau$$
$$+4\pi d^2\sum_{n=1}^{+\infty}\int_{\tau_2}^{\tau_1}Q_{1,0}(\tau)B_n^1(\tau)\frac{\mathrm{e}^{-n\tau}(n\sinh\tau+\cosh\tau)}{\sinh^3\tau}\mathrm{d}\tau$$
$$+4\pi d^2\sum_{n=1}^{+\infty}\int_{\tau_2}^{\tau_1}A^1(\tau)Q_{1,n}(\tau)\frac{\mathrm{e}^{-n\tau}(n\sinh\tau+\cosh\tau)}{\sinh^3\tau}\mathrm{d}\tau\cos n\sigma_0$$
$$+2\pi d^2\sum_{n=1}^{+\infty}\sum_{m=1}^{+\infty}\int_{\tau_2}^{\tau_1}Q_{1,n}(\tau)B_m^1(\tau)$$
$$\times\frac{\left(\mathrm{e}^{-|n-m|\tau}|n-m|+\mathrm{e}^{-|n+m|\tau}|n+m|\right)\sinh\tau+\left(\mathrm{e}^{-|n-m|\tau}+\mathrm{e}^{-|n+m|\tau}\right)\cosh\tau}{\sinh^3\tau}\mathrm{d}\tau$$
$$\times\cos n\sigma_0. \tag{2.67}$$

Analogously, we obtain for $t_2^{(2)}\left(\mathbf{x}_0\right)$:

$$\left(\frac{2D}{R^2}\right)^2\mu_{2,2}^{(2)}(\theta_2,a,c)=2d^2\int_{\tau_2}^{\tau_1}\int_0^{2\pi}\frac{G_2^{(2)}(\tau_0,\sigma_0,\tau,\sigma)T_4(\tau,\sigma)}{(\cosh\tau-\cos\sigma)^2}\,\mathrm{d}\sigma\mathrm{d}\tau$$
$$=4\pi d^2\int_{\tau_2}^{\tau_1}Q_{2,0}(\tau)A^2(\tau)\frac{\cosh\tau}{\sinh^3\tau}\mathrm{d}\tau$$

$$
\begin{aligned}
&+ 4\pi d^2 \sum_{n=1}^{+\infty} \int_{\tau_2}^{\tau_1} Q_{2,0}(\tau) B_n^2(\tau) \frac{\mathrm{e}^{-n\tau}(n\sinh\tau + \cosh\tau)}{\sinh^3\tau} \mathrm{d}\tau \\
&+ 4\pi d^2 \sum_{n=1}^{+\infty} \int_{\tau_2}^{\tau_1} A^2(\tau) Q_{2,n}(\tau) \frac{\mathrm{e}^{-n\tau}(n\sinh\tau + \cosh\tau)}{\sinh^3\tau} \mathrm{d}\tau \cos n\sigma_0 \\
&+ 2\pi d^2 \sum_{n=1}^{+\infty} \sum_{m=1}^{+\infty} \int_{\tau_2}^{\tau_1} Q_{2,n}(\tau) B_m^2(\tau) \\
&\times \frac{\left(\mathrm{e}^{-|n-m|\tau}|n-m| + \mathrm{e}^{-|n+m|\tau}|n+m|\right)\sinh\tau + \left(\mathrm{e}^{-|n-m|\tau} + \mathrm{e}^{-|n+m|\tau}\right)\cosh\tau}{\sinh^3\tau} \mathrm{d}\tau \\
&\times \cos n\sigma_0. \qquad (2.68)
\end{aligned}
$$

We plot $\mu_{2,1}^{(2)}(\theta_1, a, c)$ and $\mu_{2,2}^{(2)}(\theta_2, a, c)$ in Figure 2.25(a) and Figure 2.25(b), respectively, where we compare with numerical simulations. We observe that, as the displacement of the intracellular compartment increases, the second order moments $\mu_{2,1}^{(2)}(\theta_1, a, c)$ and $\mu_{2,1}^{(2)}(\theta_1, a, c)$, where $\theta_{1,2} = 0$, decreases as a a result of the fact that the majority of the paths starting at $\mathbf{x}_0$ will be tightly distributed around the shortest line from $\mathbf{x}_0$ to to the absorbing boundary (this is not the case for a different the starting point $\mathbf{x}_0$).

2.7.1 Average moments

We want to calculate the second order moments of $\bar{t}_1(\mathbf{x}_0)$ and $\bar{t}_2(\mathbf{x}_0)$ which are obtained by averaging $\mu_{2,1}$ and $\mu_{2,2}$ over the nuclear and cellular surface, respectively:

$$
\begin{aligned}
\left(\frac{2D}{R^2}\right)^2 \bar{\mu}_{2,i}^{(2)}(a,c) &= \frac{d\int_0^{2\pi} \frac{\mu_{2,i}^{(2)}(\theta_i,a,c)}{\cosh\tau_i - \cos\sigma_i}\,\mathrm{d}\sigma_i}{d\int_0^{2\pi} \frac{1}{\cosh\tau_i - \cos\sigma_i}\,\mathrm{d}\sigma_i} \\
&= \frac{\sinh\tau_0}{2\pi} \int_0^{2\pi} \frac{\mu_{2,i}^{(2)}(\theta_i,a,c)}{\cosh\tau_i - \cos\sigma_i}\,\mathrm{d}\sigma_i, \text{ where } i \in \{1,2\}. \qquad (2.69)
\end{aligned}
$$

Using our previous results (2.67) and (2.68) in (2.69) we obtain:

$$
\begin{aligned}
&\left(\frac{2D}{R^2}\right)^2 \bar{\mu}_{2,1}^{(2)}(a,c) = 4\pi d^2 \int_{\tau_2}^{\tau_1} Q_{1,0}(\tau) A^1(\tau) \frac{\cosh\tau}{\sinh^3\tau} \mathrm{d}\tau \\
&+ 4\pi d^2 \sum_{n=1}^{+\infty} \int_{\tau_2}^{\tau_1} Q_{1,0}(\tau) B_n^1(\tau) \frac{\mathrm{e}^{-n\tau}(n\sinh\tau + \cosh\tau)}{\sinh^3\tau} \mathrm{d}\tau
\end{aligned}
$$

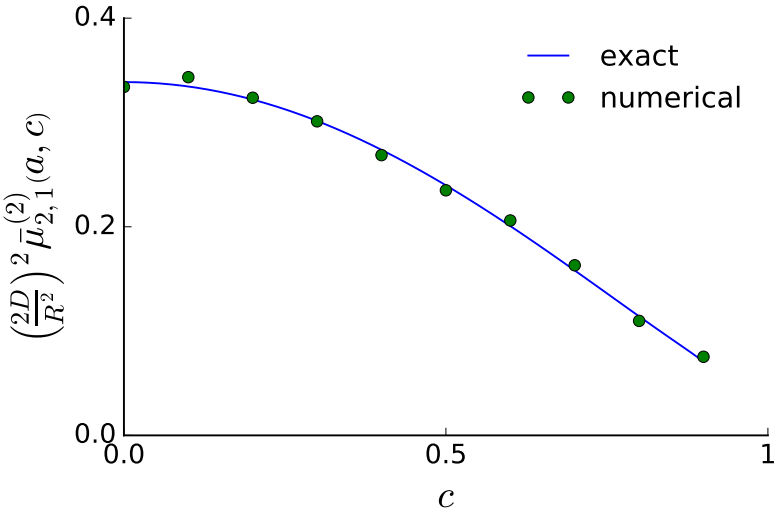

(a) $i = 1$

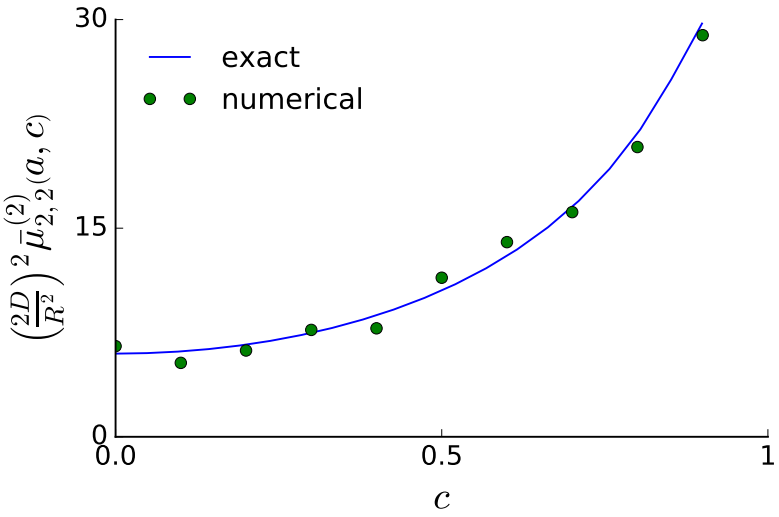

(b) $i = 2$

Figure 2.26: Second order moments $\bar{\mu}_{2,1}^{(2)}(a,c)$ of $\bar{t}_1^{(2)}(\mathbf{x}_0)$ in 2.26(a) and $\bar{\mu}_{2,2}^{(2)}(a,c)$ of $\bar{t}_2^{(2)}(\mathbf{x}_0)$ in 2.26(b), respectively, as a function of c. The green dots are numerical simulations and the blue lines are the analytic results obtained in (2.70) and (2.71), respectively. For our simulations we have chosen the following parameter values: $a = 0.1$.

$$+ 4\pi d^2 \sum_{n=1}^{+\infty} \int_{\tau_2}^{\tau_1} A^1(\tau) Q_{1,n}(\tau) \frac{\mathrm{e}^{-n\tau}(n\sinh\tau + \cosh\tau)}{\sinh^3\tau} \mathrm{d}\tau \mathrm{e}^{-n\tau_0}$$
$$+ 2\pi d^2 \sum_{n=1}^{+\infty} \sum_{m=1}^{+\infty} \int_{\tau_2}^{\tau_1} Q_{1,n}(\tau) B_m^1(\tau)$$
$$\times \frac{\left(\mathrm{e}^{-|n-m|\tau}|n-m| + \mathrm{e}^{-|n+m|\tau}|n+m|\right)\sinh\tau + \left(\mathrm{e}^{-|n-m|\tau} + \mathrm{e}^{-|n+m|\tau}\right)\cosh\tau}{\sinh^3\tau} \mathrm{d}\tau$$
$$\times \mathrm{e}^{-n\tau_0}, \tag{2.70}$$

and

$$\left(\frac{2D}{R^2}\right)^2 \bar{\mu}_{2,2}^{(2)}(a,c) = 4\pi d^2 \int_{\tau_2}^{\tau_1} Q_{2,0}(\tau) A^2(\tau) \frac{\cosh\tau}{\sinh^3\tau} \mathrm{d}\tau$$
$$+ 4\pi d^2 \sum_{n=1}^{+\infty} \int_{\tau_2}^{\tau_1} Q_{2,0}(\tau) B_n^2(\tau) \frac{\mathrm{e}^{-n\tau}(n\sinh\tau + \cosh\tau)}{\sinh^3\tau} \mathrm{d}\tau$$
$$+ 4\pi d^2 \sum_{n=1}^{+\infty} \int_{\tau_2}^{\tau_1} A^2(\tau) Q_{2,n}(\tau) \frac{\mathrm{e}^{-n\tau}(n\sinh\tau + \cosh\tau)}{\sinh^3\tau} \mathrm{d}\tau \mathrm{e}^{-n\tau_0}$$
$$+ 2\pi d^2 \sum_{n=1}^{+\infty} \sum_{m=1}^{+\infty} \int_{\tau_2}^{\tau_1} Q_{2,n}(\tau) B_m^2(\tau)$$
$$\times \frac{\left(\mathrm{e}^{-|n-m|\tau}|n-m| + \mathrm{e}^{-|n+m|\tau}|n+m|\right)\sinh\tau + \left(\mathrm{e}^{-|n-m|\tau} + \mathrm{e}^{-|n+m|\tau}\right)\cosh\tau}{\sinh^3\tau} \mathrm{d}\tau$$
$$\times \mathrm{e}^{-n\tau_0}, \tag{2.71}$$

where we have used Appendix B.3.

We plot $\bar{\mu}_{2,1}^{(2)}(a,c)$ and $\bar{\mu}_{2,2}^{(2)}(a,c)$ in Figure 2.26(a) and Figure 2.26(b), respectively, where we compare with numerical simulations. We observe from that as c increases the second order moment of $\bar{t}_1^{(2)}(\mathbf{x}_0)$ decreases as result of the fact that the paths of a Brownian particles, starting on the nuclear surface, will be centred around the line $\theta_2 = 0$ as can be seen from the hitting density in Figure 2.15. However, the second order moment of $\bar{t}_2^{(2)}(\mathbf{x}_0)$ is a increasing function of c because the length of the possible paths a Brownian particle, can take to reach the cellular surface, increases as the nucleus becomes more displaced from the cellular centre.

Additionally, we obtain the variance of $\bar{t}_1^{(2)}(\mathbf{x}_0)$ and $\bar{t}_2^{(2)}(\mathbf{x}_0)$ using the formulas:

$$V_i^{(2)}(a,c) \equiv \mathbb{V}\left[\bar{t}_i^{(2)}(\mathbf{x}_0)\right] = \bar{\mu}_{2,i}^{(2)}(a,c) - \left(\bar{T}_i^{(2)}(a,c)\right)^2, \tag{2.72}$$

which we plot in Figure 2.29 and compare with numerical simulations. We notice that the same comments about the second order moments of $\bar{t}_{1,2}^{(2)}$ apply to $V_{1,2}^{(2)}(a,c)$.

2.8 Discussion

In this chapter, using bipolar coordinates, we derive the exact Green's functions (2.13) and (2.28). They differ from the corresponding Green's functions without intracellular compartment by an amount proportional to a^2. We consider distributions of initial conditions that are (i) uniform on the nuclear surface (ii) uniform on the cellular surface, or (iii) given by the hitting density of particles diffusing from the nuclear to the cellular surface. This hitting density is also obtained from the appropriate Green's function. The exact expressions for the hitting densities and mean arrival times are (2.33), (2.45) and (2.46). When averaged over the initial surface, the mean arrival times, (2.52) and (2.53), are functions of a and c. The idea is that the point on the surface of a nucleus where a molecule emerges, or the point on the cellular surface where a molecular complex is internalised, is uniformly distributed. We further average over all possible locations of the nucleus within the cell, obtaining (2.62) and (2.63), functions of a only. We also solve Poisson's equation explicitly in bipolar coordinates, using the particular solution (2.48). From Figure 2.19 we observe that the solutions to Poisson's equation are both an increasing function of the distance from the absorbing boundary. Using the Green's functions and the solutions of Poisson's equation we obtain the higher order moments (2.67) and (2.68), and the average higher order moments (2.70) and (2.71).
We observe from Figure 2.6 and 2.12 that both $G_1^{(2)}(\mathbf{x}_0,\mathbf{x})$ and $G_2^{(2)}(\mathbf{x}_0,\mathbf{x})$ decrease in magnitude as the source point is closer to the absorbing boundary.
From Figure 2.22 and 2.29 we observe that the variance of $\bar{t}_2^{(2)}(\mathbf{x}_0)$, but not of $\bar{t}_1^{(2)}(\mathbf{x}_0)$, is of the same order of magnitude, or larger, when compared its mean, from which we deduce that the mean first passage time is not an adequate measure that captures the first passage behaviour of Brownian particles inside a cell with an absorbing trap. This is consistent with the distributions of $\bar{t}_1(\mathbf{x}_0)$ and $\bar{t}_2(\mathbf{x}_0)$ from Figure 2.28 where the distribution of $\bar{t}_2(\mathbf{x}_0)$ is wide while the distribution of

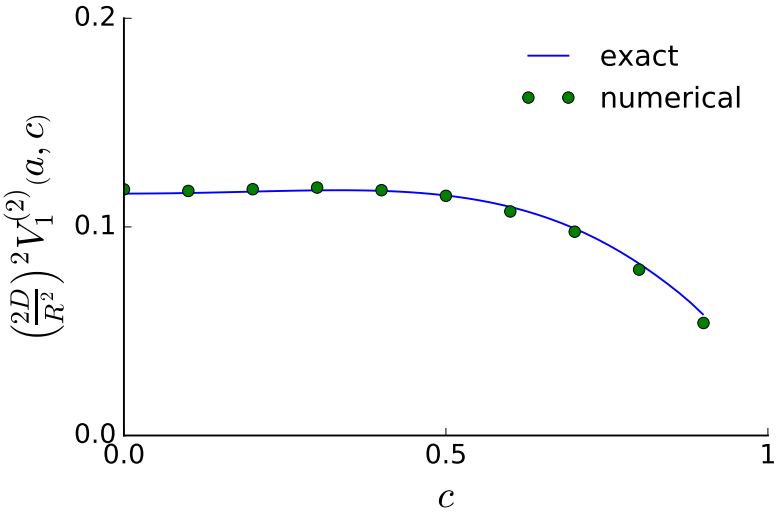

(a) $i = 1$

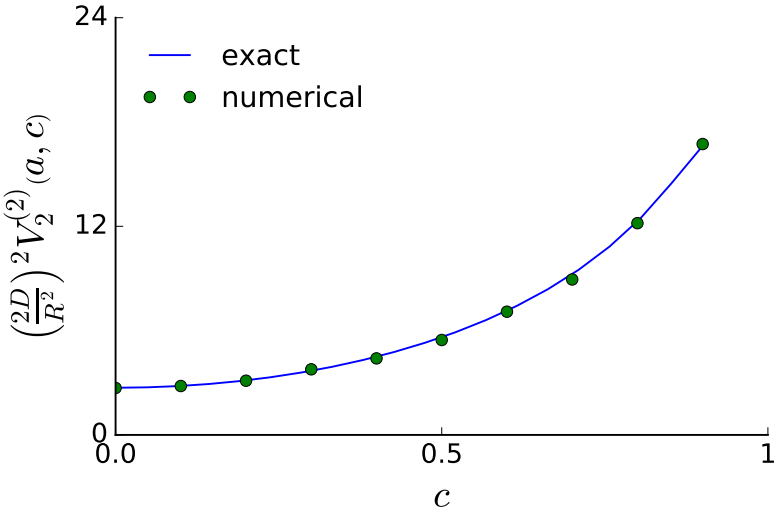

(b) $i = 2$

Figure 2.27: Variance of $\bar{t}_1^{(2)}$ in 2.27(a) and of $\bar{t}_2^{(2)}$ in 2.27(b), respectively. The green dots are numerical simulations and the blue lines are the analytic results obtained in (2.72). For our simulations we have chosen the following parameter values: $a = 0.1$.

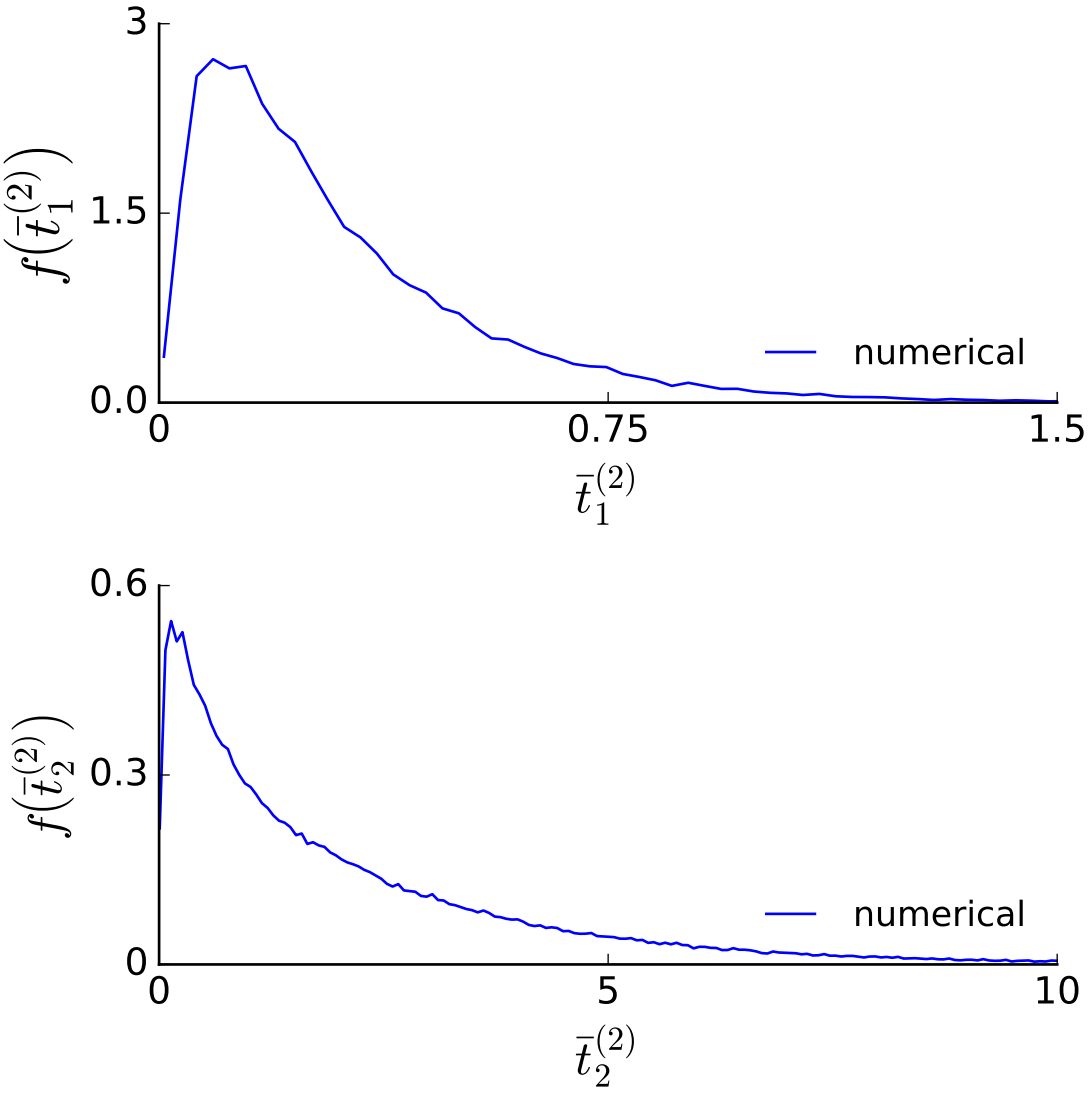

Figure 2.28: Plot of the distribution of $\bar{t}_1$ in the upper plane and the plot of the distribution of $\bar{t}_2$. The blue lines are numerical simulations for which we have chosen the following parameter values: $a = 0.4$, $c = 0.2$, $D = 0.5$.

$\bar{t}_1\left(\mathbf{x}_0\right)$ is centred around the mean (the non-smooth shape of the graphs is given by the relatively low number of Brownian particles used to obtain the distributions). The activation of many processes inside a cell requires the arrival of a single molecule at a target site and in this context the relevant timescale is given by the extreme first passage times (*i.e.* the time at which the first Brownian searcher

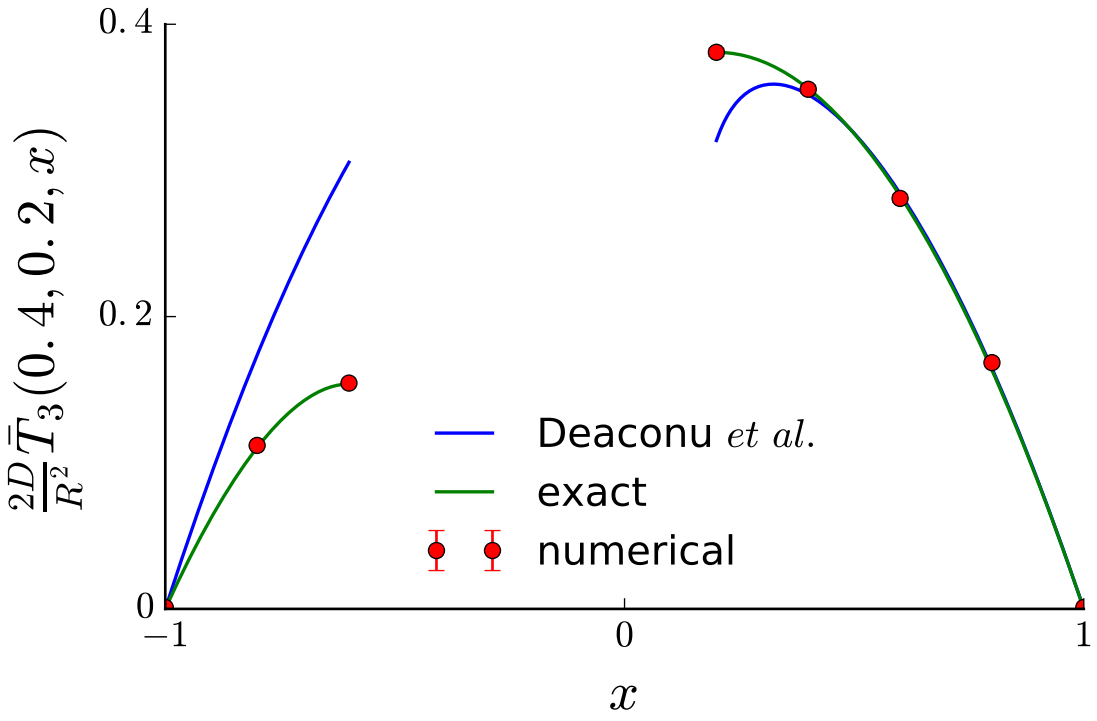

Figure 2.29: Plolt of the mean time $\bar{T}_3$ versus the horizontal distance x. The red dots are numerical simulations, the green lines are the analytic results obtained in (2.49) and the blue lines are the results obtained by Deaconu *et al.* (2000).For our simulations we have chosen the following parameter values: $a = 0.4$, $c = 0.2$, $D = 0.5$.

reaches a target) Basnayake & Holcman (2020); Lawley & Madrid (2020); Mattos *et al.* (2012).

In Section 2.5, we obtained the hitting density of a Brownian particle, starting uniformly from the nuclear surface, on the cellular surface. We observe that as c increases, the density $\varepsilon^{(2)}(\theta_2)$ becomes bimodal and we investigated the bifurcation point c^*, for which we obtained the upper and lower bounds for the bifurcation point as seen in Figure 2.16. Future work should be focused on obtaining an analytic formulae for the bifurcation point.

The two dimensional model we have explored in this chapter can be used to represent flat cell cultures where the cell can be approximated as a two dimensional

annular region, because the cells remain flat due to adhesion to the substrate and their thickens can be neglected Holcman & Schuss (2015).

The mean times calculated in this chapter have also been analytically derived by Deaconu *et al.* (2000) using conformal mapping to obtain a simpler problem to solve. However, as seen from Figure 2.29, their results are not accurate and do not constitute an alternative to our results.

The dependence on a and c of the average mean time $\bar{T}_1^{(2)}(a,c)$ is shown in Figure 2.20 from which we deduce that the average mean time $\bar{T}_1^{(2)}(a,c)$ is a decreasing function of a and c, which is intuitively correct given that a Brownian particle will take a longer time to reach the cellular surface if either the staring point is farther away from the absorbing surface. Analogously, the dependence of $\bar{T}_2^{(2)}(a,c)$ is shown in Figure 2.21 from which we observe that the average mean time is a decreasing function of a and an inverted U-shaped function of c. This is because a Brownian particle will take a longer time to reach the nuclear surface if it is a smaller target. Additionally, as the nuclear displacement c increases, a Brownian particle will take longer to reach the nucleus starting from the opposite side of the cell, however this effect is cancelled out when nucleus is sufficiently close to the cellular surface.

We notice from Figure 2.24 that $\bar{T}_2^{\varepsilon,2}(a,c)$ is a decreasing function of c when compared to $\bar{T}_2^{(2)}(a,c)$ which is an increasing function of c. This is caused by the fact that Brownian particles diffusing from the nucleus are more likely to arrive at the point of the cellular surface which is closest to the nucleus (see Figure 2.15), and, as a result, the mean time for the particle to arrive back to the nucleus is smaller than the case when its starting position is uniformly distributed on the cellular surface.

When comparing our results for $G_2^{(2)}(\mathbf{x}_0,\mathbf{x})$, $T_2^{(2)}(\theta_2,a,c)$ and $\bar{T}_2^{(2)}(a,c)$ obtained using bipolar coordiantes with the approximations derived from Condamin *et al.* (2007) in Figure 2.13, 2.17 and 2.22, respectively, we observe that our results are of superior accuracy when compared with numerical simulations.

Finding mathematical descriptions of the traffic of small molecules inside living cells and of living cells in tissues are major challenges, among them the fact that Brownian motion is not sufficient to describe their behaviour Angermann *et al.* (2012); Barkai *et al.* (2012); Brangwynne *et al.* (2009); Bressloff & Newby (2013);

Holcman (2017); Krummel *et al.* (2016); McGuffee & Elcock (2010); Metzler (2019). As well as the extension to three space dimensions, the pure diffusion model considered here can be generalised in various ways. Viral trajectories in cytoplasm may be modelled as epochs of simple diffusion and of active transport along microtubules Lagache & Holcman (2008); Lagache *et al.* (2009). Effects of crowding or of active transport mechanisms may be modelled as a type of motion that is not diffusive, with the standard time derivative replaced by a fractional one Burrage *et al.* (2017); Krummel *et al.* (2016); Metzler (2019). A reacting surface may itself contain absorbing and reflecting regions; one way to take this heterogeneity into account is via Robin boundary conditions Delgado *et al.* (2015).

Chapter 3

Diffusive transport in spherical domains

3.1 Introduction

Expanding on the results obtained in Chapter 2 we consider diffusion of a Brownian particle, with diffusivity D, in a spherical domain of radius R which contains an interior compartment of radius R_n and has displacement r_c from the centre of the domain (see Figure 3.1). We want to determine the Green's function for diffusive transport in three dimensions where the basic timescale is R^2/D.
Using bispherical coordinates, we derive the Green's functions for two cases: (i) approximation and (ii) exact. Obtaining the Green's function in three dimensions is more difficult than in two dimensions as it leads to the appearance of a second order inhomogeneous difference equation. We derive the approximate Green's function for diffusive transport from reflecting nucleus to absorbing cellular surface. The approximation is obtained using the fact that the hyperbolic cosine is usually significantly larger than the trigonometric cosine. This method only works for diffusion from the nuclear surface to cellular surface. The main result of this chapter is represented by the analytic solution to the difference equation and, subsequently the desired Green's function, by using continued fractions expansions and Perron's theorem. A limitation of our method is that it is valid only for diffusive transport where the initial position is uniformly distributed on the reflecting surface.

Hence, we derive exact expressions for arrival densities and mean arrival times, averaged over the reflecting surface. We consider distributions of initial conditions that are (i) uniform on the nuclear surface, (ii) uniform on the cellular surface, or (iii) given by the hitting density of particles diffusing from the nuclear to the cellular surface. This hitting density is also obtained from the appropriate Green's function. Numerical simulations are used for comparison. The last result is semi-analytic since we use the analytic hitting density function and the mean arrival time approximation, obtained in Section 1.7.3.2 in its derivation.

3.2 Literature review

Condamin *et al.* (2007) developed a formula for the first passage properties of a Brownian particle to reach a target while starting from a point inside a three dimensional eccentric annular region bounded on the exterior by a reflecting spherical boundary and on the interior by an absorbing sphere. These results were extended using pseudo-Green's function by Bénichou & Voituriez (2014); Chevalier *et al.* (2010) to determine the first passage properties of Brownian motion in a three dimensional domain where the absorbing targets are on an otherwise reflecting surface.

The case of multiple absorbing spherical traps contained inside a sphere with either Robin or Neumann boundary conditions has been explored, with the help of the method of matching asymptotic expansions, wielding the mean and the variance of the conditional first passage time for a Brownian particle to reach a specific trap Cheviakov & Ward (2011); Delgado *et al.* (2015). A limitation of the asymptotic method is that it is valid only when the diameter of each absorber is smaller than the diameter of the containing sphere.

Grebenkov & Traytak (2019) derived the semi-analytic Green's function for the Laplace operator in three-dimensional domains with disconnected spherical domains and diverse boundary conditions (Dirichlet, Neumann, Robin) by using the generalized method of separation of variables (GMSV). They solve the partial differential equation by reducing it to an infinite system of linear algebraic

equations (ISLAE) that is then solved numerically to a high computational efficiency by utilising the fact that the GMSV can be specifically adapted to the geometrical structure of the domain.
When the absorbing target is an absorbing disk located on a otherwise reflecting boundary the problem can be classified as a narrow escape problem and has been studied extensively Cheviakov *et al.* (2012); Grebenkov *et al.* (2020); Holcman & Schuss (2014, 2015); Reingruber *et al.* (2009). When the absorbing hole shrinks to zero the mean time to absorption diverges to infinity and the narrow escape problem becomes a singular perturbation problem and is solved by using asymptotic expansions Schuss *et al.* (2007); Singer *et al.* (2006b).
Many studies have focused on studying the MFPT of a diffusing particle to reach a specific target, either an absorbing patch on an otherwise reflecting boundary or a target in the domain. However, in many geometries the MFPT does not adequately capture the behaviour of the Brownian motion and as a result the distribution of the FPT is very important Godec & Metzler (2016a,b); Grebenkov *et al.* (2019); Lawley (2020); Lawley & Madrid (2020); Schuss *et al.* (2019).
Boundary homogenisation is used to solve problems where an otherwise reflecting boundary has absorbing traps located on it. They make use of the fact that non-uniform boundaries affect a relatively small neighbourhood near the surface and, as a result, the memory about the local properties of the boundary declines as a function of distance from the boundary Berezhkovskii *et al.* (2004); Makhnovskii *et al.* (2005).

3.3 Bispherical coordinates

In the previous chapter we have investigated diffusion in a two dimensional eccentric annular region with various boundary conditions. However, the two dimensional case is not biologically realistic, especially when considering cell biology and, consequently, we wish to study the case of diffusion in a three dimensional eccentric annular region.
We represent a cell as a sphere of radius R, containing a nucleus (or other intracellular compartment) of radius R_n. The centre of the nucleus is displaced from that of the cell by a distance r_c (Figure 3.1).

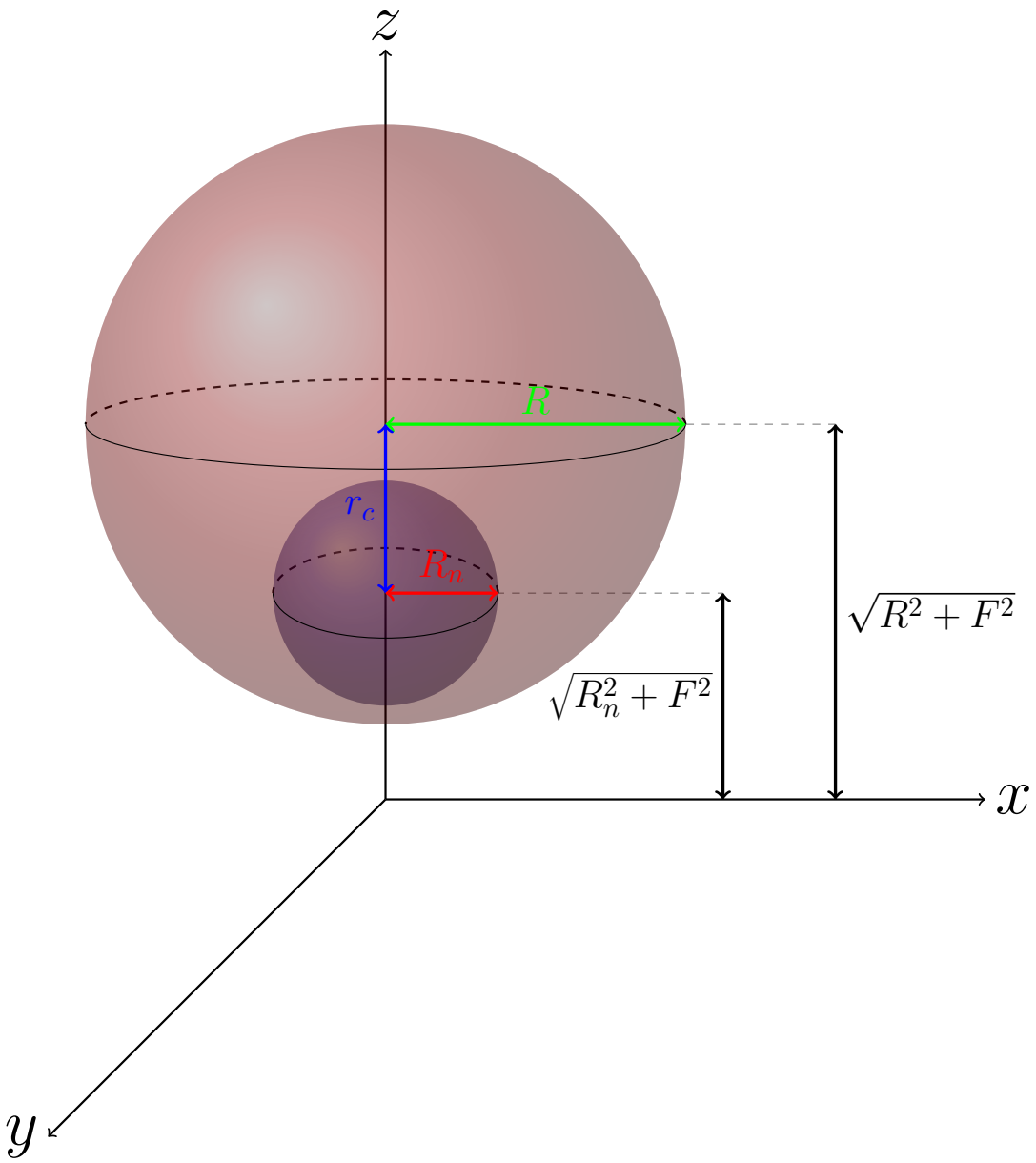

Figure 3.1: Intracellular geometry. We represent a cell as a sphere of radius R, containing a nucleus (or other intracellular compartment) of radius R_n. The centre of the nucleus is displaced from that of the cell by a distance r_c. Here $2F$ is the interfocal distance.

Analogous to the two dimensional case, we will make use of a special type of coordinate system, that of bispherical coordinate. We obtain bispherical coordinates

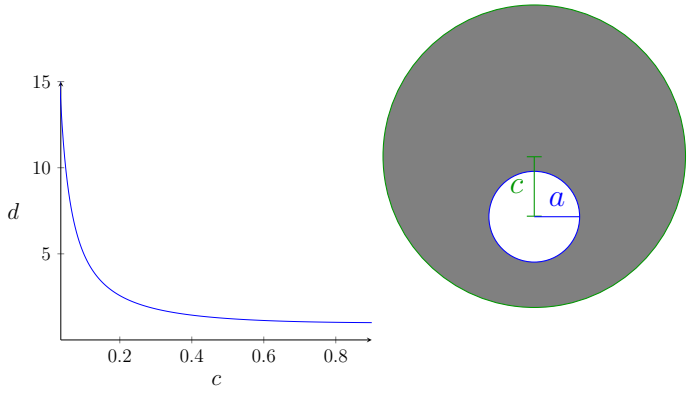

Figure 3.2: Left: the distance d used to define bispherical coordinates, as a function of c with $a = 0.1$. Right: vertical cross-section of the domain C is shown in grey.

from bipolar coordinates by rotating bipolar axes about the line between the two poles (Morse & Feshbach, 1954, p.1298).
Surfaces of constant τ are spheres of radius r, centred at $x = 0, y = 0$ and $z = \sqrt{r^2 + F^2}$, where $\tau = \log(F/r + \sqrt{1 + (F/r)^2})$ and $2F$ is the interfocal distance used to define bipolar coordinates (see Figure 2.2). We rescale lengths so that the radius of the cell is equal to 1. We shall calculate the Green's functions and mean times using the following dimensionless quantities:

$$a = \frac{R_n}{R}, \qquad c = \frac{r_c}{R} \qquad \text{and} \qquad d = \frac{F}{R}.$$

Note that $0 \leq c \leq 1 - a$, and a^3 is the fraction of the cell occupied by the nucleus. In order that the centres of the two spheres of radii 1 and a be displaced by $c = \sqrt{1 + d^2} - \sqrt{a^2 + d^2}$, we must choose

$$d = \frac{1}{2c}\sqrt{(1 + a^2 - c^2)^2 - 4a^2}. \tag{3.1}$$

Analogous to Chapter 2, we denote the nuclear surface (a sphere with scaled radius a, blue vertical cross-section in Figure 3.2) by ∂C_1 and the cellular surface (a sphere with scaled radius 1, green cross-section in Figure 3.2) by ∂C_2. The eccentric annular region C (grey cross-section in Figure 3.2) is represented by

$$\tau_2 < \tau < \tau_1, \qquad 0 \leq \sigma < \pi, \qquad 0 \leq \phi < 2\pi,$$

where $\tau_1 = \log\left(d/a + \sqrt{1+(d/a)^2}\right)$ (nuclear surface) and $\tau_2 = \log\left(d + \sqrt{1+d^2}\right)$ (cellular surface).

Chen *et al.* calculate the Green's function for an eccentric spherical annular domain, where both the inner and outer boundaries are absorbing, by using bispherical coordinates. When at least one of the boundaries is reflecting, and not absorbing, we observe the appearance of a second order difference equation due to the prefactor h_x (see (3.6) below). Stoy (1989) solves the problem of the second order inhomogeneous difference equation by approximating the prefactor to a non-trigonometric quantity and thus avoiding the appearance of the recurrence relation. Chaumet & Dufour (1998); Love (1975) obtain the analytic solution by using continued fraction method and Perron's theorem.

3.4 Bispherical Green's function

The mean time to reach an absorbing boundary of C, starting from rescaled position $\mathbf{x}_0 \in C$, can be written as

$$T(\mathbf{x}_0) = R^2 \int_C G(\mathbf{x}_0, \mathbf{x}) \mathrm{d}\mathbf{x}. \tag{3.2}$$

The Green's function $G(\mathbf{x}_0, \mathbf{x})$, the occupation density at $\mathbf{x}$, satisfies

$$D\Delta_{\mathbf{x}} G(\mathbf{x}_0, \mathbf{x}) = -\delta(\mathbf{x} - \mathbf{x}_0) \qquad \mathbf{x} \in C, \tag{3.3}$$

with suitable boundary conditions. Let (τ, σ, ϕ) be the bispherical coordinates of $\mathbf{x}$ and $(\tau_0, \sigma_0, \phi_0)$ the bispherical coordinates of $\mathbf{x}_0$. Then (Morse & Feshbach, 2010, p.1298)

$$d^2\Delta_{\mathbf{x}} = \frac{(\cosh\tau - \cos\sigma)^3}{\sin\sigma}\left[\frac{\partial}{\partial\tau}\frac{\sin\sigma}{\cosh\tau - \cos\sigma}\frac{\partial}{\partial\tau} + \frac{\partial}{\partial\sigma}\frac{\sin\sigma}{\cosh\tau - \cos\sigma}\frac{\partial}{\partial\sigma} + \frac{1}{(\cosh\tau - \cos\sigma)\sin\sigma}\frac{\partial^2}{\partial\phi^2}\right],$$

and we can write

$$T(\mathbf{x}_0) = R^2 \int_{\tau_2}^{\tau_1}\int_0^{\pi}\int_0^{2\pi} \frac{G(\mathbf{x}_0, \mathbf{x}) d^3 \sin\sigma}{(\cosh\tau - \cos\sigma)^3} \mathrm{d}\phi\mathrm{d}\sigma\mathrm{d}\tau. \tag{3.4}$$

3.4.1 From nucleus to cellular surface

We begin with the case of diffusion inside a cell with absorbing cellular surface and reflecting nucleus. We denote the Green's function by $G_1^{(3)}(\mathbf{x}_0, \mathbf{x})$ which satisfies (3.3), is equal to zero on the cellular surface and has vanishing normal derivative on the nuclear surface. As a result, we impose the following boundary conditions:

$$\frac{\partial G_1^{(3)}}{\partial \mathbf{n}_1}(\mathbf{x}_0, \mathbf{x}) = 0, \quad \mathbf{x} \in \partial C_1, \tag{3.5a}$$

$$G_1^{(3)}(\mathbf{x}_0, \mathbf{x}) = 0, \quad \mathbf{x} \in \partial C_2. \tag{3.5b}$$

where $\mathbf{n}_1$ is the unit normal outward vector to ∂C_1.
We write the Green's function's $G_1^{(3)}(\mathbf{x}_0, \mathbf{x})$ as:

$$G_1^{(3)}(\mathbf{x}_0, \mathbf{x}) = G_s^{(3)}(\mathbf{x}_0, \mathbf{x}) + G_r^{(3)}(\mathbf{x}_0, \mathbf{x}),$$

where $\Delta_{\mathbf{x}} G_r^{(3)}(\mathbf{x}_0, \mathbf{x}) = 0$. The singular part of $G_1^{(3)}(\mathbf{x}_0, \mathbf{x})$ is given by(Barton, 1989, p.100):

$$G_s^{(3)}(\mathbf{x}_0, \mathbf{x}) = \frac{1}{4\pi D|\mathbf{x} - \mathbf{x}_0|},$$

which has been expressed in bispherical coordinates by Chen *et al.*:

$$G_s^{(3)}(\mathbf{x}_0, \mathbf{x}) = \frac{1}{4\pi D d} h_x(\tau, \sigma)\, h_x(\tau_0, \sigma_0) \sum_{n=0}^{+\infty} \sum_{m=0}^{+\infty} \varepsilon_m \frac{(n-m)!}{(n+m)!} H_n^{(3)}(\mathbf{x}_0, \mathbf{x}), \tag{3.6}$$

where

$$H_n^{(3)}(\mathbf{x}_0, \mathbf{x}) = P_n^m(\cos\sigma) P_n^m(\cos\sigma_0) \cos m(\phi - \phi_0) \mathrm{e}^{-\left(n+\frac{1}{2}\right)|\tau - \tau_0|}.$$

In (3.6) we have made use of the following functions:

$$\varepsilon_m = \begin{cases} 1, & \text{if} \quad m = 0, \\ 2, & \text{if} \quad m = 1, 2, \cdots + \infty, \end{cases}$$

and

$$h_x(\tau, \sigma) = \sqrt{\cosh\tau - \cos\sigma}.$$

Our task is to find $G_1^{(3)}(\mathbf{x}_0, \mathbf{x})$ in bispherical coordinates. We seek coefficients A_{nm}, B_{nm}, C_{nm} and D_{nm} such that Chen *et al.*:

$$\begin{aligned} G_r^{(3)}(\mathbf{x}, \mathbf{x}_0) = \frac{h_x(\tau,\sigma)\, h_x(\tau_0,\sigma_0)}{4\pi D d} \sum_{n=0}^{+\infty}\sum_{m=0}^{+\infty} \Bigg[\Bigg(A_{nm} h_A(n,m) \cosh\left[\left(n+\frac{1}{2}\right)\tau\right] \\ + B_{nm} h_B(n,m) \sinh\left[\left(n+\frac{1}{2}\right)\tau\right]\Bigg) P_n^m(\cos\sigma)\cos m\phi \\ + \Bigg(C_{nm} h_C(n,m) \cosh\left[\left(n+\frac{1}{2}\right)\tau\right] \\ + D_{nm} h_D(n,m) \sinh\left[\left(n+\frac{1}{2}\right)\tau\right]\Bigg) P_n^m(\cos\sigma)\sin m\phi \Bigg], \end{aligned} \tag{3.7}$$

where

$$\begin{aligned} h_A(n,m) &= \varepsilon_m \frac{(n-m)!}{(n+m)!} P_n^m(\cos\sigma_0)\cos m\phi_0, \\ h_B(n,m) &= \varepsilon_m \frac{(n-m)!}{(n+m)!} P_n^m(\cos\sigma_0)\cos m\phi_0, \\ h_C(n,m) &= \varepsilon_m \frac{(n-m)!}{(n+m)!} P_n^m(\cos\sigma_0)\sin m\phi_0, \\ h_D(n,m) &= \varepsilon_m \frac{(n-m)!}{(n+m)!} P_n^m(\cos\sigma_0)\sin m\phi_0. \end{aligned}$$

The boundary conditions (3.5) are equivalent to in bispherical coordinates (see Appendix C.1 for Neumann boundary condition in bispherical coordinates):

$$\left.\frac{\partial G_r^{(3)}}{\partial\tau}(\tau,\sigma;\tau_0,\sigma_0)\right|_{\tau=\tau_1} = -\left.\frac{\partial G_s^{(3)}}{\partial\tau}(\tau,\sigma;\tau_0,\sigma_0)\right|_{\tau=\tau_1}, \tag{3.8a}$$

$$G_r^{(3)}(\tau_2,\sigma;\tau_0,\sigma_0) = -G_s^{(3)}(\tau_2,\sigma;\tau_0,\sigma_0). \tag{3.8b}$$

The factor $h_x(\tau,\sigma) = \sqrt{\cosh\tau - \cos\sigma}$ causes difficulties when we have non-Dirichlet boundary conditions. We show in Section 3.4.2 that the differentiation from the Neumann boundary condition (3.8a) causes the appearance of a recurrence relation which we did not see when solving the analogous case in two dimensions:

$$\alpha_{nm} A_{n-1m} + \beta_{nm} A_{nm} + \gamma_{nm} A_{n+1m} = \lambda_{nm}, \tag{3.9}$$

where α_{nm}, β_{nm}, γ_{nm} and λ_{nm} are constants. We will not solve this recurrence relation but we will make use of an approximation in Section 3.5 in order to obtain

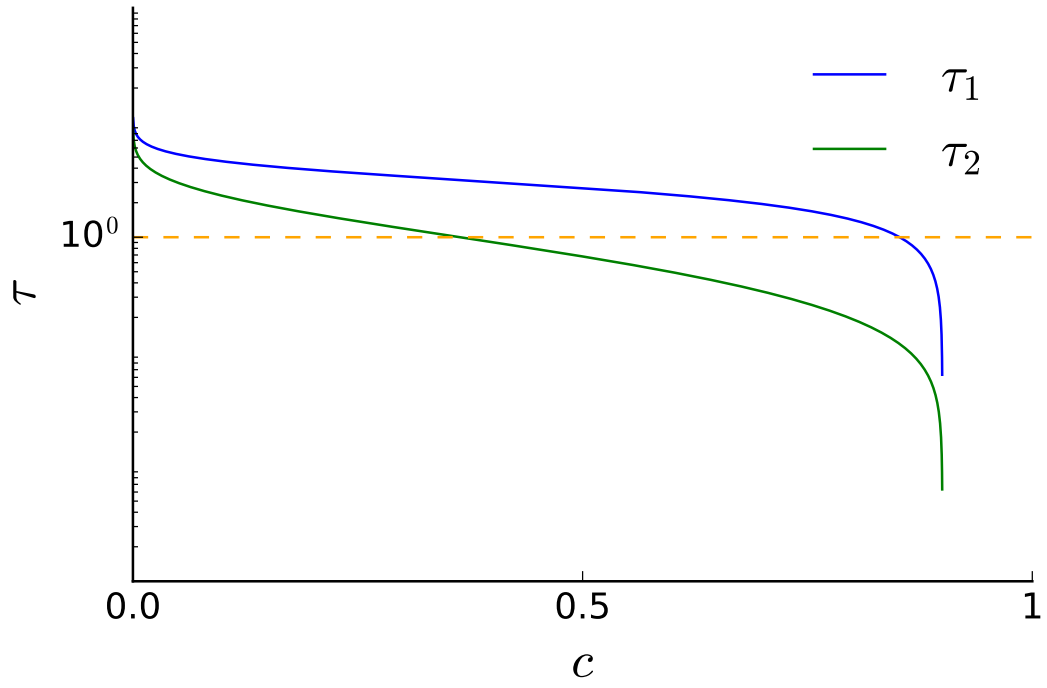

Figure 3.3: Radial bispherical coordinate evaluated for the nuclear surface τ_1 and the cellular surface τ_2 as a function of the nuclear displacement c. We observe that τ_2 decreases faster than τ_1 below 1 as a function of c. For this plot we have used the following parameters: $a = 0.1$.

$G_1^{(3)}(\mathbf{x}_0, \mathbf{x})$ by preventing the appearance of a recurrence relation altogether. An approximation can be obtained, if we observe that $\cosh\tau_1 - \cos\sigma \gg 10$ (see Figure 3.3 and 3.4) and as a result we can ignore the $\cos\sigma$ term in h_x:

$$h_x(\tau_1, \sigma) \approx \sqrt{\cosh\tau_1}.$$

As a result, the coefficients of (3.7) can be evaluated independently. We notice from Figure 3.3 and 3.4 that this approximation does not work when $\tau = \tau_2$, if the reflecting boundary is the cellular surface.
An alternative method to deal with the recurrence relation, shown in Section 3.6, is to transform it into a different recurrence relation by integrating $G_1^{(3)}(\mathbf{x}_0, \mathbf{x})$ over ∂C_1 with respect to $\mathbf{x}_0$. When the initial distribution is uniform on the surface of nucleus or of the cell, respectively, the analytic solutions involve solving

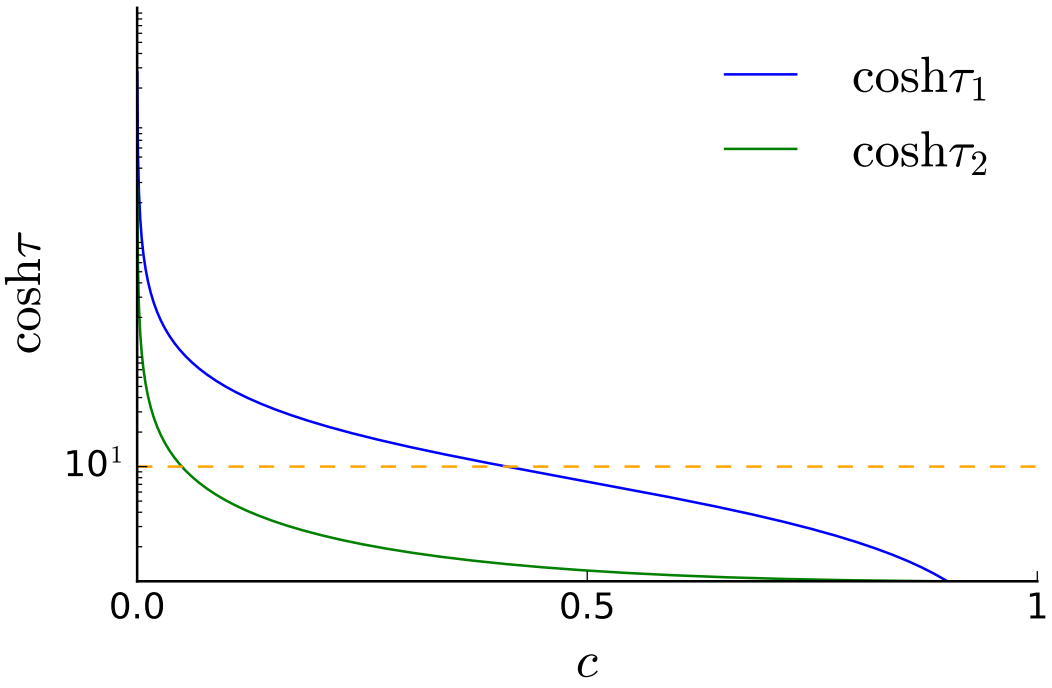

Figure 3.4: Hyperbolic cosine of the radial bispherical coordinate evaluated for the nuclear surface τ_1 and the cellular surface τ_2 as a function of the nuclear displacement c. We observe that $\cosh\tau_1$ is at least one order of magnitude larger than $\cos\sigma$ for a wider range of value of c when compared to $\cosh\tau_2$. For this plot we have used the following parameters: $a = 0.1$.

recurrence relations of the type:

$$\alpha_n A_{n-1} + \beta_n A_n + \gamma_n A_{n+1} = \lambda_n,$$

by taking advantage of the fact that:

$$\frac{\alpha_n}{\beta_n}, \frac{\gamma_n}{\beta_n} \to \text{const},$$

as $n \to +\infty$, which will allow us to use Perron's theorem and continued fraction expansion to obtain an analytic expression Chaumet & Dufour (1998). This method is useful because it allows us to deal with the recurrence relation generated by $G_2^{(3)}(\mathbf{x}_0, \mathbf{x})$.

3.4.2 Recurrence relation

In this section we will derive the recurrence relation (3.9) from the boundary conditions (3.8). From (3.8a) we deduce that:

$$\begin{aligned}
&\sum_{n=0}^{+\infty}\sum_{m=0}^{n}\Bigg\{\left[A_{nm}h_A(n,m)P_n^m(\cos\sigma)\cos m\phi + C_{nm}h_C(n,m)P_n^m(\cos\sigma)\sin m\phi\right]\\
&\times\frac{\sinh\tau_1\cosh\left[\left(n+\frac{1}{2}\right)\tau_1\right]+2\left(n+\frac{1}{2}\right)\sinh\left[\left(n+\frac{1}{2}\right)\tau_1\right](\cosh\tau_1-\cos\sigma)}{2\sqrt{\cosh\tau_1-\cos\sigma}}\\
&+\left[B_{nm}h_B(n,m)P_n^m(\cos\sigma)\cos m\phi + D_{nm}(n,m)h_DP_n^m(\cos\sigma)\sin m\phi\right]\\
&\times\frac{\sinh\tau_1\sinh\left[\left(n+\frac{1}{2}\right)\tau_1\right]+2\left(n+\frac{1}{2}\right)\cosh\left[\left(n+\frac{1}{2}\right)\tau_1\right](\cosh\tau_1-\cos\sigma)}{2\sqrt{\cosh\tau_1-\cos\sigma}}\Bigg\}\\
&=-\sum_{n=0}^{+\infty}\sum_{m=0}^{n}\varepsilon_m\frac{(n-m)!}{(n+m)!}\cos\left[m(\phi-\phi_0)\right]P_n^m(\cos\sigma)P_n^m(\cos\sigma_0)\\
&\times\frac{\sinh\tau_1-2\left(n+\frac{1}{2}\right)(\cosh\tau_1-\cos\sigma)}{2\sqrt{\cosh\tau_1-\cos\sigma}}\mathrm{e}^{-\left(n+\frac{1}{2}\right)(\tau_1-\tau_0)}.
\end{aligned}\tag{3.10}$$

We multiply (3.10) by $\cos M\phi$ and $\sin M\phi$, respectively, and by integrating with respect to ϕ from 0 to 2π we obtain:

$$\begin{aligned}
&\sum_{n=0}^{+\infty}\left\{A_{nM}h_A(n,M)P_n^M(\cos\sigma)U_1\left(n,\tau_1,\sigma\right)+B_{nM}h_B(n,M)P_n^M(\cos\sigma)U_2\left(n,\tau_1,\sigma\right)\right\}\\
&=-\sum_{n=0}^{+\infty}\varepsilon_M\frac{(n-M)!}{(n+M)!}\cos M\phi_0P_n^M(\cos\sigma)P_n^M(\cos\sigma_0)\\
&\frac{\sinh\tau_1-2\left(n+\frac{1}{2}\right)(\cosh\tau_1-\cos\sigma)}{2\sqrt{\cosh\tau_1-\cos\sigma}}\mathrm{e}^{-\left(n+\frac{1}{2}\right)(\tau_1-\tau_0)},
\end{aligned}\tag{3.11}$$

and

$$\begin{aligned}
&\sum_{n=0}^{+\infty}\left\{C_{nM}h_C(n,M)P_n^M(\cos\sigma)U_1\left(n,\tau_1,\sigma\right)+D_{nM}h_D(n,M)P_n^M(\cos\sigma)U_2\left(n,\tau_1,\sigma\right)\right\}\\
&=-\sum_{n=0}^{+\infty}\varepsilon_M\frac{(n-M!)}{(n+M)!}\cos M\phi_0P_n^M(\cos\sigma)P_n^M(\cos\sigma_0)\\
&\times\frac{\sinh\tau_1-2\left(n+\frac{1}{2}\right)(\cosh\tau_1-\cos\sigma)}{2\sqrt{\cosh\tau_1-\cos\sigma}}\mathrm{e}^{-\left(n+\frac{1}{2}\right)(\tau_1-\tau_0)},
\end{aligned}\tag{3.12}$$

where

$$U_1(n,\tau_1,\sigma) = \frac{\sinh\tau_1\cosh\left[\left(n+\frac{1}{2}\right)\tau_1\right] + 2\left(n+\frac{1}{2}\right)\sinh\left[\left(n+\frac{1}{2}\right)\tau_1\right](\cosh\tau_1-\cos\sigma)}{2\sqrt{\cosh\tau_1-\cos\sigma}},$$

$$U_2(n,\tau_1,\sigma) = \frac{\sinh\tau_1\sinh\left[\left(n+\frac{1}{2}\right)\tau_1\right] + 2\left(n+\frac{1}{2}\right)\cosh\left[\left(n+\frac{1}{2}\right)\tau_1\right](\cosh\tau_1-\cos\sigma)}{2\sqrt{\cosh\tau_1-\cos\sigma}}.$$

We observe that (3.11) and (3.12) are identical from which we deduce that $A_{nm} = C_{nm}$ and $B_{nm} = D_{nm}$ (for the remainder of this thesis we will follow this deduction and, furtheremore, we deduce that $A_n = C_n$ and $B_n = D_n$ when we define $\bar{G}_1(\mathbf{x}_0,\mathbf{x})$ and $\bar{G}_2(\mathbf{x}_0,\mathbf{x})$ in Section 3.6). As a result, we only have to solve (3.11) for A_{nm}, B_{nm} and we will also obtain C_{nm} and D_{nm}. We make use of the following notations:

$$V_1(n,\tau_1) = \sinh\tau_1\cosh\left[\left(n+\frac{1}{2}\right)\tau_1\right] + 2\left(n+\frac{1}{2}\right)\cosh\tau_1\sinh\left[\left(n+\frac{1}{2}\right)\tau_1\right], \tag{3.13a}$$

$$V_2(n,\tau_1) = \sinh\tau_1\sinh\left[\left(n+\frac{1}{2}\right)\tau_1\right] + 2\left(n+\frac{1}{2}\right)\cosh\tau_1\cosh\left[\left(n+\frac{1}{2}\right)\tau_1\right], \tag{3.13b}$$

$$W(n,\tau_1) = \sinh\tau_1 - 2\left(n+\frac{1}{2}\right)\cosh\tau_1, \tag{3.13c}$$

to rewrite (3.11) as:

$$\begin{aligned}
&\sum_{n=0}^{+\infty}\Bigg\{A_{nM}h_A(n,M)P_n^M(\cos\sigma)V_1(n,\tau_1) + B_{nM}h_B(n,M)P_n^M(\cos\sigma)V_2(n,\tau_1)\\
&- 2A_{nM}h_A(n,M)\cos\sigma P_n^M(\cos\sigma)\left(n+\frac{1}{2}\right)\sinh\left[\left(n+\frac{1}{2}\right)\tau_1\right]\\
&- 2B_{nM}h_B(n,M)\cos\sigma P_n^M(\cos\sigma)\left(n+\frac{1}{2}\right)\cosh\left[\left(n+\frac{1}{2}\right)\tau_1\right]\Bigg\}\\
&= -\sum_{n=0}^{+\infty}\varepsilon_M\frac{(n-M)!}{(n+M)!}\cos M\phi_0 P_n^M(\cos\sigma_0)\\
&\times\left[P_n^M(\cos\sigma)W(n,\tau_1) + 2\left(n+\frac{1}{2}\right)\cos\sigma P_n^M(\cos\sigma)\right]\mathrm{e}^{-\left(n+\frac{1}{2}\right)(\tau_1-\tau_0)}.
\end{aligned} \tag{3.14}$$

The associated Legendre polynomial $P_n^m(x)$ can be expressed as (Gradshteyn & Ryzhik, 2014, p.965):

$$\cos\sigma P_n^m(\cos\sigma) = \frac{n+m}{2n+1}P_{n-1}^m(\cos\sigma) + \frac{n-m+1}{2n+1}P_{n+1}^m(\cos\sigma),$$

which allows us to rewrite (3.14) as:

$$\begin{aligned}
&\sum_{n=0}^{+\infty}\Bigg\{A_{nM}h_A(n,M)P_n^M(\cos\sigma)V_1(n,\tau_1) + B_{nM}h_B(n,M)P_n^M(\cos\sigma)V_2(n,\tau_1)\\
&-2A_{nM}h_A(n,M)\left(n+\frac{1}{2}\right)\sinh\left[\left(n+\frac{1}{2}\right)\tau_1\right]\left[\frac{n+M}{2n+1}P_{n-1}^M(\cos\sigma)\right.\\
&\left.+\frac{n-M+1}{2n+1}P_{n+1}^M(\cos\sigma)\right] - 2B_{nM}h_B(n,M)\left(n+\frac{1}{2}\right)\cosh\left[\left(n+\frac{1}{2}\right)\tau_1\right]\\
&\times\left[\frac{n+M}{2n+1}P_{n-1}^M(\cos\sigma) + \frac{n-M+1}{2n+1}P_{n+1}^M(\cos\sigma)\right]\Bigg\}\\
&= -\sum_{n=0}^{+\infty}\varepsilon_M\frac{(n-M)!}{(n+M)!}\cos M\phi_0 P_n^M(\cos\sigma_0)\Bigg\{P_n^M(\cos\sigma)W(n,\tau_1) + 2\left(n+\frac{1}{2}\right)\\
&\times\left[\frac{n+M}{2n+1}P_{n-1}^M(\cos\sigma) + \frac{n-M+1}{2n+1}P_{n+1}^M(\cos\sigma)\right]\Bigg\}\mathrm{e}^{-\left(n+\frac{1}{2}\right)(\tau_1-\tau_0)}. \qquad (3.15)
\end{aligned}$$

We multiply (3.15) by $\sin\sigma P_N^M(\cos\sigma)$ and integrate with respect to σ from 0 to π and using (Gradshteyn & Ryzhik, 2014, p.769):

$$\int_0^\pi \sin\sigma P_l^m(\cos\sigma)P_{l'}^m(\cos\sigma)\,\mathrm{d}\sigma = \frac{2}{2l+1}\frac{(l+m)!}{(l-m)!}\delta_{ll'},$$

we obtain:

$$\begin{aligned}
&A_{NM}P_N^M(\cos\sigma_0)\frac{2V_1(n,\tau_1)}{2N+1} - 2\sinh\left[\left(N-\frac{1}{2}\right)\tau_1\right]\frac{N-M}{2N+1}A_{N-1M}P_{N-1}^M(\cos\sigma_0)\\
&-2\sinh\left[\left(N+\frac{3}{2}\right)\tau_1\right]\frac{N+M+1}{2N+1}A_{N+1M}P_{N+1}^M(\cos\sigma_0) + B_{NM}P_N^M(\cos\sigma_0)\\
&\times\frac{2V_2(n,\tau_1)}{2N+1} - 2\cosh\left[\left(N-\frac{1}{2}\right)\tau_1\right]\frac{N+M}{2N+1}B_{N-1M}P_{N-1}^M(\cos\sigma_0)\\
&-2\cosh\left[\left(N+\frac{3}{2}\right)\tau_1\right]\frac{N-M+1}{2N+1}B_{N+1M}P_{N+1}^M(\cos\sigma_0)\\
&= -\frac{2W(N,\tau_1)}{2N+1}\mathrm{e}^{-\left(N+\frac{1}{2}\right)(\tau_1-\tau_0)}P_N^M(\cos\sigma_0) - \frac{2(N-M)}{2N+1}\mathrm{e}^{-\left(N-\frac{1}{2}\right)(\tau_1-\tau_0)}P_{N-1}^M(\cos\sigma_0)
\end{aligned}$$

$$-\frac{2(N+M+1)}{2N+1}\mathrm{e}^{-\left(N+\frac{3}{2}\right)(\tau_1-\tau_0)}P_{N+1}^{M}\left(\cos\sigma_0\right), \tag{3.16}$$

where we have used the fact that:

$$h_A(N,M)\frac{(N+M)!}{(N-M)!}=\varepsilon_M P_N^M\left(\cos\sigma_0\right)\cos M\phi_0, \tag{3.17a}$$

$$h_B(N,M)\frac{(N+M)!}{(N-M)!}=\varepsilon_M P_N^M\left(\cos\sigma_0\right)\cos M\phi_0. \tag{3.17b}$$

For convenience we write $N=n$ and $M=m$ in the following calculations. From the Dirichlet boundary condition (3.8b) we deduce, in the same way, the following:

$$A_{nm}\cosh\left[\left(n+\frac{1}{2}\right)\tau_2\right]+B_{nm}\sinh\left[\left(n+\frac{1}{2}\right)\tau_2\right]=-\mathrm{e}^{-\left(n+\frac{1}{2}\right)(\tau_0-\tau_2)},$$

and, subsequently:

$$B_{nm}=-\mathrm{e}^{-\left(n+\frac{1}{2}\right)(\tau_0-\tau_2)}\operatorname{csch}\left[\left(n+\frac{1}{2}\right)\tau_2\right]-A_{nm}\coth\left[\left(n+\frac{1}{2}\right)\tau_2\right]. \tag{3.18}$$

Substituting B_{nm} from (3.18) into (3.16) we arrive at:

$$\begin{aligned}
&\frac{2A_{nm}}{2n+1}\left\{V_1\left(n,\tau_1\right)-V_2\left(n,\tau_1\right)\coth\left[\left(n+\frac{1}{2}\right)\tau_2\right]\right\}P_n^m(\cos\sigma_0)\\
&+A_{n-1m}\left\{-\sinh\left[\left(n-\frac{1}{2}\right)\tau_1\right]\frac{2(n-m)}{2n+1}\right.\\
&\left.+\cosh\left[\left(n-\frac{1}{2}\right)\tau_1\right]\coth\left[\left(n-\frac{1}{2}\right)\tau_2\right]\frac{2(n-m)}{2n+1}\right\}P_{n-1}^m(\cos\sigma_0)\\
&+A_{n+1m}\left\{-\sinh\left[\left(n+\frac{3}{2}\right)\tau_1\right]\frac{2(n+m+1)}{2n+1}\right.\\
&\left.+\cosh\left[\left(n+\frac{3}{2}\right)\tau_1\right]\coth\left[\left(n+\frac{3}{2}\right)\tau_2\right]\frac{2(n+m+1)}{2n+1}\right\}P_{n+1}^m(\cos\sigma_0)\\
&=-\frac{2W\left(n,\tau_1\right)}{2n+1}\mathrm{e}^{-\left(n+\frac{1}{2}\right)(\tau_1-\tau_0)}P_n^m\left(\cos\sigma_0\right)-\frac{2(n-m)}{2n+1}\mathrm{e}^{-\left(n-\frac{1}{2}\right)(\tau_1-\tau_0)}P_{n-1}^m\left(\cos\sigma_0\right)\\
&-\frac{2(n+m+1)}{2n+1}\mathrm{e}^{-\left(n+\frac{3}{2}\right)(\tau_1-\tau_0)}P_{n+1}^m\left(\cos\sigma_0\right)\\
&+\frac{2V_2\left(n,\tau_1\right)}{2n+1}\operatorname{csch}\left[\left(n+\frac{1}{2}\right)\tau_2\right]\mathrm{e}^{-\left(n+\frac{1}{2}\right)(\tau_0-\tau_2)}P_n^m\left(\cos\sigma_0\right)
\end{aligned}$$

$$
\begin{aligned}
&- \cosh\left[\left(n-\frac{1}{2}\right)\tau_1\right]\operatorname{csch}\left[\left(n-\frac{1}{2}\right)\tau_2\right]\frac{2(n-m)}{2n+1}\mathrm{e}^{-\left(n-\frac{1}{2}\right)(\tau_0-\tau_2)}P_{n-1}^{m}\left(\cos\sigma_0\right)\\
&- \cosh\left[\left(n+\frac{3}{2}\right)\tau_1\right]\operatorname{csch}\left[\left(n+\frac{3}{2}\right)\tau_2\right]\frac{2(n+m+1)}{2n+1}\mathrm{e}^{-\left(n+\frac{3}{2}\right)(\tau_0-\tau_2)}P_{n+1}^{m}\left(\cos\sigma_0\right).
\end{aligned}
$$

From which we obtain the following recurrence relation of order two for A_{nm}:

$$\alpha_{nm}A_{n-1m}+\beta_{nm}A_{nm}+\gamma_{nm}A_{n+1m}=\lambda_{nm},$$

where:

$$
\begin{aligned}
\alpha_{nm} &= \left\{-\sinh\left[\left(n-\frac{1}{2}\right)\tau_1\right]+\cosh\left[\left(n-\frac{1}{2}\right)\tau_1\right]\coth\left[\left(n-\frac{1}{2}\right)\tau_2\right]\right\} && \text{(3.19a)}\\
&\quad\times\frac{2(n-m)}{2n+1}P_{n-1}^{m}(\cos\sigma_0),\\
\beta_{nm} &= \frac{2}{2n+1}\left\{V_1\left(n,\tau_1\right)-V_2\left(n,\tau_1\right)\coth\left[\left(n+\frac{1}{2}\right)\tau_2\right]\right\}P_{n}^{m}(\cos\sigma_0), && \text{(3.19b)}\\
\gamma_{nm} &= \left\{-\sinh\left[\left(n+\frac{3}{2}\right)\tau_1\right]+\cosh\left[\left(n+\frac{3}{2}\right)\tau_1\right]\coth\left[\left(n+\frac{3}{2}\right)\tau_2\right]\right\} && \text{(3.19c)}\\
&\quad\times\frac{2(n+m+1)}{2n+1}P_{n+1}^{m}(\cos\sigma_0),\\
\lambda_{nm} &= -\frac{2W\left(n,\tau_1\right)}{2n+1}\mathrm{e}^{-\left(n+\frac{1}{2}\right)(\tau_1-\tau_0)}P_{n}^{m}\left(\cos\sigma_0\right)-\frac{2(n-m)}{2n+1}\mathrm{e}^{-\left(n-\frac{1}{2}\right)(\tau_1-\tau_0)}P_{n-1}^{m}\left(\cos\sigma_0\right)\\
&\quad-\frac{2(n+m+1)}{2n+1}\mathrm{e}^{-\left(n+\frac{3}{2}\right)(\tau_1-\tau_0)}P_{n+1}^{m}\left(\cos\sigma_0\right)\\
&\quad+\frac{2V_2\left(n,\tau_1\right)}{2n+1}\operatorname{csch}\left[\left(n+\frac{1}{2}\right)\tau_2\right]\mathrm{e}^{-\left(n+\frac{1}{2}\right)(\tau_0-\tau_2)}P_{n}^{m}\left(\cos\sigma_0\right)\\
&\quad-\cosh\left[\left(n-\frac{1}{2}\right)\tau_1\right]\operatorname{csch}\left[\left(n-\frac{1}{2}\right)\tau_2\right]\frac{2(n-m)}{2n+1}\mathrm{e}^{-\left(n-\frac{1}{2}\right)(\tau_0-\tau_2)}P_{n-1}^{m}\left(\cos\sigma_0\right)\\
&\quad-\cosh\left[\left(n+\frac{3}{2}\right)\tau_1\right]\operatorname{csch}\left[\left(n+\frac{3}{2}\right)\tau_2\right]\frac{2(n+m+1)}{2n+1}\mathrm{e}^{-\left(n+\frac{3}{2}\right)(\tau_0-\tau_2)}\\
&\quad\times P_{n+1}^{m}\left(\cos\sigma_0\right). && \text{(3.19d)}
\end{aligned}
$$

One way to solve this recurrence relation is to avoid it by making use of an approximation.

3.5 Approximation of the Green's function

We observe that the presence of the cosine term in $h_x(\tau,\sigma)$ leads to the appearance of the recurrence relation (3.9) due to the boundary conditions (3.8). As a result, we will make use of the following approximation for $h_x(\tau,\sigma)$ in oder to prevent the appearance of the recurrence relation. We observe from Figure 3.3 and 3.4 that $\cosh\tau_1 - \cos\sigma \gg 10$ for $c < 1-a$ and $\forall\sigma \in [0,\pi]$ from which we deduce that Stoy (1989):

$$h_x(\tau_1,\sigma) = \sqrt{\cosh\tau_1 - \cos\sigma} \approx \sqrt{\cosh\tau_1}, \tag{3.20}$$

and, when applied to (3.8a), gives:

$$\begin{aligned}
&\sum_{n=0}^{+\infty}\sum_{m=0}^{n}\Bigg\{\left[A_{nm}h_A(n,m)\,P_n^m(\cos\sigma)\cos m\phi + C_{nm}h_C(n,m)\,P_n^m(\cos\sigma)\sin m\phi\right]\\
&\times\frac{\sinh\tau_1\cosh\left[\left(n+\frac{1}{2}\right)\tau_1\right] + 2\left(n+\frac{1}{2}\right)\cosh\tau_1\sinh\left[\left(n+\frac{1}{2}\right)\tau_1\right]}{2\sqrt{\cosh\tau_1}}\\
&+\left[B_{nm}h_B(n,m)\,P_n^m(\cos\sigma)\cos m\phi + D_{nm}h_D(n,m)\,P_n^m(\cos\sigma)\sin m\phi\right]\\
&\times\frac{\sinh\tau_1\sinh\left[\left(n+\frac{1}{2}\right)\tau_1\right] + 2\left(n+\frac{1}{2}\right)\cosh\tau_1\cosh\left[\left(n+\frac{1}{2}\right)\tau_1\right]}{2\sqrt{\cosh\tau_1}}\Bigg\}\\
&=-\sum_{n=0}^{+\infty}\sum_{m=0}^{n}\varepsilon_m\frac{(n-m)!}{(n+m)!}\cos\left[m(\phi-\phi_0)\right]P_n^m(\cos\sigma)P_n^m(\cos\sigma_0)\\
&\times\left[\frac{\sinh\tau_1}{2\sqrt{\cosh\tau_1}} - \left(n+\frac{1}{2}\right)\sqrt{\cosh\tau_1}\right]\mathrm{e}^{-\left(n+\frac{1}{2}\right)(\tau_1-\tau_0)}.
\end{aligned}$$

We again multiply by $\cos M\phi$ and by integrating with respect to ϕ from 0 to 2π we obtain:

$$\begin{aligned}
&\sum_{n=0}^{+\infty}\Bigg\{A_{nM}h_A(n,M)\,P_n^M(\cos\sigma)\left(\frac{\sinh\tau_1\cosh\left[\left(n+\frac{1}{2}\right)\tau_1\right]}{2\sqrt{\cosh\tau_1}}\right.\\
&\left.+\frac{\left(n+\frac{1}{2}\right)\cosh\tau_1\sinh\left[\left(n+\frac{1}{2}\right)\tau_1\right]}{\sqrt{\cosh\tau_1}}\right) + B_{nM}h_B(n,M)\,P_n^M(\cos\sigma)\\
&\times\frac{\sinh\tau_1\sinh\left[\left(n+\frac{1}{2}\right)\tau_1\right] + 2\left(n+\frac{1}{2}\right)\cosh\tau_1\cosh\left[\left(n+\frac{1}{2}\right)\tau_1\right]}{2\sqrt{\cosh\tau_1}}\\
&=-\sum_{n=0}^{+\infty}\varepsilon_M\frac{(n-M)!}{(n+M)!}\cos M\phi_0 P_n^M(\cos\sigma)P_n^M(\cos\sigma_0)
\end{aligned}$$

$$\times \left[\frac{\sinh\tau_1}{2\sqrt{\cosh\tau_1}} - \left(n+\frac{1}{2}\right)\sqrt{\cosh\tau_1}\right] \mathrm{e}^{-\left(n+\frac{1}{2}\right)(\tau_1-\tau_0)}. \tag{3.21}$$

Multiplying (3.21) by $\sin\sigma P_N^M(\cos\sigma)$ and integrating with respect to σ from 0 to π results in the derivation of:

$$\begin{aligned}
&A_{NM}h_A(N,M)\,\frac{\sinh\tau_1\cosh\left[\left(N+\frac{1}{2}\right)\tau_1\right]+2\left(N+\frac{1}{2}\right)\cosh\tau_1\sinh\left[\left(N+\frac{1}{2}\right)\tau_1\right]}{2\sqrt{\cosh\tau_1}}\\
&+B_{NM}h_B(N,M)\,\frac{\sinh\tau_1\sinh\left[\left(N+\frac{1}{2}\right)\tau_1\right]+2\left(N+\frac{1}{2}\right)\cosh\tau_1\cosh\left[\left(N+\frac{1}{2}\right)\tau_1\right]}{2\sqrt{\cosh\tau_1}}\\
&=-\varepsilon_M\frac{(N-M)!}{(N+M)!}\cos M\phi_0 P_N^M(\cos\sigma_0)\left[\frac{\sinh\tau_1}{2\sqrt{\cosh\tau_1}}-\left(N+\frac{1}{2}\right)\sqrt{\cosh\tau_1}\right]\\
&\times \mathrm{e}^{-\left(N+\frac{1}{2}\right)(\tau_1-\tau_0)}.
\end{aligned}$$

Using (3.17) we simplify the above to obtain:

$$\begin{aligned}
&A_{NM}\frac{\sinh\tau_1\cosh\left[\left(N+\frac{1}{2}\right)\tau_1\right]+2\left(N+\frac{1}{2}\right)\cosh\tau_1\sinh\left[\left(N+\frac{1}{2}\right)\tau_1\right]}{2\sqrt{\cosh\tau_1}}\\
&+B_{NM}\frac{\sinh\tau_1\sinh\left[\left(N+\frac{1}{2}\right)\tau_1\right]+2\left(N+\frac{1}{2}\right)\cosh\tau_1\cosh\left[\left(N+\frac{1}{2}\right)\tau_1\right]}{2\sqrt{\cosh\tau_1}}\\
&=\left[\frac{\sinh\tau_1}{2\sqrt{\cosh\tau_1}}-\left(N+\frac{1}{2}\right)\sqrt{\cosh\tau_1}\right]\mathrm{e}^{-\left(N+\frac{1}{2}\right)(\tau_1-\tau_0)}.
\end{aligned} \tag{3.22}$$

The Dirichlet boundary condition (3.8b) can be written as:

$$\begin{aligned}
&\sum_{n=0}^{+\infty}\sum_{m=0}^{n}\Bigg\{\left[A_{nm}h_A(n,m)\,P_n^m(\cos\sigma)\cos m\phi\right.\\
&+\left.C_{nm}h_C(n,m)\,P_n^m(\cos\sigma)\sin m\phi\right]\cosh\left[\left(n+\frac{1}{2}\right)\tau_2\right]\\
&+\left[B_{nm}h_B(n,m)\,P_n^m(\cos\sigma)\cos m\phi\right.\\
&\left.+D_{nm}h_D(n,m)\,P_n^m(\cos\sigma)\sin m\phi\right]\sinh\left[\left(n+\frac{1}{2}\right)\tau_2\right]\Bigg\}\\
&=-\sum_{n=0}^{+\infty}\sum_{m=0}^{n}\varepsilon_m\frac{(n-m)!}{(n+m)!}\cos\left[m(\phi-\phi_0)\right]P_n^m(\cos\sigma)P_n^m(\cos\sigma_0)\mathrm{e}^{-\left(n+\frac{1}{2}\right)(\tau_0-\tau_2)},
\end{aligned}$$

from which we obtain by multiplying by $\cos M\phi$ and by integrating with respect to ϕ from 0 to 2π:

$$\sum_{n=0}^{+\infty}\left\{A_{nM}h_A(n,M)\,P_n^M(\cos\sigma)\cosh\left[\left(n+\frac{1}{2}\right)\tau_2\right]\right.$$

$$+ B_{nM} h_B(n,M) P_n^M(\cos\sigma) \sinh\left[\left(n+\frac{1}{2}\right)\tau_2\right]$$
$$= -\sum_{n=0}^{+\infty} \varepsilon_M \frac{(n-M)!}{(n+M)!} \cos M\phi_0 P_n^M(\cos\sigma) P_n^M(\cos\sigma_0) \mathrm{e}^{-\left(n+\frac{1}{2}\right)(\tau_0-\tau_2)}. \tag{3.23}$$

Multiplying (3.23) by $\sin\sigma P_N^M(\cos\sigma)$ and integrating with respect to σ from 0 to π results in:

$$A_{NM} h_A(N,M) \cosh\left[\left(N+\frac{1}{2}\right)\tau_2\right] + B_{NM} h_B(N,M) \sinh\left[\left(N+\frac{1}{2}\right)\tau_2\right]$$
$$= -\varepsilon_M \frac{(N-M)!}{(N+M)!} \cos M\phi_0 P_N^M(\cos\sigma_0) \mathrm{e}^{-\left(N+\frac{1}{2}\right)(\tau_0-\tau_2)},$$

which, after simplification becomes:

$$A_{NM} \cosh\left[\left(N+\frac{1}{2}\right)\tau_2\right] + B_{NM} \sinh\left[\left(N+\frac{1}{2}\right)\tau_2\right] = -\mathrm{e}^{-\left(N+\frac{1}{2}\right)(\tau_0-\tau_2)}. \tag{3.24}$$

As a result, we have from (3.22) and (3.24) the following system of equations:

$$A_{NM} \frac{\sinh\tau_1 \cosh\left[\left(N+\frac{1}{2}\right)\tau_1\right] + 2\left(N+\frac{1}{2}\right)\cosh\tau_1 \sinh\left[\left(N+\frac{1}{2}\right)\tau_1\right]}{2\sqrt{\cosh\tau_1}}$$
$$+ B_{NM} \frac{\sinh\tau_1 \sinh\left[\left(N+\frac{1}{2}\right)\tau_1\right] + 2\left(N+\frac{1}{2}\right)\cosh\tau_1 \cosh\left[\left(N+\frac{1}{2}\right)\tau_1\right]}{2\sqrt{\cosh\tau_1}}$$
$$= -\left[\frac{\sinh\tau_1}{2\sqrt{\cosh\tau_1}} - \left(N+\frac{1}{2}\right)\sqrt{\cosh\tau_1}\right] \mathrm{e}^{-\left(N+\frac{1}{2}\right)(\tau_1-\tau_0)},$$
$$A_{NM} \cosh\left[\left(N+\frac{1}{2}\right)\tau_2\right] + B_{nm} \sinh\left[\left(N+\frac{1}{2}\right)\tau_2\right]$$
$$= -\mathrm{e}^{-\left(N+\frac{1}{2}\right)(\tau_0-\tau_2)},$$

which we solve for A_{NM} and B_{NM} to obtain:

$$A_{NM} = \frac{W(N,\tau_1)\sinh\left[\left(N+\frac{1}{2}\right)\tau_2\right]\mathrm{e}^{-\left(N+\frac{1}{2}\right)(\tau_1-\tau_0)} - V_2(N,\tau_1)\,\mathrm{e}^{-\left(N+\frac{1}{2}\right)(\tau_0-\tau_2)}}{V_2(N,\tau_1)\cosh\left[\left(N+\frac{1}{2}\right)\tau_2\right] - V_1(N,\tau_1)\sinh\left[\left(N+\frac{1}{2}\right)\tau_2\right]},$$
$$B_{NM} = \frac{W(N,\tau_1)\cosh\left[\left(N+\frac{1}{2}\right)\tau_2\right]\mathrm{e}^{-\left(N+\frac{1}{2}\right)(\tau_1-\tau_0)} - V_1(N,\tau_1)\,\mathrm{e}^{-\left(N+\frac{1}{2}\right)(\tau_0-\tau_2)}}{V_1(N,\tau_1)\sinh\left[\left(N+\frac{1}{2}\right)\tau_2\right] - V_2(N,\tau_1)\cosh\left[\left(N+\frac{1}{2}\right)\tau_2\right]},$$

where $V_1(n,\tau_1), V_2(n)$ and $W(n,\tau_1)$ are defined in (3.13) and $n,m \in \mathbb{N}\cup\{0\}$. As a result we have:

$$4\pi D G_1^{(3)}(\mathbf{x}_0,\mathbf{x}) = \frac{2h_x(\tau,\sigma)\,h_x(\tau_0,\sigma_0)}{d} \sum_{n=0}^{+\infty}\sum_{m=0}^{+\infty} \varepsilon_m \frac{(n-m)!}{(n+m)!} P_n^m(\cos\sigma) P_n^m(\cos\sigma_0)$$

$$\times \cos m(\phi - \phi_0) K^{(3)}_{1,n}(\tau, \tau_0), \tag{3.25}$$

where

$$K^{(3)}_{1,n}(\tau, \tau_0) = A_{nm} \cosh\left[\left(n + \frac{1}{2}\right)\tau\right] + B_{nm} \sinh\left[\left(n + \frac{1}{2}\right)\tau\right] + \mathrm{e}^{-\left(n+\frac{1}{2}\right)|\tau - \tau_0|}.$$

Making use of the following calculations:

$$V_2(n, \tau_1) \cosh\left[\left(n + \frac{1}{2}\right)\tau_2\right] - V_1(n, \tau_1) \sinh\left[\left(n + \frac{1}{2}\right)\tau_2\right] =$$
$$\sinh\tau_1 \sinh\left[\left(n + \frac{1}{2}\right)(\tau_1 - \tau_2)\right] - 2\left(n + \frac{1}{2}\right)\cosh\tau_1 \cosh\left[\left(n + \frac{1}{2}\right)(\tau_1 - \tau_2)\right],$$
$$W(n, \tau_1) \sinh\left[\left(N + \frac{1}{2}\right)\tau_2\right] \mathrm{e}^{-\left(N+\frac{1}{2}\right)(\tau_1 - \tau_0)} - V_2(n, \tau_1)\, \mathrm{e}^{-\left(N+\frac{1}{2}\right)(\tau_0 - \tau_2)} =$$
$$= \sinh\tau_1 \left\{ \mathrm{e}^{-\left(n+\frac{1}{2}\right)(\tau_1 - \tau_0)} \sinh\left[\left(n + \frac{1}{2}\right)\tau_2\right] - \mathrm{e}^{-\left(n+\frac{1}{2}\right)(\tau_0 - \tau_2)} \sinh\left[\left(n + \frac{1}{2}\right)\tau_1\right] \right\}$$
$$- 2\left(n + \frac{1}{2}\right)\cosh\tau_1 \left\{ \mathrm{e}^{-\left(n+\frac{1}{2}\right)(\tau_1 - \tau_0)} \sinh\left[\left(n + \frac{1}{2}\right)\tau_2\right] \right\}$$
$$- 2\left(n + \frac{1}{2}\right)\cosh\tau_1 \left\{ \mathrm{e}^{-\left(n+\frac{1}{2}\right)(\tau_0 - \tau_2)} \cosh\left[\left(n + \frac{1}{2}\right)\tau_1\right] \right\},$$
$$W(n, \tau_1) \cosh\left[\left(N + \frac{1}{2}\right)\tau_2\right] \mathrm{e}^{-\left(N+\frac{1}{2}\right)(\tau_1 - \tau_0)} - V_1(n, \tau_1)\, \mathrm{e}^{-\left(N+\frac{1}{2}\right)(\tau_0 - \tau_2)} =$$
$$= \sinh\tau_1 \left\{ \mathrm{e}^{-\left(n+\frac{1}{2}\right)(\tau_1 - \tau_0)} \cosh\left[\left(n + \frac{1}{2}\right)\tau_2\right] - \mathrm{e}^{-\left(n+\frac{1}{2}\right)(\tau_0 - \tau_2)} \cosh\left[\left(n + \frac{1}{2}\right)\tau_1\right] \right\}$$
$$- 2\left(n + \frac{1}{2}\right)\cosh\tau_1 \left\{ \mathrm{e}^{-\left(n+\frac{1}{2}\right)(\tau_1 - \tau_0)} \cosh\left[\left(n + \frac{1}{2}\right)\tau_2\right] \right\}$$
$$- 2\left(n + \frac{1}{2}\right)\cosh\tau_1 \left\{ \mathrm{e}^{-\left(n+\frac{1}{2}\right)(\tau_0 - \tau_2)} \sinh\left[\left(n + \frac{1}{2}\right)\tau_1\right] \right\},$$

we obtain, after simplification, the following:

$$K^{(3)}_{1,n}(\tau, \tau_0) = \sinh\left[\left(n + \frac{1}{2}\right)(\tau_m - \tau_2)\right] \frac{\cosh\left[\left(n + \frac{1}{2}\right)(\tau_1 - \tau_M)\right]}{\cosh\left[\left(n + \frac{1}{2}\right)(\tau_1 - \tau_2)\right]}$$
$$\times \frac{\tanh\tau_1 \tanh\left[\left(n + \frac{1}{2}\right)(\tau_1 - \tau_M)\right] + 2\left(n + \frac{1}{2}\right)}{\tanh\tau_1 \tanh\left[\left(n + \frac{1}{2}\right)(\tau_1 - \tau_2)\right] + 2\left(n + \frac{1}{2}\right)}, \tag{3.26}$$

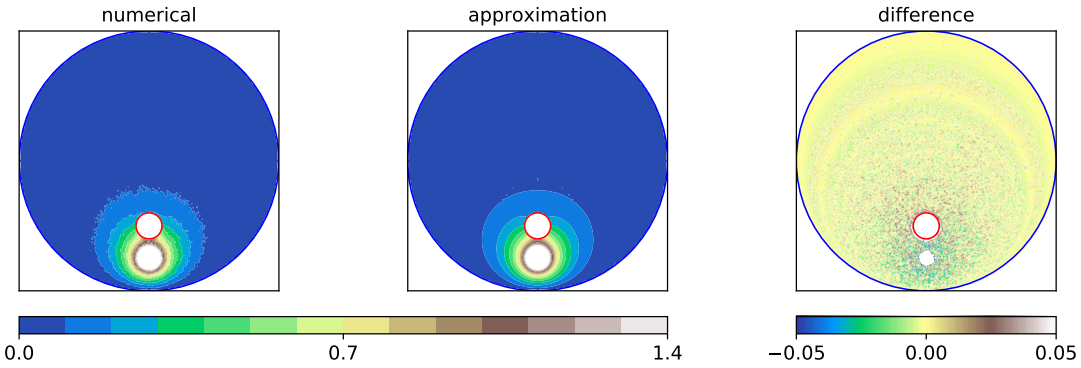

Figure 3.5: Plot of numerical simulation of $G_1^{(3)}(\mathbf{x}_0, \mathbf{x})$ (left), approximation (3.25) (centre) and difference (right). The initial condition is $\mathbf{x}_0 - \mathbf{x}_c = (0, 0, -0.75)$ and $a = 0.1, c = 0.5$. Here $\mathbf{x}_c$ is the position vector of the cellular centre.

where $\tau_m = \min\{\tau, \tau_0\}$ and $\tau_M = \max\{\tau, \tau_0\}$. We plot $G_1^{(3)}(\mathbf{x}_0, \mathbf{x})$ in Figure 3.11 and compare with numerical simulations. We observe from (3.26) that we can write $K_{1,n}^{(3)}(\tau, \tau_0)$ as:

$$K_{1,n}^{(3)}(\tau, \tau_0) = K_{1,n+\frac{1}{2}}^{(2)}(\tau, \tau_0) \times E_n(\tau, \tau_0),$$

where $K_{1,n}^{(2)}(\tau, \tau_0)$ is the summand from (2.13) and:

$$E_n(\tau, \tau_0) = \frac{\tanh\tau_1 \tanh\left[\left(n+\frac{1}{2}\right)(\tau_1 - \tau_M)\right] + 2\left(n+\frac{1}{2}\right)}{\tanh\tau_1 \tanh\left[\left(n+\frac{1}{2}\right)(\tau_1 - \tau_2)\right] + 2\left(n+\frac{1}{2}\right)}.$$

As a result, the transition from two dimensions to three dimensions leads to the appearance of the correction term $E_n(\tau, \tau_0)$ and the change of index from n to $n + \frac{1}{2}$.

3.5.1 Comparison with the interior Dirichlet Green's function

The interior Dirichlet Green's function satisfies the following equations:

$$\begin{aligned} &D\Delta_{\mathbf{x}} G_0^{(3)}(\mathbf{x}_0, \mathbf{x}) = -\delta(\mathbf{x} - \mathbf{x}_0) \quad \text{if} \quad \mathbf{x} \in C^*, \\ &G_0^{(3)}(\mathbf{x}_0, \mathbf{x}) = 0 \quad \text{if} \quad \mathbf{x} \in \partial C_2, \end{aligned} \tag{3.27}$$

where ∂C_2 is the absorbing outer boundary and $\mathbf{x}_0$ is the initial position of the point particle. $G_0^{(3)}(\mathbf{x}_0, \mathbf{x})$ is the occupation density of the time a particle spends at $\mathbf{x}$ given that it started at $\mathbf{x}_0$ and is diffusing inside a sphere of radius 1 with absorbing boundary. The solution of (3.27) is given by Barton (1989) as:

$$G_0^{(3)}(\mathbf{x}_0, \mathbf{x}) = \frac{1}{4\pi D}\left(\frac{1}{\mathrm{R}} - \frac{1}{r_0\tilde{\mathrm{R}}}\right), \tag{3.28}$$

where

$$\mathrm{R} = |\mathbf{x} - \mathbf{x}_0|, \quad \tilde{\mathrm{R}} = |\mathbf{x} - \tilde{\mathbf{x}}_0| \quad \text{and} \quad r_0 = |\mathbf{x}_0|.$$

and $\tilde{\mathbf{x}}_0$ is the image point of $\mathbf{x}_0$ with respect to the cellular boundary such that $\mathbf{x}_0 \cdot \tilde{\mathbf{x}}_0 = 1$. We expand each term in bispherical coordinates, beginning with the first Chen *et al.*:

$$\begin{aligned}\frac{1}{\mathrm{R}} &= \frac{1}{d} h_x(\tau, \sigma)\, h_x(\tau_0, \sigma_0) \sum_{n=0}^{+\infty}\sum_{m=0}^{+\infty} \varepsilon_m \frac{(n-m)!}{(n+m)!} P_n^m(\cos\sigma) P_n^m(\cos\sigma_0) \\ &\quad \times \cos m(\phi - \phi_0) \mathrm{e}^{-\left(n+\frac{1}{2}\right)|\tau - \tau_0|}.\end{aligned}$$

Analogously, the second term is written by splitting it into two parts:

$$\begin{aligned}\frac{1}{\tilde{\mathrm{R}}} &= \frac{1}{d} h_x(\tau, \sigma)\, h_x(\tilde{\tau}_0, \tilde{\sigma}_0) \sum_{n=0}^{+\infty}\sum_{m=0}^{+\infty} \varepsilon_m \frac{(n-m)!}{(n+m)!} P_n^m(\cos\sigma) P_n^m(\cos\tilde{\sigma}_0) \\ &\quad \times \cos m(\phi - \tilde{\phi}_0) \mathrm{e}^{-\left(n+\frac{1}{2}\right)|\tau - \tilde{\tau}_0|} \\ &= \frac{1}{d} h_x(\tau, \sigma)\, h_x(\tilde{\tau}_0, \tilde{\sigma}_0) \sum_{n=0}^{+\infty}\sum_{m=0}^{+\infty} \varepsilon_m \frac{(n-m)!}{(n+m)!} P_n^m(\cos\sigma) P_n^m(\cos\sigma_0) \\ &\quad \times \cos m(\phi - \phi_0) \mathrm{e}^{-\left(n+\frac{1}{2}\right)|2\tau_2 - \tau_0 - \tau|},\end{aligned}$$

and

$$\begin{aligned}\frac{1}{r_0} &= \frac{1}{d} h_x(\tau_c, \sigma_c)\, h_x(\tau_0, \sigma_0) \sum_{n=0}^{+\infty}\sum_{m=0}^{+\infty} \varepsilon_m \frac{(n-m)!}{(n+m)!} P_n^m(\cos\sigma_c) P_n^m(\cos\sigma_0) \\ &\quad \times \cos m(\phi_c - \phi_0) \mathrm{e}^{-\left(n+\frac{1}{2}\right)|\tau_0 - \tau_c|} \\ &= \frac{1}{d}\sqrt{\cosh 2\tau_2 - 1}\, h_x(\tau_0, \sigma_0) \sum_{n=0}^{+\infty}\sum_{m=0}^{+\infty} \varepsilon_m \frac{(n-m)!}{(n+m)!} P_n^m(\cos 0) P_n^m(\cos\sigma_0) \\ &\quad \times \cos m\phi_0 \mathrm{e}^{-\left(n+\frac{1}{2}\right)|2\tau_2 - \tau_0|}\end{aligned}$$

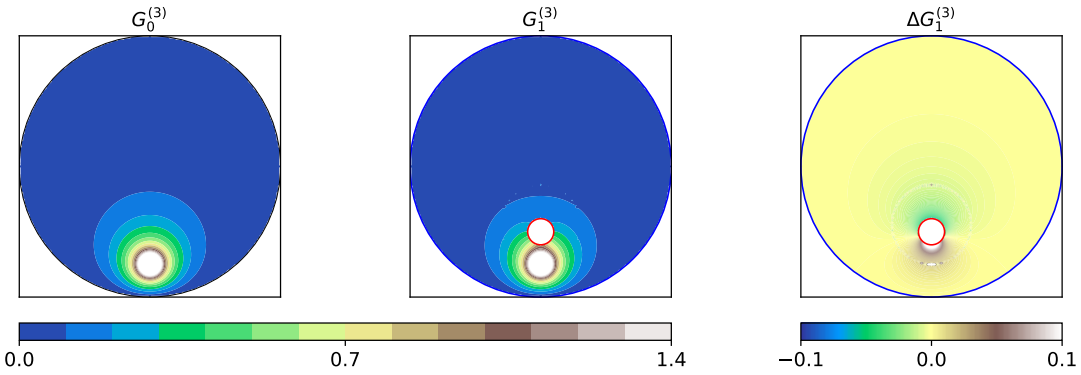

Figure 3.6: Plot of the Green's function $G_0^{(3)}(\mathbf{x}_0, \mathbf{x})$ formula (left, formula from (3.29)), the Green's function $G_1^{(3)}(\mathbf{x}_0, \mathbf{x})$ (centre, formula from (3.25)) and difference (right). The initial condition is $\mathbf{x}_0 - \mathbf{x}_c = (0, 0, -0.75)$ and $a = 0.1, c = 0.5$. Here $\mathbf{x}_c$ is the position vector of the cellular centre.

$$= \sqrt{2} h_x(\tau_0, \sigma_0) \sum_{n=0}^{+\infty} P_n(\cos\theta_0) \mathrm{e}^{-\left(n+\frac{1}{2}\right)|2\tau_2 - \tau_0|}$$
$$= \frac{h_x(\tau_0, \sigma_0)}{h_x(\tilde{\tau}_0, \tilde{\sigma}_0)},$$

where $(\tau_c, \sigma_c, \phi_c)$ are the bispherical coordinates of $\mathbf{x}_c$ (the centre of the cell) for which we have used Appendix C.3 to relate to known quantities. Additionally, we have used the fact that (Love, 1975, p.471):

$$\frac{1}{h_x(\tau, \sigma)} = \frac{1}{\sqrt{\cosh\tau - \cos\sigma}} = \sqrt{2} \sum_{n=0}^{+\infty} P_n(\cos\sigma) \mathrm{e}^{-\left(n+\frac{1}{2}\right)\tau},$$

and

$$\begin{aligned}\cosh 2\tau_2 - 1 &= \frac{\mathrm{e}^{2\log\left(d+\sqrt{1+d^2}\right)} + \mathrm{e}^{-2\log\left(d+\sqrt{1+d^2}\right)}}{2} - 1 \\ &= \frac{\left(d+\sqrt{1+d^2}\right)^4 + 1 - 2\left(d+\sqrt{1+d^2}\right)^2}{\left(d+\sqrt{1+d^2}\right)^2} \\ &= 2d^2.\end{aligned}$$

As a result, we write the three dimensional interior Dirichlet function in bispherical coordinates as:

$$4\pi D G_0^{(3)}(\mathbf{x}_0, \mathbf{x})$$

$$
\begin{aligned}
&= \frac{h_x(\tau,\sigma)\,h_x(\tau_0,\sigma_0)}{d}\sum_{n=0}^{+\infty}\sum_{m=0}^{+\infty}\varepsilon_m\frac{(n-m)!}{(n+m)!}P_n^m(\cos\sigma)P_n^m(\cos\sigma_0)\cos m(\phi-\phi_0)\\
&\times\left[\mathrm{e}^{-(n+\frac{1}{2})|\tau-\tau_0|}-\mathrm{e}^{-(n+\frac{1}{2})|\tau-\tilde{\tau}_0|}\right]\\
&= \frac{2h_x(\tau,\sigma)\,h_x(\tau_0,\sigma_0)}{d}\sum_{n=0}^{+\infty}\sum_{m=0}^{+\infty}\varepsilon_m\frac{(n-m)!}{(n+m)!}P_n^m(\cos\sigma)P_n^m(\cos\sigma_0)\cos m(\phi-\phi_0)\\
&\times\sinh\left[\left(n+\frac{1}{2}\right)(\tau_m-\tau_2)\right]\mathrm{e}^{-\left(n+\frac{1}{2}\right)(\tau_M-\tau_2)}. \qquad (3.29)
\end{aligned}
$$

Taking the difference between our Green's function approximation (3.25) and the interior Dirichlet Green's function (3.29) we obtain:

$$
\begin{aligned}
&4\pi D\Delta G_1^{(3)}(\mathbf{x}_0,\mathbf{x})\\
&= 4\pi D\left(G_1^{(3)}(\mathbf{x}_0,\mathbf{x})-G_0^{(3)}(\mathbf{x}_0,\mathbf{x})\right)\\
&= \frac{2h_x(\tau,\sigma)\,h_x(\tau_0,\sigma_0)}{d}\sum_{n=0}^{+\infty}\sum_{m=0}^{+\infty}\varepsilon_m\frac{(n-m)!}{(n+m)!}P_n^m(\cos\sigma)P_n^m(\cos\sigma_0)\cos m(\phi-\phi_0)\\
&\times\left\{\frac{\sinh\left[\left(n+\frac{1}{2}\right)(\tau_m-\tau_2)\right]\sinh\left[\left(n+\frac{1}{2}\right)(\tau_1-\tau_M)\right]}{\sinh\left[\left(n+\frac{1}{2}\right)(\tau_1-\tau_2)\right]}\right.\\
&\times\frac{\tanh\tau_1+2\left(n+\frac{1}{2}\right)\coth\left[\left(n+\frac{1}{2}\right)(\tau_1-\tau_M)\right]}{\tanh\tau_1+2\left(n+\frac{1}{2}\right)\coth\left[\left(n+\frac{1}{2}\right)(\tau_1-\tau_2)\right]}\\
&\left.-\sinh\left[\left(n+\frac{1}{2}\right)(\tau_m-\tau_2)\right]\mathrm{e}^{-\left[\left(n+\frac{1}{2}\right)(\tau_M-\tau_2)\right]}\right\}\\
&= \frac{2h_x(\tau,\sigma)\,h_x(\tau_0,\sigma_0)}{d}\sum_{n=0}^{+\infty}\sum_{m=0}^{+\infty}\varepsilon_m\frac{(n-m)!}{(n+m)!}P_n^m(\cos\sigma)P_n^m(\cos\sigma_0)\\
&\times\cos m(\phi-\phi_0)\Delta K_{1,n}^{(3)}(\tau,\tau_0), \qquad (3.30)
\end{aligned}
$$

where

$$
\begin{aligned}
\Delta K_{1,n}^{(3)}(\tau,\tau_0) = -\mathrm{e}^{-\left(n+\frac{1}{2}\right)(\tau_1-\tau_2)}&\frac{\sinh\left[\left(n+\frac{1}{2}\right)(\tau_m-\tau_2)\right]\sinh\left[\left(n+\frac{1}{2}\right)(\tau_M-\tau_2)\right]}{\sinh\left[\left(n+\frac{1}{2}\right)(\tau_1-\tau_2)\right]}\\
&\times\frac{\tanh\tau_1-2\left(n+\frac{1}{2}\right)}{\tanh\tau_1+2\left(n+\frac{1}{2}\right)\coth\left[\left(n+\frac{1}{2}\right)(\tau_1-\tau_2)\right]}.
\end{aligned}
$$

We plot (3.29) and (3.30) in Figure 3.6 and observe that the absence of the intracellular compartment has the effect that the Brownian particle will spend less time in the area defined by the direction $\sigma = 0$ and more time in the area defined by the direction $\sigma = \pi$.

3.5.2 Concentric Green's function

An interesting case which we wish to investigate is the concentric case where $c \to +0$ in (3.25). We begin with the following prerequisite calculations:

$$\begin{aligned}
\frac{h_x(\tau,\sigma)\,h_x(\tau_0,\sigma_0)}{d} &= \frac{\sqrt{(\cosh\tau-\cos\sigma)(\cosh\tau_0-\cos\sigma_0)}}{d} \\
&= \sqrt{\left(\frac{1}{r}+\sqrt{\frac{1}{d^2}+\frac{1}{r^2}}+d^{-1}\left(\frac{d}{r}+\sqrt{1+\frac{d^2}{r^2}}\right)^{-1}-\frac{\cos\sigma}{d}\right)} \\
&\times \sqrt{\left(\frac{1}{r_0}+\sqrt{\frac{1}{d^2}+\frac{1}{r_0^2}}+d^{-1}\left(\frac{d}{r_0}+\sqrt{1+\frac{d^2}{r_0^2}}\right)^{-1}-\frac{\cos\sigma}{d}\right)} \\
&\to \frac{2}{\sqrt{rr_0}}, \quad \text{as } c \to +0,
\end{aligned} \tag{3.31}$$

where we used the following identity:

$$\begin{aligned}
\cosh\tau &= \frac{\frac{d}{r}+\sqrt{1+\frac{d^2}{r^2}}+\left(\frac{d}{r}+\sqrt{1+\frac{d^2}{r^2}}\right)^{-1}}{2} \\
&= d\frac{\frac{1}{r}+\sqrt{\frac{1}{d^2}+\frac{1}{r^2}}+d^{-1}\left(\frac{d}{r}+\sqrt{1+\frac{d^2}{r^2}}\right)^{-1}}{2},
\end{aligned}$$

and $d \to +\infty$ as $c \to +0$. Using appendix B.8 and (3.31) in (3.25) as $c \to +0$ we obtain:

$$\begin{aligned}
4\pi D G_1^{(3)}(\mathbf{x}_0,\mathbf{x}) = \frac{2}{\pi\sqrt{rr_0}}\sum_{n=0}^{+\infty}\sum_{m=0}^{+\infty}\varepsilon_m\frac{(n-m)!}{(n+m)!}P_n^m(\cos\theta)P_n^m(\cos\theta_0) \\
\times\cos m(\varphi-\varphi_0)Q_n(r,r_0),
\end{aligned}$$

where (r,θ,φ) are the polar coordinates of $\mathbf{x}$, (r_0,θ_0,φ_0) are the polar coordinates of $\mathbf{x}_0$ and:

$$Q_n(r,r_0) = \frac{\left[\left(\frac{1}{r_M}\right)^{n+\frac{1}{2}}-r_M^{n+\frac{1}{2}}\right]\left[\left(\frac{r_m}{a}\right)^{n+\frac{1}{2}}-\left(\frac{a}{r_m}\right)^{n+\frac{1}{2}}\right]}{\left[\left(\frac{1}{a}\right)^{n+\frac{1}{2}}+a^{n+\frac{1}{2}}\right]}$$

$$\times \frac{1+(2n+1)\,\frac{r_m^{2n+1}+a^{2n+1}}{r_m^{2n+1}-a^{2n+1}}}{1+(2n+1)\,\frac{1+a^{2n+1}}{1-a^{2n+1}}},$$

where $r_M = \max\{r, r_0\}$ and $r_m = \min\{r, r_0\}$.

3.5.3 Hitting density on the cellular surface

Analogous to the two dimensional case discussed in Section 2.5, the density of the hitting point on the cellular surface ∂C_2, is given as a function of the Cartesian angle θ_2 (here θ_2 is the angle defined by $\mathbf{x} \in \partial C_2$, *i.e.* the angle $\angle \mathbf{O}\mathbf{x}_c\mathbf{x}$ where $\mathbf{x}_c$ is the centre of the cell and $\mathbf{O}$ is the origin of the coordinate system):

$$\varepsilon^{(3)}(\theta_2) = -D\,\frac{\partial P^{(3)}(\mathbf{x})}{\partial \mathbf{n}_2}\bigg|_{\partial C_2},$$

where $\mathbf{n}_2$ is the unit normal outward vector to ∂C_2 and

$$P^{(3)}(\mathbf{x}) = \frac{1}{4\pi a^2}\int_{\partial C_1} G_1^{(3)}\left(\mathbf{x}_0, \mathbf{x}\right)\,\mathrm{d}\mathbf{x}_0.$$

Using (3.25) we write $4\pi a^2 P^{(3)}(\mathbf{x})$ as:

$$\begin{aligned}
&d^2\int_0^{\pi}\int_0^{2\pi}\frac{G_1^{(3)}\left(\mathbf{x}_0,\mathbf{x}\right)\sin\phi_0}{\left(\cosh\tau_0-\cos\sigma_0\right)^2}\,\mathrm{d}\phi_0\mathrm{d}\sigma_0\\
&=\frac{d}{2\pi D}h_x\left(\tau,\sigma\right)\sum_{n=0}^{+\infty}\sum_{m=0}^{+\infty}\varepsilon_m\frac{(n-m)!}{(n+m)!}P_n^m(\cos\sigma)\\
&\times\int_0^{\pi}\frac{P_n^m(\cos\sigma_0)\sin\phi_0}{\left(\cosh\tau_0-\cos\sigma_0\right)^{\frac{3}{2}}}\,\mathrm{d}\sigma_0\int_0^{2\pi}\cos m(\phi-\phi_0)\,\mathrm{d}\phi_0 K_{1,n}^{(3)}(\tau,\tau_0).
\end{aligned}$$

We know that the integral:

$$\int_0^{2\pi}\cos m(\phi-\phi_0)\,\mathrm{d}\phi_0 = 2\pi\delta_{m0},$$

and the fact that $P_n^0(x) = P_n(x)$, we make use of Appendix C.4 to derive:

$$\begin{aligned}
\varepsilon^{(3)}(\theta_2) &= \frac{\sqrt{2}\left(\cosh\tau_2-\cos\sigma_2\right)^{\frac{3}{2}}}{\pi a^2\sinh\tau_1}\\
&\times\sum_{n=0}^{+\infty}\frac{\mathrm{e}^{-\left(n+\frac{1}{2}\right)\tau_1}\left(n+\frac{1}{2}\right)^2}{\sinh\left[\left(n+\frac{1}{2}\right)\left(\tau_1-\tau_2\right)\right]\tanh\tau_1+2\left(n+\frac{1}{2}\right)\cosh\left[\left(n+\frac{1}{2}\right)\left(\tau_1-\tau_2\right)\right]},
\end{aligned}\tag{3.32}$$

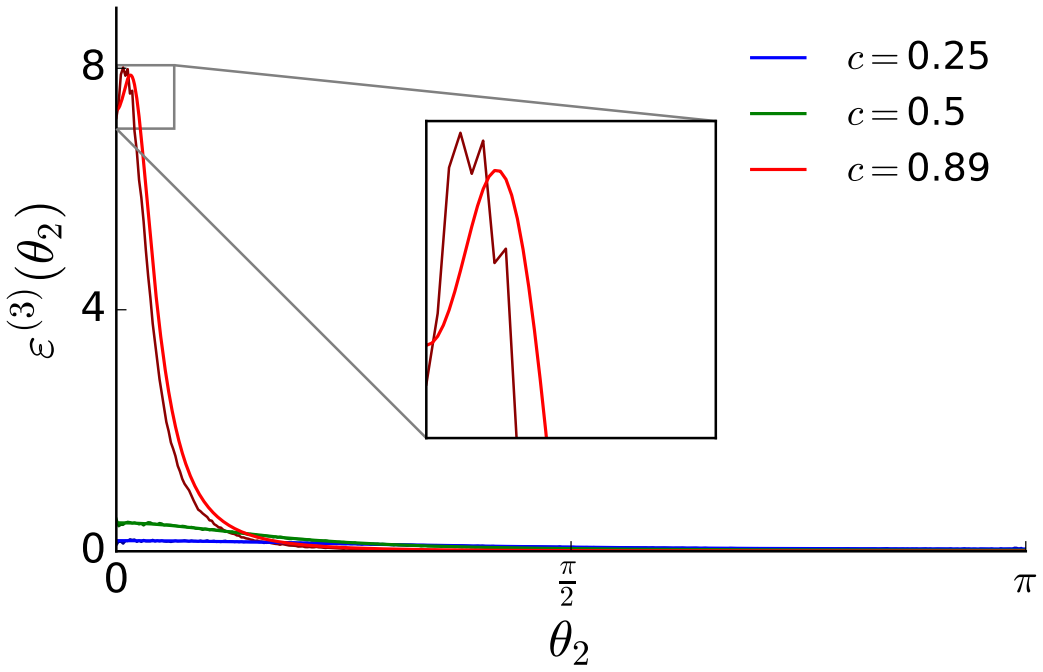

Figure 3.7: Plot of $\varepsilon^{(3)}(\theta_2)$ comparing the numerical simulation with the approximation obtained in (3.32) as a function of θ_2 for $c = 0.25$, 0.5 and 0.89. The lighter colours represent the analytic result and the darker colours represent the numerical simulations. The numerical results have been obtained by having 10^5 particles uniformly distributed on the sphere of radius a from Figure 3.1 and recording their endpoint. The inset shows $\varepsilon^{(3)}(\theta_2)$ for $c = 0.89$ and small values of θ_2. For our simulations we have chosen the following parameter values: $a = 0.1$.

where

$$\sigma_2 = \arccos \frac{1 + \cos\theta_2\sqrt{1+d^2}}{\sqrt{\left(1 + d^2 + \cos\theta_2\sqrt{1+d^2}\right)^2 - d^2\left(\cos\theta_2 + \sqrt{1+d^2}\right)^2}},$$

which we plot in Figure 3.7 and compare with numerical simulations for various values of c. We observe that, as c increases, the accuracy of our formula decreases which is predicted by the approximation (3.20) we used to derive $G_1^{(3)}(\mathbf{x}_0, \mathbf{x})$.

3.5.4 Mean time to hit the cellular surface

We use (3.25) to obtain the mean time $T_1^{(3)}(\theta_1, a, c)$ by integrating the Green's function $G_1^{(3)}(\mathbf{x}_0, \mathbf{x})$ over the annular region C:

$$\begin{aligned} T_1^{(3)}(\theta_1, a, c) &= R^2 \int_C G_1^{(3)}(\mathbf{x}_0, \mathbf{x})\, \mathrm{d}\mathbf{x} \\ &= R^2 \int_{\tau_2}^{\tau_1} \int_0^{2\pi} \int_0^{\pi} \frac{d^3 G_1^{(3)}(\mathbf{x}_0, \mathbf{x}) \sin\phi}{(\cosh\tau - \cos\sigma)^3}\, \mathrm{d}\sigma \mathrm{d}\phi \mathrm{d}\tau, \end{aligned} \tag{3.33}$$

where $\mathbf{x}_0 \in \partial C_1$ is characterized by the angle θ_1 (here θ_1 is the angle defined by $\mathbf{x} \in \partial C_1$, *i.e.* the angle $\angle \mathbf{O}\mathbf{x}_n\mathbf{x}$ where $\mathbf{x}_n$ is the centre of the nucleus and $\mathbf{O}$ is the origin of the coordinate system) and

$$\sigma_1 = \arccos \frac{a^2 + a\cos\theta_1 \sqrt{a^2 + d^2}}{\sqrt{\left(a^2 + d^2 + a\cos\theta_1 \sqrt{a^2 + d^2}\right)^2 - d^2 \left(a\cos\theta_1 + \sqrt{a^2 + d^2}\right)^2}}.$$

In (3.33) the mean time $T_1^{(3)}(\theta_1, a, c)$ is defined as:

$$\begin{aligned} T_1^{(3)}(\theta_1, a, c) &= E\left(t_1^{(3)}(\mathbf{x}_0)\right) \\ &= \text{mean time for a particle starting at } \mathbf{x}_0 \in \partial C_1 \text{ to hit } \partial C_2, \end{aligned}$$

Here, $t_1^{(3)}(\mathbf{x}_0)$ is the random variable defined as follows:

$$t_1^{(3)}(\mathbf{x}_0) = \text{time for a particle starting at } \mathbf{x}_0 \text{ on the cellular nucleus to reach the cellular surface.}$$

Making use of Appendix C.5 we determine the integral:

$$\begin{aligned} & d^3 \int_{\tau_2}^{\tau_1} \int_0^{\pi} \int_0^{2\pi} \frac{G_1^{(3)}(\mathbf{x}_0, \mathbf{x}) \sin\phi}{(\cosh\tau - \cos\sigma)^3}\, \mathrm{d}\sigma \mathrm{d}\phi \mathrm{d}\tau \\ &= \frac{d^2}{2\pi D} h_x(\tau, \sigma) \sum_{n=0}^{+\infty} \sum_{m=0}^{+\infty} \varepsilon_m \frac{(n-m)!}{(n+m)!} P_n^m(\cos\sigma_1) \\ &\times \int_{\tau_2}^{\tau_1} \left[\int_0^{\pi} \frac{P_n^m(\cos\sigma)\sin\sigma}{(\cosh\tau - \cos\sigma)^{\frac{5}{2}}}\, \mathrm{d}\sigma \int_0^{2\pi} \cos m(\phi - \phi_0)\, \mathrm{d}\phi \right] F_n(\tau, \tau_1)\, \mathrm{d}\tau \end{aligned} \tag{3.34}$$

$$= \frac{d^2}{2\pi D} h_x(\tau, \sigma) \sum_{n=0}^{+\infty} \frac{2P_n(\cos\sigma_1)}{2n+1} \int_{\tau_2}^{\tau_1} U_n(\tau) K_{1,n}^{(3)}(\tau, \tau_1)\, \mathrm{d}\tau, \tag{3.35}$$

where

$$K_{1,n}^{(3)}(\tau,\tau_1)=\frac{2\left(n+\frac{1}{2}\right)\sinh\left[\left(n+\frac{1}{2}\right)(\tau-\tau_2)\right]}{\sinh\left[\left(n+\frac{1}{2}\right)(\tau_1-\tau_2)\right]\tanh\tau_1+2\left(n+\frac{1}{2}\right)\cosh\left[\left(n+\frac{1}{2}\right)(\tau_1-\tau_2)\right]},$$

and $U_n(\tau)$ is defined in (C.5). Furthermore, in (3.34) we have made use of the following:

$$\begin{aligned}\int_0^{\pi}\frac{P_n(\cos\sigma)\sin\sigma}{(\cosh\tau-\cos\sigma)^{\frac{5}{2}}}\,\mathrm{d}\sigma&=\sum_{N=0}^{+\infty}U_N(\tau)\int_0^{\pi}P_n(\cos\sigma)P_N(\cos\sigma)\sin\sigma\,\mathrm{d}\sigma\\&=\frac{2U_n(\tau)}{2n+1}.\end{aligned}$$

The integral in (3.35) is given by:

$$\begin{aligned}&\int_{\tau_2}^{\tau_1}U_n(\tau)K_{1,n}^{(3)}(\tau,\tau_1)\,d\tau=\\&\frac{2\sqrt{2}\left(n+\frac{1}{2}\right)}{\sinh\left[\left(n+\frac{1}{2}\right)(\tau_1-\tau_2)\right]\tanh\tau_1+2\left(n+\frac{1}{2}\right)\cosh\left[\left(n+\frac{1}{2}\right)(\tau_1-\tau_2)\right]}\\&\times\int_{\tau_2}^{\tau_1}\sinh\left[\left(n+\frac{1}{2}\right)(\tau-\tau_2)\right]\left[\frac{(2n+3)(2n+1)}{3}\frac{\mathrm{e}^{-\left(n+\frac{1}{2}\right)\tau}}{\sinh^2\tau}+\frac{2}{3}(2n+1)\frac{\mathrm{e}^{-\left(n+\frac{3}{2}\right)\tau}}{\sinh^3\tau}\right]\mathrm{d}\tau,\end{aligned}\tag{3.36}$$

where the last integral is difficult to solve analytically and we will make use of numerical methods in our calculations.

Using (3.36) in (3.35) we obtain the mean time:

$$\begin{aligned}&\frac{2D}{R^2}T_1^{(3)}(\theta_1,a,c)=\\&8\sqrt{2}d^2\sum_{n=0}^{+\infty}\frac{h_x(\tau,\sigma)\left(n+\frac{1}{2}\right)P_n(\cos\sigma_1)}{\sinh\left[\left(n+\frac{1}{2}\right)(\tau_1-\tau_2)\right]\tanh\tau_1+2\left(n+\frac{1}{2}\right)\cosh\left[\left(n+\frac{1}{2}\right)(\tau_1-\tau_2)\right]}\\&\times\int_{\tau_2}^{\tau_1}\sinh\left[\left(n+\frac{1}{2}\right)(\tau-\tau_2)\right]\left[\frac{(2n+3)}{3}\frac{\mathrm{e}^{-\left(n+\frac{1}{2}\right)\tau}}{\sinh^2\tau}+\frac{2}{3}\frac{\mathrm{e}^{-\left(n+\frac{3}{2}\right)\tau}}{\sinh^3\tau}\right]\mathrm{d}\tau,\end{aligned}\tag{3.37}$$

which we plot in Figure 3.8 and compare with numerical simulations. We observe that the largest divergence of $T_1^{(3)}(\theta_1,a,c)$ occurs for values of $\theta_1=0,\pi$ (which in bispherical coordinates translate into $\sigma_1=0,\pi$) which is the value for which the cosine in the prefactor $h_x(\tau,\sigma)=\sqrt{\cosh\tau-\cos\sigma}$ obtains its maximum magnitude.

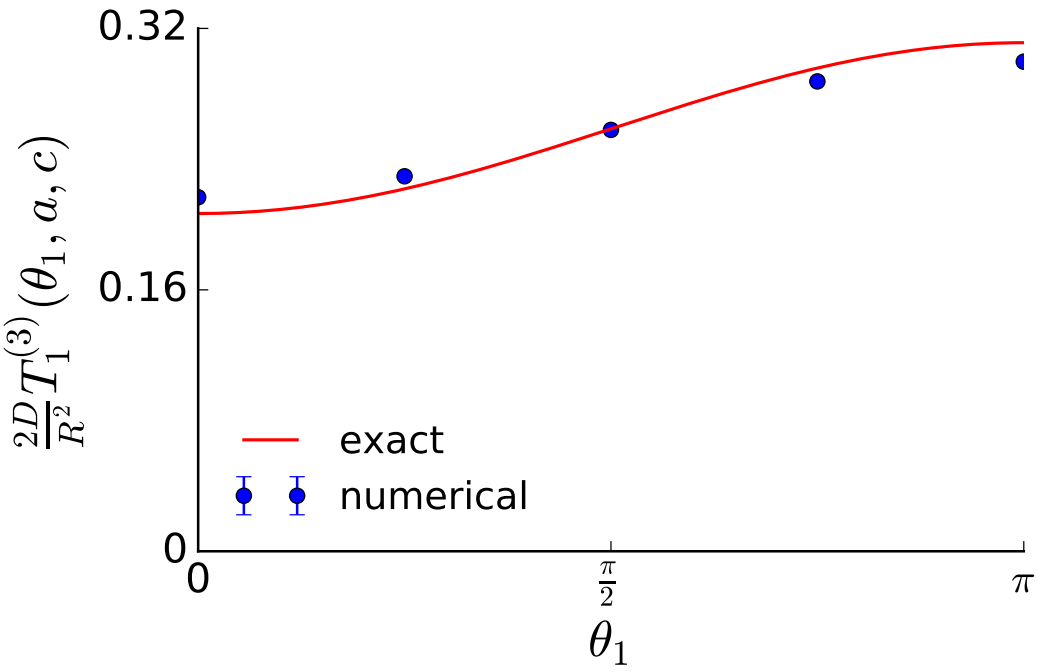

Figure 3.8: Plot of $T_1^{(3)}(\theta_1, a, c)$ as a function of θ_1 where the red line is the approximation (3.37) and the blue dots are numerical simulations. For this figure we have used the following parameters: $a = 0.1$.

3.5.5 Average mean time to hit the cellular surface

We next obtain the mean hitting time $\bar{T}_1^{(3)}(a, c)$, when the initial position $\mathbf{x}_0$ is distributed uniformly over ∂C_1. Firstly,

$$\bar{T}_1^{(3)}(a, c) = \int_{\partial C_1} \frac{T_1^{(3)}(\theta_1, a, c)}{4\pi a^2} \mathrm{d}\mathbf{x}_0 = \frac{d^2}{4\pi a^2} \int_0^{\pi} \int_0^{2\pi} \frac{T_1^{(3)}(\theta_1, a, c) \sin\sigma_1}{(\cosh\tau_1 - \cos\sigma_1)^2} \mathrm{d}\sigma_1 \mathrm{d}\phi_1, \tag{3.38}$$

which we evaluate, using Appendix C.4, to be:

$$\frac{2D}{R^2}\bar{T}_1^{(3)}(a, c) = \frac{8\sqrt{2}\pi d^3}{\pi a} \times \sum_{n=0}^{+\infty} \frac{\left(n + \frac{1}{2}\right) \mathrm{e}^{-\left(n+\frac{1}{2}\right)\tau_1} I_n}{\sinh\left[\left(n + \frac{1}{2}\right)(\tau_1 - \tau_2)\right] \tanh\tau_1 + 2\left(n + \frac{1}{2}\right) \cosh\left[\left(n + \frac{1}{2}\right)(\tau_1 - \tau_2)\right]}, \tag{3.39}$$

where in the above we have used the fact that:

$$\frac{d}{\sinh\tau_1} = a,$$

and

$$I_n = \int_{\tau_2}^{\tau_1} \sinh\left[\left(n+\frac{1}{2}\right)(\tau-\tau_2)\right]\left[\frac{(2n+3)}{3}\frac{\mathrm{e}^{-\left(n+\frac{1}{2}\right)\tau}}{\sinh^2\tau} + \frac{2}{3}\frac{\mathrm{e}^{-\left(n+\frac{3}{2}\right)\tau}}{\sinh^3\tau}\right]\mathrm{d}\tau.$$

We plot (3.39) in Figure 3.9 and we compare with numerical simulations. We observe that the accuracy of our approximation decreases as a function of the nuclear displacement c which is because of the approximation we have made in (3.20) in order to calculate $G_1^{(3)}(\mathbf{x}_0,\mathbf{x})$. Additionally, the dependence of $\bar{T}_1^{(3)}(a,c)$ on a and c is shown in Figure 3.10.

3.6 Continued fractions expression of the Green's function

From Figure 3.3 we observe that the assumption $\cosh\tau_1 \gg 1$ we have made for the nucleus does not hold for the cellular boundary characterized by τ_2. As a result, we cannot obtain an approximation for $G_2^{(3)}(\mathbf{x}_0,\mathbf{x})$ and all the quantities derived subsequently from it.

In this section, we will calculate the Green's function $\bar{G}_1^{(3)}(\mathbf{x}_0,\mathbf{x})$ and $\bar{G}_2^{(3)}(\mathbf{x}_0,\mathbf{x})$, averaged over the reflecting surface, and derive from them the first-passage properties such as the average mean time and hitting density. The reason we are assuming uniform initial conditions, on the nucleus and cellular surface, is that the method we will utilise to solve recursive relations of the form:

$$\alpha_n A_{n-1} + \beta_n A_n + \gamma_n A_{n+1} = \lambda_n,$$

will require the coefficients α_n, β_n and γ_n to have finite limits as $n \to +\infty$. However, we observe from (3.19), and from the fact that $\lim_{n\to+\infty} P_n^m(\cos\sigma)$ does not exist, that the limits $\lim_{n\to+\infty}\alpha_{nm}$, $\lim_{n\to+\infty}\beta_{nm}$ and $\lim_{n\to+\infty}\gamma_{nm}$ do not exist and we cannot make use of Theorem D.1.2.

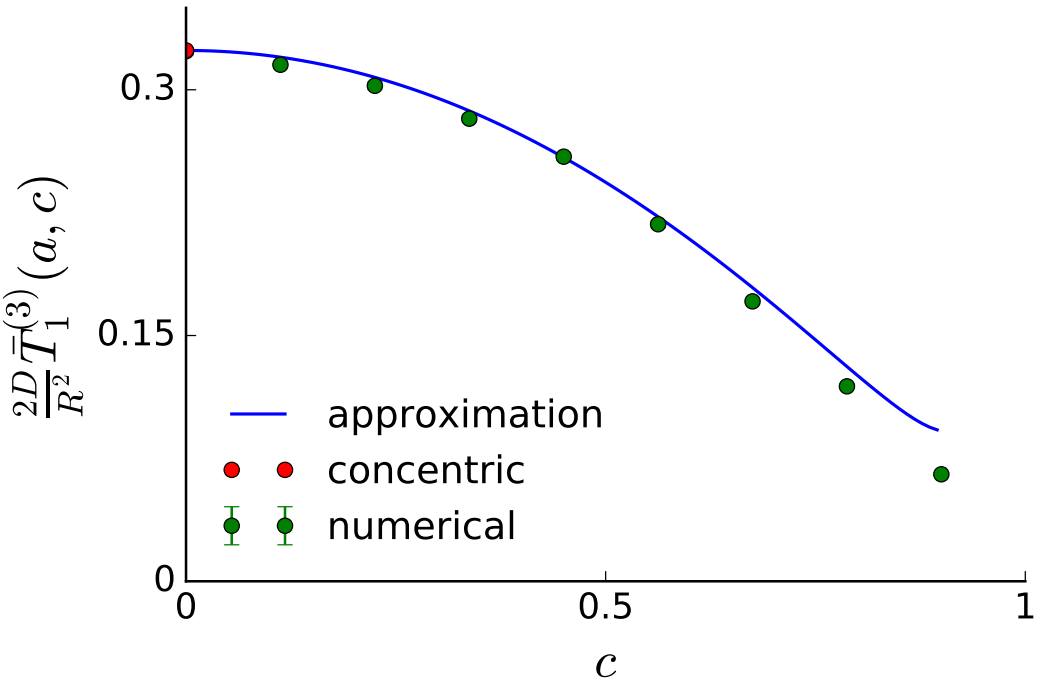

Figure 3.9: Plot of the average mean time $\bar{T}_1^{(3)}(a,c)$ as a function of the displacement of the nucleus c. The blue line represent the approximation (3.39), the green dots represent numerical simulation and the red dot is the concentric case (1.17) in rescaled coordinates. For this figure we have used the following parameters: $a = 0.1$.

3.6.1 From nucleus to cellular surface

We begin with the case of reflecting nucleus and absorbing cellular surface:

$$\frac{\partial \bar{G}_1^{(3)}}{\partial \mathbf{n}_1}(\mathbf{x}_0, \mathbf{x}) = 0, \quad \mathbf{x} \in \partial C_1, \tag{3.40}$$

$$\bar{G}_1^{(3)}(\mathbf{x}_0, \mathbf{x}) = 0, \quad \mathbf{x} \in \partial C_2. \tag{3.41}$$

The Green's function $G_1^{(3)}(\mathbf{x}_0, \mathbf{x})$ can be written as Chen *et al.*:

$$G_1^{(3)}(\mathbf{x}_0, \mathbf{x}) = G_r^{(3)}(\mathbf{x}_0, \mathbf{x}) + G_s^{(3)}(\mathbf{x}_0, \mathbf{x}).$$

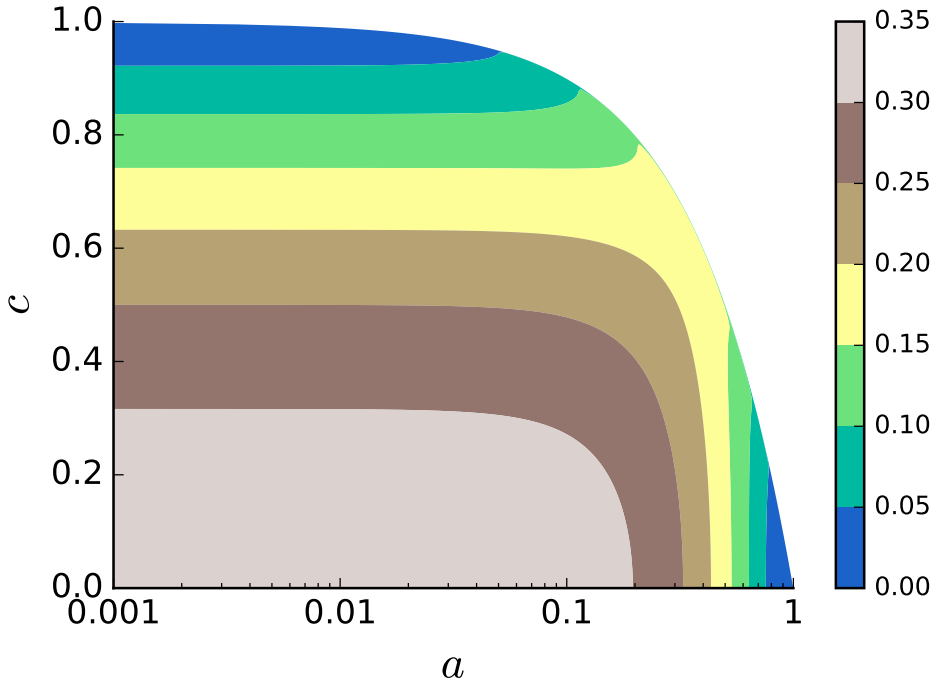

Figure 3.10: Contours of $\frac{2D}{R^2}\bar{T}_1^{(3)}(a,c)$, the mean time for a particle, whose initial condition is uniformly distributed on the nuclear surface, to reach the cellular surface, as a function of the dimensionless parameters a and c.

Integrating $G_1^{(3)}(\mathbf{x}_0,\mathbf{x})$ over the sphere characterized by τ_0 we obtain the Green's function $\bar{G}_1^{(3)}(\mathbf{x}_0,\mathbf{x})$:

$$\begin{aligned}\bar{G}_1^{(3)}(\mathbf{x}_0,\mathbf{x}) &= \frac{d^2}{S}\int_0^{2\pi}\int_0^{\pi}\frac{G^{(3)}(\mathbf{x}_0,\mathbf{x})\sin\sigma_0}{(\cosh\tau_0-\cos\sigma_0)^2}\,\mathrm{d}\sigma_0\phi_0\\ &= \frac{d^2}{S}\int_0^{2\pi}\int_0^{\pi}\frac{G_r^{(3)}(\mathbf{x}_0,\mathbf{x})\sin\sigma_0}{(\cosh\tau_0-\cos\sigma_0)^2}\,\mathrm{d}\sigma_0\phi_0\\ &+ \frac{d^2}{S}\int_0^{2\pi}\int_0^{\pi}\frac{G_s^{(3)}(\mathbf{x}_0,\mathbf{x})\sin\sigma_0}{(\cosh\tau_0-\cos\sigma_0)^2}\,\mathrm{d}\sigma_0\phi_0,\end{aligned}$$

where S is the surface area of the sphere characterized by τ_0. Making use of the following identities:

$$d^2\int_0^{2\pi}\int_0^{\pi}\frac{G_r^{(3)}(\mathbf{x}_0,\mathbf{x})\sin\sigma_0}{(\cosh\tau_0-\cos\sigma_0)^2}\,\mathrm{d}\sigma_0\phi_0$$

$$= \frac{d\sqrt{2}}{D\sinh\tau_0} h_x(\tau,\sigma) \sum_{n=0}^{+\infty} \left\{ A_n^1 \cosh\left[\left(n+\frac{1}{2}\right)\tau\right] + B_n^1 \sinh\left[\left(n+\frac{1}{2}\right)\tau\right] \right\} P_n(\cos\sigma)$$
$$\times \mathrm{e}^{-\left(n+\frac{1}{2}\right)\tau_0},$$

and

$$d^2 \int_0^{2\pi}\int_0^{\pi} \frac{G_s^{(3)}(\mathbf{x}_0,\mathbf{x})\sin\sigma_0}{(\cosh\tau_0-\cos\sigma_0)^2}\,\mathrm{d}\sigma_0\phi_0 = \frac{d\sqrt{2}}{D\sinh\tau_0} h_x(\tau,\sigma) \sum_{n=0}^{+\infty} \mathrm{e}^{-\left(n+\frac{1}{2}\right)\tau_0} P_n(\cos\sigma)$$
$$\times \mathrm{e}^{-\left(n+\frac{1}{2}\right)|\tau-\tau_0|},$$

the Green's function $\bar{G}_1^3(\mathbf{x}_0,\mathbf{x})$ can be written as:

$$S\bar{G}_1^3(\mathbf{x}_0,\mathbf{x}) = \frac{d\sqrt{2}}{D\sinh\tau_0} h_x(\tau,\sigma) \sum_{n=0}^{+\infty} \{ A_n^1 \cosh\left[\left(n+\frac{1}{2}\right)\tau\right] + B_n^1 \sinh\left[\left(n+\frac{1}{2}\right)\tau\right]$$
$$+ \mathrm{e}^{-\left(n+\frac{1}{2}\right)|\tau-\tau_0|} \} \mathrm{e}^{-\left(n+\frac{1}{2}\right)\tau_0} P_n(\cos\sigma). \tag{3.42}$$

From (3.40) we deduce that:

$$\sum_{n=0}^{+\infty} \mathrm{e}^{-\left(n+\frac{1}{2}\right)\tau_0} \Bigg\{ A_n^1 \left[\cosh\left[\left(n+\frac{1}{2}\right)\tau_1\right] \sinh\tau_1 \right.$$
$$+(2n+1)\sinh\left[\left(n+\frac{1}{2}\right)\tau_1\right](\cosh\tau_1-\cos\sigma)\Big]$$
$$+ B_n^1 \left[\sinh\left[\left(n+\frac{1}{2}\right)\tau_1\right] \sinh\tau_1 \right.$$
$$+(2n+1)\cosh\left[\left(n+\frac{1}{2}\right)\tau_1\right](\cosh\tau_1-\cos\sigma)\Big]$$
$$\left. + \left[\sinh\tau_1 - (2n+1)(\cosh\tau_1-\cos\sigma)\right] \mathrm{e}^{-\left(n+\frac{1}{2}\right)(\tau_1-\tau_0)} \right\} P_n(\cos\sigma) = 0,$$

which can be rewritten as:

$$\sum_{n=0}^{+\infty} \mathrm{e}^{-\left(n+\frac{1}{2}\right)\tau_0} \Bigg\{ A_n^1 V_1(n,\tau_1) - A_n^1(2n+1)\sinh\left[\left(n+\frac{1}{2}\right)\tau_1\right]\cos\sigma$$
$$+ B_n^1 V_2(n,\tau_1) - B_n^1(2n+1)\cosh\left[\left(n+\frac{1}{2}\right)\tau_1\right]\cos\sigma$$
$$\left. + W(n,\tau_1)\,\mathrm{e}^{-\left(n+\frac{1}{2}\right)(\tau_1-\tau_0)} + (2n+1)\cos\sigma \mathrm{e}^{-\left(n+\frac{1}{2}\right)(\tau_1-\tau_0)} \right\} P_n(\cos\sigma) = 0,$$

where $V_1(n,\tau_1), V_2(n,\tau_1)$ and $W(n,\tau_1)$ are defined in (3.13). Using the following expansion of Legendre polynomials (Gradshteyn & Ryzhik, 2014, p.985):

$$\cos\sigma P_n(\cos\sigma) = \frac{n}{2n+1}P_{n-1}(\cos\sigma) + \frac{n+1}{2n+1}P_{n+1}(\cos\sigma),$$

we obtain:

$$\begin{aligned}
&\sum_{n=0}^{+\infty} \mathrm{e}^{-\left(n+\frac{1}{2}\right)\tau_0}\Bigg\{ A_n^1 V_1\left(n,\tau_1\right) P_n(\cos\sigma) - A_n^1(2n+1)\sinh\left[\left(n+\frac{1}{2}\right)\tau_1\right] \\
&\times\left[\frac{n}{2n+1}P_{n-1}(\cos\sigma) + \frac{n+1}{2n+1}P_{n+1}(\cos\sigma)\right] + B_n^1 V_2\left(n,\tau_1\right) \\
&- B_n^1(2n+1)\cosh\left[\left(n+\frac{1}{2}\right)\tau_1\right]\left[\frac{n}{2n+1}P_{n-1}(\cos\sigma) + \frac{n+1}{2n+1}P_{n+1}(\cos\sigma)\right] \\
&+ W\left(n,\tau_1\right)\mathrm{e}^{-\left(n+\frac{1}{2}\right)(\tau_1-\tau_0)} + (2n+1)\mathrm{e}^{-\left(n+\frac{1}{2}\right)(\tau_1-\tau_0)}\left[\frac{n}{2n+1}P_{n-1}(\cos\sigma)\right. \\
&\left.+\frac{n+1}{2n+1}P_{n+1}(\cos\sigma)\right]\Bigg\} = 0.
\end{aligned}$$

Finally, we multiply the result by $P_N(\cos\sigma)\sin\sigma$ and integrate from 0 to π with respect to σ:

$$\begin{aligned}
&\frac{2V_1\left(N,\tau_1\right)\mathrm{e}^{-\left(N+\frac{1}{2}\right)\tau_0}}{2N+1}A_N^1 - \sinh\left[\left(N+\frac{3}{2}\right)\tau_1\right]\mathrm{e}^{-\left(n+\frac{3}{2}\right)\tau_0}\frac{2N+2}{2N+1}A_{N+1}^1 \\
&- \sinh\left[\left(N-\frac{1}{2}\right)\tau_1\right]\mathrm{e}^{-\left(N-\frac{1}{2}\right)\tau_0}\frac{2N}{2N+1}A_{N-1}^1 + \frac{2V_2\left(n,\tau_1\right)\mathrm{e}^{-\left(N+\frac{1}{2}\right)\tau_0}}{2N+1}B_N^1 \\
&- \cosh\left[\left(N+\frac{3}{2}\right)\tau_1\right]\mathrm{e}^{-\left(N+\frac{3}{2}\right)\tau_0}\frac{2N+2}{2N+1}B_{N+1}^1 \\
&- \cosh\left[\left(N-\frac{1}{2}\right)\tau_1\right]\mathrm{e}^{-\left(N-\frac{1}{2}\right)\tau_0}\frac{2N}{2N+1}B_{N-1}^1 \\
&= -\frac{2W\left(N,\tau_1\right)}{2N+1}\mathrm{e}^{-\left(N+\frac{1}{2}\right)\tau_1} - \frac{2N+2}{2N+1}\mathrm{e}^{-\left(N+\frac{3}{2}\right)\tau_1} - \frac{2N}{2N+1}\mathrm{e}^{-\left(N-\frac{1}{2}\right)\tau_1}, \qquad (3.43)
\end{aligned}$$

where we used the orthogonality condition (Gradshteyn & Ryzhik, 2014, p.769):

$$\int_0^\pi \sin\sigma P_l(\cos\sigma)P_{l'}(\cos\sigma)\,\mathrm{d}\sigma = \frac{2}{2l+1}\delta_{ll'}.$$

From the Dirichlet boundary condition (3.41) we obtain using analogous methods:

$$A_N^1\cosh\left[\left(N+\frac{1}{2}\right)\tau_2\right] + B_N^1\sinh\left[\left(N+\frac{1}{2}\right)\tau_2\right] = -\mathrm{e}^{-\left(N+\frac{1}{2}\right)(\tau_0-\tau_2)},$$

which allows us to express:

$$B_N^1 = -\frac{\mathrm{e}^{-\left(N+\frac{1}{2}\right)(\tau_0-\tau_2)}}{\sinh\left[\left(N+\frac{1}{2}\right)\tau_2\right]} - \coth\left[\left(N+\frac{1}{2}\right)\tau_2\right] A_N^1. \tag{3.44}$$

Consequently, we write (3.43) as a recurrence relation for A_n:

$$\alpha_n^1 A_{n-1}^1 + \beta_n^1 A_n^1 + \gamma_n^1 A_{n+1}^1 = \lambda_n^1, \tag{3.45}$$

where, for convenience, we write $N = n$ and setting $\tau_0 = \tau_1$:

$$\begin{aligned}
\alpha_n^1 &= \frac{2n}{2n+1}\mathrm{e}^{-\left(n-\frac{1}{2}\right)\tau_1}\frac{\cosh\left[\left(n-\frac{1}{2}\right)(\tau_1-\tau_2)\right]}{\sinh\left[\left(n-\frac{1}{2}\right)\tau_2\right]},\\
\beta_n^1 &= -\frac{2}{2n+1}\mathrm{e}^{-\left(n+\frac{1}{2}\right)\tau_1}\left\{\sinh\tau_1\frac{\sinh\left[\left(n+\frac{1}{2}\right)(\tau_1-\tau_2)\right]}{\sinh\left[\left(n+\frac{1}{2}\right)\tau_2\right]}\right.\\
&\quad \left.+(2n+1)\cosh\tau_1\frac{\cosh\left[\left(n+\frac{1}{2}\right)(\tau_1-\tau_2)\right]}{\sinh\left[\left(n+\frac{1}{2}\right)\tau_2\right]}\right\},\\
\gamma_n^1 &= \frac{2n+2}{2n+1}\mathrm{e}^{-\left(n+\frac{3}{2}\right)\tau_1}\frac{\cosh\left[\left(n+\frac{3}{2}\right)(\tau_1-\tau_2)\right]}{\sinh\left[\left(n+\frac{3}{2}\right)\tau_2\right]},\\
\lambda_n^1 &= -\frac{2W(n,\tau_1)}{2n+1}\mathrm{e}^{-\left(n+\frac{1}{2}\right)\tau_1} - \frac{2n+2}{2n+1}\mathrm{e}^{-\left(n+\frac{3}{2}\right)\tau_1} - \frac{2n}{2n+1}\mathrm{e}^{-\left(n-\frac{1}{2}\right)\tau_1}\\
&\quad + \frac{2V_2(n,\tau_1)\,\mathrm{e}^{-\left(n+\frac{1}{2}\right)\tau_1}}{2n+1}\frac{\mathrm{e}^{-\left(n+\frac{1}{2}\right)(\tau_1-\tau_2)}}{\sinh\left[\left(n+\frac{1}{2}\right)\tau_2\right]}\\
&\quad - \cosh\left[\left(n+\frac{3}{2}\right)\tau_1\right]\mathrm{e}^{-\left(n+\frac{3}{2}\right)\tau_1}\frac{2n+2}{2n+1}\frac{\mathrm{e}^{-\left(n+\frac{3}{2}\right)(\tau_1-\tau_2)}}{\sinh\left[\left(n+\frac{3}{2}\right)\tau_2\right]}\\
&\quad - \cosh\left[\left(n-\frac{1}{2}\right)\tau_1\right]\mathrm{e}^{-\left(n-\frac{1}{2}\right)\tau_1}\frac{2n}{2n+1}\frac{\mathrm{e}^{-\left(n-\frac{1}{2}\right)(\tau_1-\tau_2)}}{\sinh\left[\left(n-\frac{1}{2}\right)\tau_2\right]}.
\end{aligned}$$

The solution of (3.45) will be obtained by using the Green's function method for difference equations, which is analogous to the construction of solutions for differential equations Love (1975); Milne-Thomson (2000). Let $G_{n,N}$ be the solution of the difference equation:

$$\alpha_n^1 G_{n-1,N} + \beta_n^1 G_{n,N} + \gamma_n^1 G_{n+1,N} = \delta_{n,N}, \quad N = 0, 1, \ldots, \tag{3.46}$$

where δ is the Kronecker delta function. As a result, the solution of (3.45) is obtained as:

$$A_n = \sum_{N=0}^{+\infty} G_{n,N}\lambda_N^1, \quad n = 0, 1, \ldots. \tag{3.47}$$

We construct the Green's functions $G_{n,N}$ by utilising the complementary difference equation for (3.46):

$$\alpha_n^1 G_{n-1,N} + \beta_n^1 G_{n,N} + \gamma_n^1 G_{n+1,N} = 0, \tag{3.48}$$

which has two solutions given by its characteristic equation. We denote the ratio $G_{n+1,N}/G_{n,N} = \lambda$ and letting $n \to +\infty$ in (3.48) we obtain

$$\mathrm{e}^{-2\tau_2}\lambda^2 - 2\cosh\tau_1\lambda + \mathrm{e}^{2\tau_2} = 0,$$

which has solutions:

$$\lambda_1 = \mathrm{e}^{\tau_1+2\tau_2} \quad \lambda_2 = \mathrm{e}^{-\tau_1+2\tau_2}.$$

Proceding with the solution of (3.45) we will use Perron's theorem (see D.1.2) which tells us that the ratios $G_{n+1,N}/G_{n,N}$ and $G_{n-1,N}/G_{n,N}$ tend to λ_1 and $1/\lambda_2$, respectively. Furthermore, the ascending and descending fractions can be written as a function of α_n^1, β_n^1 and γ_n^1 by making use of continued fractions (see D.2):

$$\frac{G_{n+1N}}{G_{nN}} = \cfrac{\alpha_{n+1}^1}{\beta_{n+1}^1 - \cfrac{\gamma_{n+1}^1\alpha_{n+2}^1}{\beta_{n+2}^1 - \cfrac{\gamma_{n+2}^1\alpha_{n+3}^1}{\beta_{n+3}^1 - \cdots}}}} \equiv p_{n+1}^1, \tag{3.49}$$

$$\frac{G_{n-1N}}{G_{nN}} = \cfrac{\alpha_{n-1}^1}{\beta_{n-1}^1 - \cfrac{\gamma_{n-1}^1\alpha_{n-2}^1}{\beta_{n-2}^1 - \cfrac{\gamma_{n-2}^1\alpha_{n-3}^1}{\beta_{n-3}^1 - \cdots - \cfrac{\alpha_0^1\gamma_1^1}{\beta_0^1}}}}} \equiv q_{n-1}^1, \tag{3.50}$$

where

$$\lim_{n\to+\infty} p_{n+1}^1 = \lambda_1,$$
$$\lim_{n\to+\infty} q_{n-1}^1 = \frac{1}{\lambda_2}.$$

We build the solution of (3.46) by using (3.49) and (3.50) in the following way(Love, 1975, p.454):

$$\begin{aligned} G_{n+1N} &= p_{n+1}^1 G_{nN}, \quad n \geq N, \\ G_{n-1N} &= q_{n-1}^1 G_{nN}, \quad n \leq N. \end{aligned} \tag{3.51}$$

If we know $G_{N,N}$ then we will be able to determine $G_{n,N}$. As a result, we let $n = N$ in (3.51) and substitute G_{N+1N} and G_{N-1N} in (3.46) obtaining:

$$G_{NN} = \frac{1}{\alpha_N^1 q_{N-1}^1 + \beta_N^1 + \gamma_N^1 p_{N+1}^1}.$$

Consequently, we have from (3.47) and (3.44) the following:

$$\begin{aligned} A_n^1 &= \sum_{N=0}^{+\infty} \frac{\lambda_N^1}{\alpha_N^1 q_{N-1}^1 + \beta_N^1 + \gamma_N^1 p_{N+1}^1} \Bigg\{ \delta_{nN} + H(n-N) \prod_{l=N+1}^{n} p_l^1 \\ &\quad + H(N-n) \prod_{l=n}^{N-1} q_l^1 \Bigg\}, \\ B_n^1 &= -\mathrm{e}^{-\left(n+\frac{1}{2}\right)(\tau_1-\tau_2)} \operatorname{csch}\left[\left(n+\frac{1}{2}\right)\tau_2\right] \\ &\quad - A_n^1 \cosh\left[\left(n+\frac{1}{2}\right)\tau_2\right] \operatorname{csch}\left[\left(n+\frac{1}{2}\right)\tau_2\right]. \end{aligned}$$

where $H(x)$ is the Heaviside function:

$$H(x) = \begin{cases} 0, & \text{if } x < 0, \\ 1, & \text{otherwise.} \end{cases}$$

As a result, we write (3.42) as:

$$\begin{aligned} 4\pi D \bar{G}_1^3(\mathbf{x}_0, \mathbf{x}) = \frac{d\sqrt{2}}{a^2 \sinh \tau_1} h_x(\tau, \sigma) \sum_{n=0}^{+\infty} \Bigg\{ A_n^1 \cosh\left[\left(n+\frac{1}{2}\right)\tau\right] \\ + B_n^1 \sinh\left[\left(n+\frac{1}{2}\right)\tau\right] + \mathrm{e}^{-\left(n+\frac{1}{2}\right)|\tau-\tau_1|} \Bigg\} \mathrm{e}^{-\left(n+\frac{1}{2}\right)\tau_1} P_n(\cos\sigma), \end{aligned} \tag{3.52}$$

which we plot in Figure 3.11 and compare with numerical simulations.

3.6.2 From cellular surface to nucleus

Analogously, for the case of absorbing nucleus and reflecting cellular surface we obtain:

$$4\pi D \bar{G}_2^3(\mathbf{x}_0, \mathbf{x}) = \frac{d\sqrt{2}}{\sinh \tau_2} h_x(\tau, \sigma) \sum_{n=0}^{+\infty} \Bigg\{ A_n^2 \cosh\left[\left(n+\frac{1}{2}\right)\tau\right]$$

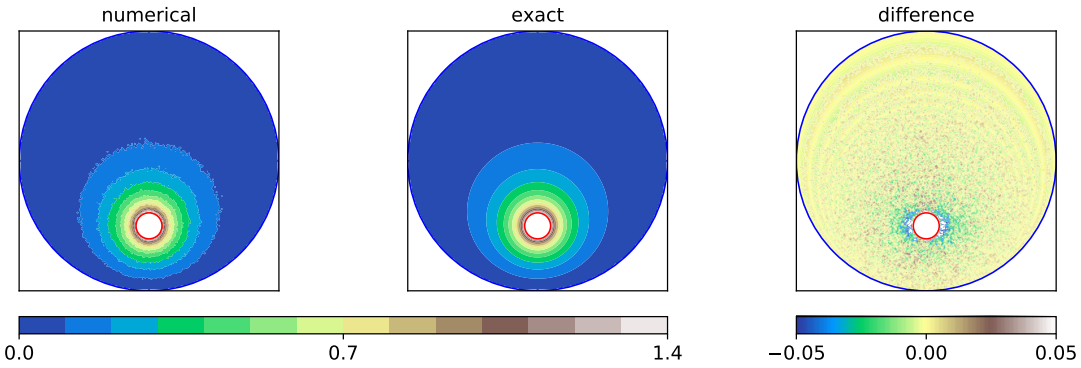

Figure 3.11: Plot of numerical simulation of $G_1^{(3)}(\mathbf{x}_0, \mathbf{x})$ (left), analytic formula (3.52) (centre) and difference (right). The initial condition is $\mathbf{x}_0 \in \partial C_1$ and $a = 0.1, c = 0.5$.

$$+ B_n^2 \sinh\left[\left(n+\frac{1}{2}\right)\tau\right] + \mathrm{e}^{-\left(n+\frac{1}{2}\right)|\tau-\tau_2|}\Big\}\mathrm{e}^{-\left(n+\frac{1}{2}\right)\tau_2} P_n(\cos\sigma),$$

where

$$\begin{aligned}
A_n^2 &= \sum_{N=0}^{+\infty} \frac{\lambda_N^2}{\alpha_N^2 q_{N-1}^2 + \beta_N^2 + \gamma_N^2 p_{N+1}^2}\Bigg\{\delta_{nN} + H(n-N)\prod_{l=N+1}^{n} p_l^2 \\
&\quad + H(N-n)\prod_{l=n}^{N-1} q_l^2\Bigg\}, \\
B_n^2 &= -\mathrm{e}^{-\left(n+\frac{1}{2}\right)(\tau_1-\tau_2)}\operatorname{csch}\left[\left(n+\frac{1}{2}\right)\tau_1\right] \\
&\quad - A_n^2 \cosh\left[\left(n+\frac{1}{2}\right)\tau_1\right]\operatorname{csch}\left[\left(n+\frac{1}{2}\right)\tau_1\right].
\end{aligned}$$

and

$$p_{n+1}^2 = \cfrac{\alpha_{n+1}^2}{\beta_{n+1}^2 - \cfrac{\gamma_{n+1}^2\alpha_{n+2}^2}{\beta_{n+2}^2 - \cfrac{\gamma_{n+2}^2\alpha_{n+3}^2}{\beta_{n+3}^2 - \cdots}}},$$

$$q_{n-1}^2 = \cfrac{\alpha_{n-1}^2}{\beta_{n-1}^2 - \cfrac{\gamma_{n-1}^2\alpha_{n-2}^2}{\beta_{n-2}^2 - \cfrac{\gamma_{n-2}^2\alpha_{n-3}^2}{\beta_{n-3}^2 - \cdots - \cfrac{\alpha_0^2\gamma_1^2}{\beta_0^2}}}}.$$

In the above calculations we have made use of the following:

$$\begin{aligned}
\alpha_n^2 &= \frac{2n}{2n+1}\mathrm{e}^{-\left(n-\frac{1}{2}\right)\tau_2}\frac{\cosh\left[\left(n-\frac{1}{2}\right)(\tau_1-\tau_2)\right]}{\sinh\left[\left(n-\frac{1}{2}\right)\tau_1\right]},\\
\beta_n^2 &= \frac{2}{2n+1}\mathrm{e}^{-\left(n+\frac{1}{2}\right)\tau_2}\left\{\sinh\tau_2\frac{\sinh\left[\left(n+\frac{1}{2}\right)(\tau_1-\tau_2)\right]}{\sinh\left[\left(n+\frac{1}{2}\right)\tau_1\right]}\right.\\
&\quad\left.-(2n+1)\cosh\tau_2\frac{\cosh\left[\left(n+\frac{1}{2}\right)(\tau_1-\tau_2)\right]}{\sinh\left[\left(n+\frac{1}{2}\right)\tau_1\right]}\right\},\\
\gamma_n^2 &= \frac{2n+2}{2n+1}\mathrm{e}^{-\left(n+\frac{3}{2}\right)\tau_2}\frac{\cosh\left[\left(n+\frac{3}{2}\right)(\tau_1-\tau_2)\right]}{\sinh\left[\left(n+\frac{3}{2}\right)\tau_1\right]},\\
\lambda_n^2 &= -\frac{2W(n,\tau_2)}{2n+1}\mathrm{e}^{-\left(n+\frac{1}{2}\right)\tau_2}-\frac{2n+2}{2n+1}\mathrm{e}^{-\left(n+\frac{3}{2}\right)\tau_2}-\frac{2n}{2n+1}\mathrm{e}^{-\left(n-\frac{1}{2}\right)\tau_2}\\
&\quad+\frac{2V_2(n,\tau_2)}{2n+1}\frac{\mathrm{e}^{-\left(n+\frac{1}{2}\right)\tau_2}}{\sinh\left[\left(n+\frac{1}{2}\right)\tau_1\right]}\\
&\quad-\cosh\left[\left(n+\frac{3}{2}\right)\tau_2\right]\frac{2n+2}{2n+1}\frac{\mathrm{e}^{-\left(n+\frac{3}{2}\right)\tau_2}}{\sinh\left[\left(n+\frac{3}{2}\right)\tau_1\right]}\\
&\quad-\cosh\left[\left(n-\frac{1}{2}\right)\tau_2\right]\frac{2n}{2n+1}\frac{\mathrm{e}^{-\left(n-\frac{1}{2}\right)\tau_2}}{\sinh\left[\left(n-\frac{1}{2}\right)\tau_1\right]},
\end{aligned}$$

where $n\in\mathbb{N}\cup\{0\}$.

3.6.3 Hitting density on the cellular surface

The hitting density of particles incoming from the nucleus is given by:

$$\varepsilon^{(3)}(\theta_2) = -D\left.\frac{\partial\bar{G}_1^3(\mathbf{x}_1,\mathbf{x})}{\partial\mathbf{n}_2}\right|_{\partial C_2},$$

which gives, after simplification:

$$\begin{aligned}
\varepsilon^{(3)}(\theta_2) = \frac{(\cosh\tau_2-\cos\sigma_2)^{\frac{1}{2}}}{4\sqrt{2}a^2\pi\sinh\tau_1}\sum_{n=0}^{+\infty}\Big[&A_n^1\bar{V}_1(n,\tau_2,\sigma_2)+B_n^1\bar{V}_2(n,\tau_2,\sigma_2)\\
&+\bar{W}(n,\tau_2,\sigma_2)\,\mathrm{e}^{-\left(n+\frac{1}{2}\right)(\tau_1-\tau_2)}\Big]\mathrm{e}^{-\left(n+\frac{1}{2}\right)\tau_1}P_n(\cos\sigma_2),
\end{aligned}\tag{3.53}$$

where

$$\bar{V}_1(n,\tau_2,\sigma_2) = V_1(n,\tau_2)-(2n+1)\sinh\left[\left(n+\frac{1}{2}\right)\tau_2\right]\cos\sigma_2,$$

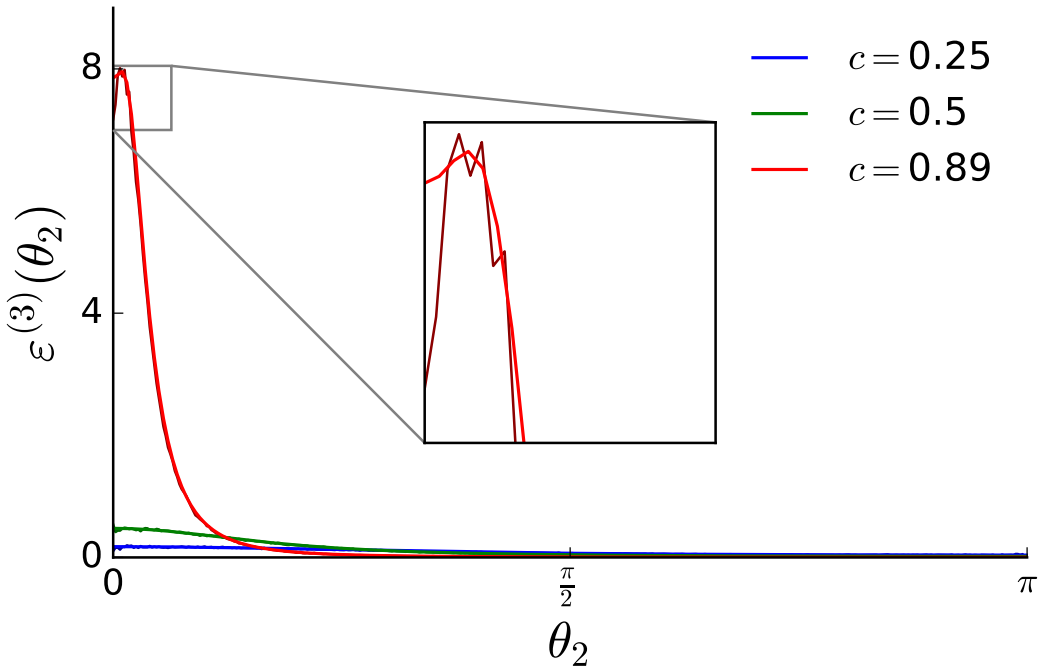

Figure 3.12: Plot of $\varepsilon^{(3)}(\theta_2)$ comparing the numerical simulation with the analytic result obtained in (3.53) as a function of θ_2 for $c = 0.25, 0.5$ and 0.89. The inset shows $\varepsilon^{(3)}(\theta_2)$ for $c = 0.89$ and small values of θ_2. The lighter colours represent the analytic result and the darker colours represent the numerical simulations. The numerical results have been obtained by having 10^5 particles uniformly distributed on the sphere of radius a from Figure 3.1 and recording their endpoint. For our simulations we have chosen the following parameter values: $a = 0.1$.

$$\bar{V}_2(n, \tau_2, \sigma_2) = V_2(n, \tau_2) - (2n+1)\cosh\left[\left(n + \frac{1}{2}\right)\tau_2\right]\cos\sigma_2,$$
$$\bar{W}(n, \tau_2, \sigma_2) = \sinh\tau_2 + (2n+1)(\cosh\tau_2 - \cos\sigma_2),$$

and

$$\sigma_2 = \arccos\frac{1 + \cos\theta_2\sqrt{1+d^2}}{\sqrt{\left(1 + d^2 + \cos\theta_2\sqrt{1+d^2}\right)^2 - d^2\left(\cos\theta_2 + \sqrt{1+d^2}\right)^2}}.$$

In calculating (3.53), we made use of (3.52) and Appendix C.1, and we plot $\varepsilon^{(3)}(\theta_2)$ in Figure 3.12 for several values of c and compare with numerical simu-

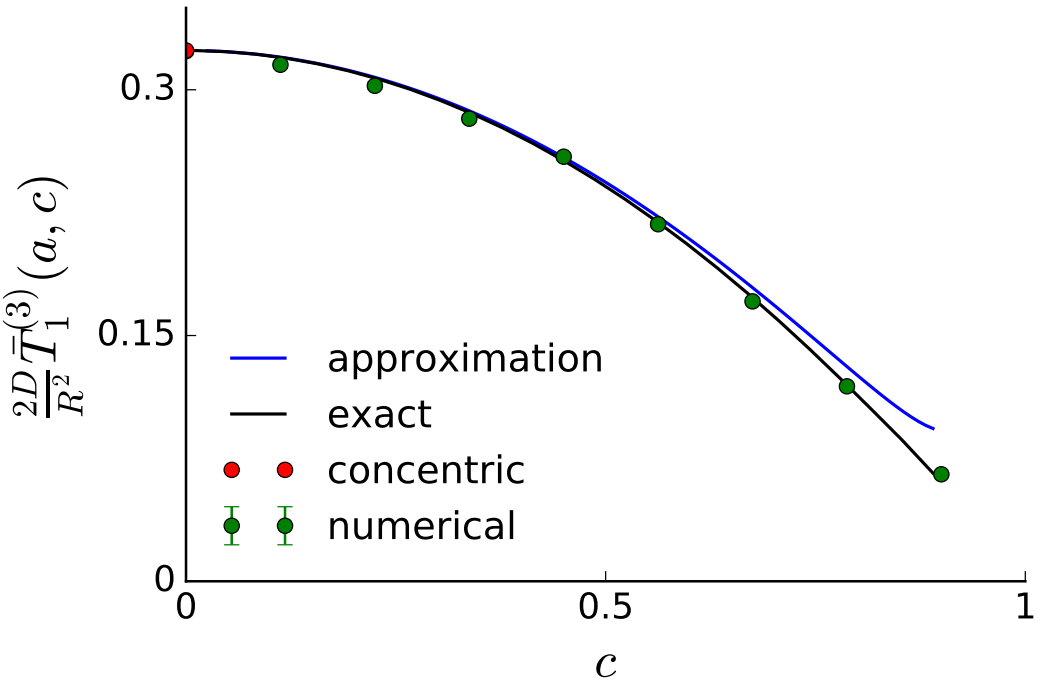

Figure 3.13: Plot of the average mean time $\bar{T}_1^{(3)}(a,c)$ as a function of the diplacement of the nucleus c. The blue line represents the approximation (3.39), the black line represents the analytic solution (3.54), the green dots represent numerical simulations and the red dot is the concentric case (1.17) in rescaled coordinates. For the numerical simulations we have used G.6.1.1 and this plot has been obtained using G.6.2.1. For this figure we have used the following parameters: $a = 0.1$.

lations. We observe that as c increases the density $\varepsilon^{(3)}(\theta_2)$ becomes bimodal in an analogous way to the two dimensional case from Figure 2.15.

3.6.4 Average mean time

We next obtain the mean hitting times, $\bar{T}_1^3(a,c)$ and $\bar{T}_2^3(a,c)$, when the initial position $\mathbf{x}_0$ is distributed uniformly over ∂C_1 and ∂C_2, respectively. Firstly,

$$\bar{T}_1^{(3)}(a,c) = R^2 d^3 \int_{\tau_2}^{\tau_1}\int_0^{2\pi}\int_0^{\pi} \frac{\bar{G}_1^{(3)}(\mathbf{x}_0,\mathbf{x})\sin\sigma}{(\cosh\tau-\cos\sigma)^3}\mathrm{d}\sigma\mathrm{d}\phi\mathrm{d}\tau,$$

which we evaluate, using Appendix C.4, to be:

$$\frac{2D}{R^2}\bar{T}_1^{(3)}(a,c) = \frac{4\pi d^3}{a}\sum_{n=0}^{+\infty} \mathrm{e}^{-\left(n+\frac{1}{2}\right)\tau_1} I_n^1, \tag{3.54}$$

where the function I_n^1 is given by:

$$I_n^1 = \int_{\tau_2}^{\tau_1} \left\{ A_n^1 \cosh\left[\left(n+\frac{1}{2}\right)\tau\right] + B_n^1 \sinh\left[\left(n+\frac{1}{2}\right)\tau\right] + \mathrm{e}^{-\left(n+\frac{1}{2}\right)(\tau_1-\tau)} \right\} \times \left[\frac{(2n+3)}{3}\frac{\mathrm{e}^{-\left(n+\frac{1}{2}\right)\tau}}{\sinh^2\tau} + \frac{2}{3}\frac{\mathrm{e}^{-\left(n+\frac{3}{2}\right)\tau}}{\sinh^3\tau}\right] \mathrm{d}\tau.$$

We plot $\bar{T}_1^{(3)}(a,c)$ in Figure 3.13 where we compare with numerical simulation and with the approximation we obtained in (3.39).
Analogously, the mean time for a particle, whose initial condition is uniformly distributed on the cellular surface, to reach the nucleus is given by:

$$\frac{2D}{R^2}\bar{T}_2^{(3)}(a,c) = 4\pi d^3 \sum_{n=0}^{+\infty} \mathrm{e}^{-\left(n+\frac{1}{2}\right)\tau_2} I_n^2, \tag{3.55}$$

where

$$I_n^2 = \int_{\tau_2}^{\tau_1} \left\{ A_n^2 \cosh\left[\left(n+\frac{1}{2}\right)\tau\right] + B_n^2 \sinh\left[\left(n+\frac{1}{2}\right)\tau\right] + \mathrm{e}^{-\left(n+\frac{1}{2}\right)(\tau-\tau_2)} \right\} \times \left[\frac{(2n+3)}{3}\frac{\mathrm{e}^{-\left(n+\frac{1}{2}\right)\tau}}{\sinh^2\tau} + \frac{2}{3}\frac{\mathrm{e}^{-\left(n+\frac{3}{2}\right)\tau}}{\sinh^3\tau}\right] \mathrm{d}\tau,$$

which we plot in Figure 3.14 where we compare with numerical simulations and with the approximation obtained from Condamin *et al.* (2007) (see (1.85)):

$$\frac{2D}{R^2}\bar{T}_2^{(3),C} = \frac{2}{3a}\left[1 + \frac{a}{1-c^2} + a\log\frac{1}{1-c^2} + a\frac{c^2-5}{2}\right].$$

When plotting $\bar{T}_1^{(3)}(a,c)$ and $\bar{T}_2^{(3)}(a,c)$ we observe that the former converges much faster the latter to the numerical simulations and, as a result, more terms are required for the sum in (3.55) and in the depth of the continued fractions in p_{n+1}^2 in order to plot $\bar{T}_2^{(3)}(a,c)$. This number of terms needed is an increasing function of c and given that the terms in the coefficients α_n^2, β_n^2 and γ_n^2 grow exponentially the plot was segmented with different number of terms used for different regions of c.

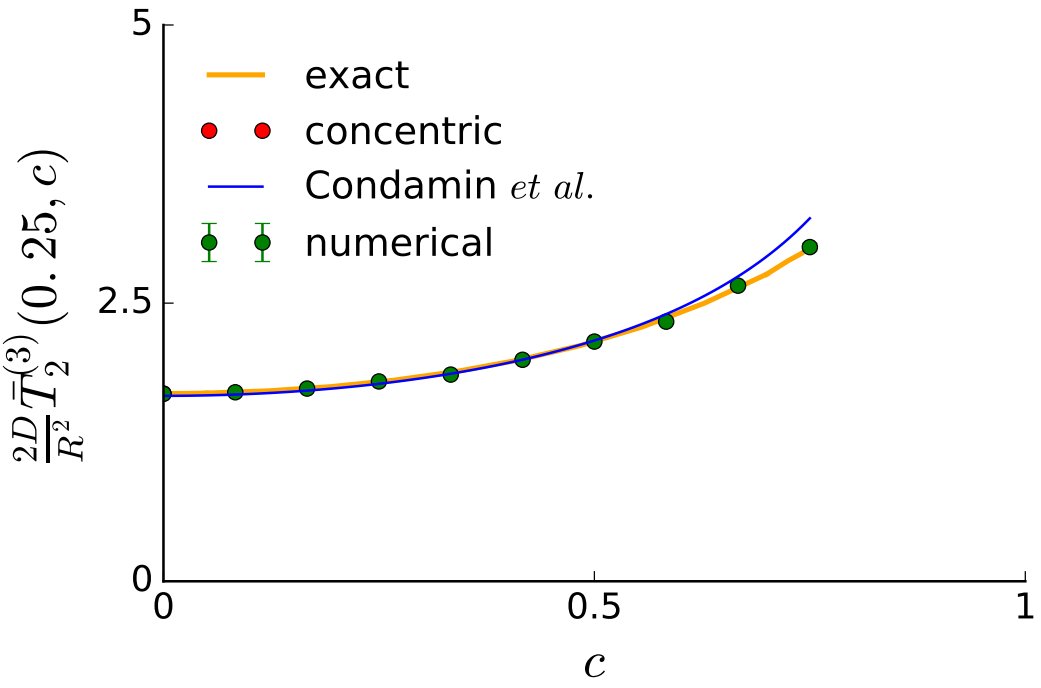

Figure 3.14: Plot of the average mean time $\bar{T}_2^{(3)}(a, c)$ as a function of the displacement of the nucleus c. The blue line represent the approximation (3.39), the black line represents the analytic solution (3.55), the green dots represent numerical simulation and the red dot is the concentric case (1.18) in rescaled coordinates. For this figure we have used the following parameters: $a = 0.25$.

3.6.5 Mean round-trip time

Calculating the total mean time for a Brownian particle to return to the nucleus given that it has touched the cellular surface is difficult and we will make use of an approximation. Let $\{\theta_2^i\}_{i\in\{0,1,\cdots,N-1\}}$ be a discretization of the interval $[0, \pi]$ (see Figure 3.15).

$$\{\theta_2^i\}_{i\in\{0,1,\cdots,N-1\}} = \left\{0, \pi \times \frac{1}{N}, \cdots, \pi \times \frac{N-1}{N}\right\}.$$

Consequently, we create the following vectors:

$$\mathbf{v} = \{T_2^{(3)}(\theta_2^i, a, c)\}_{i\in\{0,1,\cdots,N-1\}}, \quad \mathbf{w} = \{\varepsilon^3(\theta_2^i)\}_{i\in\{0,1,\cdots,N-1\}},$$

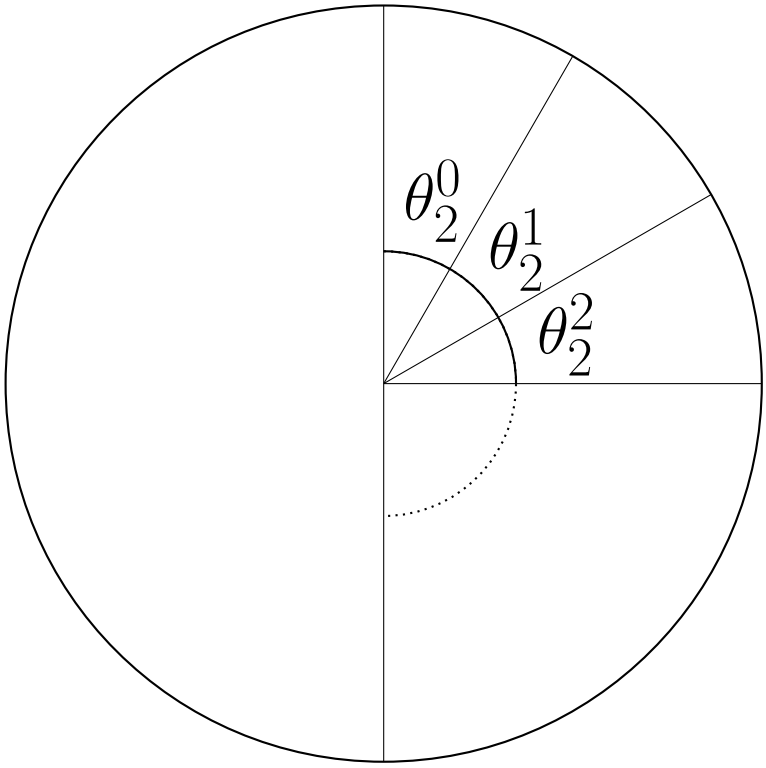

Figure 3.15: Diagram of the discretization of the spherical θ_2 angle used to obtain a semi-analytic mean time $\bar{T}_2^{\varepsilon,3}(c)$.

where $T_2^{(3)}(\theta_i, a, c)$ is the approximation provided by Condamin *et al.* (2007) and $\varepsilon^{(3)}(\theta_i)$ is the hitting density deduced in (3.53). As a result, the mean time, starting on the cellular surface with initial distribution $\varepsilon^{(3)}(\theta_2)$, can be approximated by:

$$\frac{2D}{R^2}\bar{T}_2^{\varepsilon,3}(a,c) = \frac{2\pi^2}{N}\sum_{i=0}^{N-1}\varepsilon^{(3)}(\theta_2^i)T_2^{(3)}(\theta_2^i, a, c)\sin\theta_2^i, \tag{3.56}$$

which we plot in Figure 3.16 where we compare with numerical simulations. We deduce from Figure 3.14 and 3.16 that, while $\bar{T}_2^{(3)}(a,c)$ is an increasing function of c, $\bar{T}_2^{\varepsilon,3}(a,c)$ is a decreasing function which is explained by the fact that the initial position of the Brownian particle, on the cellular surface, is concentrated at the point of shortest distance to the nuclear surface (see Figure 3.12).

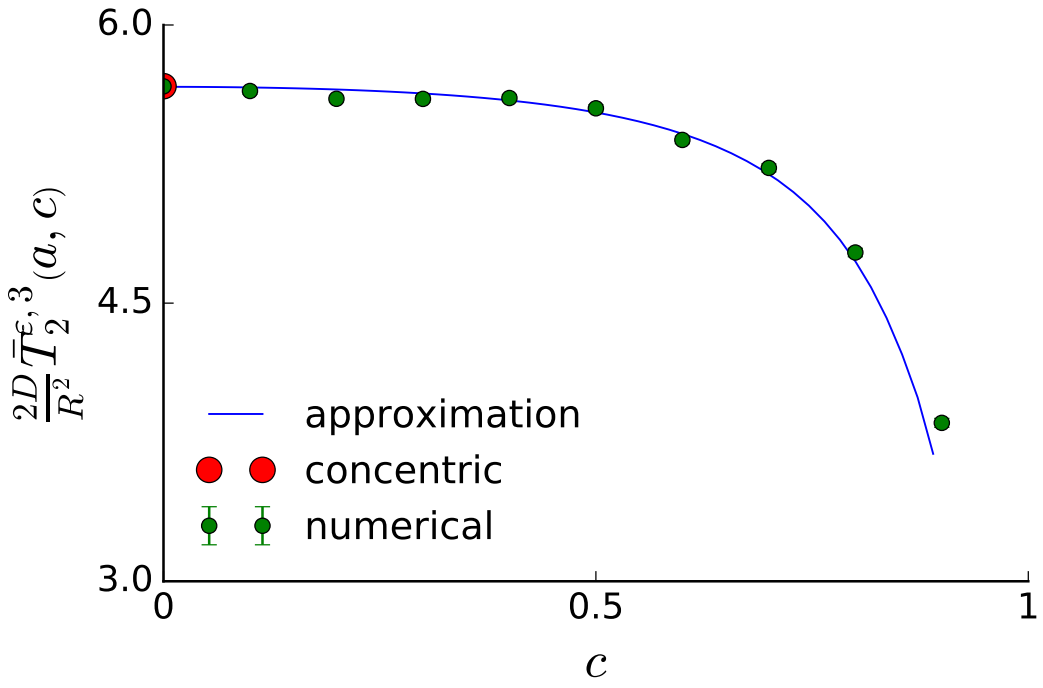

Figure 3.16: Plot of the mean time $\bar{T}_2^{\epsilon,3}$ as a function of the displacement of the nucleus c. The blue line is the semi-analytic solution obtained in (3.56), green dots are numeric simulations and the red dot is the concentric case (1.18) in rescaled coordinates. For this plot we have used the following parameters: $a = 0.1$.

3.7 Discussion

In this chapter we have derived the Green's function, using bispherical coordinates, under two scenarios: (i) approximation and (ii) exact. For the approximation we have made use of the fact that the prefactor $h_x(\tau,\sigma) = \sqrt{\cosh\tau - \cos\sigma}$ can be approximated as $h_x(\tau,\sigma) \approx \sqrt{\cosh\tau}$ when $\tau \gg 0$. This approximation is useful for calculating $G_1^{(3)}(\mathbf{x}_0,\mathbf{x})$ but not $G_2^{(3)}(\mathbf{x}_0,\mathbf{x})$. From the Green's function we calculate the first passage properties of diffusion from the nuclear surface to the cellular surface: hitting density (3.32), mean time (3.37) and average mean time (3.39).

We observe, from Figure 3.9, that as the displacement of the nucleus c increases the accuracy of our approximation (3.39) for $\bar{T}_1^{(3)}(a,c)$ decreases when compared

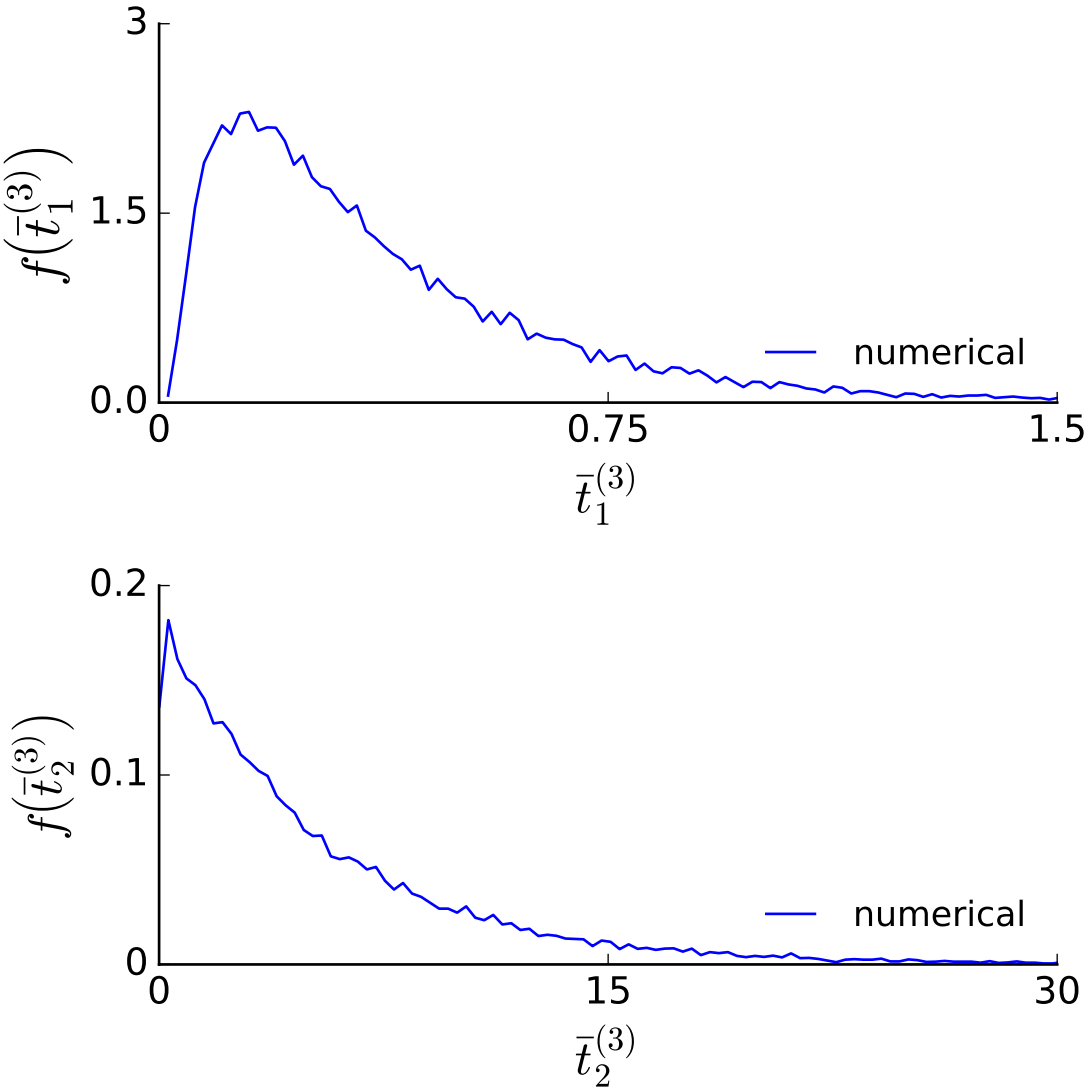

Figure 3.17: Plot of the distribution of $\bar{t}_1^{(3)}$ in the upper plane and the plot of the distribution of $\bar{t}_2^{(3)}$ in the lower plane. The blue lines are numerical simulations for which we have chosen the following parameter values: $a = 0.1$, $c = 0.45$, $D = 0.5$.

with numerical simulations which is consistent with the approximation (3.20) we used to obtain our results.

The existence of a Neumann boundary condition leads to the appearance of a second order difference equation which we solve by using the Green's function method for difference equations, which allows us to calculate the Green's function

for two scenarios: (i) diffusion from the nuclear surface to the cellular surface and (ii) diffusion from the cellular surface to the nuclear surface. A limitation of this method is that it is only applicable when the initial position of the Brownian particle is uniformly distributed on the surface of the nucleus or of the cell, respectively.

In order to obtain the Green's function with uniform initial condition over the surface of the nucleus and of the cell, $\bar{G}_1^{(3)}(\mathbf{x}_0, \mathbf{x})$ and $\bar{G}_2^{(3)}(\mathbf{x}_0, \mathbf{x})$, respectively, we make use of Perron's theorem and continued fraction expansion. From the Green's function we calculate the first passage properties of diffusion from the nuclear surface to the cellular surface: hitting density (3.53) and average mean time (3.54). Analogously, we derive from $\bar{G}_2^{(3)}(\mathbf{x}_0, \mathbf{x})$ the first passage properties of diffusion from the cellular surface to the nuclear surface: average mean time (3.55). We notice from Figure 3.13, when comparing the average mean time of diffusion from the nuclear surface to the cellular surface, that unlike our approximation (3.39), our analytic formula does not decrease in accuracy as the displacement of the nucleus c increases. To our knowledge, the analytic formula for $\bar{G}_1^{(3)}(\mathbf{x}_0, \mathbf{x})$, and all the derived quantities, is unique to the literature.

We derived a semi-analytic formula for the mean round trip time $\left(\bar{T}_1^{(3)} + \bar{T}_2^{\varepsilon,3}\right)(a, c)$ from the approximation derived by Condamin *et al.* (2007) for $T_2^{(3)}(\theta_2)$ and our analytic formula (3.53) for $\varepsilon^{(3)}(\theta_2)$. We notice from Figure 3.16 that $\bar{T}_2^{\varepsilon,3}(a, c)$ is a decreasing function of c as opposed to $\bar{T}_2^{(3)}(a, c)$ which is an increasing function of c. This is because the Brownian particles diffusing from the nucleus are more likely to arrive at the point of the cellular surface which is closest to the nucleus, and, as a result, the mean time for the particle to arrive back to the nucleus is smaller than the case when its starting position is uniformly distributed on the cellular surface.

The dependence on a and c, of the approximation $\bar{T}_1^{(3)}(a, c)$, is shown in Figure 3.10 from which we deduce that the average mean time $\bar{T}_1^{(3)}(a, c)$ is a decreasing function of a and c which is intuitively correct given that a Brownian particle will take a longer time to reach a cellular surface if the staring point is farther away from the absorbing surface.

Our formulas have applications in mathematical immunology to estimate the mean time for a transport molecules (for example STAT molecules Imada &

Leonard (2000); Kerr *et al.* (2003); Speil *et al.* (2011); Vinkemeier (2004)) to start a immune reaction by transporting a signal molecule from the surface of the cell to a intracellular compartment.

The higher order moments of $\bar{t}_1^{(3)}(\mathbf{x}_0)$ and $\bar{t}_2^{(3)}(\mathbf{x}_0)$ should be the focus of extending the results from Chapter 2. We observe from Figure 3.17 that the distribution of $\bar{t}_2^{(3)}(\mathbf{x}_0)$ is wider around the mean than the distribution of $\bar{t}_1^{(3)}(\mathbf{x}_0)$ from which we deduce that $\bar{T}_2^{(3)}(a,c)$ does not capture the most important aspects of Brownian motion from the cellular surface to the nuclear surface. The activation of many processes inside a cell requires the arrival of a single molecule at a target site and in this context the relevant timescale is given by the extreme first passage times (*i.e.* the time at which the first Brownian searcher reaches a target) Basnayake & Holcman (2020); Lawley & Madrid (2020); Mattos *et al.* (2012).

Future work should be on modeling Robin boundary conditions for nuclear or cellular surface given that the reacting surface may itself contain absorbing and reflecting regions. Additionally, future work should be done on expanding the mean times and average mean times in powers of a and comparing with the formulae derived from Condamin *et al.* (2007) in a similar fashion to Chapter 2.

Chapter 4

Simulating intracellular distribution of *Coxiella burnetii* assay

4.1 Introduction

An experimental procedure designed to measure a property of a system in fields such as pharmacology and medicine is often called an assay. In this Chapter, we develop a theoretical model of an assay carried out at the Defence Science and Technology Laboratory (Dstl) to measure intracellular bacterial load of THP-1 (monocytic cell line derived from the peripheral blood of a childhood case of acute monocytic leukemia Bosshart & Heinzelmann (2016)) human monocytes exposed to *Coxiella burnetii* bacteria.

Coxiella burnetii is the agent of Q fever and is transmitted as a zoonotic pathogenic agent to humans (sheep, goats, and cattle are the main source of infection)(Dalton *et al.*, 2014, p.60). The pathogenic agent was used in the biological weapons program of the United States and Soviet Union, and is classified as a Category B pathogen by the Centers for Disease Control and Prevention (CDC) Madariaga *et al.* (2003). In infected humans, *Coxiella burnetii* is phagocytosed by immune cells such as monocytes and macrophages which are then subsequently subverted by the bacteria which replicate intracellularly. The importance of *Coxiella burnetii* is given by the consideration of it as a prototype in cell-free culture for

bacterium, which replicate inside eukaryotic cells Dalton *et al.* (2014).
In the experiments performed by Dstl, a cylindrical well is filled with a composite medium of 90% Leibovitz's L-15 Medium and 10% fetal calf serum containing *Coxiella burnetii bacteria*. Monocytes are distributed on the base of the cylindrical container. After 24 hours, fluorescence microscopy reveals the location of intracellular and extracellular bacteria (see Appendix E.1).
An important parameter is the multiplicity of infection (MOI): the ratio of the total number of bacteria initially in the medium to the total number of monocytes on the well bottom. Let the number of monocytes be N_0 and the the initial number of bacteria be M_0 then

$$M_0 = \text{MOI} \times N_0.$$

In our theoretical model, we assume a cylindrical container of radius b and height h. We assume that *Coxiella burnetii* bacteria are, initially, uniformly distributed in the medium and they diffuse with diffusion coefficient D until they are phagocytosed by the monocytes. The monocytes form a monolayer on the bottom of the well (see Figure 4.1). We assume that the bacteria do not stick to the walls of the well.
The monocytes are assumed to be disks of radius r_m on the bottom of the vessel. The distribution of r_m is shown in Figure 4.2 from the experimental data provided by Dstl.
We assume that the height of the assay well is given to be $h = 1\text{cm}$ and the radius of the well horizontal cross-section $b = 1/\sqrt{\pi}\text{cm}$. The initial number of monocytes distributed on the well bottom is assumed to be $N_0 = 1.5 \times 10^5$ and the multiplicity of infection is $\text{MOI} = 2 \times 10^2$. Finally, we assume that the *Coxiella burnetii* bacteria diffuse with diffusion coefficient $D = 0.5\text{cm}^2\,\text{s}^{-1}$. The parameters used for the assay simulation are shown in table F.1. A graphical representation of the assay experiment is shown in Figure 4.1.
We want to determine the intracellular distribution of phagocytosed *Coxiella burnetii* at any point in time and for that purpose we will make use of boundary homogenisation: the bottom of the vessel can be assumed to be a reflecting surface (given that the bacteria do not stick to the assay well) covered with absorbing

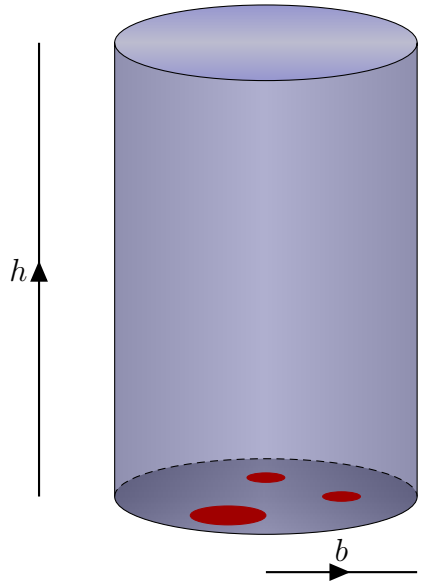

Figure 4.1: Diagram of the assay well where b is the radius of the cross-section and h is the height of the well. The red circles on the bottom denote the monocytes distributed in a monolayer.

disks, which can be approximated to a homogeneous surface using methods which we will discuss below.
In this chapter we will be using the following boundary conditions which are equivalent Barton (1989); Bou-Rabee & Holmes-Cerfon (2020); Erban & Chapman (2007):

- Dirichlet boundary condition ≡ absorbing boundary.
- Neumann boundary condition ≡ reflecting boundary.
- Robin boundary condition ≡ partially reflecting/absorbing boundary.

Numerical simulations highlighted in Appendix E.3 are used to validate our results.

4.2 Literature review

Problems arising when diffusing particles are captured by patchy surfaces are ubiquitous in physics, biology and chemistry. A sample includes ligand bind-

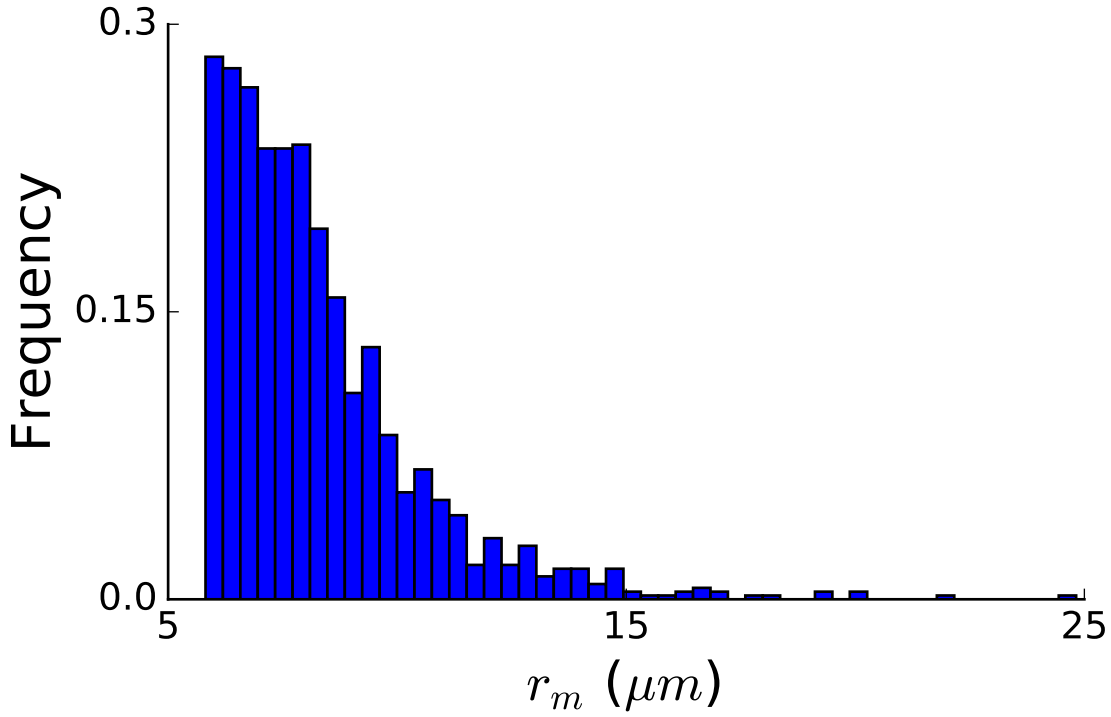

Figure 4.2: Histogram of the radii r_m of monocytes which are assumed to be disks on the bottom of the well (experimental data provided by Dstl).

ing to cell surface receptors, electric current through arrays of electrodes, reactions on supported catalysts and water exchange in plants. Of particular interest are reflecting surfaces covered with non-overlapping circular absorbing traps (Berezhkovskii *et al.*, 2004, p.11390).

The method of matched asymptotic expansion has been used extensively to study narrow escape problems when the absorbing target is a absorbing circular hole located on a otherwise reflecting boundary. This is because when the absorbing hole shrinks to zero the mean time to absorption diverges to infinity and the narrow escape problem becomes a singular perturbation problem and is solved by using asymptotic expansions Holcman & Schuss (2015); Schuss *et al.* (2007); Singer *et al.* (2006b). Matched asymptotic expansion has been used to calculate the diffusive flux to a boundary covered by circular absorbers in the case of a flat boundary Bernoff & Lindsay (2018); Bernoff *et al.* (2018) and a spherical

boundary Lindsay *et al.* (2017).

The problem of periodic absorbers located on a reflecting boundary has been investigated extensively using boundary homogenization Berezhkovskii *et al.* (2006); Bernoff *et al.* (2018); Muratov & Shvartsman (2008).

Eun (2018) calculated the rate constant of a cell membrane covered by multiple receptors by using surface curvature-dependent kinetic theory with a correction for the asymptotic behaviour as the fraction of the surface covered goes to 1.

Partial differential equations with heterogeneous boundary conditions are difficult to solve analytically and, as a consequence, boundary homogenisation is used to solve these problems. This entails replacing the heterogeneous patchy surface with a homogeneous partially absorbing surface with appropriate trapping parameter κ as seen in Figure 4.3.

A key strength of boundary homogenisation is its universality, that is, it can be used to solve both internal and external problems where particles diffuse to a trapping surface from inside and outside of a region, respectively. Furthermore, this method can be used to solve both steady state and time-dependent problems Berezhkovskii *et al.* (2004).

Boundary homogenisation belongs to a class of methods called "effective medium theories" which treat phenomena in non-uniform media by changing the real medium with a fictitious uniform media with adequate parameters. The fundamental idea behind boundary homogenisation is that non-uniform boundaries affect a relatively small neighbourhood near the surface and, as a result, the memory about the local properties of the boundary declines as a function of distance from the boundary (Berezhkovskii *et al.*, 2004, p.11390).

Berg and Purcell (Berg & Purcell, 1977, p.194-196) analysed the binding of ligand to receptors on the surface of a cell which they approximated to a sphere of radius R, covered with N_0 perfectly absorbing disks of radius r_m, where they assumed that $r_m \ll R$. They used the analogous problem, from electrostatics, of an insulating sphere of radius R covered by N_0 conducting disks of radius r_m connected by infinitesimal wires to derive the diffusing current to the sphere:

$$J = k_{BP} c_\infty, \quad k_{BP} = k_{SM} \frac{N_0 k_{disk}}{k_{SM} + N_0 k_{disk}},$$

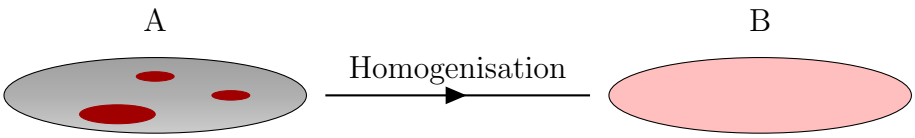

Figure 4.3: Graphical representation of boundary homogenisation. The heterogeneous boundary condition on surface A is replaced by a homogeneous partially absorbing boundary in B with trapping rate κ. On surface A, the boundary conditions are $p(\mathbf{r},t) = 0$ on the red circles and $\nabla_{\mathbf{n}} p(\mathbf{r},t) = 0$ on the rest of the boundary, where $p(\mathbf{r},t)$ is the particle density and $\mathbf{n}$ is the unit normal outward vector to the surface. However, the boundary condition on B is given by $D\nabla_{\mathbf{n}} p(\mathbf{r},t) = \kappa p(\mathbf{r},t)$.

where J is the steady state diffusion current and c_∞ is the ligand concentration sufficiently far from the cell surface. The Berg-Purcell rate constant k_{BP} is the product of the Smoluchowski rate constant $k_{SM} = 4\pi DR$ (which is the forward rate constant for ligand molecules diffusing to the cell surface (Lauffenburger & Linderman, 1993, p.147)), and the capture probability of a particle starting on the surface of a sphere of radius R with trapping rate $\kappa_{BP} = N_0 k_{disk}/4\pi R^2$ where $k_{disk} = 4Dr_m$ is the rate constant of a perfectly absorbing disk of radius a placed on a perfectly reflecting plane (the number of disks per unit area is $N_0/4\pi R^2$ and if the disks are sufficiently far apart then κ_{BP} can be approximated as the product of k_{disk} and the number of disks per area) (Shoup & Szabo, 1982, p.33). We rewrite the Berg-Purcell trapping rate:

$$\kappa_{BP} = \frac{4D}{\pi r_m}\sigma, \quad \sigma = \frac{N_0 r_m^2}{4R^2},$$

where σ is the fraction of the spherical surface covered in absorbing disks. This formula has been improved by Zwanzig (Zwanzig, 1990, p. 5857) to arbitrary surface coverage:

$$\kappa_{ZW} = \frac{1}{1-\sigma}\kappa_{BP} = \frac{4D}{\pi a}\frac{\sigma}{1-\sigma}.$$

Berezhkovskii *et al.* (Berezhkovskii *et al.*, 2004, p.11391) used the following notation for the trapping rate:

$$\kappa = \frac{4D}{\pi r_m}F(\sigma), \tag{4.1}$$

where $F(\sigma)$ is a dimensionless function of the trap-coverage fraction. Thus, the problem of boundary homogenisation consists of finding the appropriate function F for a patchy surface with trap surface fraction σ.
We observe that the boundary is perfectly absorbing ($F \to +\infty \Rightarrow \kappa \to +\infty$, see Appendix E.2) when $\sigma \to 1$ and perfectly reflecting ($F \to 0 \Rightarrow \kappa \to 0$) when $\sigma \to 0$. Furthermore, from (4.1) we observe that $\kappa \to +\infty$ when $r_m \to 0$ and σ is held constant, which means that the boundary behaves as perfectly absorbing when the disks cover a small fraction of the surface. For example, a cell of radius $R = 5\mu m$ covered with N_0 transport proteins of radius $r_m = 10\text{Å}$ (where 1Å= 1 ångström $= 10^{-10}m$) can absorb at half the rate of a perfectly absorbing sphere when $\sigma = 1.6 \times 10^{-4}$(Berg, 1993, p.33).
From the Berg-Purcell and Zwanzig formulae for κ we observe that:

$$F_{BP}(\sigma) = \sigma, \quad F_{ZW}(\sigma) = \frac{\sigma}{1-\sigma},$$

where $F_{BP}(\sigma)$ is only valid for $\sigma \ll 1$ while $F_{ZW}(\sigma)$ captures the asymptotic behaviour as $\lim_{\sigma\to 0} F_{ZW}(\sigma) = 0$ and $\lim_{\sigma\to 1} F_{ZW}(\sigma) = +\infty$.
Berezhkovskii et al. (Berezhkovskii *et al.*, 2004, p.11392) proposed the following formula for F:

$$F(\sigma) = \frac{\sigma}{1-\sigma}(1 + A\sigma^B),$$

where the parameters A, B where obtained by using numerical simulations to calculate the mean time for a diffusing particle to be absorbed by a partially reflecting surface and related the numerical result to the analytic formula for the mean time which is a function of κ. As a result, the function F becomes:

$$F(\sigma) = \frac{\sigma}{1-\sigma}(1 + 3.8\sigma^{1.25}).$$

The use of these formulae for boundary homogenisation is justified when the trap radius r_m is much smaller than the characteristic length R of the boundary (in the case of a sphere it is the sphere radius).
In the case of non-overlapping disks of different radii we take advantage of the fact that $F(\sigma)$ only depends on the trap-coverage fraction and not on the disk radius. This allows us to derive a formula for the effective trapping rate κ for a

patchy surface covered by N_0 absorbing disks of varying radii r_m^i, $i \in \{1, \ldots, N_0\}$ (Makhnovskii *et al.*, 2005, p. 236102):

$$\kappa(\sigma_1, \ldots, \sigma_{N_0}) = \frac{4D}{\pi} F(\sigma) \sum_{i=1}^{N_0} \frac{\sigma_i}{r_m^i \sigma}, \tag{4.2}$$

where

$$\sigma = \sum_{i=1}^{N_0} \sigma_i,$$

and $\sigma_i = \pi \left(r_m^i\right)^2 n_i$ is the surface fraction occupied by n_i disks of radius r_m^i. We introduce the following notation:

$$\kappa_i(\sigma) = \frac{4D}{\pi r_m^i} F(\sigma),$$

and we rewrite (4.2) as :

$$\kappa(\sigma_1, \ldots, \sigma_{N_0}) = \sum_{i=1}^{N_0} \nu_i \kappa_i(\sigma), \tag{4.3}$$

where $\nu_i = \sigma_i / \sigma$ is the relative fraction of the surface covered by disks of radius r_m^i and:

$$\sum_{i=1}^{N_0} \nu_i = 1.$$

We will use this formula for the rest of this chapter when discussing boundary homogenisation. We plot κ as a function of N_0 in Figure 4.4 where the radii r_m^i are sampled from the data provided by Dstl (see Figure 4.2). Given the fact that the radius of a monocyte is a continuous variable the chance of duplicates in the experimental data provided by Dstl is very unlikely. As a result, the number disks of radius r_m^i is $n_i = 1$ and the trapping is given by (4.3) is:

$$\kappa = \frac{4D}{\pi} F\left(\pi \sum_{i=1}^{N_0} \left(r_m^i\right)^2\right) \frac{\sum_{i=1}^{N_0} r_m^i}{\sum_{i=1}^{N_0} \left(r_m^i\right)^2}. \tag{4.4}$$

Using (4.4) and the monocyte radii data provided by Dstl we obtain the trapping rate $\kappa \approx 762\, cm/s$ for $N_0 = 1.5 \times 10^5$ monocytes, which we will use in our subsequent calculations. In the remainder of this chapter, boundary homogenisation

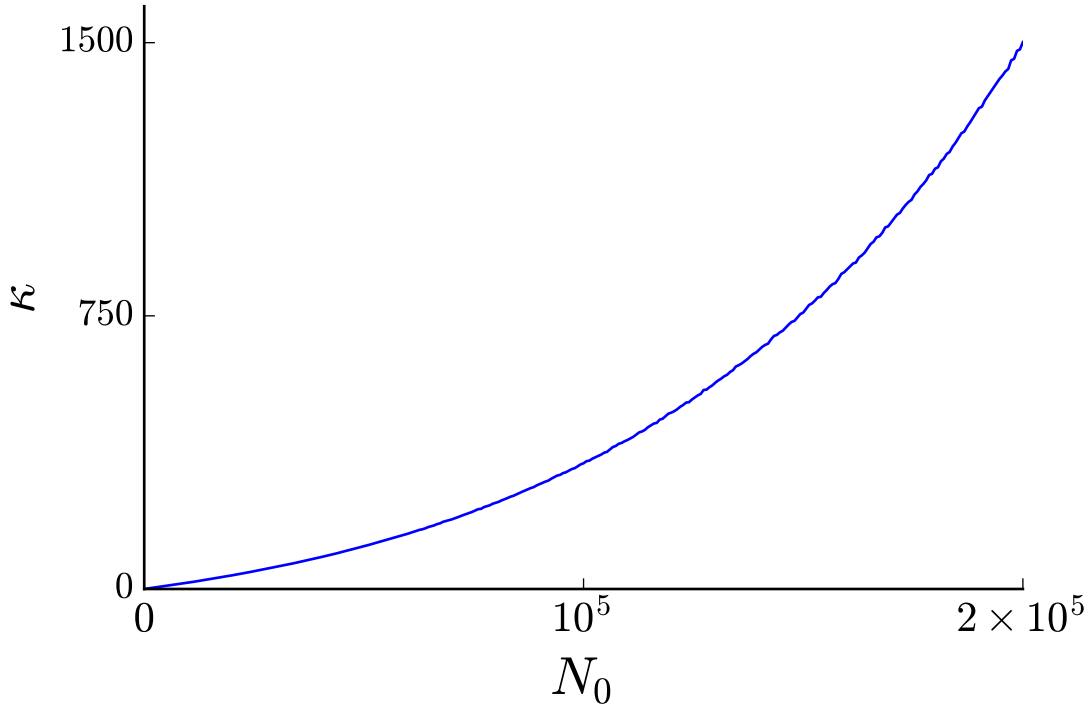

Figure 4.4: Plot of the trapping rate κ as a function of N_0 where N_0 is the number of absorbing traps. The blue line represents the formula derived in (4.2). The radii r_m^i are sampled from the experimental data provided by Dstl (see Figure 4.2).

is discussed in the context of producing a mathematical model of assays with the hope of obtaining the intracellular distribution of bacteria phagocytosed during the experiment. The homogenised boundary will have Robin boundary condition and we will highlight this type of boundary in the case of one dimensional diffusion in Section 4.5. The assay experiment was described in Section 4.1 and we apply boundary homogenisation deriving the relevant results in Section 4.6.

4.3 Diffusive current

Following the example of Berg (Berg, 1993, p.33), we want to investigate how many traps must be placed in order that the absorption rate be half that of the

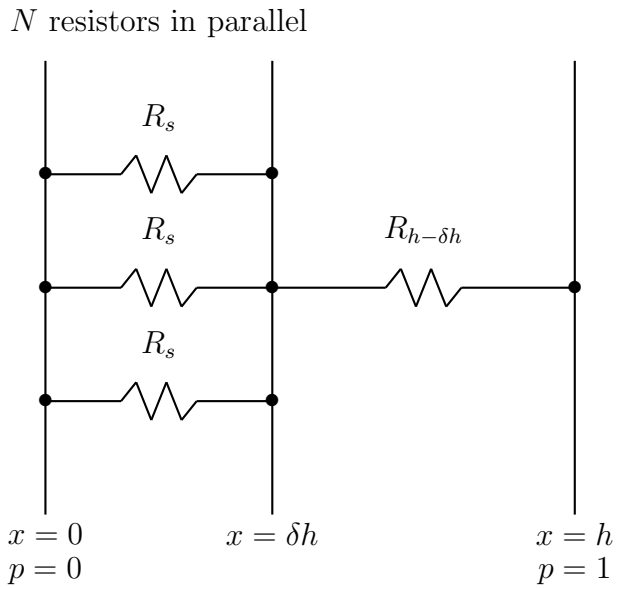

Figure 4.5: Electrical model for the problem of N_0 absorbers of radius s on the bottom of an assay of radius b and height h, the problem illustrated in Figure 4.1.

case when the boundary is fully absorbing.

Consider the case when the top of the assay well is a constant source of new bacteria (*i.e.* $p(x) = 1$ at $x = 1$, where $p\,(x)$ is the particle concentration). We define the diffusion current to be the rate at which bacteria are absorbed by the monocytes at the bottom of the assay and we wish to calculate the ratio I/I_0, where I_0 and I are the diffusive current when the bottom of the assay is absorbing or covered with absorbing circular traps, respectively.

The problem is formally equivalent to the one in electricity where current flows through a medium of finite resistivity to N_0 conductive patches on an otherwise insulated surface (see Figure 4.5) (Berg, 1993, p.31-33). The concentration p is analogous to the voltage V and using Ohm's law, which states that the current through a resistor is equal to the potential drop across its terminals divided by its resistance, we derive that $I = p/R_e$ where R_e is the diffusion resistance.

Exploiting this relation, we note that the diffusion resistance for diffusion in the cylinder is $R_h = h/D\pi b^2$ and the diffusion resistance for one of the traps of radius

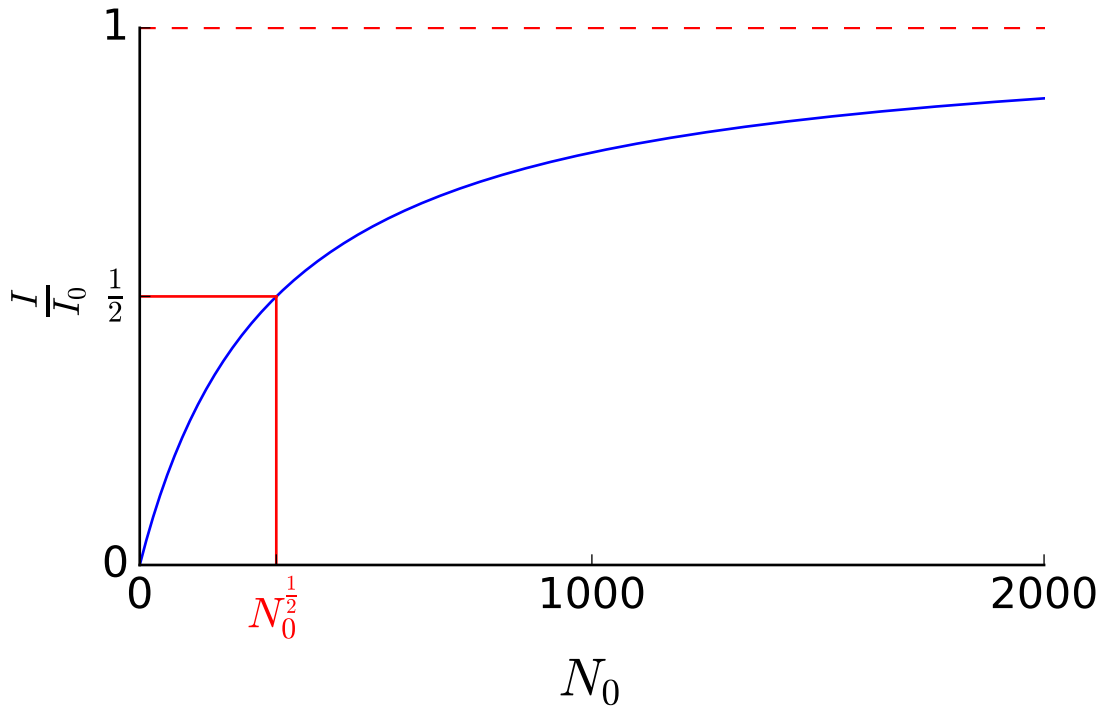

Figure 4.6: The diffusion current fraction I/I_0 as a function of the number N_0 of disk-like absorbers on the bottom of the assay. The blue line represents the formula derived in (4.5).

s is $1/4Ds$. As a result, the total resistance of the circuit is:

$$R_e = R_{h-\delta h} + \frac{R_s}{N_0} = \frac{h-\delta h}{D\pi b^2} + \frac{1}{4DN_0 s}.$$

Given that $\delta h \ll h$ the resistance becomes:

$$R_e \approx \frac{h}{D\pi b^2}\left(1 + \frac{\pi b^2}{4hN_0 s}\right).$$

Consequently, the ratio of the diffusion current is:

$$\frac{I}{I_0} = \frac{1}{1+\frac{\pi b^2}{4hN_0 s}}. \tag{4.5}$$

Denoting the diffusive current fraction by α we obtain the number of traps:

$$\frac{I}{I_0} = \alpha \Rightarrow N_0^{\alpha} = \frac{\alpha}{1-\alpha}\frac{\pi b^2}{4hs}. \tag{4.6}$$

We want to know how many traps have to be placed on the bottom of the assay in order to obtain a value of the diffusion current half of the case when the entire assay bottom is absorbing. Using $\alpha = 0.5$ and $s = \mathbb{E}[r_m]$ in (4.6) we obtain:

$$N_0^{\frac{1}{2}} = \frac{\pi b^2}{4hs} = 302,$$

which means that just $\sigma = \pi N_0^{\frac{1}{2}} \mathbb{E}([r_m])^2 \approx 6 \times 10^{-4}$ of the surface of the assay well is covered with traps.
Interestingly, letting $N_0 = 1.5 \times 10^5$ we obtain $I/I_0 \approx 0.997$ which means that in our experiment the bottom of the assay well is equivalent to fully absorbing boundary.

4.4 Monocyte surface coverage

A quantity of importance for our analysis is the fraction σ of the bottom surface of the well covered with $N_0 = 1.5 \times 10^5$ monocytes of radius r_m (see Figure 4.2). In order to estimate σ we begin with Figure 4.7(a), provided by Dstl, and using the image processing program ImageJ we obtain Figure 4.7(b) by making use of the following sequence of commands:

1. Plugins→Filters→Enhance Local Contrast (blocksize:60; histogram bins:256; maximum slope:6.00);
2. Process→Smooth;
3. Plugins→Filters→Enhance Local Contrast (blocksize:20; histogram bins:256; maximum slope:6.00);
4. Image→Adjust→Brightness/Contrast→Contrast such that the lower limit is 55 and the upper limit is 198;
5. Save as a .jpeg.

We observe from Figure 4.7(b) and 4.8 that the interior of the cells are characterised by low grayscale values and the cellular boundaries are characterised by high grayscale values. We plot the distribution of the grayscale values of 768×768

pixels of the transformed image from Figure 4.7(b) in Figure 4.8 and observe that the distribution is symmetrical. Additionally, we observe that the grayscale values are concentrated at the endpoint of the range with a local maximum at medium values of the grayscale. We observe that the points which separate the cellular from the extracellular domain are represented by the points where the grayscale distribution obtained its local minima. Because we utilise the Python code G.1 to obtain the cumulative distribution function of the grayscale interval $[0, X] \cup [255 - X, 255]$, shown in Figure 4.9, these two points will overlap into a single point, due to the symmetry of the distribution, and are determined by the value of X for which:

$$\frac{\mathrm{d}^2}{\mathrm{d}X^2} CDF(X) = 0,$$

where $CDF\,(x)$ is the cumulative distribution function of the grayscale distribution shown in Figure 4.8. As a result, we observe that for $X = 15$ the second order derivative in X becomes zero and we obtain $\sigma \approx 1/3$. To justify our choice of $X = 15$ we use Python code G.2 to produce Figure 4.10 in which every pixel in the set $[0, X] \cup [255 - X, 255]$ is coloured red and all other pixels are coloured blue. We observe that the red pixels coincide with the monocytes from Figure 4.7(b). Additionally, our estimate of σ is also consistent with experimental data provided by Dstl which gives:

$$\sigma = \frac{N_0 \times \pi \left(\mathbb{E}\left[r_m\right]\right)^2}{\pi b^2} \approx 0.322.$$

For our analysis we choose the value of $\sigma = 1/3$ as the surface fraction of the bottom of the well covered with monocytes.

4.5 One dimension diffusion equation

We are interested in how the position of a particle, starting uniformly on a interval $[0, h]$, changes with time due to diffusion. The boundary conditions are the following: Robin boundary conditions at $x = 0$ and Neumann boundary conditions at $x = h$. Let $p(x, t)$ be the density of particles at position x at time t given that their initial position is distributed uniformly on the interval $[0, h]$. As

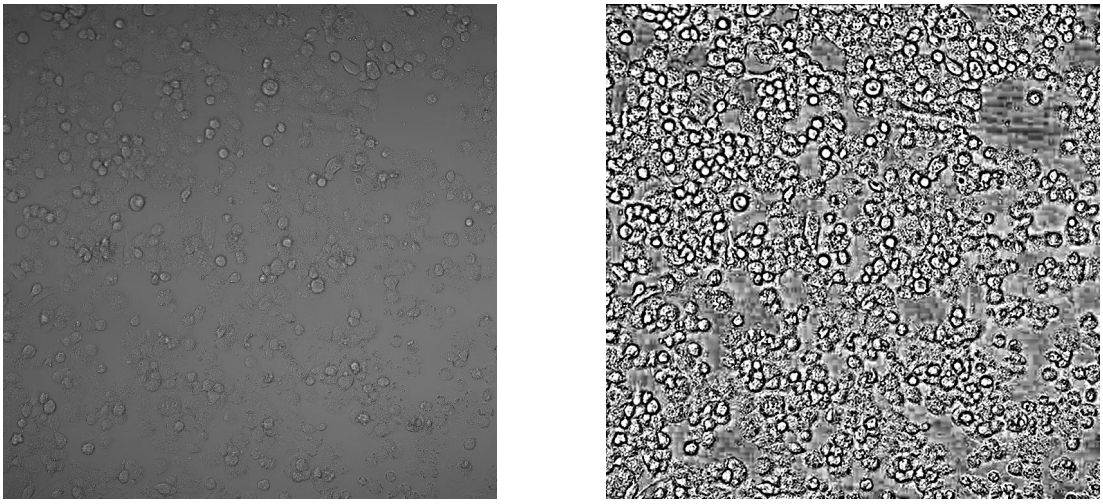

(a) (b)

Figure 4.7: Image of the cells on the bottom of the well provided by Dstl (left) and the same image after being transformed using ImageJ.

a result we have:

$$\frac{\partial}{\partial t}p(x,t) = D\nabla_x^2 p(x,t), \tag{4.7}$$

with boundary and initial conditions, respectively:

$$D\left.\frac{\partial}{\partial x}p(x,t)\right|_{x=0} = \kappa p(0,t), \quad \forall t \geq 0, \tag{4.8a}$$

$$\left.\frac{\partial}{\partial x}p(x,t)\right|_{x=h} = 0, \quad \forall t \geq 0, \tag{4.8b}$$

$$p(x,0) = \frac{1}{h}, \quad \text{for } x \in (0,h). \tag{4.8c}$$

We look for a separable solution of (4.7) of the form $p(x,t) = \mathcal{X}(x)\mathcal{T}(t)$ and as a result the diffusion equation becomes after simplification:

$$\frac{\mathcal{X}}{D}\frac{\mathrm{d}\mathcal{T}}{\mathrm{d}t} = T\frac{\mathrm{d}^2\mathcal{X}}{\mathrm{d}x^2}. \tag{4.9}$$

Multiplying equation (4.9) by $\frac{1}{\mathcal{X}\mathcal{T}}$ we obtain:

$$\frac{1}{D\mathcal{T}}\frac{\mathrm{d}\mathcal{T}}{\mathrm{d}t} = \frac{1}{\mathcal{X}}\frac{\mathrm{d}^2\mathcal{X}}{\mathrm{d}x^2}. \tag{4.10}$$

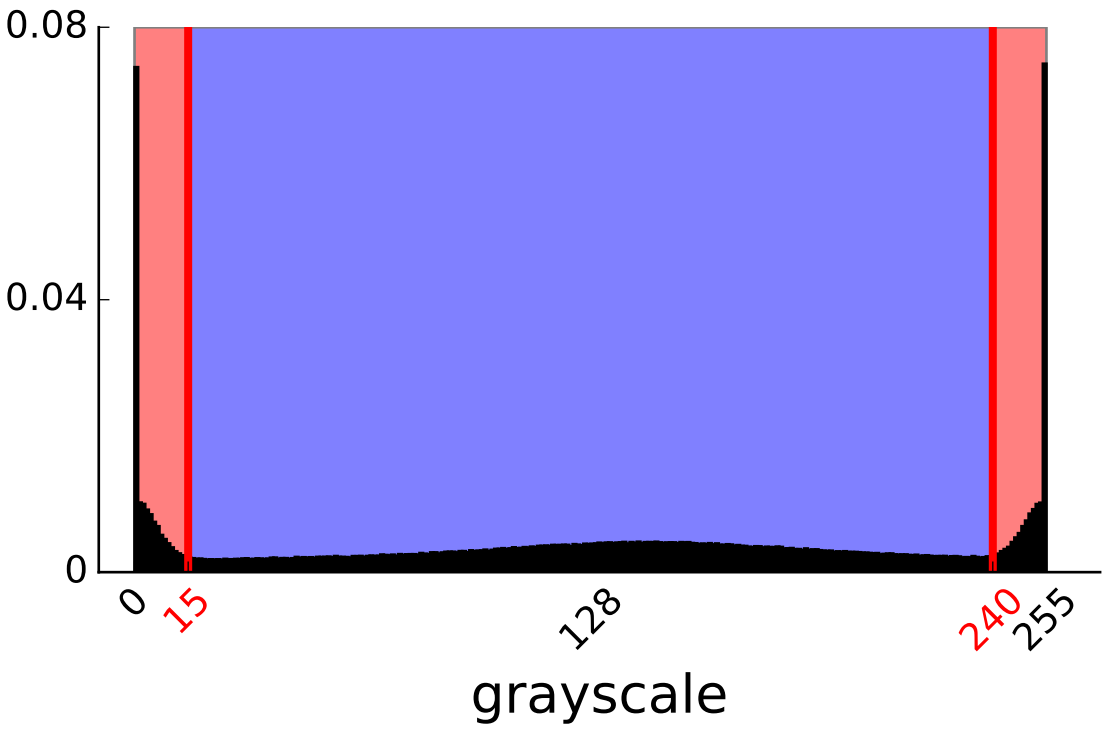

Figure 4.8: Distribution of grayscale values of Figure 4.7(b). We calculate the grayscale value for each pixel and we obtain the distribution of these values. The light red regions represents the monocytes, while the light blue region represents the bottom of the assay well.

We observe that the left-hand side of (4.10) is a function of t while the right-hand side is a function of x and we deduce that:

$$\frac{1}{D\mathcal{T}}\frac{\mathrm{d}\mathcal{T}}{\mathrm{d}t} = \frac{1}{\mathcal{X}}\frac{\mathrm{d}^2\mathcal{X}}{\mathrm{d}x^2} = -\lambda^2,$$

where λ is a constant. Here we choose the constant to be $-\lambda^2$ in order to ensure that the time function does not grow exponentially and as a consequence the density $p(x,t)$ will be finite when $t \to +\infty$ (the particle will eventually be absorbed and as a result $p(x,t) \to 0$ when $t \to +\infty, \forall x \in [0,h]$, see Section 1.3). The time equation is:

$$\frac{1}{\mathcal{T}}\frac{\mathrm{d}\mathcal{T}}{\mathrm{d}t} = -\lambda^2 D,$$

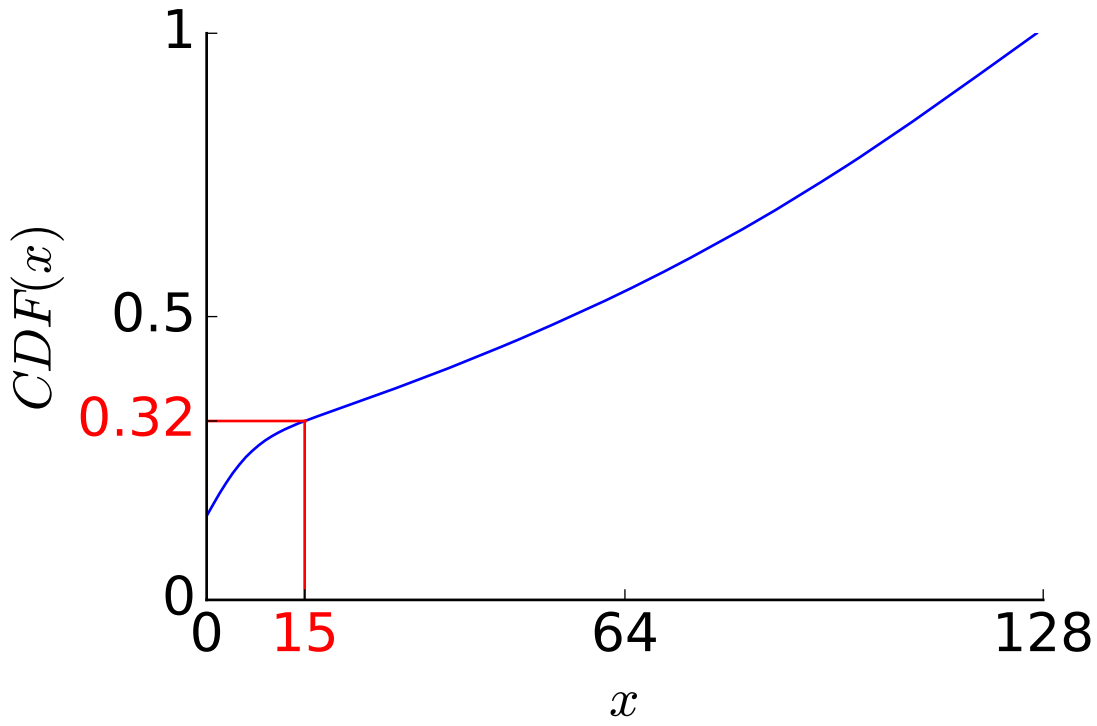

Figure 4.9: Cumulative distribution function of the grayscale interval $[0, x] \cup [255 - x, 255]$ of Figure 4.7(b).

which has the solution:

$$\mathcal{T}(t) = C\mathrm{e}^{-\lambda^2 Dt}, \tag{4.11}$$

where C is a constant.

Solving the x equation we obtain:

$$\frac{\mathrm{d}^2\mathcal{X}}{\mathrm{d}x^2} + \lambda^2\mathcal{X} = 0 \Rightarrow \mathcal{X}(x) = A\cos(\lambda x) + B\sin(\lambda x).$$

Given the boundary condition (4.8a) and (4.8b) we deduce the following:

$$D\left.\frac{\partial}{\partial x}p(x,t)\right|_{x=0} = \kappa p(0,t), \forall t > 0 \Rightarrow D\left.\frac{\mathrm{d}\mathcal{X}}{\mathrm{d}x}\right|_{x=0} = \kappa\mathcal{X}(0),$$
$$\frac{\partial}{\partial r}p(b,t) = 0, \forall t > 0 \Rightarrow \left.\frac{\mathrm{d}\mathcal{X}}{\mathrm{d}x}\right|_{x=h} = 0,$$

which gives us:

$$D\left.\frac{\mathrm{d}\mathcal{X}}{\mathrm{d}x}\right|_{x=0} = \kappa\mathcal{X}(0) \Rightarrow D\lambda B = \kappa A \Rightarrow A = \frac{D\lambda B}{\kappa},$$

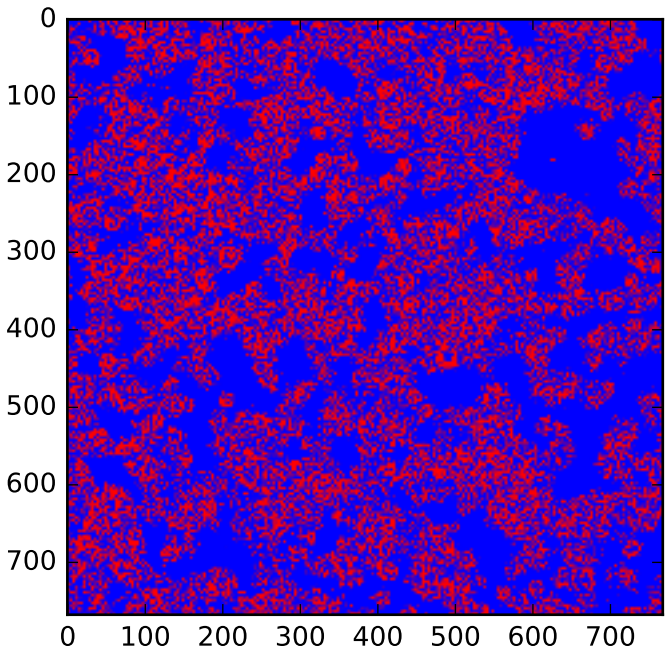

Figure 4.10: Heat map of Figure 4.7(b) where all pixels whose grayscale value is contained in the interval $[0, 15] \cup [240, 255]$ are coloured red and all other pixels are coloured blue. This figure was obtained using Python code G.2.

$$\left.\frac{\mathrm{d}\mathcal{X}}{\mathrm{d}x}\right|_{x=h} = 0 \Rightarrow -A\lambda \sin(\lambda z) + B\lambda \cos(\lambda z) = 0.$$

As a result, the x component turns out to be:

$$\mathcal{X}_n(x) = \frac{D\lambda_n}{\kappa} \cos(\lambda_n x) + \sin(\lambda_n x), \quad n \in \mathbb{N} \cup \{0\}, \tag{4.12}$$

where λ_n is the n-th root of:

$$\frac{D\lambda}{\kappa} \sin(\lambda h) - \cos(\lambda h) = 0. \tag{4.13}$$

Using (4.11), (4.12) and the principle of superposition we write $p(x, t)$ as:

$$p(x,t) = \sum_{n=0}^{+\infty} A_n \left[\frac{D\lambda_n}{\kappa} \cos(\lambda_n x) + \sin(\lambda_n x)\right] \mathrm{e}^{-\lambda_n^2 Dt}, \tag{4.14}$$

where A_n's are coefficients to be determined. From the initial condition (4.8c) we have:

$$p(x,0) = \frac{1}{h} \Rightarrow \sum_{n=0}^{+\infty} A_n \left[\frac{D\lambda_n}{\kappa} \cos(\lambda_n x) + \sin(\lambda_n x) \right] = \frac{1}{h}, \tag{4.15}$$

We multiply (4.15) by $\mathcal{X}_m(x)$ integrate from 0 to h with respect to x obtaining:

$$\sum_{n=0}^{+\infty} A_n \int_0^h \mathcal{X}_m \mathcal{X}_n \, \mathrm{d}x = \frac{1}{h} \int_0^h \mathcal{X}_m \, \mathrm{d}x.$$

The right-hand side is calculated to be:

$$\begin{aligned}
\int_0^h \mathcal{X}_m(x) \, \mathrm{d}x &= \int_0^h \left[\frac{D\lambda_m}{\kappa} \cos(\lambda_m x) + \sin(\lambda_m x) \right] \mathrm{d}x \\
&= \frac{D\lambda_m}{\kappa} \int_0^h \cos(\lambda_m x) \, \mathrm{d}x + \int_0^h \sin(\lambda_m x) \, \mathrm{d}x \\
&= \frac{D\lambda_m}{\kappa} \left[\frac{\sin(\lambda_m x)}{\lambda_m} \right]_0^h - \left[\frac{\cos(\lambda_m x)}{\lambda_m} \right]_0^h \\
&= \frac{1}{\lambda_m} \left[\frac{D\lambda_m}{\kappa} \sin(\lambda_m h) - \cos(\lambda_m h) \right] + \frac{1}{\lambda_m} \\
&= \frac{1}{\lambda_m},
\end{aligned} \tag{4.16}$$

where in the penultimate line we have used (4.13) and, which gives us the following:

$$\sum_{n=0}^{+\infty} A_n \int_0^h \mathcal{X}_m \mathcal{X}_n \, \mathrm{d}x = \frac{1}{h\lambda_m}. \tag{4.17}$$

If $n \neq m$ then we have:

$$\begin{aligned}
&\int_0^h \mathcal{X}_n \mathcal{X}_m \, \mathrm{d}x = \int_0^h \left[\frac{D\lambda_n}{\kappa} \cos(\lambda_n x) + \sin(\lambda_n x) \right] \left[\frac{D\lambda_m}{\kappa} \cos(\lambda_m x) + \sin(\lambda_m x) \right] \mathrm{d}x \\
&= \frac{D^2\lambda_n\lambda_m}{\kappa^2} \int_0^h \cos(\lambda_n x) \cos(\lambda_m x) \, \mathrm{d}x + \frac{D\lambda_n}{\kappa} \int_0^h \cos(\lambda_n x) \sin(\lambda_m x) \, \mathrm{d}x \\
&+ \frac{D\lambda_m}{\kappa} \int_0^h \cos(\lambda_m x) \sin(\lambda_n x) \, \mathrm{d}x + \int_0^h \sin(\lambda_n x) \sin(\lambda_m x) \, \mathrm{d}x \\
&= \frac{D^2\lambda_n\lambda_m}{2\kappa^2} \left\{ \left[\frac{\sin\left[(\lambda_n - \lambda_m)x\right]}{\lambda_n - \lambda_m} \right]_0^h + \left[\frac{\sin\left[(\lambda_n + \lambda_m)x\right]}{\lambda_n + \lambda_m} \right]_0^h \right\} \\
&- \frac{D\lambda_n}{2\kappa} \left\{ \left[\frac{\cos\left[(\lambda_m - \lambda_n)x\right]}{\lambda_m - \lambda_n} \right]_0^h + \left[\frac{\cos\left[(\lambda_n + \lambda_m)x\right]}{\lambda_n + \lambda_m} \right]_0^h \right\}
\end{aligned}$$

$$
\begin{aligned}
&- \frac{D\lambda_m}{2\kappa}\left\{ \left[\frac{\cos\left[(\lambda_n-\lambda_m)x\right]}{\lambda_n-\lambda_m}\right]_0^h + \left[\frac{\cos\left[(\lambda_n+\lambda_m)x\right]}{\lambda_n+\lambda_m}\right]_0^h \right\} \\
&+ \frac{1}{2}\left\{ \left[\frac{\sin\left[(\lambda_n-\lambda_m)x\right]}{\lambda_n-\lambda_m}\right]_0^h - \left[\frac{\sin\left[(\lambda_n+\lambda_m)x\right]}{\lambda_n+\lambda_m}\right]_0^h \right\} \\
&= \frac{D^2\lambda_n\lambda_m}{2\kappa^2}\left\{ \frac{\sin\left[(\lambda_n-\lambda_m)h\right]}{\lambda_n-\lambda_m} + \frac{\sin\left[(\lambda_n+\lambda_m)h\right]}{\lambda_n+\lambda_m} \right\} \\
&- \frac{D\lambda_n}{2\kappa}\left\{ \frac{\cos\left[(\lambda_m-\lambda_n)h\right]}{\lambda_m-\lambda_n} + \frac{\cos\left[(\lambda_n+\lambda_m)h\right]}{\lambda_n+\lambda_m} \right\} \\
&- \frac{D\lambda_m}{2\kappa}\left\{ \frac{\cos\left[(\lambda_n-\lambda_m)h\right]}{\lambda_n-\lambda_m} + \frac{\cos\left[(\lambda_n+\lambda_m)h\right]}{\lambda_n+\lambda_m} \right\} \\
&+ \frac{1}{2}\left\{ \frac{\sin\left[(\lambda_n-\lambda_m)h\right]}{\lambda_n-\lambda_m} - \frac{\sin\left[(\lambda_n+\lambda_m)h\right]}{\lambda_n+\lambda_m} \right\} \\
&= \frac{1}{\lambda_n-\lambda_m}\left[\frac{D^2\lambda_n\lambda_m}{2\kappa^2}\sin\left[(\lambda_n-\lambda_m)h\right] + \frac{D\lambda_n}{2\kappa}\cos\left[(\lambda_n-\lambda_m)h\right] \right. \\
&\left. - \frac{D\lambda_m}{2\kappa}\cos\left[(\lambda_n-\lambda_m)h\right] + \frac{1}{2}\sin\left[(\lambda_n-\lambda_m)h\right] \right] \\
&+ \frac{1}{\lambda_n+\lambda_m}\left[\frac{D^2\lambda_n\lambda_m}{2\kappa^2}\sin\left[(\lambda_n+\lambda_m)h\right] - \frac{D\lambda_n}{2\kappa}\cos\left[(\lambda_n+\lambda_m)h\right] \right. \\
&\left. - \frac{D\lambda_m}{2\kappa}\cos\left[(\lambda_n+\lambda_m)h\right] - \frac{1}{2}\sin\left[(\lambda_n+\lambda_m)h\right] \right] \\
&= \frac{1}{\lambda_n-\lambda_m}\left[\frac{D^2\lambda_n\lambda_m}{2\kappa^2}\left(\sin\lambda_n h\cos\lambda_m h - \cos\lambda_n h\sin\lambda_m h\right) \right. \\
&+ \frac{D\lambda_n}{2\kappa}\left(\cos\lambda_n h\cos\lambda_m h + \sin\lambda_n h\sin\lambda_m h\right) \\
&- \frac{D\lambda_m}{2\kappa}\left(\cos\lambda_n h\cos\lambda_m h + \cos\lambda_n h\cos\lambda_m h\right) \\
&\left. + \frac{1}{2}\left(\sin\lambda_n h\cos\lambda_m h - \cos\lambda_n h\sin\lambda_m h\right) \right] \\
&+ \frac{1}{\lambda_n+\lambda_m}\left[\frac{D^2\lambda_n\lambda_m}{2\kappa^2}\left(\sin\lambda_n h\cos\lambda_m h + \cos\lambda_n h\sin\lambda_m h\right) \right.
\end{aligned}
$$

$$
\begin{aligned}
&- \frac{D\lambda_n}{2\kappa}\left(\cos\lambda_n h\cos\lambda_m h - \sin\lambda_n h\sin\lambda_m h\right)\\
&- \frac{D\lambda_m}{2\kappa}\left(\cos\lambda_n h\cos\lambda_m h - \sin\lambda_n h\sin\lambda_m h\right)\\
&- \frac{1}{2}\left(\sin\lambda_n h\cos\lambda_m h + \cos\lambda_n h\sin\lambda_m h\right)\Bigg]\\
&= \frac{1}{\lambda_n-\lambda_m}\Bigg[\frac{D\lambda_m}{2\kappa}\cos\lambda_m h\left(\frac{D\lambda_n}{\kappa}\sin\lambda_n h - \cos\lambda_n h\right)\\
&- \frac{D\lambda_n}{2\kappa}\cos\lambda_n h\left(\frac{D\lambda_m}{\kappa}\sin\lambda_m h - \cos\lambda_m h\right)\\
&+ \frac{\sin\lambda_m h}{2}\left(\frac{D\lambda_n}{\kappa}\sin\lambda_n h - \cos\lambda_n h\right) - \frac{\sin\lambda_n h}{2}\left(\frac{D\lambda_m}{\kappa}\sin\lambda_m h - \cos\lambda_m h\right)\Bigg]\\
&+ \frac{1}{\lambda_n+\lambda_m}\Bigg[\frac{D\lambda_m}{2\kappa}\cos\lambda_m h\left(\frac{D\lambda_n}{\kappa}\sin\lambda_n h - \cos\lambda_n h\right)\\
&+ \frac{D\lambda_n}{2\kappa}\cos\lambda_n h\left(\frac{D\lambda_m}{\kappa}\sin\lambda_m h - \cos\lambda_m h\right)\\
&+ \frac{\sin\lambda_m h}{2}\left(\frac{D\lambda_n}{\kappa}\sin\lambda_n h - \cos\lambda_n h\right) - \frac{\sin\lambda_n h}{2}\left(\frac{D\lambda_m}{\kappa}\sin\lambda_m h - \cos\lambda_m h\right)\Bigg]\\
&= 0,
\end{aligned}
\tag{4.18}
$$

where we have used (4.13).
If $n = m$ we have

$$
\begin{aligned}
&\int_0^h \mathcal{X}_m^2\,\mathrm{d}x = \int_0^h\left[\frac{D\lambda_m}{\kappa}\cos(\lambda_m x) + \sin(\lambda_m x)\right]^2\mathrm{d}x\\
&= \frac{D^2\lambda_m^2}{\kappa^2}\int_0^h\cos^2(\lambda_m x)\,\mathrm{d}x + \int_0^h\sin^2(\lambda_m x)\,\mathrm{d}x + \frac{2D\lambda_m}{\kappa}\int_0^h\sin(\lambda_m x)\cos(\lambda_m x)\,\mathrm{d}x\\
&= \frac{D^2\lambda_m^2}{2\kappa^2}\int_0^h\left[1+\cos(2\lambda_m x)\right]\mathrm{d}x + \frac{1}{2}\int_0^h\left[1-\cos(2\lambda_m x)\right]\mathrm{d}x + \frac{D\lambda_m}{\kappa}\int_0^h\sin(2\lambda_m x)\,\mathrm{d}x\\
&= \frac{D^2\lambda_m^2}{2\kappa^2}\left[x + \frac{\sin(2\lambda_m x)}{2\lambda_m}\right]_0^h + \frac{1}{2}\left[x - \frac{\sin(2\lambda_m x)}{2\lambda_m}\right]_0^h - \frac{D\lambda_m}{\kappa}\left[\frac{\cos(2\lambda_m x)}{2\lambda_m}\right]_0^h\\
&= \frac{D^2\lambda_m^2}{2\kappa^2}h + \frac{D^2\lambda_m}{4\kappa^2}\sin(2\lambda_m h) + \frac{h}{2} - \frac{\sin(2\lambda_m h)}{4\lambda_m} - \frac{D\cos(2\lambda_m h)}{2\kappa} + \frac{D}{2\kappa}\\
&= \frac{D^2\lambda_m^2}{2\kappa^2}h + \frac{h}{2} + \frac{D}{2\kappa} + \frac{D^2\lambda_m}{2\kappa^2}\sin(\lambda_m h)\cos(\lambda_m h) - \frac{\sin(\lambda_m h)\cos(\lambda_m h)}{2\lambda_m}
\end{aligned}
$$

$$
\begin{aligned}
&- \frac{D}{2\kappa}\left[\cos^2(\lambda_m h) - \sin^2(\lambda_m h)\right] \\
&= \frac{D^2\lambda_m^2}{2\kappa^2}h + \frac{h}{2} + \frac{D}{2\kappa} + \frac{D}{2\kappa}\cos(\lambda_m h)\left[\frac{D\lambda_m}{\kappa}\sin(\lambda_m h) - \cos(\lambda_m h)\right] \\
&+ \frac{\sin(\lambda_m h)}{\lambda_m}\left[\frac{D\lambda_m}{\kappa}\sin(\lambda_m h) - \cos(\lambda_m h)\right] \\
&= \frac{D^2\lambda_m^2}{2\kappa^2}h + \frac{h}{2} + \frac{D}{2\kappa}. \qquad (4.19)
\end{aligned}
$$

From (4.17) , (4.18) and (4.19) we deduce that:

$$
A_m = \frac{1}{h\lambda_m\left[\frac{D^2\lambda_m^2}{2\kappa^2}h + \frac{h}{2} + \frac{D}{2\kappa}\right]}, \quad m \in \mathbb{N} \cup \{0\}
$$

We plot $p(x,t)$ in Figure 4.11 versus numerical simulations (see Appendix E.3).

4.5.1 Survival function

We want to obtain the probability that a particle is still diffusing at time t and as a result we integrate $p\,(x,t)$ over the interval $[0,h]$ with respect to x:

$$
\begin{aligned}
S(t,\kappa) &= \int_0^h p(x,t)\,\mathrm{d}x, \\
&= \sum_{n=0}^{+\infty} A_n \int_0^h \left[\frac{D\lambda_n}{\kappa}\cos(\lambda_n x) + \sin(\lambda_n x)\right]\,\mathrm{d}x\mathrm{e}^{-\lambda_n^2 Dt}. \qquad (4.20)
\end{aligned}
$$

We know from (4.16) that:

$$
\int_0^h X_m(x)\,\mathrm{d}x = \int_0^h \left[\frac{D\lambda_m}{\kappa}\cos(\lambda_m x) + \sin(\lambda_m x)\right]\,\mathrm{d}x = \frac{1}{\lambda_m}.
$$

As a result we have:

$$
S(t,\kappa) = \sum_{n=0}^{+\infty} B_n \mathrm{e}^{-\lambda_n^2 Dt}, \qquad (4.21)
$$

where

$$
B_n = \frac{1}{h\lambda_m^2\left[\frac{D^2\lambda_n^2}{2\kappa^2}h + \frac{h}{2} + \frac{D}{2\kappa}\right]},
$$

and λ_n is the n-th root of:

$$
\frac{D\lambda}{\kappa}\sin(\lambda h) - \cos(\lambda h) = 0.
$$

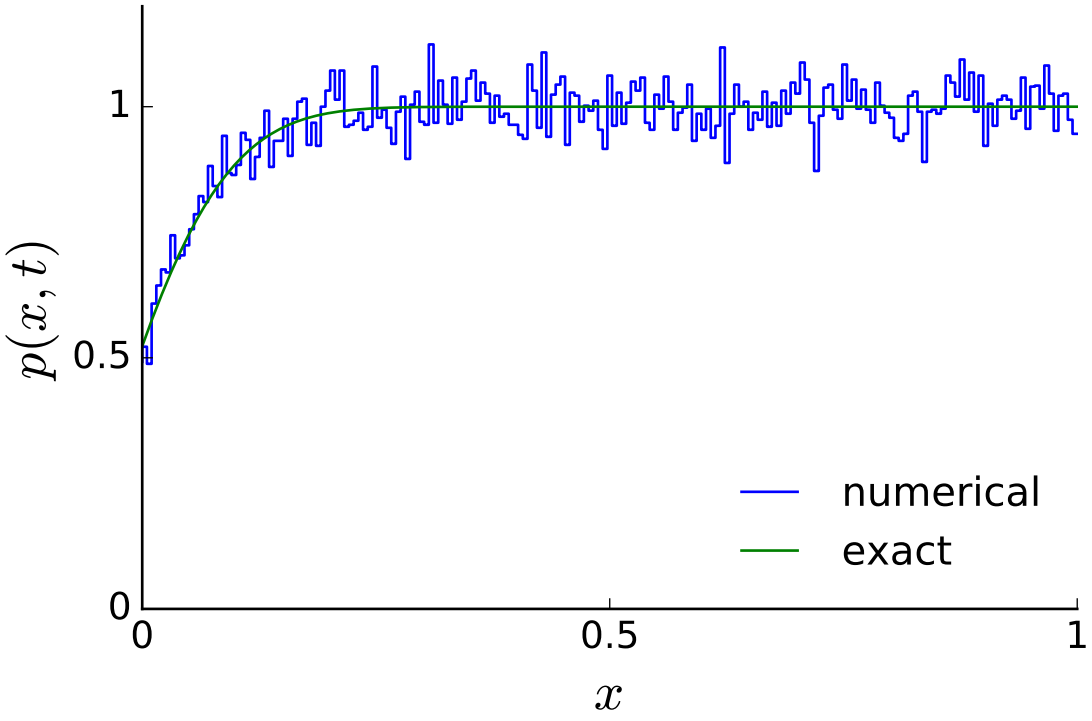

Figure 4.11: Plot of $p(x,t)$ as a function of $x \in [0,h]$. The blue line represents numerical simulations and the green line represents the analytic solution (4.14). Here $p(x,t)$ is the particle density at point $x \in [0,h]$, at time t, gives uniform initial conditions. We observe that at the left boundary, at $x = 0$, the density is not zero, which is given by the fact that the boundary is partially reflecting (see Appendix E.2). Here we have chosen the following parameter values: $h = 1\,\text{cm}, D = 0.5\,\text{cm}^2\,\text{s}^{-1}, \kappa = 1\,\text{cm}\,\text{s}^{-1}, t = 0.01\,\text{s}$.

We plot our result and compare with numerical simulations in Figure 4.12. We observe that, as t increases, the probability that a Brownian particle is "alive" decreases to zero which means that absorption at $x = 0$ is guaranteed.

4.5.2 Mean time to absorption

Given that we know the survival function we can now obtain the mean time for the diffusing particle to be absorbed by the $x = 0$ boundary (Redner, 2001, p.27):

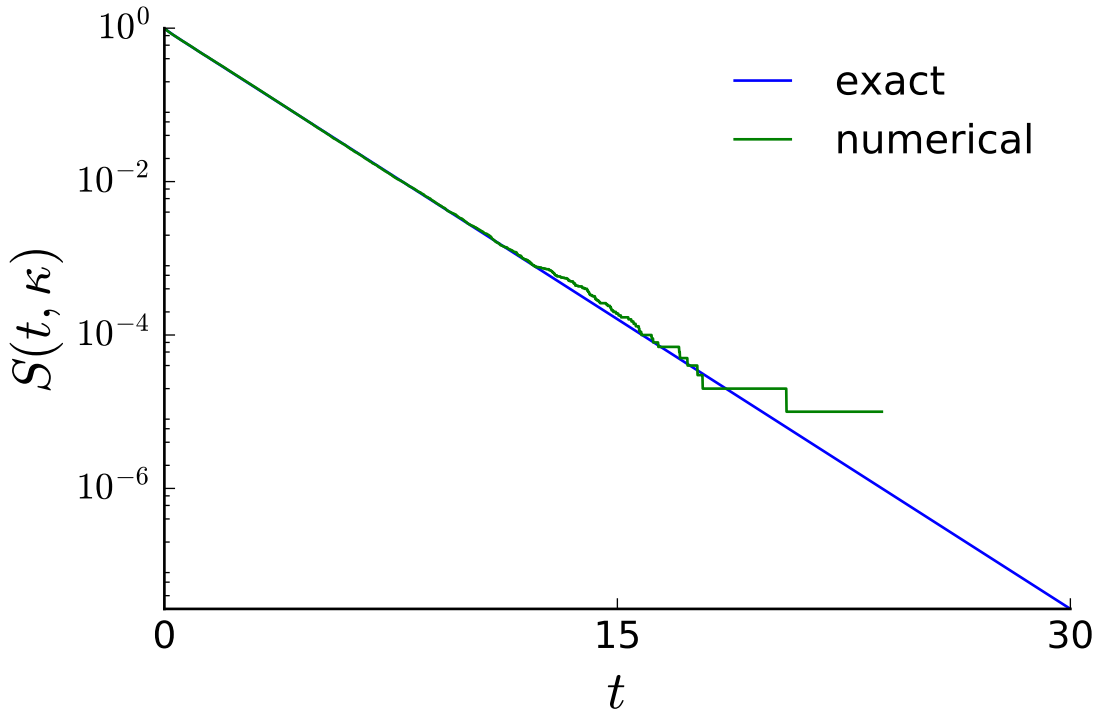

Figure 4.12: Plot of $S(t,\kappa)$ as a function of t. The green line represents numerical simulations and the blue line represents analytic solution (4.21). Here we have chosen the following parameter values: $h = 1\,\text{cm}, D = 0.5\,\text{cm}^2\,\text{s}^{-1}, \kappa = 1\,\text{cm}\,\text{s}^{-1}$.

$$T(\kappa) = -\int_0^{+\infty} t\frac{\partial S}{\partial t}(t,\kappa)\,\mathrm{d}t = \sum_{n=0}^{+\infty} \frac{1}{hD\lambda_n^4\left[\left(\frac{D^2\lambda_n^2}{\kappa^2}+1\right)\frac{h}{2}+\frac{D}{2\kappa}\right]}, \tag{4.22}$$

which we plot in Figure 4.13 and compare with numerical simulations. We observe that as $\kappa \to 0$ the mean time tends to infinity which is expected given that particles cannot be absorbed because the boundary at $x = 0$ becomes reflecting (see Appendix E.2).

4.6 Cylinder diffusion

We are interested in how the position of a particle, starting uniformly in a cylinder of radius b and height h, changes with time due to diffusion. The boundary

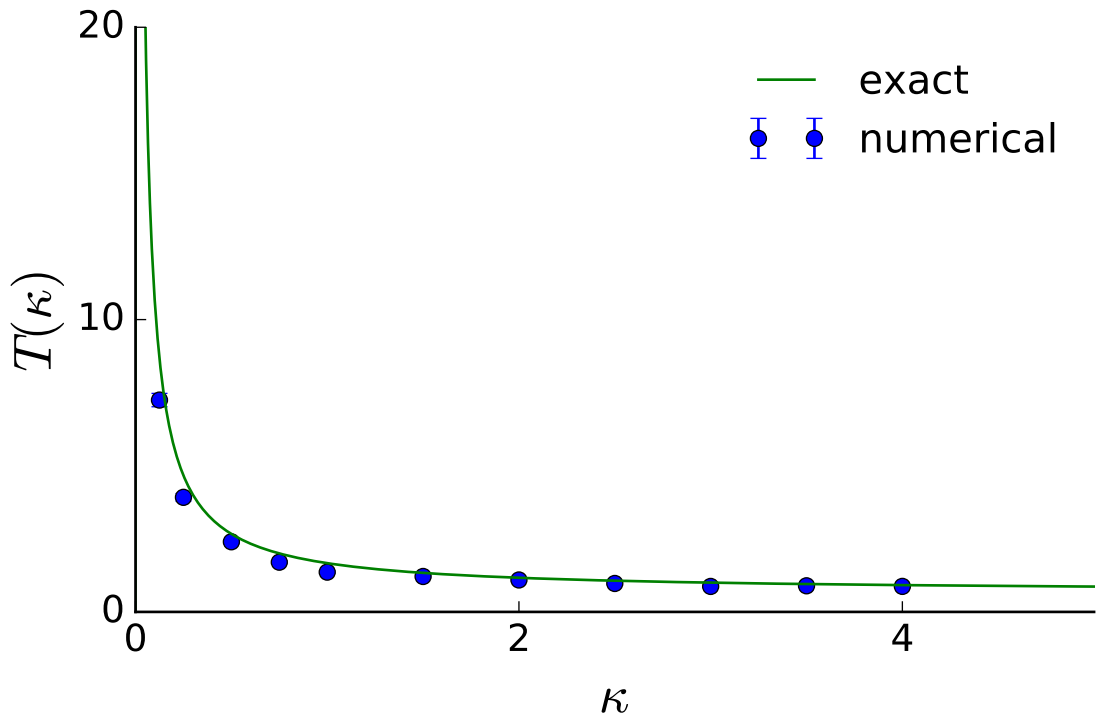

Figure 4.13: Plot of $T(\kappa)$ as a function of κ. The blue dots represent numerical simulations and the green line represents analytic solution (4.22). Here we have chosen the following parameter values: $h = 1\,\mathrm{cm}, D = 0.5\,\mathrm{cm}^2\,\mathrm{s}^{-1}$.

conditions are the following: Neumann boundary conditions at all walls with the exception of the floor which has Robin boundary condition with trapping rate κ. We again define $p(\mathbf{x}, t)$ be the density of particles at position $\mathbf{x}$ at time t given that their initial position is distributed uniformly in the cylinder of radius b and height h. As a result we have:

$$\frac{\partial}{\partial t} p\left(\mathbf{x}, t\right) = D \nabla_{\mathbf{x}}^2 p\left(\mathbf{x}, t\right), \tag{4.23}$$

with boundary and initial conditions, respectively:

$$\left.\frac{\partial p}{\partial r}\right|_{r=b} = 0, \tag{4.24a}$$

$$\left.\frac{\partial p}{\partial z}\right|_{z=h} = 0, \tag{4.24b}$$

$$D\left.\frac{\partial p}{\partial z}\right|_{z=0} = \kappa p(r, z=0, t), \tag{4.24c}$$

$$p(r, z, t=0) = \frac{1}{\pi b^2 h}. \tag{4.24d}$$

We look for a separable solution of the form $p(r,z,t) = \mathcal{Z}(z)\mathcal{T}(t)$ for (4.23) (we ignore the radial component because of radial symmetry) which gives:

$$\mathcal{Z}\frac{\mathrm{d}\mathcal{T}}{\mathrm{d}t} = D\mathcal{T}\frac{\mathrm{d}^2\mathcal{Z}}{\mathrm{d}z^2}.$$

Dividing by $\frac{1}{D\mathcal{Z}\mathcal{T}}$ we observe that the left-hand side is a function of t while the right-hand side is a function of z:

$$\frac{1}{D\mathcal{T}}\frac{\mathrm{d}\mathcal{T}}{\mathrm{d}t} = \frac{1}{\mathcal{Z}}\frac{\mathrm{d}^2\mathcal{Z}}{\mathrm{d}z^2} = -\lambda^2,$$

where λ is a constant. Here, similarly to the one dimensional case, we choose the constant to be $-\lambda^2$ in order to ensure that the time function does not grow exponentially. As a result, $\mathcal{T}(t)$ is:

$$\frac{1}{D\mathcal{T}}\frac{\mathrm{d}\mathcal{T}}{\mathrm{d}t} = -\lambda^2 \Rightarrow \mathcal{T}(t) = A\mathrm{e}^{-\lambda^2 D t},$$

where A is a constant. The z equation is:

$$\frac{\mathrm{d}^2\mathcal{Z}}{\mathrm{d}z^2} + \lambda^2\mathcal{Z} = 0,$$

which has the solution:

$$\mathcal{Z}(z) = C\cos(\lambda z) + E\sin(\lambda z),$$

where C and E are constants.
We deduce from the boundary conditions (4.24b) and (4.24c):

$$\left.\frac{\partial p}{\partial z}\right|_{z=h} = 0 \Rightarrow \left.\frac{\mathrm{d}\mathcal{Z}}{\mathrm{d}z}\right|_{z=h} = 0 \Rightarrow -C\lambda\sin(\lambda z) + E\lambda\cos(\lambda z) = 0,$$

$$D\left.\frac{\partial p}{\partial z}\right|_{z=0} = \kappa p(r, z=0, t) \Rightarrow D\left.\frac{\mathrm{d}\mathcal{Z}}{\mathrm{d}z}\right|_{z=0} = \kappa\mathcal{Z}(0) \Rightarrow D\lambda E = \kappa C \Rightarrow C = \frac{D\lambda E}{\kappa}.$$

As a result, the z equation turns out to be:

$$\mathcal{Z}_n(z) = \frac{D\lambda_n}{\kappa}\cos(\lambda_n z) + \sin(\lambda_n z), \quad n \in \mathbb{N}\cup\{0\},$$

where λ_n is the n-th root of:

$$\frac{D\lambda}{\kappa}\sin(\lambda h) - \cos(\lambda h) = 0.$$

Using the principle of superposition, the solution of the diffusion equation is the linear combination:

$$p(z,t) = \sum_{n=0}^{+\infty} A_n \left[\frac{D\lambda_n}{\kappa}\cos(\lambda_n z) + \sin(\lambda_n z)\right] \mathrm{e}^{-\lambda_n^2 Dt}.$$

Using the initial condition (4.24d) we can obtain the coefficients A_n:

$$\frac{1}{\pi b^2 h} = \sum_{n=0}^{+\infty} A_n \left[\frac{D\lambda_n}{\kappa}\cos(\lambda_n z) + \sin(\lambda_n z)\right].$$

We multiply the above equation by $\mathcal{Z}_m(z)$ and we integrate it from 0 to h with respect to z:

$$\frac{1}{\pi b^2 h}\int_0^h \mathcal{Z}_m(z)\,\mathrm{d}z = \sum_{n=0}^{+\infty}\left(A_n \int_0^h \mathcal{Z}_m(z)\,\mathcal{Z}_n(z)\,\mathrm{d}z\right),$$

and using the orthogonality condition (4.18) we obtain:

$$\frac{1}{\pi b^2 h}\int_0^h \mathcal{Z}_m(z)\,\mathrm{d}z = A_m \int_0^h \mathcal{Z}_m^2(z)\,\mathrm{d}z, \tag{4.25}$$

where

$$\int_0^h \mathcal{Z}_m(z)\,\mathrm{d}z = \frac{1}{\lambda_m}, \tag{4.26}$$

and

$$\int_0^h \mathcal{Z}_m^2(z)\,\mathrm{d}z = \left(\frac{D^2\lambda_m^2}{\kappa^2}+1\right)\frac{h}{2} + \frac{D}{2\kappa}.$$

As a result, we have:

$$A_m = \frac{1}{\pi b^2 h}\frac{1}{\lambda_m\left[\left(\frac{D^2\lambda_m^2}{\kappa^2}+1\right)\frac{h}{2}+\frac{D}{2\kappa}\right]}, \quad m \in \mathbb{N}\cup\{0\}.$$

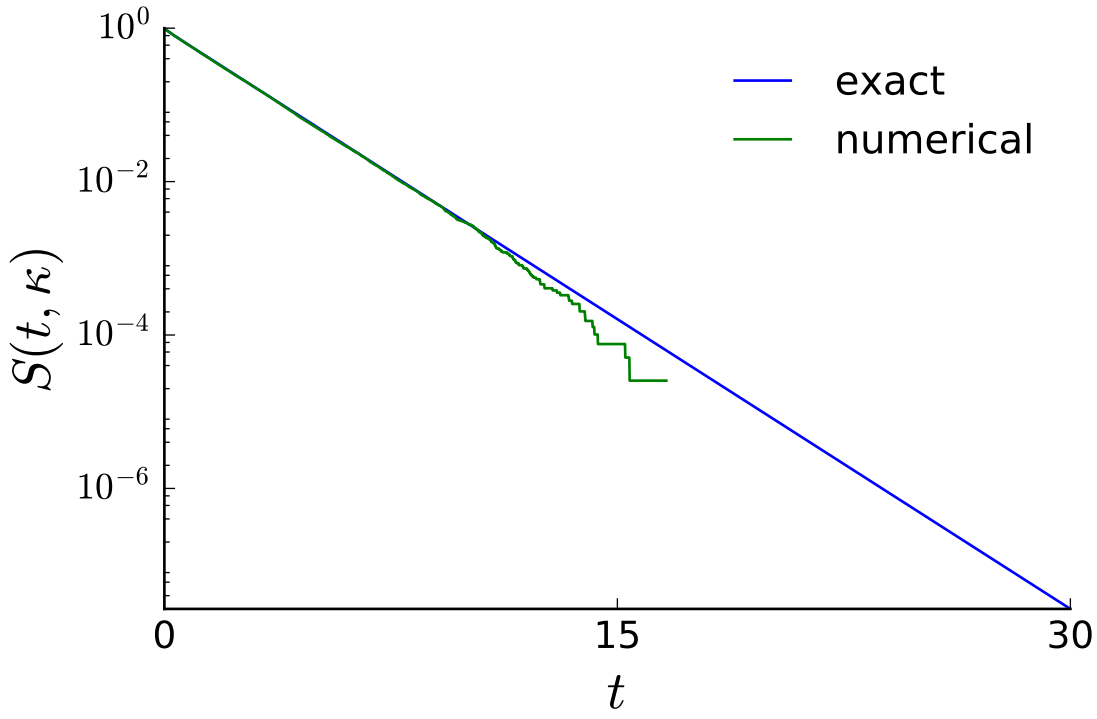

Figure 4.14: Plot of $S(t,\kappa)$ as a function t. The green line represents numerical simulations and the blue line represents analytic solution (4.27). Here we have chosen the following parameter values: $b = 1/\sqrt{\pi}\,\mathrm{cm}, h = 1\,\mathrm{cm}, D = 0.5\,\mathrm{cm}^2\,\mathrm{s}^{-1}, \kappa = 1\,\mathrm{cm}\,\mathrm{s}^{-1}$.

4.6.1 Survival function

We want to obtain the probability that a Brownian particle is still diffusing at time t and as a result we integrate $p(z,t)$ over the cylinder:

$$\begin{aligned} S(t,\kappa) &= \int_0^{2\pi}\int_0^h\int_0^b rp(z,t)\,\mathrm{d}\theta\mathrm{d}z\mathrm{d}r, \\ &= \pi b^2 \sum_{m=0}^{+\infty} A_m \int_0^h \left[\frac{D\lambda_m}{\kappa}\cos(\lambda_m z) + \sin(\lambda_m z)\right] \mathrm{d}z\mathrm{e}^{-\lambda_m^2 Dt}. \end{aligned}$$

We know from (4.26) that:

$$\int_0^h \left[\frac{D\lambda_m}{\kappa}\cos(\lambda_m z) + \sin(\lambda_m z)\right] \mathrm{d}z = \frac{1}{\lambda_m}.$$

As a result

$$S(t,\kappa) = \sum_{n=0}^{+\infty} B_n \mathrm{e}^{-\lambda_n^2 Dt}, \tag{4.27}$$

where

$$B_m = \frac{1}{h\lambda_m^2 \left[\left(\frac{D^2\lambda_m^2}{\kappa^2}+1\right)\frac{h}{2}+\frac{D}{2\kappa}\right]}, \quad m \in \mathbb{N}\cup\{0\},$$

and we plot our result and compare with numerical simulations in Figure 4.14. We observe that, as t increases, the probability that a Brownian particle is "alive" decreases to zero which means that absorption at the bottom of the well $z = 0$ is guaranteed.

4.6.2 Mean time to absorption

Given that we know the survival function we can now obtain the mean time for the diffusing particle to be absorbed by the bottom of the assay well (Redner, 2001, p.27):

$$T(\kappa) = -\int_0^{+\infty} t\frac{\partial S}{\partial t}(t,\kappa)\,\mathrm{d}t = \sum_{n=0}^{+\infty} \frac{1}{hD\lambda_n^4 \left[\left(\frac{D^2\lambda_n^2}{\kappa^2}+1\right)\frac{h}{2}+\frac{D}{2\kappa}\right]}, \tag{4.28}$$

which we plot in Figure 4.15 and compare with numerical simulations. We observe that (4.28) is identical to (4.22) which is due to cylindrical symmetry (only the height h matters when calculating the mean time). Additionally, we notice that as $\kappa \to 0$ the meant time tends to infinity which is expected given that particles cannot be absorbed because the boundary at $x = 0$ becomes reflecting (see Appendix E.2).

4.6.3 Intracellular distribution of *Coxiella burnetii*

Now that we have the survival function we can calculate the intracellular distribution of bacteria phagocytosed by monocytes. Given M balls and N containers then the fraction of containers with r balls is given by Poisson's formula Ellis & Delbrück (1939); Shabram & Aguilar-Cordova (2000)

$$p(r) = \frac{n^r \mathrm{e}^{-n}}{r!}, \quad r \in \mathbb{N}\cup\{0\},$$

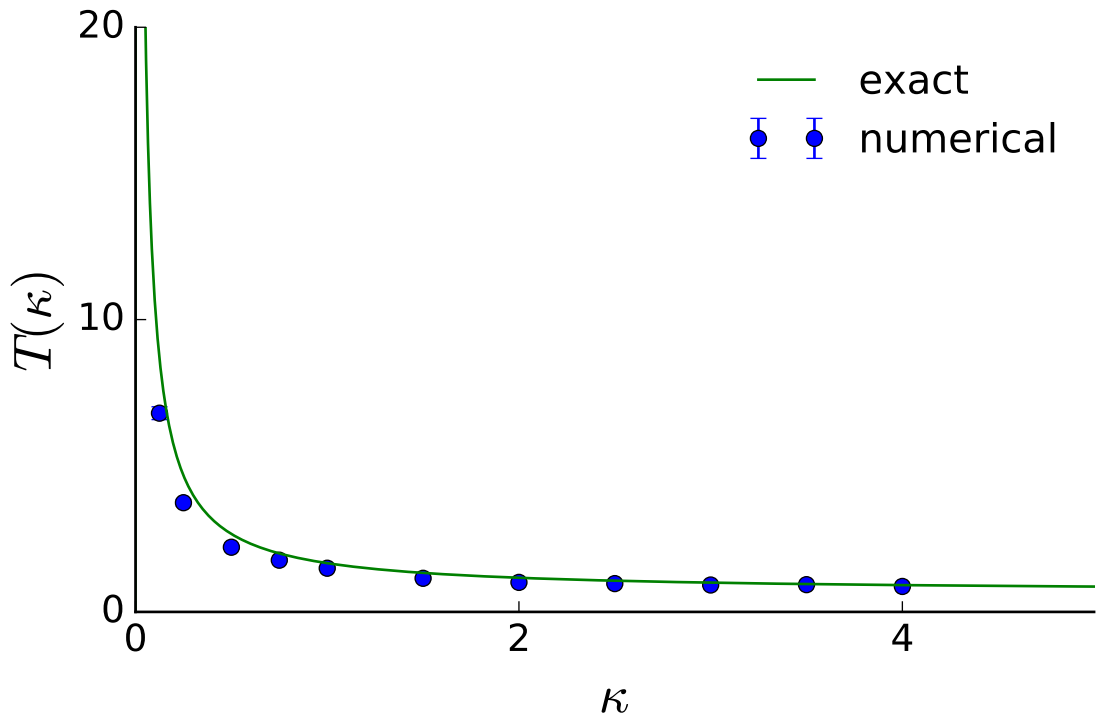

Figure 4.15: Plot of $T(\kappa)$ as a function of κ. The blue dots represent numerical simulations and the green line represents analytic solution (4.28). Here we have chosen the following parameter values: $b = 1/\sqrt{\pi}\,\text{cm}, h = 1\,\text{cm}, D = 0.5\,\text{cm}^2\,\text{s}^{-1}$.

where

$$n = \frac{M}{N},$$

is the average number balls per container. If, as in our case, the balls are the *Coxiella burnetii* bacteria and the containers are the monocytes, then the number bacteria phagocytosed by time t is:

$$M(t, \kappa) = M_0(1 - S(t, \kappa)),$$

and, as a result, we get:

$$n(t, \kappa) = \frac{M(t, \kappa)}{N_0} = \frac{M_0(1 - S(t, \kappa))}{N_0} = MOI[1 - S(t, \kappa)],$$

which is also the mean and variance of the Poisson distribution plotted in Figure 4.17.

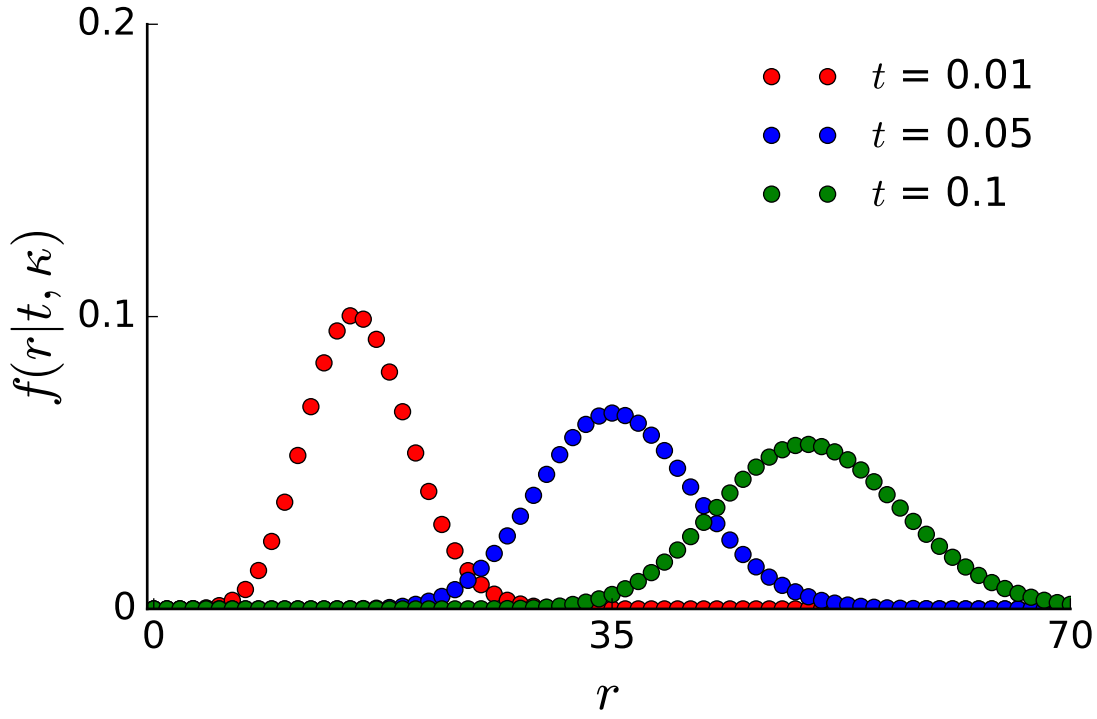

Figure 4.16: Histogram of intracellular loads from (4.29). The red dots represent the intracellular loads for time $t = 0.01$s, the blue dots for time $t = 0.05$s and green dots represent time $t = 0.1$s. Here $M_0 = MOI \times N_0$ is the initial number of *Coxiella burnetii* bacteria distributed in the assay well. This figure was obtained using Python code G.3. Here we have used the following parameters $N_0 = 1.5 \times 10^5, MOI = 200, D = 0.5\,\mathrm{cm}^2\,\mathrm{s}^{-1}, \kappa = 762\,\mathrm{cm}\,\mathrm{s}^{-1}$.

The fraction of monocytes containing r bacteria is:

$$f(r|t,\kappa) = \frac{[MOI(1 - S(t,\kappa))]^r \, \mathrm{e}^{-MOI(1-S(t,\kappa))}}{r!}, \tag{4.29}$$

which we plot for $t = 0.01\,\mathrm{s}, t = 0.05\,\mathrm{s}$ and $t = 0.1\,\mathrm{s}$, respectively, in Figure 4.16. We observe that as time t increases the mean number of particles absorbed increases and the distribution becomes wider given by the fact that as more particles absorbed and previously empty monocytes are subsequently filled with bacteria.

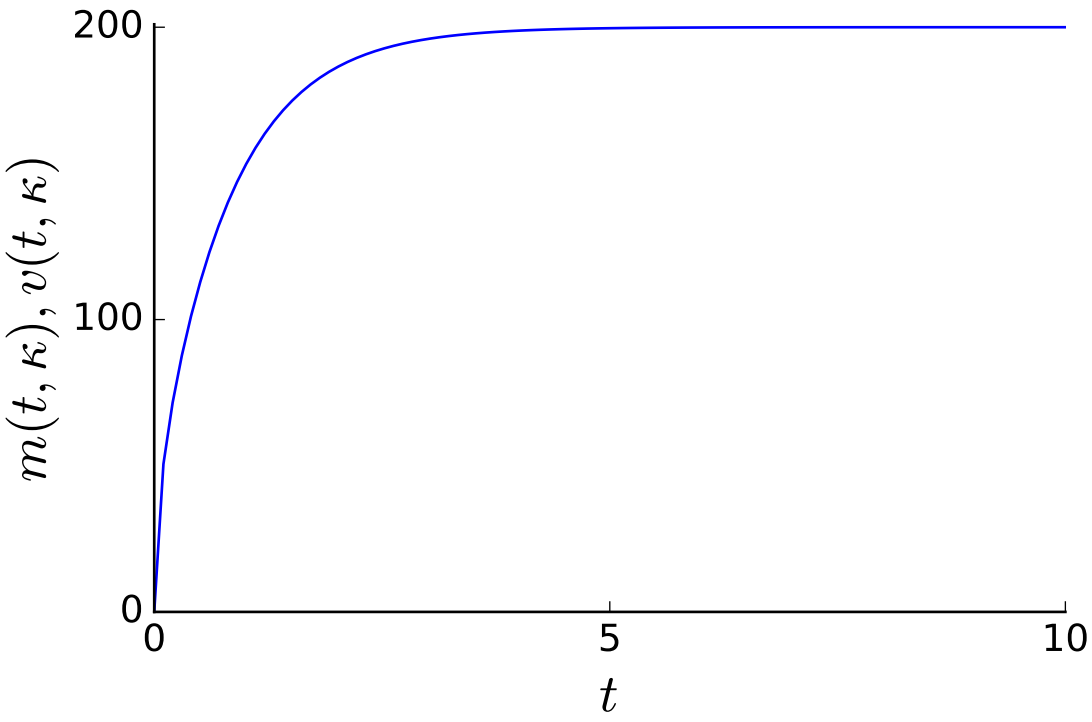

Figure 4.17: Plot of the mean and variance of the intracellular load distribution as a function of time t. For this plot we have selected $MOI = 200, N = 1.5 \times 10^5, D = 0.5\,\mathrm{cm}^2\,\mathrm{s}^{-1}, \kappa = 762\,\mathrm{cm}\,\mathrm{s}^{-1}$.

4.7 Discussion

In this chapter we have studied the problem of boundary homogenisation applied to the case of assays where the bottom of the assay has a monolayer of monocytes distributed on it and *Coxiella burnetii* bacteria are placed uniformly in large number in the medium.

We observe from Figure 4.17 that the mean and variance of the intracellular bacterial load distribution are both increasing functions of time. This means that as time increases the number of intracellular bacteria will increase but the spread around the mean will also increase. This is confirmed in Figure 4.16 where, for smaller times, the distribution is more clustered around the mean when compared to larger times. Additionally, we observe from Figure 4.17 that both the mean

time and the variance converge to their maximum value of 200 for $t \approx 2s$ which is the timescale $\frac{h^2}{D} = 2s$ of diffusion inside a cylinder with an absorbing floor.
From Section 4.4, we observe remarkable agreement between the monocyte coverage obtained by image analysis and the results obtained using Dstl parameters, of the same assay, with both reaching the conclusion that $\sigma = 1/3$.
Mean times to absorption were shown in Figure 4.15 to increase to infinity as the trapping rate κ decreased to zero which is intuitively correct, given that, as $\kappa \to 0$ the boundary becomes reflecting and Brownian particles will not be able to be absorbed.
The distribution of the intracellular bacterial load (4.29) is the main result of this chapter, as it allows an alternative to expensive and time-consuming experiments. Additionally, it offers an alternative to difficult numerical simulations which must analyse interactions between 1.5×10^5 monocytes and 3×10^7 bacteria. In order to increase accuracy, we must implement boundary tests to account for particles whose path crosses the boundary of a monocyte during a timestep but whose endpoints are outside the monocytes Jansons & Lythe (2000, 2005). This requires having a timestep parameter Δt which satisfies $\sqrt{D\Delta t} < \mathbb{E}[r_m]$ where D is the diffusion coefficient and r_m is the radius of a monocyte (see Figure 4.2). Replacing Brownian particle simulations with Monte Carlo method or the finite element method, in order to check the validity of our results, should be the subject of future work Bernoff *et al.* (2018); Eun (2020).
Future work should be on modelling the behaviour of monocytes which we assumed are static but, in reality, they are mobile. Additionally, bacteria replicate inside the monocytes and some escape, back into the assay medium, which alters our results and should be included in a future extension of the model developed here.

Chapter 5

Concluding remarks

In this thesis, mathematical models have been developed for Brownian particles diffusing in three geometries: i) circular eccentric annular region, ii) spherical eccentric annular region and iii) cylindrical region of an assay well. The first two geometries are useful for modelling intracellular transport of particles while the third geometry is useful for modelling an assay involving *Coxiella burnetii*. Numerical simulations are developed to test the accuracy of our models and are shown in Appendix G.

In Chapter 2 we have used bipolar coordinates to derive the exact Green's functions (2.13) and (2.28). They differ from the corresponding Green's functions without intracellular compartment by an amount proportional to a^2. We consider distributions of initial conditions that are (i) uniform on the nuclear surface (ii) uniform on the cell surface, or (iii) given by the hitting density of particles diffusing from the nuclear surface to the cellular surface. This hitting density is also obtained from the appropriate Green's function. The exact expressions for the hitting densities and mean arrival times are (2.33), (2.45) and (2.46). When averaged over the initial surface, the mean arrival times, (2.52) and (2.53), are functions of a and c. The idea is that the point on the surface of a nucleus where a molecule emerges, or the point on the cell surface where a molecular complex is internalised, is uniformly distributed. We further average over all possible locations of the nucleus within the cell, obtaining (2.62) and (2.63), functions of a only. We also solve Poisson's equation explicitly in bipolar coordinates, using the particular solution (2.48). Using the Green's functions $G_1^{(2)}(\mathbf{x}_0, \mathbf{x})$ and

$G_2^{(3)}(\mathbf{x}_0, \mathbf{x})$ together with the solutions of Poisson's equation $T_3(\mathbf{x}_0)$ and $T_4(\mathbf{x}_0)$ we obtain the higher order moments (2.67) and (2.68), and the average higher order moments (2.70) and (2.71).

In Chapter 3 we extend the results from Chapter 2 to three dimensions in order to obtain the Green's function with uniform initial condition over the surface of the nucleus and the cell $\bar{G}_1^{(3)}(\mathbf{x}_0, \mathbf{x})$ and $\bar{G}_2^{(3)}(\mathbf{x}_0, \mathbf{x})$, respectively. As a result, we make use of Perron's theorem and continued fraction expansion. From the Green's function we calculate the first passage properties of diffusion from the nuclear surface to the cellular surface: hitting density (3.53) and average mean time (3.54). Analogously, we derive from $\bar{G}_2^{(3)}(\mathbf{x}_0, \mathbf{x})$ the first passage properties of diffusion from the nuclear surface to the cellular surface: average mean time (3.55). We notice from Figure 3.13, when comparing the average mean time of diffusion from the nuclear surface to the cellular surface, that unlike our approximation (3.39), our analytic formula does not decrease in accuracy as the displacement of the nucleus c increases. To our knowledge, the analytic formula for $\bar{G}_1^{(3)}(\mathbf{x}_0, \mathbf{x})$, and all the derived quantities, is unique to the literature. We derived a semi-analytic formula for the mean round trip time $\bar{T}_2^{3,\varepsilon}(c)$ from the approximation derived by Condamin *et al.* (2007) for $T_2^{(3)}(\theta_2, a, c)$ and our analytic formula (3.53) for $\varepsilon^{(3)}(\theta_2)$. We notice from Figure 3.16 that $\bar{T}_2^{3,\varepsilon}(a, c)$ is a decreasing function of c as opposed to $\bar{T}_2^{(3)}(a, c)$ which is an increasing function of c. This is because the Brownian particles diffusing from the nucleus are more likely to arrive at the point of the cellular surface which is closest to the nucleus, and, as a result, the mean time for the particle to arrive back to the nucleus is smaller then the case when its starting position is uniformly distributed on the cellular surface.

A limitation with both our two dimensional and three dimensional results is that we have assumed a uniform interior environment which gives a constant diffusion coefficient. One solution would be to include more excluded region that are present inside a cell besides the nucleus such as the Golgi apparatus, but this would make deriving an analytic solution significantly more difficult. Alternatively we could apply homogenisation theory to the interior environment to result in a uniform diffusion coefficient.

Additionally, we have assumed when calculating the mean round-trip time that the Brownian particles do not spend time on the surface of the cell. However this is not biologically realistic given that molecules diffuse on the cellular surface and, as result, future work should be on modelling cellular surface behaviour Habib *et al.* (2001); Lythe (2006).

In Chapter 4 we have studied the problem of boundary homogenisation applied to the case of assay where the bottom of the assay well has a monolayer of monocytes distributed on it and *Coxiella burnetii* bacteria are placed uniformly in large number in the medium. We have studied the problem of diffusing particles in and otherwise reflecting cylinder with a number of circular traps on the bottom surface. Using boundary homogenisation we have been able to replace the bottom surface of the cylinder with a reactive boundary having a Robin boundary condition. This allowed us to solve the diffusion equation for the assay domain and obtain the survival function of a particle starting uniformly in the cylinder. From the survival function we are able to derive the mean time for the Brownian particle to reach the reactive surface. Assuming that the distribution of *Coxiella burnetii* absorbed by the monocytes follow a Poisson distribution, we deduce the the intracellular distribution of *Coxiella burnetii* as a function of time and of the trapping rate κ. This result represents the most import derivation of Chapter 4 and it offers an alternative to difficult numerical simulations which, in order simulate the assay, must analyse interactions between 1.5×10^5 monocytes and 3×10^7 bacteria. Accuracy can be increased by reducing the simulation time step or implementing a boundary tests to account for particles whose path crosses the boundary of a monocyte during a timestep but whose endpoints are outside the monocytes.

Currently, our model does not account for the behaviour of monocytes which we assumed are static but, in reality, they are mobile. Additionally, bacteria replicate inside the monocytes and some escape, back into the assay medium, which alters our results and should be included in a future extension of the model developed here.

A limitation to the model we have constructed for simulation *Coxiella burnetii* assay is the unavailability of estimates for the diffusion coefficient D without which the determination of the intracellular distribution cannot be undertaken.

Future work should be concentrated on the determining D by either determining the value experimentally or by determining it from the constituent parts of the composite medium of 90% Leibovitz's L-15 Medium and 10% foetal calf serum. For this thesis we have used Brownian simulations in Appendix G, with exponential timestepping and the boundary tests developed by Jansons & Lythe (2000, 2005) for absorbing boundaries, to verify our results. However, reflecting boundaries are approximated by flat boundaries and, as a result, future work should focus on developing a reflecting boundary algorithm. Additionally, boundary element method could extend the analysis of this analytical study to deal with non-circular irregular shapes of solution domains, as well as any type of inhomogeneous or even nonlinear boundary conditions.

Appendix A

Integration

This appendix is dedicated to the properties of various integrals.

A.1 Integration of $H_2^{(2)}$ over disk

In the following we will prove the following relation:

$$\int_{C^*} H_2^{(2)}(\mathbf{v},\mathbf{z})\,\mathrm{d}\mathbf{z} = \frac{3}{8D} \quad \forall \mathbf{v} \in C^*,$$

where C^* is a circle of radius 1.
We begin by noting that:

$$\begin{aligned}\int_{C^*} H_2^{(2)}(\mathbf{v},\mathbf{z})\,\mathrm{d}\mathbf{z} &= \frac{1}{2\pi D}\int_{C^*}\left(\ln\frac{1}{v}+\ln\frac{1}{R\tilde{R}}+\frac{z^2+v^2}{2}\right)\mathrm{d}\mathbf{z}\\ &= \frac{1}{2\pi D}\int_{C^*}\left(\log\frac{1}{|\mathbf{z}-\mathbf{v}|}+\log\frac{1}{|\mathbf{z}-\tilde{\mathbf{v}}|}+\log\frac{1}{v}+\frac{z^2+v^2}{2}\right)\mathrm{d}\mathbf{z},\end{aligned} \tag{A.1}$$

where $0 \le |\mathbf{v}| = v \le 1-a$.
We use the following identities from (Barton, 1989, p.413–414):

$$\log\frac{1}{|\mathbf{z}-\mathbf{v}|} = \log\frac{1}{r_>} + \sum_{m=1}^{\infty}\frac{\cos(m\theta)}{m}\left(\frac{r_<}{r_>}\right)^m,$$

and

$$\log\frac{1}{|\mathbf{z}-\tilde{\mathbf{v}}|} = \log v + \sum_{m=1}^{\infty}\frac{\cos(m\theta)}{m}\left(\frac{r_<}{r_>}\right)^m,$$

where $r_<(r_>) = \min(\max)(z, v)$ to obtain the first two terms in the left-hand side of (A.1):

$$\begin{aligned}
\int_C \log\frac{1}{|\mathbf{z}-\mathbf{v}|}\mathrm{d}\mathbf{z} &= \int_0^1\int_0^{2\pi} r\log\frac{b}{R}\,\mathrm{d}r\mathrm{d}\theta \\
&= \int_0^1\int_0^{2\pi} r\left[\log\frac{1}{r_>} + \sum_{m=1}^{\infty}\frac{\cos(m\theta)}{m}\left(\frac{r_<}{r_>}\right)^m\right]\mathrm{d}\theta\mathrm{d}r \\
&= \int_0^{2\pi}\int_0^{r'} r\left[\log\frac{1}{v} + \sum_{m=1}^{\infty}\frac{\cos(m\theta)}{m}\left(\frac{r}{v}\right)^m\right]\mathrm{d}r\mathrm{d}\theta \\
&+ \int_0^{2\pi}\int_{r'}^1 r\left[\log\frac{1}{r} + \sum_{m=1}^{\infty}\frac{\cos(m\theta)}{m}\left(\frac{v}{r}\right)^m\right]\mathrm{d}r\mathrm{d}\theta \\
&= \int_0^{2\pi}\left[\sum_{m=1}^{\infty}(m+2)\frac{\cos(m\theta)}{m}\frac{r^{m+2}}{(v)^m} + \frac{1-(v)^2}{4}\right. \\
&\left. + \sum_{m=1}^{\infty}(2-m)\frac{\cos(m\theta)}{m}\frac{(v)^m}{r^{m-2}}\right]\mathrm{d}\theta \\
&= \int_0^{2\pi}\left[\frac{1-v^2}{4} + \sum_{m=1}^{\infty}\frac{\cos(m\theta)}{m}\left[(m+2)\frac{r^{m+2}}{(v)^m} - (m-2)\frac{(v)^m}{r^{m-2}}\right]\right]\mathrm{d}\theta \\
&= \pi\frac{1-v^2}{2},
\end{aligned} \tag{A.2}$$

and

$$\begin{aligned}
\int_C \log\frac{1}{|\mathbf{z}-\tilde{\mathbf{v}}|}\,\mathrm{d}\mathbf{z} &= \int_0\int_0^{2\pi} r\log\frac{1}{\tilde{R}}\,\mathrm{d}\theta\mathrm{d}r \\
&= \int_0^1\int_0^{2\pi} r\left[\log v + \sum_{m=1}^{\infty}\frac{\cos(m\theta)}{m}\left(\frac{r_<}{r_>}\right)^m\right]\mathrm{d}\theta\mathrm{d}r \\
&= \int_0^1\int_0^{2\pi} r\left[\log v + \sum_{m=1}^{\infty}\frac{\cos(m\theta)}{m}v^m r^{m+1}\right]\mathrm{d}\theta\mathrm{d}r \\
&= \int_0^{2\pi}\left[\frac{1}{2}\log v + \sum_{m=1}^{\infty}\frac{m+2}{m}\cos(m\theta)v^m\right]\mathrm{d}\theta \\
&= \pi\log v.
\end{aligned} \tag{A.3}$$

The last two terms of (A.1) are straightfoward to calculate:

$$\int_C \log\left(\frac{1}{v}\right)\mathrm{d}\mathbf{z} = \int_0^1\int_0^{2\pi} r\log\frac{1}{v}\,\mathrm{d}\theta\mathrm{d}r = \pi\log\frac{1}{v}, \tag{A.4}$$

and

$$\int_C \frac{z^2+v^2}{2}\mathrm{d}\mathbf{z} = \int_0^1 \int_0^{2\pi} r\frac{r^2+v^2}{2}\,\mathrm{d}\theta\mathrm{d}r = \pi\left(\frac{1}{4}+\frac{v^2}{2}\right). \tag{A.5}$$

Using (A.2), (A.3), (A.4) and (A.5) we obtain:

$$\int_{C^*} H_2^{(2)}(\mathbf{v},\mathbf{z})\,\mathrm{d}\mathbf{z} = \frac{3}{8D} \quad \forall \mathbf{v}\in C^*.$$

A.2 Integration of $H_2^{(3)}$ over disk

In the following we will prove the following relation:

$$\int_{C^*} H_2^{(3)}(\mathbf{v},\mathbf{z})\,\mathrm{d}\mathbf{z} = \frac{56}{60D} - \frac{1}{3D}\log 2, \quad \forall \mathbf{v}\in C^*. \tag{A.6}$$

We begin by noting that:

$$\begin{aligned}
&\int_{C^*} H^{(3)}(\mathbf{v},\mathbf{z})\,\mathrm{d}\mathbf{z} \\
&= \frac{1}{4\pi D}\int_{C^*}\left(\frac{1}{R}+\frac{1}{v\tilde{R}}-\log\left(v\tilde{R}+1-zv\mu\right)+\frac{z^2+v^2}{2}\right)\mathrm{d}\mathbf{z} \\
&= \frac{1}{4\pi D}\int_{C^*}\left(\frac{1}{|\mathbf{z}-\mathbf{v}|}+\frac{1}{y|\mathbf{z}-\tilde{\mathbf{v}}|}-\log\left(v\tilde{R}+1-zv\mu\right)+\frac{z^2+v^2}{2}\right)\mathrm{d}\mathbf{z},
\end{aligned} \tag{A.7}$$

where $0\le|\mathbf{v}|=v\le 1-a$, $\mu=\cos\theta$ and θ is the angle between $\mathbf{z}$ and $\mathbf{v}$.
We use the following identities from (Barton, 1989, p.417–418):

$$\frac{1}{|\mathbf{z}-\mathbf{v}|} = \sum_{m=0}^{\infty} P_m(\mu)\frac{r_<^m}{r_>^{m+1}},$$

and

$$\frac{1}{|\mathbf{z}-\tilde{\mathbf{v}}|} = v\sum_{m=0}^{\infty} P_m(\mu)\,(zv)^m,$$

where $r_<(r_>) = \min(\max)(z,v)$ to obtain the first two terms in the left-hand side of (A.7):

$$\int_{C^*}\frac{1}{|\mathbf{z}-\mathbf{v}|}\mathrm{d}\mathbf{z} = \int_0^1\int_0^{2\pi}\int_0^{\pi} r^2\sin\theta\sum_{m=0}^{\infty}P_m(\cos\theta)\frac{r_<^m}{r_>^{m+1}}\,\mathrm{d}\theta\mathrm{d}\phi\mathrm{d}r$$

$$
\begin{aligned}
&= 2\pi \sum_{m=0}^{\infty} \int_0^1 \int_0^{\pi} P_m(\cos\theta) \sin\theta \frac{r^2 r_<^m}{r_>^{m+1}} \,\mathrm{d}\theta \mathrm{d}r \\
&= 4\pi \int_0^v r^2 \frac{1}{v} \,\mathrm{d}r + 4\pi \int_v^1 r^2 \frac{1}{r} \,\mathrm{d}r \\
&= 2\pi \left(1 - \frac{v^2}{3}\right), \qquad \text{(A.8)}
\end{aligned}
$$

and

$$
\begin{aligned}
\int_{C^*} \frac{1}{v|\mathbf{z} - \tilde{\mathbf{v}}|} \mathrm{d}\mathbf{z} &= \int_0^1 \int_0^{2\pi} \int_0^{\pi} r^2 \sin\theta v \sum_{m=0}^{\infty} P_m(\cos\theta) \left(rv\right)^m \, d\theta \mathrm{d}\phi \mathrm{d}r \\
&= 2\pi \sum_{m=0}^{\infty} \int_0^1 \int_0^{\pi} P_m(\cos\theta) \sin\theta r^{m+2} v^m \,\mathrm{d}\theta \mathrm{d}r \\
&= 4\pi \int_0^1 r^2 \,\mathrm{d}\theta \mathrm{d}r \\
&= \frac{4\pi}{3}. \qquad \text{(A.9)}
\end{aligned}
$$

In order to calculate the third term of (A.7) we make use of (Barton, 1989, p.425):

$$
\log\left(\frac{2}{v\tilde{R} + 1 - zv\mu}\right) = \sum_{m=1}^{\infty} \frac{P_m(\mu)}{m} \left(zv\right)^m, \qquad \text{(A.10)}
$$

and this gives us:

$$
\begin{aligned}
&\int_{C^*} \log\left(v\tilde{R} + 1 - zv\mu\right) \,\mathrm{d}\mathbf{z} \\
&= -\int_{C^*} \left(\log\left(\frac{2}{v\tilde{R} + 1 - zv\mu}\right) - \log 2\right) \,\mathrm{d}\mathbf{z} \\
&= -\int_0^1 \int_0^{2\pi} \int_0^{\pi} r^2 \sin\theta \left(\sum_{m=1}^{\infty} \frac{P_m(\cos\theta)}{m} \left(zv\right)^m - \log 2\right) \,\mathrm{d}\theta \mathrm{d}\phi \mathrm{d}r \\
&= \log 2 \int_0^1 \int_0^{2\pi} \int_0^{\pi} r^2 \sin\theta \,\mathrm{d}\theta \mathrm{d}\phi \mathrm{d}r \\
&= \frac{4\pi}{3} \log 2. \qquad \text{(A.11)}
\end{aligned}
$$

The last term of (A.7) is straightforward to calculate:

$$
\int_{C^*} \frac{z^2 + v^2}{2} \mathrm{d}\mathbf{z} = \int_0^1 \int_0^{2\pi} \int_0^{\pi} r^2 \frac{r^2 + v^2}{2} \sin\theta \,\mathrm{d}\theta \mathrm{d}\phi \mathrm{d}r = 2\pi \left(\frac{1}{5} + \frac{v^2}{3}\right). \qquad \text{(A.12)}
$$

Using (A.8), (A.9), (A.11) and (A.12) we obtain:

$$\int_{C^*} H_2^{(3)}(\mathbf{v},\mathbf{z})\,\mathrm{d}\mathbf{z} = \frac{56}{60D} - \frac{1}{3D}\log 2, \quad \forall \mathbf{v} \in C^*. \tag{A.13}$$

A.3 Commentary on Pinsky (2003)

Let $D \subseteq \mathbb{R}^d$, where $d \geq 2$, be a domain. If $D \neq \mathbb{R}^d$, assuming that D has a smooth boundary, we let $v : \partial D \to S^d$ be smooth and satisfy $v(x) \cdot n(x) > 0$ for all $x \in \partial D$, where $n(x)$ denotes the inward unit normal to D at $x \in \partial D$. We call v a reflection vector. Let $X(t)$ be the diffusion process in D with $v-$reflection and ∂D (if $D \neq \mathbb{R}^d$).
For a positive definite $d \times d$ matrix Γ, we define the norm:

$$||v||_\Gamma = \left(v, \frac{\Gamma}{Det^{\frac{1}{d}}(\Gamma)}\right)^{\frac{1}{2}}.$$

We observe that this norm preserves the Euclidean norm but distorts directions. For $x \in D$ and $r > 0$, we define $B_r^\Gamma(x) = \{y \in \mathbb{R}^d : ||y - x||_\Gamma < r\}$ as the open ball of radius r in the $\Gamma-$norm and centered at x. Furthermore, we denote $\tau_{B_r^\Gamma(x)} = \inf\{t \geq 0 : X(t) \in \bar{B}_r^\Gamma(x)\}$. In the case of the standard Euclidean norm, when Γ is a scalar multiple of I, we will use the notation $|v|$ and $B_r(x)$ in place of $||v||_I$ and $B_r^I(x)$. Let ω_d denote the volume of the unit ball in $\mathbb{R}^d$.
Condamin *et al.* (2007) make reference to Pinsky (2003) for deriving the mean first passage time (MFPT) for a domain with a small sphere inside the domain. This a reference to Theorem 2 on page 180 of Pinsky (2003):

Theorem. *Let $X(t)$ by $v-$reflected Brownian motion in a domain $D \subset \mathbb{R}^d$. Assume that the process is positive recurrent and let μ denote the invariant probability density. Let $x \in D$ be such that $\bar{B}_l(x) \subset D$. For each $R \in (0, l)$, there exists $z_{l;R} \in \partial B_l(x)$ such that*

1. *if $d = 2$, then*

$$E_{z_{l;R}}\tau_{B_R(x)} = \frac{1}{\mu(B_R(x))}R^2 \log\frac{1}{R} - \frac{1}{2}\left(l^2 - R^2\right);$$

2. if $d \geq 3$, then

$$E_{z_{l;R}}\tau_{B_R(x)} = \frac{2R^d}{d(d-2)\mu(B_R(x))}\left(R^{2-d} - l^{2-d}\right) - \frac{1}{d}\left(l^2 - R^2\right).$$

Remark. *Consider Theorem when the reflection vector is normal, in which case we assume that $Vol(D) < \infty$ and we have $\mu(B_R(x)) = \frac{\omega_d R^d}{Vol(D)}$. Then the theorem indicates that for $x \in D$ and for $0 < R < l$ such that $\bar{B}_l(x) \subset D$, one can find a point $z_{l;R}$ such that $E_{z_{l;R}}\tau_{B_R(x)}$ is equal to the common value that one obtains for the expected value of $\tau_{B_R(x)}$ starting from any point on $\partial B_l(x)$ in the case that the domain is a ball of the same volume centered at x.*

These results tell us that if all the conditions mentioned in the theorem are satisfied then for the domain D there exists circle/sphere of radius l (where $R < l$) then there exists a point on the surface of the circle/sphere such that the mean time to reach the ball of radius R is given by a explicit formula. Then the theorem indicates that for $x \in D$ and for $0 < R < l$ such that $\bar{B}_l(x) \subset D$, one can find a point $z_{l;R}$ such that $E_{z_{l;R}}\tau_{B_R(x)}$ is equal to the common value that one obtains for the expected value of $\tau_{B_R(x)}$ starting from any point on $\partial B_l(x)$ in the case that the domain is a ball of the same volume centered at x. This result does not depend on the starting site as (Condamin *et al.*, 2007, 021111-1) mentioned themselves.

Appendix B

Bipolar coordinates

B.1 Normal derivative in bipolar coordinates

We are interested in the normal derivative of a function $f(\tau, \sigma)$ evaluated on a circle ∂C of constant $\tau = \tau_*$ and for that purpose we will investigate the following hypothesis:

$$\mathbf{n} = \left(\frac{1 - \cosh\tau_* \cos\sigma}{\cosh\tau_* - \cos\sigma}, -\frac{\sinh\tau_* \sin\sigma}{\cosh\tau_* - \cos\sigma} \right),$$

where $\mathbf{n}$ is the normal vector to the $\tau = \tau_*$ surface. Let $\mathbf{v}$ be a point:

$$\mathbf{v} = (x, y) = \left(d\frac{\sinh\tau}{\cosh\tau - \cos\sigma}, d\frac{\sin\sigma}{\cosh\tau - \cos\sigma} \right),$$

whose derivative evaluated on ∂C is:

$$\left.\frac{\partial \mathbf{v}}{\partial \tau}\right|_{\tau=\tau_*} = \left(d\frac{1 - \cosh\tau_* \cos\sigma}{(\cosh\tau_* - \cos\sigma)^2}, -d\frac{\sinh\tau_* \sin\sigma}{(\cosh\tau_* - \cos\sigma)^2} \right),$$

and

$$\left| \left.\frac{\partial \mathbf{v}}{\partial \tau}\right|_{\tau=\tau_*} \right|^2 = \frac{d^2}{(\cosh\tau_* - \cos\sigma)^2}.$$

As a result we obtain the unit vector:

$$\mathbf{e}_\tau = \frac{\left.\frac{\partial \mathbf{v}}{\partial \tau}\right|_{\tau=\tau_*}}{\left| \left.\frac{\partial \mathbf{v}}{\partial \tau}\right|_{\tau=\tau_*} \right|} = \left(\frac{1 - \cosh\tau_* \cos\sigma}{\cosh\tau_* - \cos\sigma}, -\frac{\sinh\tau_* \sin\sigma}{\cosh\tau_* - \cos\sigma} \right).$$

The vector $\mathbf{v} = (x, y) \in \partial C$ also satisfies:

$$y^2 + (x - d\coth\tau_*)^2 = \frac{d^2}{\sinh^2\tau_*}.$$

Changing the system of coordinates such that the origin is the centre of the circle $\tau = \tau_*$. Let θ be the angular coordinate of a point of the circle and as a result:

$$\tan\theta = \frac{y}{x - d\coth\tau_*} = \frac{d\frac{\sin\sigma}{\cosh\tau_* - \cos\sigma}}{d\frac{\sinh\tau_*}{\cosh\tau_* - \cos\sigma} - d\coth\tau_*} = -\frac{\sin\sigma\sinh\tau_*}{1 - \cos\sigma\cosh\tau_*}.$$

Using standard trigonometric identifies we express $\cos\theta$ and $\sin\theta$ in terms of $\tan\theta$:

$$\cos\theta = \frac{1}{\sqrt{1+\tan^2\theta}} = -\frac{1 - \cos\sigma\cosh\tau_*}{\cosh\tau_* - \cos\sigma},$$
$$\sin\theta = \frac{\tan\theta}{\sqrt{1+\tan^2\theta}} = \frac{\sinh\tau_*\sin\sigma}{\cosh\tau_* - \cos\sigma}.$$

This gives us the vector normal to the surface of the circle:

$$\mathbf{e}_\theta = (\cos\theta, \sin\theta) = -\left(\frac{1 - \cosh\tau_*\cos\sigma}{\cosh\tau_* - \cos\sigma}, -\frac{\sinh\tau_*\sin\sigma}{\cosh\tau_* - \cos\sigma}\right) = -\mathbf{e}_\tau.$$

As a result we have the following identity for the normal derivative on a circle of constant $\tau = \tau_*$

$$\left.\frac{\partial f}{\partial \mathbf{n}}\right|_{\mathbf{x}\in\partial C} = \nabla f\cdot\mathbf{e}_\tau|_{\mathbf{x}\in\partial C} = -\frac{\cosh\tau_* - \cos\sigma}{d}\left.\frac{\partial f}{\partial\tau}\right|_{\tau=\tau_*}.$$

B.2 Convolution of Fourier Series

Suppose we have two Fourier series:

$$f(\sigma) = \frac{A_0}{2} + \sum_{n=1}^{\infty}\left(A_n\cos n\sigma + A'_n\sin n\sigma\right),$$

and

$$g(\sigma) = \frac{B_0}{2} + \sum_{n=1}^{\infty}\left(B_n\cos n\sigma + B'_n\sin n\sigma\right),$$

for which we want to write their product as a Fourier series:

$$h(\sigma) = f(\sigma)g(\sigma) = \frac{C_0}{2} + \sum_{n=1}^{\infty}\left(C_n\cos n\sigma + C'_n\sin n\sigma\right).$$

The product of the two Fourier series can be written as:

$$\begin{aligned}&\left[\frac{A_0}{2}+\sum_{n=1}^{\infty}\left(A_n\cos n\sigma+A'_n\sin n\sigma\right)\right]\\&\times\left[\frac{B_0}{2}+\sum_{n=1}^{\infty}\left(B_n\cos n\sigma+B'_n\sin n\sigma\right)\right]\\&=\left(\sum_{n=-\infty}^{\infty}a_n\mathrm{e}^{in\sigma}\right)\left(\sum_{n=-\infty}^{\infty}b_n\mathrm{e}^{in\sigma}\right),\end{aligned}$$

where

$$\begin{aligned}a_0 = A_0/2, \quad a_n = \frac{A_n - iA'_n}{2}, \quad a_{-n} = \frac{A_n + iA'_n}{2},\\ b_0 = B_0/2, \quad b_n = \frac{B_n - iB'_n}{2}, \quad b_{-n} = \frac{B_n + iB'_n}{2},\end{aligned}$$

Rearranging the product we obtain:

$$\left(\sum_{n=-\infty}^{\infty}a_n\mathrm{e}^{in\sigma}\right)\left(\sum_{n=-\infty}^{\infty}b_n\mathrm{e}^{in\sigma}\right)=\sum_{n=-\infty}^{\infty}c_n\mathrm{e}^{in\sigma},$$

where

$$c_n = \sum_{k=-\infty}^{\infty} a_{n-k}b_k. \tag{B.1}$$

As a result, we have:

$$h(\sigma) = \frac{C_0}{2}+\sum_{n=1}^{\infty}\left(C_n\cos n\sigma + C'_n\sin n\sigma\right),$$

where

$$C_0 = 2c_0, \quad C_n = c_n + c_{-n}, \quad C'_n = i\left(c_n - c_{-n}\right). \tag{B.2}$$

We observe that if $A'_n = 0$ and $B'_n = 0$ then we have $a_n = a_{-n}$ and $b_n = b_{-n}$. As a result, $c_n = c_{-n}$ from which we deduce that $C'_n = 0$.

B.3 Evaluation of $I_{n,k} = \int_0^{2\pi} \frac{\cos n(\sigma-\sigma_0)}{(\cosh\tau-\cos\sigma)^k}\,\mathrm{d}\sigma$

We want to evaluate the following integral:

$$I_{n,k} = \int_0^{2\pi}\frac{\cos n(\sigma-\sigma_0)}{(\cosh\tau-\cos\sigma)^k}\,\mathrm{d}\sigma$$

which can be written as:

$$\int_0^{2\pi} \frac{\cos n(\sigma-\sigma_0)}{(\cosh\tau-\cos\sigma)^k}\,\mathrm{d}\sigma = \int_0^{2\pi} \frac{\cos n\sigma\cos n\sigma_0}{(\cosh\tau-\cos\sigma)^k}\,\mathrm{d}\sigma + \int_0^{2\pi} \frac{\sin n\sigma\sin n\sigma_0}{(\cosh\tau-\cos\sigma)^k}\,\mathrm{d}\sigma$$

We observe that the second integrand of the right-hand side of the previous equation:

$$h(\sigma) = \frac{\sin n\sigma}{(\cosh\tau-\cos\sigma)^k},$$

is an odd function and as a result:

$$\int_0^{2\pi} h(\sigma)\,\mathrm{d}\sigma = 0.$$

Therefore we have:

$$\int_0^{2\pi} \frac{\cos n(\sigma-\sigma_0)}{(\cosh\tau-\cos\sigma)^k}\,\mathrm{d}\sigma = \cos n\sigma_0 \int_0^{2\pi} \frac{\cos n\sigma}{(\cosh\tau-\cos\sigma)^k}\,\mathrm{d}\sigma$$

Let $\cosh\tau = a > 1$ and using the complex representation of the cosine function:

$$\cos\sigma = \frac{\mathrm{e}^{i\sigma}+\mathrm{e}^{-i\sigma}}{2},$$

we obtain:

$$\int_0^{2\pi} \frac{\cos n\sigma}{(\cosh\tau-\cos\sigma)^k}\,\mathrm{d}\sigma = \frac{1}{2}\int_0^{2\pi} \frac{\mathrm{e}^{in\sigma}+\mathrm{e}^{-in\sigma}}{\left(a-\frac{\mathrm{e}^{i\sigma}+\mathrm{e}^{-i\sigma}}{2}\right)^k}\,\mathrm{d}\sigma. \tag{B.3}$$

Performing the following change of variables:

$$z = \mathrm{e}^{i\sigma} \Rightarrow \frac{\mathrm{d}z}{iz} = \mathrm{d}\sigma,$$

the integral (B.3) becomes:

$$\begin{aligned}\int_0^{2\pi} \frac{\cos n\sigma}{(\cosh\tau-\cos\sigma)^k}\,\mathrm{d}\sigma &= \frac{1}{2}\int_0^{2\pi} \frac{\mathrm{e}^{in\sigma}+\mathrm{e}^{-in\sigma}}{\left(a-\frac{\mathrm{e}^{i\sigma}+\mathrm{e}^{-i\sigma}}{2}\right)^k}\,\mathrm{d}\sigma,\\ &= \frac{(-2)^k}{2}\int_{|z|=1} \frac{z^n+z^{-n}}{iz\left(z-2a+z^{-1}\right)^k}\,\mathrm{d}z,\\ &= -\frac{(-2)^{k-1}}{i}\int_{|z|=1} \frac{z^{2n}+1}{z^{n-k+1}(z^2-2az+1)^k}\,\mathrm{d}z,\end{aligned}$$

$$= -\frac{(-2)^{k-1}}{i}\int_{|z|=1}\frac{z^{2n}+1}{z^{n-k+1}(z-z_1)^k(z-z_2)^k}\,\mathrm{d}z,$$

where

$$z_1 = a-\sqrt{a^2-1} = \mathrm{e}^{-\tau}, \quad z_2 = a+\sqrt{a^2-1} = \mathrm{e}^{\tau}.$$

We notice that $z_1 z_2 = 1$ and $z_2 > a > 1 > z_1$ because $a = \cosh\tau > 1$ and as a result:

$$\int_{|z|=1}\frac{z^{2n}+1}{z^{n-k+1}(z-z_1)^k(z-z_2)^k}\,\mathrm{d}z = 2\pi i\left[\mathrm{Res}(f,z_1)+\mathrm{Res}(f,0)\right],$$

where

$$f(z) = \frac{z^{2n}+1}{iz^{n-k+1}(z-z_1)^k(z-z_2)^k}.$$

We express $f(z)$ in Laurent series:

$$f(z) = \sum_{m=-\infty}^{\infty} a_m z^m = \frac{1}{z^{n-k+1}}\sum_{m=-\infty}^{\infty} a_m z^{m-(n-k+1)}$$
$$= \frac{1}{z^{n-k+1}}\sum_{m'=-\infty}^{\infty} b_{m'} z^{m'} \Rightarrow a_{-1} = b_{n-k},$$

and we observe that:

$$\frac{z^{2n}+1}{(z-z_1)^k(z-z_2)^k} = \sum_{m'=-\infty}^{\infty} b_{m'} z^{m'},$$

Furthermore

$$\frac{1}{(z-z_1)^k(z-z_2)^k} = c_0 + c_1 z + \cdots + c_{n-k}z^{n-k} + \cdots,$$

which tells us that:

$$\sum_{m'=-\infty}^{\infty} b_{m'} z^{m'} = (z^{2n}+1)(c_0 + c_1 z + \cdots + c_{n-k}z^{n-k} + \cdots)$$

As a result we have $c_{n-k} = b_{n-k}$ if $n \geq -k+1$. We know that:

$$\frac{1}{(z-a)^k} = (-1)^k \sum_{j=0}^{\infty}\binom{j+k-1}{k-1}\frac{z^j}{a^{j+k}}$$

and this gives us the residue of f evaluated at $z = 0$:

$$\frac{1}{(z-z_1)(z-z_2)} = \left[\sum_{j=0}^{\infty}\binom{j+k-1}{k-1}\frac{z^j}{z_1^{j+1}}\right]\left[\sum_{j=0}^{\infty}\binom{j+k-1}{k-1}\frac{z^j}{z_2^{j+1}}\right],$$

$$\Rightarrow \mathrm{Res}(f,0) = \sum_{i=0}^{n-k}\binom{i+k-1}{k-1}\binom{n+i-1}{k-1}\frac{1}{z_1^{i+k}z_2^{n+i}}$$

As a result, the residue of f at 0 is:

$$\mathrm{Res}(f,0) = \sum_{i=0}^{n-k}\binom{i+k-1}{k-1}\binom{n+i-1}{k-1}\frac{1}{z_1^{i+k}z_2^{n+i}},$$

if $n \geq -k+1$, otherwise f has no pole at $z = 0$. Furthermore, the residue of f at z_1 is:

$$\mathrm{Res}(f,z_1) = \frac{1}{(n-1)!}\lim_{z\to z_1}\frac{\partial^{k-1}}{\partial z^{k-1}}\left[(z-z_1)^k f(z)\right]$$

As a result we have:

$$\begin{aligned}\frac{1}{i}\int_{|z|=1}\frac{z^{2n}+1}{z^{n-k+1}(z^2-2az+1)^k}\,\mathrm{d}z &= 2\pi\left[\mathrm{Res}(f,0)+\mathrm{Res}(f,z_1)\right],\\ &= 2\pi\left[\frac{1}{(n-1)!}\lim_{z\to z_1}\frac{\partial^{k-1}}{\partial z^{k-1}}\left[(z-z_1)^k f(z)\right]\right.\\ &\quad\left.+\sum_{i=0}^{n-k}\binom{i+k-1}{k-1}\binom{n+i-1}{k-1}\frac{1}{z_1^{i+k}z_2^{n+i}}\right],\end{aligned}$$

which gives us:

$$\begin{aligned}I_{n,k} &= \int_0^{2\pi}\frac{\cos n(\sigma-\sigma_0)}{(\cosh\tau-\cos\sigma)^k}\,\mathrm{d}\sigma,\\ &= (-2)^k\pi\cos n\sigma_0\left[\frac{1}{(n-1)!}\lim_{z\to z_1}\frac{\partial^{k-1}}{\partial z^{k-1}}\left[(z-z_1)^k f(z)\right]\right.\\ &\quad\left.+\sum_{i=0}^{n-k}\binom{i+k-1}{k-1}\binom{n+i-1}{k-1}\frac{1}{z_1^{i+k}z_2^{n+i}}\right].\end{aligned}$$

If $k = 1$ then we have:

$$I_{n,1} = \int_0^{2\pi}\frac{\cos n(\sigma-\sigma_0)}{\cosh\tau-\cos\sigma}\,\mathrm{d}\sigma = \frac{2\pi\cos n\sigma_0}{\mathrm{e}^{n\tau}\sinh\tau},$$

and when $k = 2$ we have:

$$I_{n,2} = \int_0^{2\pi}\frac{\cos n(\sigma-\sigma_0)}{(\cosh\tau-\cos\sigma)^2}\,\mathrm{d}\sigma = 2\pi\cos n\sigma_0\frac{\mathrm{e}^{-n\tau}(n\sinh\tau+\cosh\tau)}{\sinh^3\tau}.$$

B.3.1 Alternative Derivation

Alternatively, we can write (B.3) as:

$$I_{n,k} = \cos n\sigma_0 \int_0^{2\pi} \frac{\cos n\sigma}{(\cosh\tau-\cos\sigma)^k}\,\mathrm{d}\sigma = \cos n\sigma_0 \Re\left[\int_0^{2\pi} \frac{\mathrm{e}^{in\sigma}}{(\cosh\tau-\cos\sigma)^k}\,\mathrm{d}\sigma\right] \tag{B.4}$$

where $\Re[z]$ is real part of a complex number z. Performing the following change of variables:

$$z = \mathrm{e}^{i\sigma} \Rightarrow \frac{\mathrm{d}z}{iz} = \mathrm{d}\sigma,$$

and using the fact that:

$$\cos\sigma = \frac{\mathrm{e}^{i\sigma}+\mathrm{e}^{-i\sigma}}{2},$$

the integral (B.4) becomes:

$$\begin{aligned}
I_{n,k} &= \cos n\sigma_0 \Re\left[\int_0^{2\pi} \frac{\mathrm{e}^{in\sigma}}{(\cosh\tau-\frac{\mathrm{e}^{i\sigma}+\mathrm{e}^{-i\sigma}}{2})^k}\,\mathrm{d}\sigma\right] \\
&= \cos n\sigma_0 \Re\left[\int_0^{2\pi} \frac{\mathrm{e}^{in\sigma}}{(-2)^{-k}\,(\mathrm{e}^{i\sigma}-2a+\mathrm{e}^{-i\sigma})^k}\,\mathrm{d}\sigma\right] \\
&= (-2)^k \cos n\sigma_0 \Re\left[\int_0^{2\pi} \frac{\mathrm{e}^{in\sigma}}{(\mathrm{e}^{i\sigma}-2a+\mathrm{e}^{-i\sigma})^k}\,\mathrm{d}\sigma\right] \\
&= (-2)^k \cos n\sigma_0 \Re\left[\int_0^{2\pi} \frac{\mathrm{e}^{in\sigma}}{\mathrm{e}^{-ik\sigma}(\mathrm{e}^{2i\sigma}-2a\mathrm{e}^{i\sigma}+1)^k}\,\mathrm{d}\sigma\right] \\
&= (-2)^k \cos n\sigma_0 \Re\left[\int_0^{2\pi} \frac{\mathrm{e}^{i(n+k)\sigma}}{(\mathrm{e}^{2i\sigma}-2a\mathrm{e}^{i\sigma}+1)^k}\,\mathrm{d}\sigma\right] \\
&= (-2)^k \cos n\sigma_0 \Re\left[\int_{|z|=1} \frac{z^{n+k}}{iz(z^2-2az+1)^k}\,\mathrm{d}z\right] \\
&= (-2)^k \cos n\sigma_0 \Re\left[\frac{1}{i}\int_{|z|=1} \frac{z^{n+k-1}}{(z^2-2az+1)^k}\,\mathrm{d}z\right] \\
&= (-2)^k \cos n\sigma_0 \Re\left[\frac{1}{i}\int_{|z|=1} \frac{z^{n+k-1}}{(z-z_1)^k(z-z_2)^k}\,\mathrm{d}z\right],
\end{aligned}$$

where

$$\begin{aligned}
z_1 &= a-\sqrt{a^2-1} = \mathrm{e}^{-\tau}, \\
z_2 &= a+\sqrt{a^2-1} = \mathrm{e}^{\tau}.
\end{aligned}$$

and $a = \cosh\tau$. We notice that $z_1 z_2 = 1$ and $z_2 > a > 1 > z_1$ because $a = \cosh\tau > 1$ and as a result:

$$\int_{|z|=1} \frac{z^{n+k-1}}{(z-z_1)^k(z-z_2)^k}\,\mathrm{d}z = 2\pi i\left[\mathrm{Res}(f, z_1)\right],$$

where

$$f_{n,k}(z) = \frac{z^{n+k-1}}{(z-z_1)^k(z-z_2)^k}.$$

We know that the residue of f at z_1 is:

$$\mathrm{Res}(f, z_1) = \frac{1}{(n-1)!}\lim_{z\to z_1}\frac{\partial^{k-1}}{\partial z^{k-1}}\left[(z-z_1)^k f_{n,k}(z)\right],$$

if $n \geq 0$. As a result, we have:

$$\begin{aligned} I_{n,k} &= \cos n\sigma_0 \int_0^{2\pi} \frac{\cos n\sigma}{(\cosh\tau-\cos\sigma)^k}\,\mathrm{d}\sigma \\ &= 2\pi\cos n\sigma_0 \Re\left[\lim_{z\to z_1}\frac{\partial^{k-1}}{\partial z^{k-1}}\left[\frac{(-2)^k(z-z_1)^k}{(n-1)!}f_{n,k}(z)\right]\right], \\ &= 2\pi\cos n\sigma_0 \Re\left[\lim_{z\to z_1}\frac{\partial^{k-1}}{\partial z^{k-1}} g_{n,k}(z)\right], \end{aligned} \tag{B.5}$$

where

$$g_{n,k}(z) = \frac{(-2)^k}{(n-1)!}\frac{z^{n+k-1}}{(z-z_2)^k}$$

If we let $k = 1$ in (B.5) then we have:

$$\begin{aligned} I_{n,1} &= 2\pi\cos n\sigma_0 \Re\left[\lim_{z\to z_1} g_{n,1}(z)\right] = -4\pi\cos n\sigma_0 \Re\left[\frac{z_1^n}{(z_1-z_2)}\right] \\ &= -4\pi\cos n\sigma_0 \frac{\mathrm{e}^{-n\tau}}{\mathrm{e}^{-\tau}-\mathrm{e}^{\tau}} = \frac{2\pi\cos n\sigma_0}{\mathrm{e}^{n\tau}\sinh\tau}. \end{aligned} \tag{B.6}$$

When $k = 2$ we have:

$$\begin{aligned} I_{n,2} &= 2\pi\cos n\sigma_0 \Re\left[\lim_{z\to z_1}\frac{\partial}{\partial z} g_{n,2}(z)\right], \\ &= 8\pi\cos n\sigma_0 \Re\left[\lim_{z\to z_1}\frac{\partial}{\partial z}\frac{z^{n+1}}{(z-z_2)^2}\right], \\ &= 8\pi\cos n\sigma_0 \frac{(n+1)\,z_1^n\,(z_1-z_2)^2 - 2\,(z_1-z_2)\,z_1^{n+1}}{(z_1-z_2)^4}, \end{aligned}$$

$$
\begin{aligned}
&= 8\pi\cos n\sigma_0 \frac{(n+1)\,z_1^n\,(z_1-z_2)-2z_1^{n+1}}{(z_1-z_2)^3},\\
&= 8\pi\cos n\sigma_0 \frac{z_1^n}{(z_1-z_2)^3}\left[n\,(z_1-z_2)-(z_1+z_2)\right],\\
&= 2\pi\cos n\sigma_0 \frac{\mathrm{e}^{-n\tau}(n\sinh\tau+\cosh\tau)}{\sinh^3\tau},
\end{aligned}
\tag{B.7}
$$

and, if we set $k=3$, we obtain:

$$
\begin{aligned}
I_{n,3} &= 2\pi\cos n\sigma_0 \Re\left[\lim_{z\to z_1}\frac{\partial^2}{\partial^2 z} g_{n,3}(z)\right] = -8\pi\cos n\sigma_0\Re\left[\lim_{z\to z_1}\frac{\partial^2}{\partial^2 z}\frac{z^{n+2}}{(z-z_2)^3}\right]\\
&= -8\pi\cos n\sigma_0\Re\left[\lim_{z\to z_1}\frac{\partial}{\partial z}\frac{(n+2)\,z^{n+1}\,(z-z_2)^3-3\,(z-z_2)^2\,z^{n+2}}{(z-z_2)^6}\right]\\
&= -8\pi\cos n\sigma_0\Re\left[\lim_{z\to z_1}\frac{\partial}{\partial z}\frac{(n+2)\,z^{n+1}\,(z-z_2)-3z^{n+2}}{(z-z_2)^4}\right]\\
&= -8\pi\cos n\sigma_0\Re\left[\lim_{z\to z_1}\frac{(n+2)\,z^n\left[(n-1)\,z-(n+1)\,z_2\right](z-z_2)}{(z-z_2)^5}\right.\\
&\left.- \frac{4z^{n+1}\left[n\,(z-z_2)-(z+z_2)-z_2\right]}{(z-z_2)^5}\right]\\
&= \pi\cos n\sigma_0\left[\frac{(n+2)\,\mathrm{e}^{-n\tau}\left[n\sinh\tau+\cosh\tau\right]\sinh\tau}{\sinh^5\tau}\right.\\
&\left.+\frac{2\mathrm{e}^{-(n+1)\tau}\left[n\sinh\tau+\cosh\tau\right]+\mathrm{e}^{-n\tau}}{\sinh^5\tau}\right].
\end{aligned}
\tag{B.8}
$$

B.3.2 Recurrence relation

Writing the integral $I_{n,k}$ as:

$$I_{n,k} = \cos n\sigma_0 \times I'_{n,k},$$

where

$$I'_{n,k} = \int_0^{2\pi}\frac{\cos n\sigma}{(\cosh\tau-\cos\sigma)^k}\mathrm{d}\sigma,$$

and, using integration by parts, we obtain:

$$
\begin{aligned}
I'_{n,k} &= \int_0^{2\pi}\frac{\cos n\sigma}{(\cosh\tau-\cos\sigma)^k}\mathrm{d}\sigma,\\
&= \left[\frac{\sin n\sigma}{(\cosh-\cos\sigma)^k}\right]_0^{2\pi} + k\int_0^{2\pi}\frac{\sin n\sigma}{(\cosh-\cos\sigma)^{k+1}}\sin\sigma\mathrm{d}\sigma,
\end{aligned}
$$

$$
\begin{aligned}
&= \frac{k}{2}\int_0^{2\pi}\left[\frac{\cos\left(n-1\right)\sigma}{\left(\cosh\tau-\cos\sigma\right)^{k+1}} - \frac{\cos\left(n+1\right)\sigma}{\left(\cosh\tau-\cos\sigma\right)^{k+1}}\right]\mathrm{d}\sigma,\\
&= \frac{k}{2}\int_0^{2\pi}\frac{\cos\left(n-1\right)\sigma}{\left(\cosh\tau-\cos\sigma\right)^{k+1}}\mathrm{d}\sigma - \frac{k}{2}\int_0^{2\pi}\frac{\cos\left(n+1\right)\sigma}{\left(\cosh\tau-\cos\sigma\right)^{k+1}}\mathrm{d}\sigma,\\
&= \frac{k}{2}I'_{n-1,k+1} - \frac{k}{2}I'_{n+1,k+1},
\end{aligned}
$$

Consequently, we obtain the following reccurence relation:

$$kI'_{n-1,k+1} - 2I'_{n,k} - kI'_{n+1,k+1} = 0.$$

B.4 Bipolar expansion

From (2.55) we obtain the following expansions in powers of a:

$$dc = \frac{1-c^2}{2} - \frac{a^2(1+c^2)}{2(1-c^2)} + \mathcal{O}(a^4), \tag{B.9a}$$

$$\tau_1 - \tau_2 = \log\left(1-c^2\right) - \log a - \frac{a^2}{(1-c^2)^2} + \frac{a^2}{1-c^2} + \mathcal{O}(a^4). \tag{B.9b}$$

Making use of the expansions in powers of a for τ_1 and τ_2 derived in (2.22) we obtain:

$$
\begin{aligned}
\mathrm{e}^{-2n\tau_1} &= \mathrm{e}^{-2n\left[\log\left(1-c^2\right)-\log a-\log c-\frac{a^2}{(1-c^2)^2}+\mathcal{O}(a^5)\right]},\\
&= \left(\frac{ac}{1-c^2}\right)^{2n}\left(1+\mathcal{O}(a^2)\right) = \left(\frac{ac}{1-c^2}\right)^{2n} + \mathcal{O}(a^{(2+2n)}),
\end{aligned} \tag{B.10a}
$$

$$
\begin{aligned}
1 \pm \mathrm{e}^{-2n(\tau_1-\tau_2)} &= 1 \pm \mathrm{e}^{-2n\left[\log\left(1-c^2\right)-\log a-\frac{a^2}{(1-c^2)^2}+\frac{a^2}{1-c^2}+\mathcal{O}(a^4)\right]},\\
&= 1 \pm \left(\frac{a}{1-c^2}\right)^{2n} + \mathcal{O}(a^{(2+2n)}).
\end{aligned} \tag{B.10b}
$$

Subsequently, we have:

$$\frac{1}{1+\mathrm{e}^{-2n(\tau_1-\tau_2)}} = \left(1+\mathrm{e}^{-2n(\tau_1-\tau_2)}\right)^{-1} = 1 - \left(\frac{a}{1-c^2}\right)^{2n} + \mathcal{O}(a^{(2+2n)})$$

and finally:

$$
\begin{aligned}
\tanh n(\tau_1-\tau_2) = \frac{1-\mathrm{e}^{-2n(\tau_1-\tau_2)}}{1+\mathrm{e}^{-2n(\tau_1-\tau_2)}} &= \left[1 - \left(\frac{a}{1-c^2}\right)^{2n} + \mathcal{O}(a^{(2+2n)})\right]^2,\\
&= 1 - 2\left(\frac{a}{1-c^2}\right)^{2n} + \mathcal{O}(a^{4n}).
\end{aligned}
$$

B.4.1 Bipolar coefficients in the limit $c \to 0$

From the definition (2.1) the following limits for $c \to 0$ are obtained:

$$d = \frac{1}{2c}\sqrt{(1+a^2-c^2)^2 - 4a^2} \to \infty,$$
$$cd = \frac{1}{2}\sqrt{(1+a^2-c^2)^2 - 4a^2} \to \frac{1-a^2}{2}.$$

Subsequently, using the definitions $\tau_1 = \log\left(d/a + \sqrt{1+(d/a)^2}\right)$ and $\tau_2 = \log\left(d + \sqrt{1+d^2}\right)$ we find the limit as $c \to 0$:

$$\tau_1 = \log\left(d/a + \sqrt{1+(d/a)^2}\right) \to \infty, \tag{B.12a}$$
$$\tau_2 = \log\left(d + \sqrt{1+d^2}\right) \to \infty, \tag{B.12b}$$
$$\begin{aligned}\tau_1 - \tau_2 &= \log\left(d/a + \sqrt{1+(d/a)^2}\right) - \log\left(d + \sqrt{1+d^2}\right) \\ &= \log\frac{d/a + \sqrt{1+(d/a)^2}}{d + \sqrt{1+d^2}} = \log\frac{1/a + \sqrt{1/d^2 + 1/a^2}}{1 + \sqrt{1/d^2+1}} \to \log\frac{1}{a}.\end{aligned} \tag{B.12c}$$

B.5 Proof of $\sum_{n=1}^{\infty} \frac{1}{n} \mathrm{e}^{-2n\tau_2} = -\log 2d + \tau_2$

In this appendix we will prove that:

$$\sum_{n=1}^{\infty} \frac{1}{n} \mathrm{e}^{-2n\tau_2} = -\log 2d + \tau_2,$$

for the cases when $a = 0$ and $a \neq 0$.

If $a = 0$ we have:

$$\begin{aligned}\sum_{n=1}^{\infty} \frac{1}{n} \mathrm{e}^{-2n\tau_2} &= \sum_{n=1}^{\infty} \frac{\left(\mathrm{e}^{-2\tau_2}\right)^n}{n} = -\log\left(1 - \mathrm{e}^{-2\tau_2}\right) = -\log\left(1 - \mathrm{e}^{2\log c}\right) \\ &= -\log\left(1-c^2\right) = -\log 2d + \tau_2,\end{aligned}$$

where we have used the fact that:

$$\tau_2 = -\log c, \quad d = \frac{1-c^2}{2c},$$

and

$$\log 2d = \log\left(1-c^2\right) - \log c = \log\left(1-c^2\right) + \tau_2. \tag{B.13}$$

If $a \neq 0$ then we have:

$$\begin{aligned}\sum_{n=1}^{\infty} \frac{1}{n} \mathrm{e}^{-2n\tau_2} &= \sum_{n=1}^{\infty} \frac{\left(\mathrm{e}^{-2\tau_2}\right)^n}{n} = -\log\left(1 - \mathrm{e}^{-2\tau_2}\right) = -\log\left(1 - \mathrm{e}^{-2\log\left(d+\sqrt{1+d^2}\right)}\right) \\ &= -\log\left(1 - \left(d + \sqrt{1+d^2}\right)^{-2}\right) = -\log\left(\frac{2d}{d+\sqrt{1+d^2}}\right) \\ &= -\log 2d + \log\left(d + \sqrt{1+d^2}\right) = -\log 2d + \tau_2.\end{aligned}$$

B.6 Proof of $\tilde{\tau}_0 = 2\tau_2 - \tau_0, \quad \tilde{\sigma}_0 = \sigma_0$

The image point $\tilde{\mathbf{x}}$ in Cartesian coordinates is:

$$\tilde{\mathbf{x}} = (\tilde{x}, \tilde{y}) = \left(\frac{x - \sqrt{1+d^2}}{(x - \sqrt{1+d^2})^2 + y^2} + \sqrt{1+d^2}, \frac{y}{(x - \sqrt{1+d^2})^2 + y^2}\right).$$

We use the following identities:

$$\begin{aligned}\tilde{x} + d &= \frac{x - \sqrt{1+d^2} + (\sqrt{1+d^2} + d)\left[(x - \sqrt{1+d^2})^2 + y^2\right]}{(x - \sqrt{1+d^2})^2 + y^2}, \\ \tilde{x} - d &= \frac{x - \sqrt{1+d^2} + (\sqrt{1+d^2} - d)\left[(x - \sqrt{1+d^2})^2 + y^2\right]}{(x - \sqrt{1+d^2})^2 + y^2}, \\ (\tilde{x}+d)^2 + \tilde{y}^2 &= \frac{1 + 2(x - \sqrt{1+d^2})(\sqrt{1+d^2} + d)}{(x - \sqrt{1+d^2})^2 + y^2} \\ &\quad + \frac{(\sqrt{1+d^2} + d)^2\left[(x - \sqrt{1+d^2})^2 + y^2\right]^2}{\left[(x - \sqrt{1+d^2})^2 + y^2\right]^2}, \\ (\tilde{x}-d)^2 + \tilde{y}^2 &= \frac{1 + 2(x - \sqrt{1+d^2})(\sqrt{1+d^2} - d)}{(x - \sqrt{1+d^2})^2 + y^2} \\ &\quad + \frac{(\sqrt{1+d^2} - d)^2\left[(x - \sqrt{1+d^2})^2 + y^2\right]^2}{\left[(x - \sqrt{1+d^2})^2 + y^2\right]^2},\end{aligned}$$

to obtain that:

$$\begin{aligned}\tilde{\tau} &= \frac{1}{2}\log\frac{(\tilde{x}+d)^2 + \tilde{y}^2}{(\tilde{x}-d)^2 + \tilde{y}^2} \\ &= \frac{1}{2}\log\frac{1 + 2(x - \sqrt{1+d^2})(\sqrt{1+d^2} + d) + (\sqrt{1+d^2} + d)\left[(x - \sqrt{1+d^2})^2 + y^2\right]}{1 + 2(x - \sqrt{1+d^2})(\sqrt{1+d^2} - d) + (\sqrt{1+d^2} - d)\left[(x - \sqrt{1+d^2})^2 + y^2\right]}\end{aligned}$$

$$
\begin{aligned}
&= \frac{1}{2}\log\frac{\left[1+(x-\sqrt{1+d^2})(\sqrt{1+d^2}+d)\right]^2+(\sqrt{1+d^2}+d)^2y^2}{\left[1+(x-\sqrt{1+d^2})(\sqrt{1+d^2}-d)\right]^2+(\sqrt{1+d^2}-d)^2y^2}\\
&= \frac{1}{2}\log\frac{(\sqrt{1+d^2}+d)^2}{(\sqrt{1+d^2}-d)^2}+\frac{1}{2}\log\frac{\left(x-\sqrt{1+d^2}+\frac{1}{\sqrt{1+d^2}+d}\right)^2+y^2}{\left(x-\sqrt{1+d^2}+\frac{1}{\sqrt{1+d^2}-d}\right)^2+y^2}\\
&= \log\frac{\sqrt{1+d^2}+d}{\sqrt{1+d^2}-d}+\frac{1}{2}\log\frac{\left(x-\sqrt{1+d^2}+\sqrt{1+d^2}-d\right)^2+y^2}{\left(x-\sqrt{1+d^2}+\sqrt{1+d^2}+d\right)^2+y^2}\\
&= \log\left(\sqrt{1+d^2}+d\right)^2+\frac{1}{2}\log\frac{(x-d)^2+y^2}{(x+d)^2+y^2}\\
&= 2\tau_2-\tau,
\end{aligned}
$$

and

$$
\begin{aligned}
\pi-\tilde{\sigma} &= 2\arctan\frac{2d\tilde{y}}{d^2-\tilde{x}^2-\tilde{y}^2-\sqrt{(d^2-\tilde{x}^2-\tilde{y}^2)^2+4d^2\tilde{y}^2}}\\
&= 2\arctan\frac{\frac{2dy}{\left(x-\sqrt{1+d^2}\right)^2+y^2}}{\frac{d^2-x^2-y^2}{\left(x-\sqrt{1+d^2}\right)^2+y^2}+\frac{\sqrt{(d^2-x^2-y^2)^2+4d^2y^2}}{\left(x-\sqrt{1+d^2}\right)^2+y^2}}\\
&= 2\arctan\frac{2dy}{d^2-x^2-y^2-\sqrt{(d^2-x^2-y^2)^2+4d^2y^2}}\\
&= \pi-\sigma \Rightarrow \tilde{\sigma}=\sigma,
\end{aligned}
$$

where we have used the fact that:

$$
d^2-\tilde{x}^2-\tilde{y}^2=\frac{d^2-x^2-y^2}{\left(x-\sqrt{1+d^2}\right)^2+y^2}.
$$

B.7 Proof of $(\tau_c, \sigma_c) = (2\tau_2, 0)$

We want to proove that the position (τ_c, σ_c) of the centre of the circle in bipolar coordinates is equal to $(2\tau_2, 0)$. The angular component σ_c is zero given the fact that the point is on the Ox axis. For the τ-component we have:

$$
\begin{aligned}
\tau_c &= \log\frac{(x+d)^2}{(x-d)^2}=\log\frac{\sqrt{1+d^2}+d}{\sqrt{1+d^2}-d}=\log\left(\sqrt{1+d^2}+d\right)^2=2\log\left(\sqrt{1+d^2}+d\right)\\
&= 2\tau_2.
\end{aligned}
$$

B.8 Bipolar coordinates - concentric case

We want know how do expressions involving bipolar coordinates (τ, σ) relate to polar coordinates (r, θ) as $c \to 0$. We begin with:

$$\begin{aligned}
\tau - \tau_2 &= \frac{1}{2}\log\frac{\left(x+\sqrt{1+d^2}+d\right)^2+y^2}{\left(x+\sqrt{1+d^2}-d\right)^2+y^2} - \log\left(d+\sqrt{1+d^2}\right) \\
&= \frac{1}{2}\log\frac{\left(x+\sqrt{1+d^2}+d\right)^2+y^2}{\left[\left(x+\sqrt{1+d^2}-d\right)^2+y^2\right]\left(d+\sqrt{1+d^2}\right)^2} \\
&= \frac{1}{2}\log\frac{\left(d+\sqrt{1+d^2}\right)^2\left[\left(\frac{x}{d+\sqrt{1+d^2}}+1\right)^2+\left(\frac{y}{d+\sqrt{1+d^2}}\right)^2\right]}{\left(d+\sqrt{1+d^2}\right)^2\left[\left(x+\frac{1}{\sqrt{1+d^2}+d}\right)^2+y^2\right]} \\
&\to \frac{1}{2}\log\frac{1}{r^2} = \log\frac{1}{r} \quad \text{as } c \to 0,
\end{aligned}$$

where $r = \sqrt{x^2+y^2}$.
Similarly we have for:

$$\begin{aligned}
\tau_1 - \tau &= \log\left(d/a+\sqrt{1+d^2/a^2}\right) - \frac{1}{2}\log\frac{\left(x+\sqrt{1+d^2}+d\right)^2+y^2}{\left(x+\sqrt{1+d^2}-d\right)^2+y^2} \\
&= -\frac{1}{2}\log\frac{\left(x+\sqrt{1+d^2}+d\right)^2+y^2}{\left[\left(x+\sqrt{1+d^2}-d\right)^2+y^2\right]\left(d/a+\sqrt{1+d^2/a^2}\right)^2} \\
&= -\frac{1}{2}\log\frac{d^2\left[\left(\frac{x}{d}+\sqrt{\frac{1+d^2}{d^2}}\right)^2+\left(\frac{y}{d}\right)^2\right]}{d^2\left(1/a+\sqrt{1/d^2+1/a^2}\right)^2\left[\left(x+\frac{1}{\sqrt{1+d^2}+d}\right)^2+y^2\right]} \\
&\to -\frac{1}{2}\log\frac{a^2}{r^2} = \log\frac{r}{a} \quad \text{as } c \to 0.
\end{aligned}$$

We know that the tangent of the bipolar angular component can be written as:

$$\begin{aligned}
\tan\sigma &= \frac{2dy}{\left(x+\sqrt{1+d^2}\right)^2+y^2-d^2} = \frac{2dy}{x^2+2x\sqrt{1+d^2}+1+d^2+y^2-d^2} \\
&= \frac{2dy}{d\left((x^2+y^2+1)/d+2x\sqrt{1+d^2}/d\right)} \to \frac{y}{x} \quad \text{as } c \to 0
\end{aligned}$$

$$= \tan\theta,$$

where θ is the standard polar angular coordinate of (x, y). From this we deduce the following:

$$\sigma - \sigma_0 = \theta - \theta_0.$$

Here (r, θ) and (r_0, θ_0) are the polar representation of (x, y) and (x_0, y_0), respectively.

Appendix C

Bispherical coordinates

C.1 Normal derivative in bispherical coordinates

We are interested in the normal derivative of a function $f(\tau, \sigma, \phi)$ evaluated on a sphere of constant $\tau = \tau_1$ and for that purpose we will investigate the following hypothesis:

$$\mathbf{n} = \left(-\frac{\sin\sigma\cos\phi\sinh\tau}{\cosh\tau - \cos\sigma}, -\frac{\sin\sigma\sin\phi\sinh\tau}{\cosh\tau - \cos\sigma}, \frac{1 - \cosh\tau\cos\sigma}{\cosh\tau - \cos\sigma} \right),$$

where $\mathbf{n}$ is the normal vector to the $\tau = \tau_1$ surface. Let $\mathbf{v}$ be a point on the sphere $\tau = \tau_1$:

$$\mathbf{v} = (x, y, z) = \left(d\frac{\sin\sigma\cos\phi}{\cosh\tau - \cos\sigma}, d\frac{\sin\sigma\sin\phi}{\cosh\tau - \cos\sigma}, d\frac{\sinh\tau}{\cosh\tau - \cos\sigma} \right).$$

Then we have

$$\frac{\partial\mathbf{v}}{\partial\tau} = \left(-d\frac{\sin\sigma\cos\phi\sinh\tau}{(\cosh\tau - \cos\sigma)^2}, -d\frac{\sin\sigma\sin\phi\sinh\tau}{(\cosh\tau - \cos\sigma)^2}, d\frac{1 - \cosh\tau\cos\sigma}{(\cosh\tau - \cos\sigma)^2} \right),$$

and

$$\left| \frac{\partial\mathbf{v}}{\partial\tau} \right|^2 = \frac{d^2}{(\cosh\tau - \cos\sigma)^2}.$$

As a result we obtain the unit vector:

$$\mathbf{e}_\tau = \left(-\frac{\sin\sigma\cos\phi\sinh\tau}{\cosh\tau - \cos\sigma}, -\frac{\sin\sigma\sin\phi\sinh\tau}{\cosh\tau - \cos\sigma}, \frac{1 - \cosh\tau\cos\sigma}{\cosh\tau - \cos\sigma} \right).$$

The vector $\mathbf{v} = (x, y, z)$ also satisfies:

$$(z - d\coth\tau)^2 + y^2 + x^2 = d^2\,\mathrm{csch}^2\,\tau.$$

Changing the system of coordinates such that the origin is the centre of the sphere $\tau = \tau_1$. Let θ and ϕ be the polar angle and azimuthal angle, respectively, of a point on the sphere and as a result:

$$\begin{aligned}\tan\varphi = \frac{y}{x} = \frac{\sin\phi}{\cos\phi} = \tan\phi \Rightarrow \phi = \varphi,\\ \theta = \arccos\frac{z - d\coth\tau}{\sqrt{x^2 + y^2 + (z - d\coth\tau)^2}} = \arccos\left(\frac{\cos\sigma\cosh\tau - 1}{\cosh\tau - \cos\sigma}\right).\end{aligned}$$

Using standard trigonometric identifies we express $\cos\theta$ and $\sin\theta$ in terms of $\tan\theta$:

$$\cos\arccos x = x, \quad \sin\arccos x = \sqrt{1 - x^2},$$

where $x \in [0, \pi]$. This gives us the vector normal to the surface of the circle:

$$\begin{aligned}\mathbf{e}_\theta &= (\sin\theta\cos\varphi, \sin\theta\sin\varphi, \cos\theta)\\ &= \left(\frac{\sin\sigma\cos\phi\sinh\tau}{\cosh\tau - \cos\sigma}, \frac{\sin\sigma\sin\phi\sinh\tau}{\cosh\tau - \cos\sigma}, \frac{\cosh\tau\cos\sigma - 1}{\cosh\tau - \cos\sigma}\right)\\ &= -\mathbf{e}_\tau.\end{aligned}$$

As a result we have the following identity for the normal derivative on a circle of constant τ

$$\frac{\partial f}{\partial \mathbf{n}} = \nabla f \cdot \mathbf{e}_\tau = -\frac{\cosh\tau - \cos\sigma}{d}\frac{\partial f}{\partial \tau}.$$

C.2 Proof of $\left(\tilde{\tau}_0, \tilde{\sigma}_0, \tilde{\phi}_0\right) = (2\tau_2 - \tau_0, \sigma_0, \phi_0)$

The image point $\tilde{\mathbf{x}}$ in Cartesian coordinates is:

$$\begin{aligned}\tilde{\mathbf{x}} = (\tilde{x}, \tilde{y}, \tilde{z}) = \Bigg(&\frac{x}{x^2 + y^2 + (z - \sqrt{1 + d^2})^2}, \frac{y}{x^2 + y^2 + (z - \sqrt{1 + d^2})^2},\\ &\frac{z - \sqrt{1 + d^2}}{x^2 + y^2 + (z - \sqrt{1 + d^2})^2} + \sqrt{1 + d^2}\Bigg).\end{aligned} \tag{C.1}$$

We begin with the τ-coordinate of the image point:

$$
\begin{aligned}
\tilde{\tau} &= \operatorname{arcsinh}\left(\frac{2d\tilde{z}}{\tilde{Q}}\right) = \log\left(\frac{2d\tilde{z}}{\tilde{Q}} + \sqrt{1 + \left(\frac{2d\tilde{z}}{\tilde{Q}}\right)^2}\right) \\
&= \log\left(\frac{2d\tilde{z}}{\tilde{Q}} + \frac{\sqrt{Q^2 + (2d\tilde{z})^2}}{\tilde{Q}}\right) \\
&= \log\left(\frac{2d\tilde{z}}{\tilde{Q}} + \frac{\sqrt{\left(\tilde{R}^2 + d^2\right)^2 - (2d\tilde{z})^2 + (2d\tilde{z})^2}}{\tilde{Q}}\right) \\
&= \log\left(\frac{\tilde{R}^2 + d^2 + 2d\tilde{z}}{\tilde{Q}}\right) = \log\left(\frac{\tilde{R}^2 + d^2 + 2d\tilde{z}}{\sqrt{\left(\tilde{R}^2 + d^2\right)^2 - (2d\tilde{z})^2}}\right) \\
&= \log\left(\frac{\tilde{R}^2 + d^2 + 2d\tilde{z}}{\sqrt{\left(\tilde{R}^2 + d^2 + 2d\tilde{z}\right)\left(\tilde{R}^2 + d^2 - 2d\tilde{z}\right)}}\right) \\
&= \frac{1}{2}\log\left(\frac{\tilde{R}^2 + d^2 + 2d\tilde{z}}{\tilde{R}^2 + d^2 - 2d\tilde{z}}\right) = \frac{1}{2}\log\left(\frac{\tilde{x}^2 + \tilde{y}^2 + \tilde{z}^2 + d^2 + 2d\tilde{z}}{\tilde{x}^2 + \tilde{y}^2 + \tilde{z}^2 + d^2 - 2d\tilde{z}}\right) \\
&= \frac{1}{2}\log\left(\frac{\tilde{x}^2 + \tilde{y}^2 + (\tilde{z} + d)^2}{\tilde{x}^2 + \tilde{y}^2 + (\tilde{z} - d)^2}\right) \\
&= \frac{1}{2}\log\left(\frac{x^2 + y^2 + \left[z - \sqrt{1+d^2} + \left(x^2 + y^2 + (z - \sqrt{1+d^2})^2\right)\left(\sqrt{1+d^2} + d\right)\right]^2}{x^2 + y^2 + \left[z - \sqrt{1+d^2} + \left(x^2 + y^2 + (z - \sqrt{1+d^2})^2\right)\left(\sqrt{1+d^2} - d\right)\right]^2}\right) \\
&= \frac{1}{2}\log\left(\frac{1 + \left(\sqrt{1+d^2} + d\right)^2\left(x^2 + y^2 + (z - \sqrt{1+d^2})^2\right)}{1 + \left(\sqrt{1+d^2} - d\right)^2\left(x^2 + y^2 + (z - \sqrt{1+d^2})^2\right)}\right. \\
&\left.\frac{+2\left(z - \sqrt{1+d^2}\right)\left(\sqrt{1+d^2} + d\right)}{+2\left(z - \sqrt{1+d^2}\right)\left(\sqrt{1+d^2} - d\right)}\right) \\
&= \frac{1}{2}\log\frac{\left(\sqrt{1+d^2} + d\right)^2\left[\frac{1}{\left(\sqrt{1+d^2}+d\right)^2} + x^2 + y^2 + (z - \sqrt{1+d^2})^2 + \frac{2\left(z - \sqrt{1+d^2}\right)}{\sqrt{1+d^2}+d}\right]}{\left(\sqrt{1+d^2} - d\right)^2\left[\frac{1}{\left(\sqrt{1+d^2}-d\right)^2} + x^2 + y^2 + (z - \sqrt{1+d^2})^2 + \frac{2\left(z - \sqrt{1+d^2}\right)}{\sqrt{1+d^2}-d}\right]}
\end{aligned}
$$

$$
\begin{aligned}
&= \frac{1}{2}\log\frac{\left(\sqrt{1+d^2}+d\right)^2\left[\left(\sqrt{1+d^2}-d\right)^2+x^2+y^2+(z-\sqrt{1+d^2})^2\right.}{\left(\sqrt{1+d^2}-d\right)^2\left[\left(\sqrt{1+d^2}+d\right)^2+x^2+y^2+(z-\sqrt{1+d^2})^2\right.} \\
&\frac{\left.+2\left(z-\sqrt{1+d^2}\right)\left(\sqrt{1+d^2}-d\right)\right]}{\left.+2\left(z-\sqrt{1+d^2}\right)\left(\sqrt{1+d^2}+d\right)\right]} \\
&= \frac{1}{2}\log\left(d+\sqrt{1+d^2}\right)^4 + \frac{1}{2}\log\frac{x^2+y^2+\left(z-\sqrt{1+d^2}+\sqrt{1+d^2}-d\right)^2}{x^2+y^2+\left(z-\sqrt{1+d^2}+\sqrt{1+d^2}+d\right)^2} \\
&= 2\log\left(d+\sqrt{1+d^2}\right) - \frac{1}{2}\log\frac{x^2+y^2+(z+d)^2}{x^2+y^2+(z-d)^2} \\
&= 2\tau_2 - \tau,
\end{aligned}
$$

where in the above we have utilised:

$$
\begin{aligned}
&\tilde{x}^2+\tilde{y}^2+(\tilde{z}\pm d)^2 \\
&\quad= \frac{x^2+y^2+\left[z-\sqrt{1+d^2}+\left(x^2+y^2+(z-\sqrt{1+d^2})^2\right)\left(\sqrt{1+d^2}\pm d\right)\right]^2}{x^2+y^2+(z-\sqrt{1+d^2})^2}.
\end{aligned}
$$

Making use of the following identities:

$$
\begin{aligned}
\tilde{R}^2-d^2 &= \frac{x^2+y^2+\left[z-\sqrt{1+d^2}+\sqrt{1+d^2}\left(x^2+y^2+(z-\sqrt{1+d^2})^2\right)\right]^2}{\left(x^2+y^2+(z-\sqrt{1+d^2})^2\right)^2} \\
&\quad+\frac{d^2\left(x^2+y^2+(z-\sqrt{1+d^2})^2\right)^2}{\left(x^2+y^2+(z-\sqrt{1+d^2})^2\right)^2} \\
&= \frac{1+2\sqrt{1+d^2}\left(z-\sqrt{1+d^2}\right)+(1+d^2)\left(x^2+y^2+(z-\sqrt{1+d^2})^2\right)}{x^2+y^2+(z-\sqrt{1+d^2})^2} \\
&\quad-\frac{d^2\left(x^2+y^2+(z-\sqrt{1+d^2})^2\right)}{x^2+y^2+(z-\sqrt{1+d^2})^2} \\
&= \frac{1+d^2-d^2+2\sqrt{1+d^2}\left(z-\sqrt{1+d^2}\right)+x^2+y^2+(z-\sqrt{1+d^2})^2}{x^2+y^2+(z-\sqrt{1+d^2})^2} \\
&= \frac{x^2+y^2+\left(z-\sqrt{1+d^2}+\sqrt{1+d^2}\right)^2-d^2}{x^2+y^2+(z-\sqrt{1+d^2})^2} \\
&= \frac{x^2+y^2+z^2-d^2}{x^2+y^2+(z-\sqrt{1+d^2})^2} \\
&= \frac{R^2-d^2}{x^2+y^2+(z-\sqrt{1+d^2})^2},
\end{aligned}
$$

and

$$\begin{aligned}\tilde{Q} &= \sqrt{\left(\tilde{R}^2 + d^2\right)^2 - (2d\tilde{z})^2} = \sqrt{\left(\tilde{R}^2 + d^2 + 2d\tilde{z}\right)\left(\tilde{R}^2 + d^2 - 2d\tilde{z}\right)} \\ &= \sqrt{\left(\tilde{x}^2 + \tilde{y}^2 + (\tilde{z} + d)^2\right)\left(\tilde{x}^2 + \tilde{y}^2 + (\tilde{z} - d)^2\right)} \\ &= \frac{\sqrt{\left(x^2 + y^2 + (z + d)^2\right)\left(x^2 + y^2 + (z - d)^2\right)}}{x^2 + y^2 + (z - \sqrt{1 + d^2})^2} \\ &= \frac{Q}{x^2 + y^2 + (z - \sqrt{1 + d^2})^2},\end{aligned}$$

we obtain that:

$$\tilde{\sigma} = \arccos\left(\frac{\tilde{R}^2 - d^2}{\tilde{Q}}\right) = \arccos\left(\frac{\frac{R^2 - d^2}{x^2+y^2+(z-\sqrt{1+d^2})^2}}{\frac{Q}{x^2+y^2+(z-\sqrt{1+d^2})^2}}\right) = \arccos\left(\frac{R^2 - d^2}{Q}\right) = \sigma.$$

Finally, from the definition of $\tilde{x}$ and $\tilde{y}$ from (C.1) we see that:

$$\tilde{\phi} = \arctan\left(\frac{\tilde{y}}{\tilde{x}}\right) = \arctan\left(\frac{\frac{y}{x^2+y^2+(z-\sqrt{1+d^2})^2}}{\frac{x}{x^2+y^2+(z-\sqrt{1+d^2})^2}}\right) = \arctan\left(\frac{y}{x}\right) = \phi.$$

C.3 Proof of $(\tau_c, \sigma_c, \phi_c) = (2\tau_2, 0, 0)$

We want to prove that the position $(\tau_c, \sigma_c, \phi_c)$ of the centre of the sphere in bispherical coordinates is equal to $(2\tau_2, 0, 0)$. The angular component ϕ_c is zero given the fact that the point is on the Ox axis. The centre of the sphere can be written as:

$$(x_c, y_c, z_c) = \left(0, 0, \sqrt{1 + d^2}\right).$$

Making use of the following:

$$\begin{aligned}R &= \sqrt{{x_c}^2 + {y_c}^2 + {z_c}^2} = \sqrt{1 + d^2}, \\ Q &= \sqrt{\left(1 + d^2 + d^2\right)^2 - 4d^2\left(1 + d^2\right)} = \sqrt{\left(1 + d^2 - d^2\right)^2} = 1,\end{aligned}$$

we obtain the τ-component as:

$$\tau_c = \operatorname{arcsinh}\left(\frac{2dz_c}{Q}\right) = \operatorname{arcsinh} 2d\sqrt{1 + d^2} = \log\left(2d\sqrt{1 + d^2} + \sqrt{4d^2\left(1 + d^2\right) + 1}\right)$$

$$= \log\left(2d\sqrt{1+d^2}+2d^2+1\right) = \log\left(d+\sqrt{1+d^2}\right)^2 = 2\log\left(d+\sqrt{1+d^2}\right)$$
$$= 2\tau_2.$$

Finally, the σ-component we have:

$$\sigma_c = \arccos\left(\frac{R^2-d^2}{Q}\right) = \arccos\left(\frac{1+d^2-d^2}{1}\right) = \arccos 1 = 0.$$

C.4 Bispherical integral

From (Jeffery, 1912, p.118) we know the following properties of Legendre polynomials:

$$\int_0^\pi \frac{P_n(\cos\sigma_0)\sin\sigma_0}{(\cosh\tau_0-\cos\sigma_0)^{\frac{1}{2}}}\,\mathrm{d}\sigma_0 = \frac{2\sqrt{2}}{2n+1}\mathrm{e}^{-\left(n+\frac{1}{2}\right)\tau_0},$$
$$\int_0^\pi \frac{P_n(\cos\sigma_0)\sin\sigma_0}{(\cosh\tau_0-\cos\sigma_0)^{\frac{3}{2}}}\,\mathrm{d}\sigma_0 = 2\sqrt{2}\frac{\mathrm{e}^{-\left(n+\frac{1}{2}\right)\tau_0}}{\sinh\tau_0}.$$

C.5 Legendre polynomial expansion

A generating function for Legendre polynomials P_n is given by (Barton, 1989, p.417):

$$\frac{1}{(1-2xt+t^2)^{\frac{1}{2}}} = \sum_{n=0}^{\infty} P_n(x)t^n. \tag{C.2}$$

Differentiating with respect to t and multiplying by $2t$ we obtain:

$$t\frac{-2x+2t}{(1-2xt+t^2)^{\frac{3}{2}}} = \sum_{n=0}^{\infty} 2nP_n(x)t^n. \tag{C.3}$$

Adding (C.2) and (C.3) we have after rearrangement:

$$\frac{1}{(1-2xt+t^2)^{\frac{3}{2}}} = \sum_{n=0}^{\infty}(2n+1)\,P_n(x)\frac{t^n}{1-t^2}.$$

Repeating the previous step we arrive at:

$$\frac{1}{(1-2xt+t^2)^{\frac{5}{2}}} = \sum_{n=0}^{\infty}\left[\frac{(2n+3)\,(2n+1)}{3}\frac{t^n}{(1-t^2)^2}+\frac{4}{3}(2n+1)\frac{t^{n+2}}{(1-t^2)^3}\right]P_n(x). \tag{C.4}$$

Let $x = \cos\sigma$ and $t = \mathrm{e}^{-\tau}$ in (C.4) we obtain:

$$\frac{1}{(\cosh\tau - \cos\sigma)^{\frac{5}{2}}} = \sum_{n=0}^{\infty} U_n(\tau) P_n(\cos\sigma),$$

where

$$U_n(\tau) = \sqrt{2}\left[\frac{(2n+3)\,(2n+1)}{3}\frac{\mathrm{e}^{-\left(n+\frac{1}{2}\right)\tau}}{\sinh^2\tau} + \frac{2}{3}\,(2n+1)\,\frac{\mathrm{e}^{-\left(n+\frac{3}{2}\right)\tau}}{\sinh^3\tau}\right]. \tag{C.5}$$

Appendix D

Difference equations

D.1 Theorems

For the theorems of this section we have used (Milne-Thomson, 2000, p.523-534).

D.1.1 Poincaré's theorem

If $u(n)$ is any solution of a homogeneous linear difference equation whose coefficients tend to constants, when $n \to \infty$, then:

$$\lim_{n\to\infty} \frac{u(n+1)}{u(n)},$$

exists and is equal to one of the zeros of the characteristic equation of the associated difference equation with constant coefficients if the moduli of the zeroes of the characteristic equation are distinct.

D.1.2 Perron's theorem

If the coefficients of $u(n)$ in the difference equation of order n are not zero where $n = 0, 1, 2, \ldots$, and the other hypotheses be fulfilled, then the equation has n fundamental solutions $u_1(n), \ldots, u_n(n)$ such that

$$\lim_{n\to\infty} \frac{u_i(n+1)}{u_i(n)} = \alpha_i, \quad i = 1, 2, 3, \ldots, n,$$

where α_i is a root of the characteristic equation.

D.2 Continued fraction theorem

We begin by defining the following:

$$z_s = \frac{x_s - x_{s+1}}{x_s - x_{s+2}} \frac{x_{s+2} - x_{s+3}}{x_{s+1} - x_{s+3}}, \quad s \in \{1, 2, 3, \ldots, n-3\},$$
$$v_s = \frac{x_n - x_s}{x_n - x_{s+1}} \frac{x_{s+1} - x_{s+2}}{x_s - x_{s+2}}, \quad v_{n-2} = 1,$$

from which results:

$$\frac{z_s}{v_{s+1}} = \frac{x_s - x_{s+1}}{x_s - x_{s+2}} \frac{x_n - x_{s+2}}{x_n - x_{s+1}},$$

and subsequently:

$$1 - \frac{z_s}{v_{s+1}} = v_s, \quad s \in \{1, 2, 3, \ldots, n-3\}. \tag{D.1}$$

Letting $s = 1$ in the above we have:

$$v_1 = 1 - \frac{z_1}{v_2} = 1 - \frac{z_1}{1 - \frac{z_2}{v_3}}.$$

Applying (D.1) multiple times we obtain:

$$v_1 = 1 - \frac{z_1}{1 - \frac{z_2}{1 - \cdots}}. \tag{D.2}$$

Let us now consider the following Poincare difference equation:

$$u(n+2) + p(n)u(n+1) + q(n)u(n) = 0, \tag{D.3}$$

where

$$\lim_{n\to\infty} p(n) = a_1, \quad \lim_{n\to\infty} q(n) = a_2.$$

As a result, the characteristic equation of (D.3) is

$$t^2 + a_1 t + a_2 = 0,$$

which we suppose has two roots α and β such that $|\alpha| > |\beta|$.
Let $u_1(n)$ and $u_2(n)$ be a fundamental system of solutions from which we obtain from the difference equation:

$$p(n) = \frac{u_1(n+2)u_2(n) - u_2(n+2)u_1(n)}{u_1(n)u_2(n+1) - u_2(n)u_1(n+1)},$$

$$q(n) = \frac{u_1(n+1)u_2(n+2) - u_2(n+1)u_1(n+2)}{u_1(n)u_2(n+1) - u_2(n)u_1(n+1)},$$

Taking

$$x_s = \frac{u_1(n+s-2)}{u_2(n+s-2)},$$

then we obtain

$$z_s = \frac{q(n+s-1)}{p(n+s-2)p(n+s-1)}. \tag{D.4}$$

Performing the change of variables $n \to n+2$ we obtain after simplifications:

$$v_s - 1 = \frac{u_1(n+m)u_2(n+1) - u_2(n+m)u_1(n+1)}{u_1(n+m)u_2(n) - u_2(n+m)u_1(n)} \frac{1}{p(n-1)}.$$

Substituting in (D.2) and making use of (D.4) we have the identity:

$$\frac{u_1(n+m)u_2(n+1) - u_2(n+m)u_1(n+1)}{u_1(n+m)u_2(n) - u_2(n+m)u_1(n)} \equiv \frac{-q(n)}{p(n) - \frac{q(n+1)}{p(n+1) - \cdots - \frac{q(n+m+1)}{p(n+m+1)}}}. \tag{D.5}$$

We notice that the right-hand side of the previous equation is only dependent on the coefficients of the difference equation (D.3) and is therefore independent of the fundamental system of solutions we have chosen. As a result, we choose our fundamental solutions such that:

$$\lim_{m\to\infty} \frac{u_1(n+m+1)}{u_1(n+m)} = \alpha, \quad \lim_{m\to\infty} \frac{u_2(n+m+1)}{u_2(n+m)} = \beta,$$

which is possible given Perron's theorem D.1.2. Therefore

$$\lim_{n\to\infty} \left| \frac{u_2(n+m+1)}{u_1(n+m+1)} \frac{u_1(n+m)}{u_2(n+m)} \right| = \left| \frac{\beta}{\alpha} \right| < 1,$$

from which we deduce that:

$$\lim_{n\to\infty} \frac{u_2(n+m)}{u_1(n+m)} = 0.$$

Dividing the numerator and denominator of (D.5) by $u(n+1)$ and we let $n \to \infty$ to obtain:

$$\frac{u_2(n+1)}{u_2(n)} = \frac{-q(n)}{p(n) - \frac{q(n+1)}{p(n+1) - \cdots}},$$

and $u_2(n)$ is obtained as a solution of the equation of the first order.

Analogously, by performing the change of variables $n \to -t-2$ in the difference equation we obtain a second solution given by:

$$\frac{u_3(n)}{u_3(n+1)} = \frac{-1}{p(n-1) - \frac{q(n-2)}{p(n-2)-\cdots}}.$$

Appendix E

Numerical simulations

E.1 Experimental methodology

The *Coxiella* bacteria are stained using the following process:

- the infected cells are washed twice with 0.5 ml of PS (phosphate-buffered saline);
- they are covered with 4 % paraformaldehyde, fumigated out of the cabinet and stored at 4 for more than 40 hours;
- the paraformaldehyde is removed and 200m μl cell perm/fix buffer (BD biosciences) is added in each well to permeablise the cells and are left for 20 minutes at room temperature;
- 2 μl of anti-Coxiella LPS (lipopolysaccharides) antibody (BBI) is added to each well and left for 1 hour at room temperature in order for the antibodies to bind to the Coxiella;
- the cells are washed with PBS;
- 2 μl of FITC (Fluorescein isothiocyanate) labeled anti-mouse antibody (Invitrogen) is added to each well and left for 1 hour at room temperature which labels the previous antibodies green;
- cells are washed and left in PBS;

- the cells are viewed under laser confocal microscope (LSM 710, Zeiss) using $488nm$ laser;
- images are processed using Zeiss Zen 2012 Blue software;

E.2 Robin boundary condition

Suppose $p(\mathbf{x})$ is a function which satisfies the following Robin boundary condition:

$$\nabla_{\mathbf{n}} p = \kappa p$$

where $\mathbf{n}$ is the normal vector to the surface and κ is the trapping rate. If $\kappa \to 0$ then:

$$\nabla_{\mathbf{n}} p = 0$$

and the boundary becomes reflecting, while if $\kappa \to \infty$ then:

$$p = 0$$

and the boundary becomes absorbing.

E.3 Numerical algorithm

In order to simulate $p(x,t)$ we use the following algorithm(Erban & Chapman, 2007, p.4):

- we distribute N particles uniformly over the interval $[0,h]$;
- let Δt be the timestep. and $x_i(t), i = 1,\ldots,N$ be the position of the i-th particle at time t. The the position $x_i(t+\Delta t)$ is given by:

$$x_i(t+\Delta t) = x_i(t) + \Delta x \tag{E.1}$$

  where $\Delta x \sim N(0, 2D\Delta t)$ and D is the diffusion coefficient.
- if a particle crosses the reflecting boundary at step i then position x_{i+1} is given by:

$$x_i(t+\Delta t) = 2h - x_i(t) - \Delta x$$

- for the partially absorbing boundary we utilise the following:
  - if $x_i < 0$ then $x_i(t + \Delta t) = -x_i(t) - \Delta x$ with probability $1 - P\sqrt{\Delta t}$, where $P = \kappa\sqrt{\pi}/2\sqrt{D}$, otherwise the particle is removed from the system.
  - if $x_i > 0$ the particle is removed from the system with probability

$$\mathrm{e}^{-\frac{x_i x_{i+1}}{D\Delta t}} P\sqrt{\Delta t} \tag{E.2}$$

- at the end of each time step the position of each particle is recorded which gives $p(x, t)$.

Appendix F

Tables

This appendix contains tables of different parameters used in this thesis.

Table F.1: *Coxiella burnetii* assay parameters

Parameter	Definition	Value
b	radius of assay well	$\frac{1}{\sqrt{\pi}}\,\mathrm{cm}$
h	height of assay well	$1\,\mathrm{cm}$
κ	trapping rate	$762\,\mathrm{cm\,s^{-1}}$
D	diffusion coefficient	$0.5\,\mathrm{cm^2\,s^{-1}}$
N	initial number of monocytes	1.5×10^5
MOI	multiplicity of infection	2×10^2
M_0	initial number of bacteria	3×10^7

Appendix G

Python code

This appendix contains the Python code used to produce plots in this thesis.

G.1 Grayscale interval plot

```
"""We plot the cummulative distribution function of the
   grayscale distribution of
the image provided by dstl for the monocytes covering the
   bottom of the
assay well"""
from PIL import Image
import matplotlib.pyplot as plt
import numpy as np
"""We change the python plot such that it does not have
   upper or rightward
border"""
fig = plt.figure(frameon=False)
ax = plt.subplot(111)
ax.spines['top'].set_visible(False)
ax.spines['right'].set_visible(False)
ax.yaxis.set_ticks_position('left')
ax.xaxis.set_ticks_position('bottom')
"""We upload the dstl image"""
imag = Image.open("preinfection2thesis.jpg")
```

```
"""Convert the image te RGB if it is a .gif for example"""
imag = imag.convert ('RGB')
"""We record the height and width of the image in pixels"""
width, height = imag.size
"""We define a matrix of -1 of the same size as the iamge
    """
cdens = np.ones(shape=(width,height))*(-1)
z1,z2=np.linspace(width,0,width),np.linspace(0,height,
    height)
def open_image(path):
  newImage = Image.open(path)
  return newImage
"""Save Image"""
def save_image(image, path):
  image.save(path, 'png')
"""Create a new image with the given size"""
def create_image(i, j):
  image = Image.new("RGB", (i, j), "white")
  return image
"""Get the pixel from the given image"""
def get_pixel(image, i, j):
    width, height = image.size
    if i > width or j > height:
      return None
    """Get Pixel"""
    pixel = image.getpixel((i, j))
    return pixel
X,Y = 15,240
def convert_grayscale(image,X):
  """Get size"""
  width, height = image.size
  S = 0
  """Transform to grayscale"""
  for i in range(width):
      for j in range(height):
          """Get Pixel"""
```

```
            pixel = get_pixel(image, i, j)
            """Get R, G, B values (This are int from 0 to
               255)"""
            red =   pixel[0]
            green = pixel[1]
            blue =  pixel[2]
            """Transform to grayscale"""
            gray = int(1/3*(red+green+blue))
            if gray<=X or gray>=255-X:
                S += 1
    """Return grayscale cumulative distribution"""
    return  S/(width*height)
N=127
x=np.linspace(0,N,N+1)
y=[]
for i in x:
    print(i)
    y.append(convert_grayscale(imag,i))
plt.plot(x,y)
"""We highlight the grayscale value for which the monocytes
    occupy 1/3 of the
 image"""
plt.axvline(x=15,ymin=0,ymax=convert_grayscale(imag,15),
   color='r')
plt.axhline(y=convert_grayscale(imag,15),xmin=0,xmax
   =1500/12700, color='r')
plt.xticks([0,15,64,128], [0,15,64,128],fontsize=14)
plt.gca().get_xticklabels()[1].set_color("red")
plt.yticks([0,convert_grayscale(imag,15),0.5,1], [0,'%.2f'%
   convert_grayscale(imag,15),0.5,1],fontsize=14)
plt.gca().get_yticklabels()[1].set_color("red")
plt.xlim([0,128])
plt.ylim([0,1])
plt.xlabel(r'$x$',fontsize=20)
plt.ylabel(r'$CDF(x)$',fontsize=20)
plt.tight_layout()
```

```
plt.savefig("ColormapIntervalNumber.pdf")
plt.show()
```

G.2 Grayscale heat map

```
"""We plot the grayscale trasformation of the image
   provided by dstl for the
monocytes covering the bottom of the assay well"""
from PIL import Image
import matplotlib.pyplot as plt
import numpy as np
imag = Image.open("preinfection2thesis.jpg")
"""Convert the image te RGB if it is a .gif for example"""
imag = imag.convert ('RGB')
"""We record the height and width of the image in pixels"""
width, height = imag.size
"""We define a matrix of -1 of the same size as the iamge
   """
cdens = np.ones(shape=(width,height))*(-1)
z1,z2=np.linspace(width,0,width),np.linspace(0,height,
   height)
def open_image(path):
  newImage = Image.open(path)
  return newImage
"""Save Image"""
def save_image(image, path):
  image.save(path, 'png')
"""Create a new image with the given size"""
def create_image(i, j):
  image = Image.new("RGB", (i, j), "white")
  return image
"""Get the pixel from the given image"""
def get_pixel(image, i, j):
    # Inside image bounds?
    width, height = image.size
```

```
    if i > width or j > height:
      return None
    # Get Pixel
    pixel = image.getpixel((i, j))
    return pixel
X,Y = 15,240
def convert_grayscale(image):
  """Get size"""
  width, height = image.size
  print(width,height)
  S = 0
  """Create new Image and a Pixel Map"""
  new = create_image(width, height)
  pixels = new.load()
  """Transform to grayscale"""
  for i in range(width):
      for j in range(height):
          """Get Pixel"""
          pixel = get_pixel(image, i, j)
          """Get R, G, B values (This are int from 0 to
             255)"""
          red =   pixel[0]
          green = pixel[1]
          blue =  pixel[2]
          """Transform to grayscale
          gray = (red * 0.299) + (green * 0.587) + (blue *
             0.114)"""
          gray = int(1/3*(red+green+blue))
          if gray<=X or gray>=Y:
              pixels[i, j] = (int(255),0,0)
              S += 1
          else:
              pixels[i, j] = (0,0,int(255))
  """Return new image"""
  return new, S/(width*height)*100
plt.imshow(convert_grayscale(imag)[0])
```

```
plt.savefig("GrayscaleColormapInterval.pdf")
plt.show()
```

G.3 Intracellular distribution of *Coxiella burnetii*

```
"""We plot the intracellular distribution of Coxiella
   burnetii"""
import numpy as np
from scipy.spatial.distance import pdist, squareform
import matplotlib.pyplot as plt
import math
import scipy.special as sp
import csv
from scipy.optimize import brentq
from decimal import *
getcontext().prec = 40
"""We change the python plot such that it does not have
   upper or rightward
border"""
fig = plt.figure(frameon=False)
ax = plt.subplot(111)
ax.spines['top'].set_visible(False)
ax.spines['right'].set_visible(False)
ax.yaxis.set_ticks_position('left')
ax.xaxis.set_ticks_position('bottom')
def Func(y):
    return y/K*np.sin(y*h)-np.cos(y*h)
"""We define the signchange function which we will help us
   find the solutions
of the Bessel function defined above"""
def signchange(r,f,start):
    sol=[]
    before=start
    sol.append(before)
    for x in r:
```

```
        if x>before and f(x)*f(before)<0:
            before=x
            sol.append(before)
    return sol
"""We define the root_finder function which will find the
   solutionsof the
Bessel function defined above"""
def root_finder(r,f):
    roots=[]
    for n in range(len(r)-1):
        roots.append(brentq(f, r[n], r[n+1], ()))
    return roots
"""We define the survival function"""
def Survival(x,n,W,K):
    s=0.0
    for j in range(0,n+1):
        A_ij=1/(W[j]**2*(h/2*(W[j]**2/K**2+1)+1/(2*K)))
        s+=A_ij/h*np.exp(-(W[j]**2)*D*x)
    return s
"""We define the Poisson distribution"""
def Poisson(n,m):
    return np.exp(-m)*m**n/sp.factorial(n)
"""We define the radius of the assay well, the trapping
   rate, the diffusion
coefficient, the fraction of the spherical surface covered
   in absorbing disks,
the number of traps and the number of diffusing particles
   """
global b,K,h,D,sigma,N,C0
b=1/np.sqrt(np.pi)
K=0
h=1
D=0.5
sigma=0
N=150000
C0=200*N
```

```
"""We upload the data provided by Dstl for the radius of
   the radius of the
trap"""
coxiella_radius_1=[]
with open('Expt4_THP1_CellSize.csv') as csvfile:
    readCSV = csv.reader(csvfile, delimiter=',')
    for row in readCSV:
        coxiella_radius_1.append(row[0])
coxiella_radius_1=np.delete(coxiella_radius_1, 0, axis=0)
coxiella_radius_1=[np.sqrt((float(x)*10**(-14))/np.pi) for
   x in coxiella_radius_1]
coxiella_radius_2=[]
with open('Expt5_THP1_CellSize.csv') as csvfile:
    readCSV = csv.reader(csvfile, delimiter=',')
    for row in readCSV:
        coxiella_radius_2.append(row[0])
coxiella_radius_2=np.delete(coxiella_radius_2, 0, axis=0)
coxiella_radius_2=[np.sqrt((float(x)*10**(-14))/np.pi) for
   x in coxiella_radius_2]
coxiella_radius=coxiella_radius_1+coxiella_radius_2
"""We upload the position of the traps"""
txt=str("DATAfile_3D_Gillard_Position_Traps_1.0")+str(".txt
   ")
text_file = open(txt, "r")
lines = text_file.read().split()
pos_x=[]
pos_y=[]
pos_z=[]
for i in range(len(lines)):
    if i%3==0:
        pos_x.append(float(lines[i]))
    if i%3==1:
        pos_y.append(float(lines[i]))
    if i%3==2:
        pos_z.append(float(lines[i]))
print(len(pos_x),len(pos_y),len(pos_z))
```

```
pos=np.c_[pos_x, pos_y, pos_z]

"""We plot the intracellular distribution of the capture
   Coxiella burnetii at
different times"""
Color=['ro','bo','go']
Ts=[0.01,0.05,0.1]
for i in [0,1,2]:
    ts=Ts[i]
    K=0
    Radius=np.mean(coxiella_radius)*np.ones(N)
    sigma=np.pi*sum([x**2 for x in Radius])
    def f(sigma):
        return (1+3.8*sigma**(5/4))/(1-sigma)
    for r_i in Radius:
        V = np.pi*r_i**2/sigma
        K += 4*V*D/(np.pi*r_i)*sigma*f(sigma)
    K=K/D
    x = np.linspace(0.001, 6000, 5000)
    S=Survival(ts,500,root_finder(signchange(x,Func
       ,0.00000001),Func),K)
    M=int(C0*(1-S))
    m=M/N
    print(m,'hello')
    Q=70
    n=np.linspace(0,Q,Q+1)
    ax.plot(n,Poisson(n,m),Color[i],label=r'$t$ = '+str(ts)
       )
plt.xlabel(r'$r$',fontsize=20)
plt.ylabel(r'$f(r|t,\kappa)$',fontsize=20)
plt.legend(loc=1,fontsize=15,frameon=False)
plt.xlim([-0.5,Q])
plt.xticks([0,35,70], [r'0',r'35',r'70'],fontsize=14)
plt.yticks([0,0.10,0.20], [r'0',r'0.1',r'0.2'],fontsize=14)
plt.tight_layout()
plt.savefig('Intracellular_Distribution.pdf')
```

```
plt.show()
```

G.4 Survival function for circular domains

G.4.1 Numerical simulations

```
"""
Simulation of diffusing particles inside a concentric
   annular region bounded
two circles. The outher circle is reflecting and the inner
   circle is absorbing.
We record the number of particles still alive at each time
   step in order to
determine the survival function
"""
import random as random
import numpy as np
from scipy.spatial.distance import pdist, squareform
import matplotlib.pyplot as plt
import matplotlib.animation as animation
import math

class ParticleBox:
    """
    init_state is an [N x 2] array, where N is the number
       of particles:
       [[x1, y1],
        [x2, y2],
        ...               ]

    bounds is the size of the box: [xmin, xmax, ymin, ymax]
    """
    def __init__(self,
                 init_state = [[1, 0],
                               [-0.5, 0.5],
```

```
                                [-0.5, -0.5]],
                bounds = [-10, 10, -10, 10],
                size = 0.00,
                M = 0.05,
                G = 9.8):
        self.init_state = np.asarray(init_state, dtype=
            float)
        self.M = M * np.ones(self.init_state.shape[0])
        self.size = size
        self.state = self.init_state.copy()
        self.time_elapsed = 0
        self.bounds = bounds
        self.G = G
    def step(self, dt):
        global nr,time, init_k, nrprt, b, a, c, D
        """step once by dt seconds"""
        self.time_elapsed += dt
        """We create a copy of the particle positions"""
        self.state_backup=self.state.copy()
        """We update the position of the particles"""
        self.state[:,1] += np.random.normal(0,np.sqrt(2*D*
            dt),nrprt)
        self.state[:,0] += np.random.normal(0,np.sqrt(2*D*
            dt),nrprt)
        """We determine which particles have crossed inside
             the nucleus and we
        delete them"""
        Distance_1 = np.where(self.state[:, 0]**2+(self.
            state[:, 1]+c)**2<(a)**2)
        self.state[Distance_1,0]=0
        self.state[Distance_1,1]=-c
        self.state=np.delete(self.state, Distance_1, axis
            =0)
        self.state_backup=np.delete(self.state_backup,
            Distance_1, axis=0)
        nrprt=len(self.state[:,0])
```

```
        state_backup_2=self.state.copy()
        """We determine which particles have crossed the
           cellular surface and
        we reflect them"""
        Distance_2 = np.where(self.state[:, 0]**2+self.
           state[:, 1]**2>(b)**2)
        self.state[Distance_2,1]=(2*b-np.sqrt(
           state_backup_2[Distance_2,0]**2+state_backup_2[
           Distance_2,1]**2))*np.sin(np.arctan2(
           state_backup_2[Distance_2,1], state_backup_2[
           Distance_2,0]))
        self.state[Distance_2,0]=(2*b-np.sqrt(
           state_backup_2[Distance_2,0]**2+state_backup_2[
           Distance_2,1]**2))*np.cos(np.arctan2(
           state_backup_2[Distance_2,1], state_backup_2[
           Distance_2,0]))
        """We determine which particles have crossed the
           boundary of nucleus
        between the beginning and end of the time step. We
           delete these
        particles"""
        r1=[math.sqrt(x**2+y**2) for x,y in zip(self.state
           [:,0],self.state[:,1])]
        r2=[math.sqrt(x**2+y**2) for x,y in zip(self.
           state_backup[:,0],self.state_backup[:,1])]
        C=[math.exp(-1*(a-R1)*(a-R2)/(D*dt)) for R1,R2 in
           zip(r1,r2)]
        u=np.random.uniform(0,1,nrprt)
        sterg=np.where(C>u)
        self.state=np.delete(self.state, sterg, axis=0)
        nrprt=len(self.state[:,0])
        time+=dt
        """We record the number of particles stll remaining
            and the time"""
        if nrprt!=0:
                file.write(str(nrprt)+" "+str(time)+" ")
```

```
        else:
            file.close()
global nrprt, nr, tlist, nlist, time, init_k,b, a, c,D
"Outer radius"
b=1
"Inner radius"
a=0.1
"Position of nucleus"
c=0
"Diffusion coefficient"
D=0.5
txt=str("SurvFile.txt")
file = open(txt, "w")
time=0
nrprt=100000
""" set up initial state """
p=0
np.random.seed()
"""We create 10^5 particles which will diffuse in the
   annular region"""
init_state= np.random.uniform(-b,b,(nrprt, 2))
n=[]
m=[]
for i in range(nrprt):
    if ((a)**2<=(init_state[i, 0])**2+(init_state[i, 1]+c)
       **2)and(init_state[i, 0])**2+init_state[i, 1]**2<=(b
       )**2:
        p+=1
        n.append(init_state[i,0])
        m.append(init_state[i,1])
init_state_1=np.c_[n, m]
nrprt=p
move=np.ones(nrprt)
tlist=[0]
nlist=[nrprt]
box = ParticleBox(init_state_1, size=0.004)
```

```
dt = 0.0001
""" set up figure and animation """
fig = plt.figure()
fig.subplots_adjust(left=0, right=1, bottom=0, top=1)
ax = fig.add_subplot(111, aspect='equal', autoscale_on=
   False,
                     xlim=(-1.1, 1.1), ylim=(-1.1, 1.1))
""" particles holds the locations of the particles """
particles, = ax.plot([], [], 'ro', ms=6)
""" rect is the box edge """
rect = plt.Rectangle(box.bounds[::2],
                     box.bounds[1] - box.bounds[0],
                     box.bounds[3] - box.bounds[2],
                     ec='none', lw=2, fc='none')
circle_1=plt.Circle((0,0),b,color='b',fill=False)
circle_2=plt.Circle((0,-c),a,color='b',fill=False)
ax.add_patch(rect)
ax.add_patch(circle_1)
ax.add_patch(circle_2)
def init():
    """ initialize animation """
    global box, rect
    particles.set_data([], [])
    rect.set_edgecolor('none')
    return particles, rect
def animate(i):
    """perform animation step """
    global box, rect, dt, ax, fig, circle
    box.step(dt)
    ms = int(fig.dpi * 2 * box.size * fig.get_figwidth()
             / np.diff(ax.get_xbound())[0])
    """ update pieces of the animation """
    rect.set_edgecolor('none')
    particles.set_data(box.state[:, 0], box.state[:, 1])
    particles.set_markersize(ms)
    return particles, rect
```

```
ani = animation.FuncAnimation(fig, animate, frames=100,
                              interval=10, blit=True,
                                 init_func=init)
plt.show()
```

G.4.2 Figure plot

```
"""
We plot the two dimensional survival function for a
   Brownian particle diffusing
inside a concentric annular region where the inner boundary
    is absorbing and
the outer boundary is reflecting
"""
import numpy as np
from scipy.spatial.distance import pdist, squareform
import matplotlib.pyplot as plt
import math
import scipy.special as sp
from scipy.optimize import brentq
"""
We define the radius of the cell and the radius of the
   nucleus
"""
b=1
a=0.1
x = np.linspace(0.1, 6000, 5000)
"""We change the python plot such that it does not have
   upper or rightward
border"""
fig = plt.figure(frameon=False)
ax = plt.subplot(111)
ax.spines['top'].set_visible(False)
ax.spines['right'].set_visible(False)
ax.yaxis.set_ticks_position('left')
ax.xaxis.set_ticks_position('bottom')
```

```
def Bessel(y):
    return sp.jv(0,a*y)*sp.yv(1,b*y)-sp.jv(1,b*y)*sp.yv(0,a
       *y)
"""We define the signchange function which we will help us
   find the solutions
of the Bessel function defined above"""
def signchange(r,f,start):
    sol=[]
    before=start
    sol.append(before)
    for x in r:
        if x>before and f(x)*f(before)<0:
            before=x
            sol.append(before)
    return sol
"""We define the root_finder function which will find the
   solutionsof the
Bessel function defined above"""
def root_finder(r,f):
    roots=[]
    for n in range(len(r)-1):
        roots.append(brentq(f, r[n], r[n+1], ()))
    return roots
u = np.linspace(0, 1000, 201)
"""We define the integral of the Bessel function"""
def Bessel_int(a,b,v,j):
    if j==0:
        return (b*sp.jv(1,b*v)-a*sp.jv(1,a*v))/v
    if j==1:
        return (b*sp.yv(1,b*v)-a*sp.yv(1,a*v))/v
"""We define the survival function"""
def Bessel_comp(x,n,v):
    s=0.0
    for i in range(n):
        s+=((np.pi*sp.yv(0,a*v[i])*(sp.yv(1,b*v[i])**2))/((
           sp.yv(1,b*v[i])**2)-(sp.yv(0,a*v[i]))**2))*(
```

```
            Bessel_int(a,b,v[i],0)-(sp.jv(0,a*v[i])/sp.yv(0,
            a*v[i]))*Bessel_int(a,b,v[i],1))*np.exp(-(v[i
            ]**2)*0.5*x)
    return s
v = np.linspace(0, 16, 2001)
"""We plot the survival function"""
plt.semilogy(v,2*Bessel_comp(v,5,root_finder(signchange(x,
   Bessel,0.00000001),Bessel))/(b**2-a**2),label='exact')
plt.xticks([0,9,18],['0','9','18'],fontsize=14)
plt.yticks([1,10**(-2),10**(-4)], [r'$10^0$',r'$10^{-2}$',r
   '$10^{-4}$'],fontsize=16)
plt.xlim([0,18])
"""We upload the survival data from numerical simulations
   """
text_file = open("SurvFile.txt", "r")
lines = text_file.read().split(" ")
text_file.close()
tlist=[0]
nlist=[float(lines[0])]
for i in range(len(lines)-1):
    if i%2==0:
        nlist.append(float(lines[i]))
    else:
        tlist.append(float(lines[i]))
c=nlist[0]
nlist=[x/c for x in nlist]
tlist=[x for x in tlist]
plt.xlabel(r'$t\,$(seconds)',fontsize=16)
plt.ylabel(r'$s(t)$',fontsize=16)
"""We plot the numerical simulations of the survival
   function"""
plt.plot(tlist,nlist,label='numerical')
plt.legend(loc=1,fontsize=14,frameon=False)
plt.tight_layout()
plt.savefig('SurvPlot2D.pdf')
plt.show()
```

G.5 Green's function

G.5.1 $G_1^{(2)}(\mathbf{x}_0, \mathbf{x})$

G.5.1.1 Numerical simulations

```
""" Two space dimensions
mean time to hit target at x from initial position y
makes two contour plots: numerical and analytical"""
from numpy import *
import random
import os, sys
from pylab import contourf,savefig,show,subplot,colorbar,
   clabel,title,figure
import matplotlib.pyplot as plt
import numpy as np
from scipy.integrate import quad
"""We define the radius of the nucleus and the diffusion
   coefficient"""
a=0.1
D=0.5
#Boundary paramenter
BC="NeumanntoDirichlet"
#Starting condition
SC="Uniform"
NR=500000 # number of realisations
dt=0.001
sfac=sqrt(2*D*dt)
random.seed()
"""We define the position of the nulceus and the starting
   position of the
Brownian particles"""
rt=-0.25
rs=-0.35
xt=rt
yt=0.0
```

```
"""We define the matrix which will be used to calculate the
    Green's function"""
N=100
xyhist = np.ones((2*N+1,2*N+1))*(-1)
ireal=0
sumt=0.0
global x,y
x=rs
y=0.0
while ireal < NR:
    ireal += 1
    x=rs
    y=0.0
    t=0.0
    dist1=abs(rt-rs)
#    do ten steps with dt*0.0001
    for i in range(10):
        x += 0.01*sfac*random.gauss(0,1)
        y += 0.01*sfac*random.gauss(0,1)
        t += 0.0001*dt
        rr=(x-xt)*(x-xt)+(y-yt)*(y-yt)
        c=xt
        k=yt
        """If the particle crosses the boundary of the
           nucleus we reflect it"""
        if rr <a*a:
            yy=y
            xx=x
            y=k+(2*a-np.sqrt((xx-c)**2+(yy-k)**2))*np.sin(
               np.arctan2(yy-k, xx-c))
            x=c+(2*a-np.sqrt((xx-c)**2+(yy-k)**2))*np.cos(
               np.arctan2(yy-k, xx-c))
        xyhist[int(round(x*N))+N][int(round(y*N))+N] +=
           0.0001
#    do ten steps with dt*0.01
    for i in range(10):
```

```
        x += 0.1*sfac*random.gauss(0,1)
        y += 0.1*sfac*random.gauss(0,1)
        t += 0.01*dt
        rr=(x-xt)*(x-xt)+(y-yt)*(y-yt)
        c=xt
        k=yt
        """If the particle crosses the boundary of the
           nucleus we reflect it"""
        if rr <a*a:
            yy=y
            xx=x
            y=k+(2*a-np.sqrt((xx-c)**2+(yy-k)**2))*np.sin(
               np.arctan2(yy-k, xx-c))
            x=c+(2*a-np.sqrt((xx-c)**2+(yy-k)**2))*np.cos(
               np.arctan2(yy-k, xx-c))
        xyhist[int(round(x*N))+N][int(round(y*N))+N] +=
           0.01
    while True:
        X=x
        Y=y
        x += sfac*random.gauss(0,1)
        y += sfac*random.gauss(0,1)
        t += dt
        """If the particle crosses the cellular surface we
           determine if it
        absorbed or reflected"""
        r1=np.sqrt(x**2+y**2)
        r2=np.sqrt(X**2+Y**2)
        C=math.exp(-2*min(1-r1,1-r2)/(np.sqrt(D*dt)))
        u=np.random.uniform(0,1,1)
        if C>u:
            sumt += t
            break
        rr=x*x+y*y
        if rr >1:
            sumt += t
```

```
            break
        rr=(x-xt)*(x-xt)+(y-yt)*(y-yt)
        c=xt
        k=yt
        """If the particle crosses the boundary of the
           nucleus we reflect it"""
        if rr <a*a:
            yy=y
            xx=x
            y=k+(2*a-np.sqrt((xx-c)**2+(yy-k)**2))*np.sin(
               np.arctan2(yy-k, xx-c))
            x=c+(2*a-np.sqrt((xx-c)**2+(yy-k)**2))*np.cos(
               np.arctan2(yy-k, xx-c))
        xyhist[int(round(x*N))+N][int(round(y*N))+N] += 1
xyarea=1.0/(N*N)
myrange=0.05*arange(60)
z1,z2=linspace(-1,1,2*N+1),linspace(-1,1,2*N+1)
hist=xyhist.transpose()
CC=hist*dt/(xyarea*NR)
txt=str(BC)+"_"+str(SC)+str(".txt")
file = open(txt, "w")
for i in range(len(CC[:,1])):
    for j in CC[i,:]:
        file.write(str(j)+' ')
file.close()
```

G.5.1.2 Plot

```
"""We plot the numerical simulation for the Green's
   function G_1^{(2)} and
compare them with the analytic formula derived using
   bipolar coordinates"""
import numpy as np
import matplotlib.pyplot as plt
from matplotlib.colors import LogNorm
```

```
from pylab import contourf,savefig,show,subplot,colorbar,
   clabel,title,figure
from matplotlib import cm
matrix = np.random.random((10, 10, 3))
"""We define the radius of the cell, the radisu of the
   nucleus, the diplacement
of the nucleus, the diffusion coefficient, the size of the
   matrix and the
starting position of Brownian particles"""
b=1
a=0.1
c=+0.25
D=0.5
N=100
rs=-0.5
z1,z2=np.linspace(-1,1,2*N+1),np.linspace(-1,1,2*N+1)
(Z1,Z2) = np.meshgrid(z1,z2)
def bipolar(x,y):
    """We convert Cartesian coordinates into bipolar
       coordinates """
    c=+0.25
    d=1/c*(0.25*(b**2+a**2-c**2)**2-a**2*b**2)**0.5
    tau=0.5*np.log(((x+d)**2+y**2)/((x-d)**2+y**2))
    rho=np.pi-np.arctan2(2*d*y,x**2+y**2-d**2)
    return tau,rho
def Green_bipolar_dirichlet_neumann(y1,y2,Z1,Z2,n):
    '''Green function G_1^{(2)}'''
    c=+0.25
    d=1/c*(0.25*(b**2+a**2-c**2)**2-a**2*b**2)**0.5
    A=(b**2+d**2)**0.5
    tau=bipolar(Z1+A,Z2)[0]
    rho=bipolar(Z1+A,Z2)[1]
    tau0=bipolar(y1+A,y2)[0]
    rho0=bipolar(y1+A,y2)[1]
    tau2=np.log(d/b+(1+(d/b)**2)**0.5)
    tau1=np.log(d/a+(1+(d/a)**2)**0.5)
```

```
    ret=0
    if tau>tau0:
        for i in range(1,n):
            ret+=np.cos(i*(rho-rho0))/(i*np.pi)*(np.sinh(i
               *(tau0-tau2))*np.cosh(i*(tau1-tau)))/np.cosh
               (i*(tau2-tau1))
        ret+=1/(2*np.pi)*(tau0-tau2)
    if tau0>tau:
        for i in range(1,n):
            ret+=np.cos(i*(rho-rho0))/(i*np.pi)*(np.sinh(i
               *(tau-tau2))*np.cosh(i*(tau1-tau0)))/np.cosh
               (i*(tau2-tau1))
        ret+=1/(2*np.pi)*(tau-tau2)
    return ret/D
CD = np.ones(shape=(2*N+1,2*N+1))*(-1)
"""We upload the numerical simulations for G_1^{(2)}"""
new_data = np.loadtxt('DatafileNumerical.txt')
new_data = new_data.reshape((2*N+1,2*N+1))
hist=new_data.transpose()
rt=c
x1,x2=rt,0
"""We mask the excluded region and the extracellular region
   """
exterior = np.sqrt((Z1**2) + (Z2**2)) > b
interior = np.sqrt(((Z1+x2)**2) + ((Z2+x1)**2)) < a
hist[interior] = -100
hist[exterior] = -100
HIST=hist.transpose()
z2,z3=np.linspace(-1,1,2*N+1),np.linspace(-1,1,2*N+1)
(Z2,Z3) = np.meshgrid(z2,z3)
rs=-0.5
y1,y2=rs,0
for I in range(2*N+1):
    for J in range(2*N+1):
        CD[I,J]=Green_bipolar_dirichlet_neumann(y1,y2, z1[I
           ], z2[J],200)
```

```
        print(I,J,CD[I,J])
HIST_1=CD.transpose()
"""We mask the excluded region and the extracellular region
   """
exterior = np.sqrt((Z2**2) + (Z3**2)) > b
interior = np.sqrt((Z2+rt)**2 + ((Z3)**2)) < a
HIST_1[interior] = -100
HIST_1[exterior] = -100
"""We take the difference between the numerical simulation
   and the analytic
formula"""
HIST_2=HIST-HIST_1
"""We mask the excluded region and the extracellular region
   """
exterior = np.sqrt((Z2**2) + (Z3**2)) > b
interior = np.sqrt((Z2+rt)**2 + ((Z3)**2)) < a
HIST_2[interior] = -100
HIST_2[exterior] = -100
fig, ax = plt.subplots(1,3, figsize=(12, 3))
plt.subplots_adjust(left=0.05, right=0.85)
myrange=0.05*np.arange(0.0,25)
z2,z3=np.linspace(1,-1,2*N+1),np.linspace(1,-1,2*N+1)
(Z2,Z3) = np.meshgrid(z2,z3)
im=ax[0].contourf(z2,z3,np.rot90(np.rot90(HIST)),myrange,
   cmap=cm.terrain)
"""We change the python plot such that it the window is a
   square and there are
not ticks"""
ax[0].set_aspect("equal")
ax[0].set_xticks([])
ax[0].set_yticks([])
ax[0].set_title('numerical')
"""We draw the outer boundary as a blue circle and the
   inner boundary as a red
circle"""
```

```
circle = plt.Circle((0,0), 1, color='blue', fill=False,
    linewidth=1)
ax[0].add_artist(circle)
circle = plt.Circle((-c,0), a, color='red', fill=False,
    linewidth=1)
ax[0].add_artist(circle)
im=ax[1].contourf(z2,z3,np.rot90(np.rot90(HIST_1)),myrange,
    cmap=cm.terrain)
"""We change the python plot such that it the window is a
    square and there are
not ticks"""
ax[1].set_aspect("equal")
ax[1].set_xticks([])
ax[1].set_yticks([])
ax[1].set_title('exact')
"""We draw the outer boundary as a blue circle and the
    inner boundary as a red
circle"""
circle = plt.Circle((0,0), 1, color='blue', fill=False,
    linewidth=1)
ax[1].add_artist(circle)
circle = plt.Circle((-c,0), a, color='red', fill=False,
    linewidth=1)
ax[1].add_artist(circle)
myrange=0.001*np.arange(-5,5.1)
im2=ax[2].contourf(z2,z3,np.rot90(np.rot90(HIST_2)),myrange
    ,cmap=cm.terrain)
"""We change the python plot such that it the window is a
    square and there are
not ticks"""
ax[2].set_aspect("equal")
ax[2].set_xticks([])
ax[2].set_yticks([])
ax[2].set_title('difference')
"""We draw the outer boundary as a blue circle and the
    inner boundary as a red
```

```
circle"""
circle = plt.Circle((0,0), 1, color='blue', fill=False,
    linewidth=1)
ax[2].add_artist(circle)
circle = plt.Circle((-c,0), a, color='red', fill=False,
    linewidth=1)
ax[2].add_artist(circle)
plt.draw()
"""We add the colorbars to the plot"""
p0 = ax[0].get_position().get_points().flatten()
p1 = ax[1].get_position().get_points().flatten()
p2 = ax[2].get_position().get_points().flatten()
ax_cbar = fig.add_axes([p0[0], 0, p1[2]-p0[0], 0.05])
cb=plt.colorbar(im, cax=ax_cbar, ticks=[0,0.6,1.2],
    orientation='horizontal')
font_size = 12 # Adjust as appropriate.
cb.ax.tick_params(labelsize=font_size)
ax_cbar1 = fig.add_axes([p2[0], 0, p2[2]-p2[0], 0.05])
cb=plt.colorbar(im2, cax=ax_cbar1,ticks=[-0.005,0,0.005],
    orientation='horizontal')
font_size = 12 # Adjust as appropriate.
cb.ax.tick_params(labelsize=font_size)
plt.savefig('twoDcomparisonG1.pdf',bbox_inches='tight')
plt.show()
```

G.6 Average mean time

G.6.1 Numerical simulations

G.6.1.1 From nuclear surface to cellular surface in an eccentric spherical domain

```
"""Brownian simulation start at nucleus and run until hit
    cell surface in two
dimensions"""
```

```
import numpy as np
import scipy.stats as stats
import pylab as pl
import matplotlib.pyplot as plt
from numpy import random as r
from mpmath import csch,coth
"""We define the diffusion coefficient, the radius of the
   nucleus, the radius
of the cell, the number of realisations of the Brownian
   simulations and time
step"""
D = 0.5
a = 0.1
b = 1.0
nreal = 50000
dt = 0.001
def sdistnucl(x,y,z):
    '''square of distance from centre of nucleus'''
    return x**2 + y**2 + (z-c)**2
def sdistsurf(x,y,z):
    ''' square of distance from centre of cell'''
    return x**2 + y**2 + z**2
def reflectnucl(x,y,z):
    ''' find new position by simple reflection off nuclear
       surface'''
    X,Y,Z = x,y,z
    oldr = np.sqrt(sdistnucl(x,y,z))
    z = c+(2*a-oldr)*np.cos(np.arccos((Z-c)/(X**2+Y**2+(Z-c
       )**2)**0.5))
    y = (2*a-oldr)*np.sin(np.arctan2(Y, X))*np.sin(np.
       arccos((Z-c)/(X**2+Y**2+(Z-c)**2)**0.5))
    x = (2*a-oldr)*np.cos(np.arctan2(Y, X))*np.sin(np.
       arccos((Z-c)/(X**2+Y**2+(Z-c)**2)**0.5))
    return x,y,z
def reflectsurf(x,y,z):
```

```
    ''' find new position by simple reflection off cellular
        surface'''
    X,Y,Z = x,y,z
    oldr = np.sqrt(sdistsurf(x,y,z))
    z = (2*b-oldr)*np.cos(np.arccos(Z/(X**2+Y**2+Z**2)
       **0.5))
    y = (2*b-oldr)*np.sin(np.arctan2(Y, X))*np.sin(np.
       arccos(Z/(X**2+Y**2+Z**2)**0.5))
    x = (2*b-oldr)*np.cos(np.arctan2(Y, X))*np.sin(np.
       arccos(Z/(X**2+Y**2+Z**2)**0.5))
    return x,y,z
def expotimeT1(c):
    '''Exponential timestep with boundary test for
       diffusion from the nuclear
    surface to the cellular surface'''
    """We define the initial position of the Brownian
       particle uniformly on the
    surface of the nucleus"""
    X = np.random.uniform(-1,1)
    Y = np.random.uniform(-1,1)
    z = np.random.uniform(-1,1)
    while(X**2+Y**2==1):
        X = np.random.uniform(-1,1)
        Y = np.random.uniform(-1,1)
    x = a*np.sqrt(1-z**2)*(X**2-Y**2)/(X**2+Y**2)
    y = a*np.sqrt(1-z**2)*(2*X*Y)/(X**2+Y**2)
    z = a*z + c
    istep = 0
    r1s = sdistsurf(x,y,z)
    phit = 0
    """While the Brownian particle has not hit the cellular
        surface it will
    keep diffusing"""
    while phit < r.random():
        """We update the position of the Brownian particle
           after one
```

```
        timestep"""
        r0s = r1s
        w = np.sqrt(np.random.normal(0,1)**2+np.random.
           normal(0,1)**2+np.random.normal(0,1)**2)
        mod = pl.sqrt(-2*pl.log(r.random()))*w/nu
        rs = 2.0
        Z = np.random.uniform(-1,1)
        while rs > 1:
            v1,v2 = 2*r.random()-1,2*r.random()-1
            rs = v1*v1+v2*v2
        x += mod*np.sqrt(1-Z**2)*(v1*v1-v2*v2)/rs
        y += mod*np.sqrt(1-Z**2)*2*v1*v2/rs
        z += mod*Z
        """If the particle cross the surface of the nucleus
            it is reflected"""
        if sdistnucl(x,y,z) < a*a:
            x,y,z = reflectnucl(x,y,z)
        istep += 1
        r1s = sdistsurf(x,y,z)
        """We update the probability that the Brownian
           particle hit the
        cellular surface"""
        phit = pl.exp(-2*nu*(b-max(pl.sqrt(r0s),pl.sqrt(r1s
           ))))
    """We return the position of the Brownian particle on
       the cellular surface
    and the number of steps it took to reach the cellular
       surface"""
    return istep
np.random.seed()
dtlist,emlist,esemlist = [],[],[]
sdt = pl.sqrt(2*D*dt)
nu = 1.0/pl.sqrt(D*dt)
txt=str("T1BAR")+str(".txt")
file = open(txt, "w")
```

```
"""We define the range of value the displacement of the
   nucleus takes"""
C=np.linspace(0,1-a,10)
for c in C:
    tone = [dt*expotimeT1(c) for i in range(nreal)]
    print(dt,pl.mean(tone),'+-',stats.sem(tone),)
    print(tone[:5])
    dtlist.append(dt)
    emlist.append(pl.mean(tone))
    esemlist.append(stats.sem(tone))
    """We record the position of the nucleus, the mean time
        and standard error
    of the mean """
    file.write(str(pl.mean(tone))+' '+str(stats.sem(tone))+
       ' ')
file.close()
```

G.6.1.2 Mean round-trip time in an eccentric circular domain

```
"""Brownian simulation start at nucleus, run until hit cell
    surface and then
returns to the nucleus"""
import numpy as np
import scipy.stats as stats
import pylab as pl
from numpy import random as r
from mpmath import csch,coth
import matplotlib.pyplot as plt
"""We define the diffusion coefficient, the radius of the
   nucleus, the radius
of the cell, the number of realisations of the Brownian
   simulations and time
step"""
D = 0.5
a = 0.1
b = 1.0
```

```
nreal = 5000
dt = 0.001
def sdistnucl(x,y):
    '''square of distance from centre of nucleus'''
    return (x-c)**2 + y**2
def sdistsurf(x,y):
    ''' square of distance from centre of cell'''
    return x**2 + y**2
def reflectnucl(x,y):
    ''' find new position by simple reflection off nuclear
       surface'''
    oldr = pl.sqrt(sdistnucl(x,y))
    newr = 2*a-oldr
    return c+(x-c)*newr/oldr,y*newr/oldr
def reflectsurf(x,y):
    ''' find new position by simple reflection off the
       cellular surface'''
    oldr = pl.sqrt(sdistsurf(x,y))
    newr = 2*b-oldr
    return x*newr/oldr,y*newr/oldr
def reflectsurffin(x,y):
    ''' find new position by projecting on the cellular
       surface'''
    oldr = pl.sqrt(sdistsurf(x,y))
    return x/oldr,y/oldr
def expotime1(c):
    '''Exponential timestep with boundary test for
       diffusion from the nuclear
    surface to the cellular surface'''
    """We define the initial position of the Brownian
       particle uniformly on the
    surface of the nucleus"""
    theta = np.random.uniform(0,2*np.pi,1)
    x, y = c + a*np.cos(theta), a*np.sin(theta)
    ir,istep = 0,0
    r1s = sdistsurf(x,y)
```

```
    phit = 0
    """While the Brownian particle has not hit the cellular
        surface it will
    keep diffusing"""
    while phit < r.random():
        """We update the position of the Brownian particle
           after one
        timestep"""
        r0s = r1s
        mod = 2*pl.sqrt(pl.log(r.random())*pl.log(r.random
           ()))/nu
        rs = 2.0
        while rs > 1:
            v1,v2 = 2*r.random()-1,2*r.random()-1
            rs = v1*v1+v2*v2
        x += mod*(v1*v1-v2*v2)/rs
        y += mod*2*v1*v2/rs
        """If the particle crosses the surface of the
           nucleus it is reflected"""
        if sdistnucl(x,y) < a*a:
            x,y = reflectnucl(x,y)
            ir += 1
        istep += 1
        r1s = sdistsurf(x,y)
        """We update the probability that the Brownian
           particle hit the
        cellular surface"""
        phit = pl.exp(-2*nu*(b-max(r0s**0.5,r1s**0.5)))
    """After the Brownian particle has crossed the cellular
        surface it is
    placed on the cellular surface while preserving the
       angle"""
    x,y = reflectsurffin(x,y)
    """We return the position of the Brownian particle on
       the cellular surface
```

```
    and the number of steps it took to reach the cellular
       surface"""
    return x, y, istep
def expotime2():
    '''Exponential timestep with boundary test for
       diffusion from the cellular
    surface to the nuclear surface'''
    """We define the initial position of the Brownian
       particle to be the end
    point of the outward path"""
    x, y, istep = expotime1(c)
    print(c,np.sqrt(x**2+y**2),istep)
    r1s = sdistnucl(x,y)
    phit = 0
    """While the Brownian particle has not hit the nuclear
       surface it will
    keep diffusing"""
    while phit < r.random():
        """We update the position of the Brownian particle
           after one
        timestep"""
        r0s = r1s
        mod = 2*pl.sqrt(pl.log(r.random())*pl.log(r.random
           ()))/nu
        rs = 2.0
        while rs > 1:
            v1,v2 = 2*r.random()-1,2*r.random()-1
            rs = v1*v1+v2*v2
        x += mod*(v1*v1-v2*v2)/rs
        y += mod*2*v1*v2/rs
        """If the particle crosses the surface of the cell
           it is reflected"""
        if sdistsurf(x,y) > b*b:
            x,y = reflectsurf(x,y)
        istep += 1
        r1s = sdistnucl(x,y)
```

```
        """We update the probability that the Brownian
           particle hit the
        cellular surface"""
        phit = pl.exp(-2*nu*(min(r0s**0.5,r1s**0.5)-a))
    """We return the number of steps it took for the
       Brownian particle to reach
    the nuclear surface"""
    return istep
"""We define the range of value the displacement of the
   nucleus takes"""
C = np.linspace(0,1-a,10)
txt=str("2Dt2Simulation.txt")
file = open(txt, "w")
for c in C:
    print(c)
    sdt = pl.sqrt(2*D*dt)
    nu = 1.0/pl.sqrt(D*dt)
    tone = [dt*expotime2() for i in range(nreal)]
    print(c,pl.mean(tone),'+-',stats.sem(tone))
    """We record the position of the nucleus, the mean time
        and standard error
    of the mean """
    file.write(str(c)+' '+str(pl.mean(tone))+' ' +str(stats
       .sem(tone))+' ')
file.close()
```

G.6.1.3 From nuclear surface to the cellular surface in an eccentric circular domain

```
"""Brownian simulation start at nucleus and run until hit
   cell surface in two
dimensions"""
import numpy as np
import scipy.stats as stats
import pylab as pl
from numpy import random as r
```

```
from mpmath import csch,coth
import matplotlib.pyplot as plt
"""We define the diffusion coefficient, the radius of the
   nucleus, the radius
of the cell, the number of realisations of the Brownian
   simulations and time
step"""
D = 0.5
a = 0.1
b = 1.0
nreal = 10000
dt = 0.001
def sdistnucl(x,y,c):
    '''square of distance from centre of nucleus'''
    return (x-c)**2 + y**2
def sdistsurf(x,y):
    ''' square of distance from centre of cell'''
    return x**2 + y**2
def reflectnucl(x,y):
    ''' find new position by simple reflection off nuclear
       surface'''
    oldr = pl.sqrt(sdistnucl(x,y,c))
    newr = 2*a-oldr
    return c+(x-c)*newr/oldr,y*newr/oldr
def reflectsurf(x,y):
    ''' find new position by simple reflection off cellular
        surface'''
    oldr = pl.sqrt(sdistsurf(x,y))
    newr = 2*b-oldr
    return x*newr/oldr,y*newr/oldr
def expotime1():
    '''Exponential timestep with boundary test for
       diffusion from the nuclear
    surface to the cellular surface'''
    """We define the initial position of the Brownian
       particle uniformly on the
```

```
    surface of the nucleus"""
    theta = np.random.uniform(0,2*np.pi,1)
    x, y = c + a*np.cos(theta), a*np.sin(theta)
    istep = 0,0
    r1s = sdistsurf(x,y)
    phit = 0
    """While the Brownian particle has not hit the cellular
        surface it will
    keep diffusing"""
    while phit < r.random():
        """We update the position of the Brownian particle
           after one
        timestep"""
        r0s = r1s
        mod = 2*pl.sqrt(pl.log(r.random())*pl.log(r.random
           ()))/nu
        rs = 2.0
        while rs > 1:
            v1,v2 = 2*r.random()-1,2*r.random()-1
            rs = v1*v1+v2*v2
        x += mod*(v1*v1-v2*v2)/rs
        y += mod*2*v1*v2/rs
        """If the particle cross the surface of the nucleus
            it is reflected"""
        if sdistnucl(x,y,c) < a*a:
            x,y = reflectnucl(x,y)
        istep += 1
        r1s = sdistsurf(x,y)
        """We update the probability that the Brownian
           particle hit the
        cellular surface"""
        phit = pl.exp(-2*nu*(b-max(r0s**0.5,r1s**0.5)))
    """We return the position of the Brownian particle on
       the cellular surface
    and the number of steps it took to reach the cellular
       surface"""
```

```
    return istep
"""We define the range of value the displacement of the
   nucleus takes"""
C=np.linspace(0,1-a,10)
txt=str("barT1.txt")
file = open(txt, "w")
for c in C:
    sdt = pl.sqrt(2*D*dt)
    nu = 1.0/pl.sqrt(D*dt)
    tone = [dt*expotime1() for i in range(nreal)]
    print(pl.mean(tone),'+-',stats.sem(tone))
    """We record the position of the nucleus, the mean time
        and standard error
    of the mean """
    file.write(str(c)+' '+str(pl.mean(tone))+' ' +str(stats
       .sem(tone))+' ')
file.close()
```

G.6.1.4 From cellular surface to nuclear surface in an eccentric circular domain

```
"""Brownian simulation start at cellular surface and runs
   until hit nucleus in
two dimensions"""
import numpy as np
import scipy.stats as stats
import pylab as pl
from numpy import random as r
from mpmath import csch,coth
import matplotlib.pyplot as plt
"""We define the diffusion coefficient, the radius of the
   nucleus, the radius
of the cell, the number of realisations of the Brownian
   simulations and time
step"""
D = 0.5
```

```
a = 0.25
b = 1.0
nreal = 10000
dt = 0.001
def sdistnucl(x,y,c):
    '''square of distance from centre of nucleus'''
    return (x-c)**2 + y**2
def sdistsurf(x,y):
    ''' square of distance from centre of cell'''
    return x**2 + y**2
def reflectnucl(x,y):
    ''' find new position by simple reflection off the
       nuclear surface'''
    oldr = pl.sqrt(sdistnucl(x,y))
    newr = 2*a-oldr
    return c+(x-c)*newr/oldr,y*newr/oldr
def reflectsurf(x,y):
    ''' find new position by simple reflection off the
       cellular surface'''
    oldr = pl.sqrt(sdistsurf(x,y))
    newr = 2*b-oldr
    return x*newr/oldr,y*newr/oldr
def expotime2():
    '''Exponential timestep with boundary test for
       diffusion from the cellular
    surface to the nuclear surface'''
    """We define the initial position of the Brownian
       particle uniformly on the
    surface of the cell"""
    theta = np.random.uniform(0,2*np.pi)
    x, y = b*np.cos(theta), b*np.sin(theta)
    istep = 0,0
    r1s = sdistnucl(x,y,c)
    phit = 0
    """While the Brownian particle has not hit the nuclear
       surface it will
```

```
    keep diffusing"""
    while phit < r.random():
        """We update the position of the Brownian particle
           after one
        timestep"""
        r0s = r1s
        mod = 2*pl.sqrt(pl.log(r.random())*pl.log(r.random
           ()))/nu
        rs = 2.0
        while rs > 1:
            v1,v2 = 2*r.random()-1,2*r.random()-1
            rs = v1*v1+v2*v2
        x += mod*(v1*v1-v2*v2)/rs
        y += mod*2*v1*v2/rs
        """If the particle crosses the surface of the cell
           it is reflected"""
        if sdistsurf(x,y) > b*b:
            x,y = reflectsurf(x,y)
        istep += 1
        r1s = sdistnucl(x,y,c)
        """We update the probability that the Brownian
           particle hit the
        cellular surface"""
        phit = pl.exp(-2*nu*(min(r0s**0.5,r1s**0.5)-a))
    """We return the number of steps it took for the
       Brownian particle to reach
    the nuclear surface"""
    return istep
"""We define the range of value the displacement of the
   nucleus takes"""
C=np.linspace(0,1-a,10)
txt=str("barT2.txt")
file = open(txt, "w")
for c in C:
    sdt = pl.sqrt(2*D*dt)
    nu = 1.0/pl.sqrt(D*dt)
```

```
    tone = [dt*expotime2() for i in range(nreal)]
    print(pl.mean(tone),'+-',stats.sem(tone))
    """We record the position of the nucleus, the mean time
        and standard error
    of the mean """
    file.write(str(c)+' '+str(pl.mean(tone))+' ' +str(stats
       .sem(tone))+' ')
file.close()
```

G.6.2 Plots

G.6.2.1 From nuclear surface to cellular surface

```
"""We plot the average mean time \bar{T}_1^{(3)} in an
   eccentric spherical
annular region """
import numpy as np
from scipy.spatial.distance import pdist, squareform
import matplotlib.pyplot as plt
import math
import scipy.special as sp
import scipy.stats as stats
from pylab import contourf,savefig,show,subplot,colorbar,
   clabel,title,figure
import scipy.integrate as integrate
"""We define the radius of the cell, the radius of the
   nucleus and the
diffusion coefficient"""
b=1
a=0.1
D=0.5
"""We define the functions necessary to construct continued
    fractions"""
def alphan(n,tau1,tau2):
    return 2*n/(2*n+1)*np.exp(-(n-0.5)*tau1)*(np.cosh((n
       -0.5)*(tau1-tau2))/np.sinh((n-0.5)*tau2))
```

```
def gamman(n,tau1,tau2):
    return (2*n+2)/(2*n+1)*np.exp(-(n+1.5)*tau1)*(np.cosh((
        n+1.5)*(tau1-tau2))/np.sinh((n+1.5)*tau2))
def betan(n,tau1,tau2):
    return np.exp(-(n+0.5)*tau1)/(n+0.5)*(-(2*n+1)*np.cosh(
        tau1)*(np.cosh((n+0.5)*(tau1-tau2))/np.sinh((n+0.5)*
        tau2))-np.sinh(tau1)*(np.sinh((n+0.5)*(tau1-tau2))/
        np.sinh((n+0.5)*tau2)))
def alphanB(n,tau1,tau2):
    return -2*n/(2*n+1)*np.exp(-(n-0.5)*tau1)*(np.cosh((n
        -0.5)*tau1)-np.sinh((n-0.5)*tau1)*np.sinh((n-0.5)*
        tau2)/np.cosh((n-0.5)*tau2))
def gammanB(n,tau1,tau2):
    return -(2*n+2)/(2*n+1)*np.exp(-(n+1.5)*tau1)*(np.cosh
        ((n+1.5)*tau1)-np.sinh((n+1.5)*tau1)*np.sinh((n+1.5)
        *tau2)/np.cosh((n+1.5)*tau2))
def betanB(n,tau1,tau2):
    return np.exp(-(n+0.5)*tau1)/(n+0.5)*((2*n+1)*np.cosh(
        tau1)*(np.cosh((n+0.5)*(tau1-tau2))/np.cosh((n+0.5)*
        tau2))+np.sinh(tau1)*(np.sinh((n+0.5)*(tau1-tau2))/
        np.cosh((n+0.5)*tau2)))
def lambdan(n,tau1,tau2):
    V2 = np.sinh((n+0.5)*tau1)*np.sinh(tau1)+2*(n+0.5)*np.
        cosh((n+0.5)*tau1)*np.cosh(tau1)
    W = np.sinh(tau1)-2*(n+0.5)*np.cosh(tau1)
    return 2*W/(2*n+1)*np.exp(-(n+0.5)*tau1)+(2*n+2)/(2*n
        +1)*np.exp(-(n+1.5)*tau1)+2*n/(2*n+1)*np.exp(-(n
        -0.5)*tau1)-2*V2*np.exp(-(n+0.5)*(2*tau1-tau2))/((2*
        n+1)*np.sinh((n+0.5)*tau2))+np.cosh((n+1.5)*tau1)*np
        .exp(-(n+1.5)*(2*tau1-tau2))/np.sinh((n+1.5)*tau2)
        *(2*n+2)/(2*n+1)+np.cosh((n-0.5)*tau1)*np.exp(-(n
        -0.5)*(2*tau1-tau2))/np.sinh((n-0.5)*tau2)*(2*n)/(2*
        n+1)
def lambdanB(n,tau1,tau2):
    V1 = np.cosh((n+0.5)*tau1)*np.sinh(tau1)+2*(n+0.5)*np.
        sinh((n+0.5)*tau1)*np.cosh(tau1)
```

```
    W = np.sinh(tau1)-2*(n+0.5)*np.cosh(tau1)
    return 2*W/(2*n+1)*np.exp(-(n+0.5)*tau1)+(2*n+2)/(2*n
       +1)*np.exp(-(n+1.5)*tau1)+2*n/(2*n+1)*np.exp(-(n
       -0.5)*tau1)-2*V1*np.exp(-(n+0.5)*(2*tau1-tau2))/((2*
       n+1)*np.cosh((n+0.5)*tau2))+np.sinh((n+1.5)*tau1)*np
       .exp(-(n+1.5)*(2*tau1-tau2))/np.cosh((n+1.5)*tau2)
       *(2*n+2)/(2*n+1)+np.sinh((n-0.5)*tau1)*np.exp(-(n
       -0.5)*(2*tau1-tau2))/np.cosh((n-0.5)*tau2)*(2*n)/(2*
       n+1)
"""We construct the continued fractions"""
def pn(n,N,tau1,tau2):
    s = 0
    for i in range(0,N-1):
        S = gamman(N+n-(i+1),tau1,tau2)*alphan(N+n-i,tau1,
           tau2)
        s = S/(betan(N+n-i,tau1,tau2)-s)
    s = - alphan(n+1,tau1,tau2)/(betan(n+1,tau1,tau2)-s)
    return s
def qn(n,tau1,tau2):
    s = 0
    for i in range(0,n-1):
        S = alphan(i+1,tau1,tau2)*gamman(i,tau1,tau2)
        s = S/(betan(i,tau1,tau2)-s)
    s = - gamman(n-1,tau1,tau2)/(betan(n-1,tau1,tau2)-s)
    return s
def pnB(n,N,tau1,tau2):
    s = 0
    for i in range(0,N-1):
        S = gammanB(N+n-(i+1),tau1,tau2)*alphanB(N+n-i,tau1
           ,tau2)
        s = S/(betanB(N+n-i,tau1,tau2)-s)
    s = - alphanB(n+1,tau1,tau2)/(betanB(n+1,tau1,tau2)-s)
    return s
def qnB(n,tau1,tau2):
    s = 0
    for i in range(0,n-1):
```

```
        S = alphanB(i+1,tau1,tau2)*gammanB(i,tau1,tau2)
        s = S/(betanB(i,tau1,tau2)-s)
    s = - gammanB(n-1,tau1,tau2)/(betanB(n-1,tau1,tau2)-s)
    return s
def GN(N,n,tau1,tau2):
    return 1/(alphan(N,tau1,tau2)*qn(N,tau1,tau2)+betan(N,
       tau1,tau2)+gamman(N,tau1,tau2)*pn(N,n,tau1,tau2))
def GNB(N,n,tau1,tau2):
    return 1/(alphanB(N,tau1,tau2)*qnB(N,tau1,tau2)+betanB(
       N,tau1,tau2)+gammanB(N,tau1,tau2)*pnB(N,n,tau1,tau2)
       )
def delta(n,m):
    if n==m:
        return 1
    else:
        return 0
def prodp(r,t,tau1,tau2):
    p = 1
    for i in range(r,t+1):
        p = p*pn(i-1,15,tau1,tau2)
    return p
def prodq(r,t,tau1,tau2):
    q = 1
    for i in range(r,t+1):
        q = q*qn(i+1,tau1,tau2)
    return q
def prodpB(r,t,tau1,tau2):
    p = 1
    for i in range(r,t+1):
        p = p*pnB(i-1,15,tau1,tau2)
    return p
def prodqB(r,t,tau1,tau2):
    q = 1
    for i in range(r,t+1):
        q = q*qnB(i+1,tau1,tau2)
    return q
```

```
"""We define the Heaviside function"""
def heaviside(x,y):
    if x<0:
        return 0
    if x==0:
        return y
    if x>0:
        return 1
"""We use the continued fractions to construct the
   coefficients of the Green's
functions"""
def An(n,L,c):
    s = 0
    d = 1/c*(0.25*(b**2+a**2-c**2)**2-a**2*b**2)**0.5
    tau2 = np.log(d/b+(1+(d/b)**2)**0.5)
    tau1 = np.log(d/a+(1+(d/a)**2)**0.5)
    for NN in range(0,L):
        s += lambdan(NN,tau1,tau2)*GN(NN,10,tau1,tau2)*(
           delta(NN,n)+heaviside(n-NN,0)*prodp(NN+1,n,tau1,
           tau2)+heaviside(NN-n,0)*prodq(n,NN-1,tau1,tau2))
    return s
def Bn(n,L,c):
    s = 0
    d = 1/c*(0.25*(b**2+a**2-c**2)**2-a**2*b**2)**0.5
    tau2 = np.log(d/b+(1+(d/b)**2)**0.5)
    tau1 = np.log(d/a+(1+(d/a)**2)**0.5)
    for NN in range(0,L):
        s += lambdanB(NN,tau1,tau2)*GNB(NN,10,tau1,tau2)*(
           delta(NN,n)+heaviside(n-NN,0)*prodpB(NN+1,n,tau1
           ,tau2)+heaviside(NN-n,0)*prodqB(n,NN-1,tau1,tau2
           ))
    return s
def AN(n,L,c):
    d = 1/c*(0.25*(b**2+a**2-c**2)**2-a**2*b**2)**0.5
    tau2 = np.log(d/b+(1+(d/b)**2)**0.5)
    tau1 = np.log(d/a+(1+(d/a)**2)**0.5)
```

```
    s = np.exp(-(n+0.5)*(tau1-tau2))/np.cosh((n+0.5)*tau2)-
       Bn(n,L,c)*np.sinh((n+0.5)*tau2)/np.cosh((n+0.5)*tau2
       )
    return s
def BN(n,L,c):
    d = 1/c*(0.25*(b**2+a**2-c**2)**2-a**2*b**2)**0.5
    tau2 = np.log(d/b+(1+(d/b)**2)**0.5)
    tau1 = np.log(d/a+(1+(d/a)**2)**0.5)
    s = np.exp(-(n+0.5)*(tau1-tau2))/np.sinh((n+0.5)*tau2)-
       An(n,L,c)*np.cosh((n+0.5)*tau2)/np.sinh((n+0.5)*tau2
       )
    return s
"""We construct the exact Green's function \bar{G}_1^{(3)}
   """
def G(x,c,n):
    d = 1/c*(0.25*(b**2+a**2-c**2)**2-a**2*b**2)**0.5
    tau1 = np.log(d/a+(1+(d/a)**2)**0.5)
    return  (An(n,10,c)*np.cosh((n+0.5)*x)+Bn(n,10,c)*np.
       sinh((n+0.5)*x)-np.exp(-(n+0.5)*(tau1-x)))*((2*n+3)
       /3*np.exp(-(n+1/2)*x)/np.sinh(x)**2+2/3*np.exp(-(n
       +3/2)*x)/np.sinh(x)**3)
"""We construct the approximate Green's function \bar{G}_1
   ^{(3)}"""
def Gg(x,c,n):
    d = 1/c*(0.25*(b**2+a**2-c**2)**2-a**2*b**2)**0.5
    tau2 = np.log(d/b+(1+(d/b)**2)**0.5)
    return  np.sinh((n+0.5)*(x-tau2))*2**(1/2)*((2*n+3)/3*
       np.exp(-(n+1/2)*x)/np.sinh(x)**2+2/3*np.exp(-(n+3/2)
       *x)/np.sinh(x)**3)
"""We construct the approximate average mean time \bar{T}_1
   ^{(3)}"""
def AvgMeanTime(c,m):
    s=0
    d = 1/c*(0.25*(b**2+a**2-c**2)**2-a**2*b**2)**0.5
    tau2 = np.log(d/b+(1+(d/b)**2)**0.5)
    tau1 = np.log(d/a+(1+(d/a)**2)**0.5)
```

```
    for n in range(0,m+1):
        I = integrate.quad(lambda x: Gg(x,c,n), tau2, tau1)
            [0]
        s += I*(n+0.5)*np.exp(-(n+0.5)*tau1)/(np.sinh((n
            +0.5)*(tau1-tau2))*np.tanh(tau1)+2*(n+0.5)*np.
            cosh((n+0.5)*(tau1-tau2)))
    s = 16*np.sqrt(2)*np.pi*d**4*s/(D*np.sinh(tau1))/(4*np.
        pi*a**2)
    return s
"""We construct the exact average mean time \bar{T}_1^{(3)}
    """
def AvgMeanTimeG(c,m):
    s=0
    d = 1/c*(0.25*(b**2+a**2-c**2)**2-a**2*b**2)**0.5
    tau2 = np.log(d/b+(1+(d/b)**2)**0.5)
    tau1 = np.log(d/a+(1+(d/a)**2)**0.5)
    for n in range(0,m+1):
        I = integrate.quad(lambda x: G(x,c,n), tau2, tau1)
            [0]
        s += -I*np.exp(-(n+0.5)*tau1)
    s = 2*d**4*s/(D*np.sinh(tau1)*a**2)
    return s
"""We change the python plot such that it does not have
    upper or rightward
border"""
fig = plt.figure(frameon=False)
ax = plt.subplot(111)
ax.spines['top'].set_visible(False)
ax.spines['right'].set_visible(False)
ax.yaxis.set_ticks_position('left')
ax.xaxis.set_ticks_position('bottom')
"""We plot the approximate average mean time \bar{T}_1^{(3)
    }"""
NRPRT=np.linspace(0.025,0.89,100)
h=[AvgMeanTime(x,20) for x in NRPRT]
```

```
ax.plot(NRPRT,h,color='blue',label=r'approximation',
   linewidth=1.25)
"""We plot the exact average mean time \bar{T}_1^{(3)}"""
NRPRT=np.linspace(0.01,0.89,25)
h=[AvgMeanTimeG(x,5) for x in NRPRT]
ax.plot(NRPRT,h,color='k',label=r'exact',linewidth=1.25)
"""We upload the numerical simulations for average mean
   time \bar{T}_1^{(3)}
and plot them"""
txt=str("3DUDMeanTime")+str(".txt")
text_file = open(txt, "r")
lines = text_file.read().split(" ")
text_file.close()
T=[float(lines[0])]
V=[float(lines[1])]
for i in range(2,len(lines)-1):
    if i%2==0:
        T.append(float(lines[i]))
    else:
        V.append(float(lines[i]))
C=np.linspace(0,1-a,9)
ax.errorbar(C,T,V,fmt='o',color='green',label='numerical')
x=0
y=(b**2-a**2)/(6*D)+a**3/(3*D)*(1/b-1/a)
plt.plot(x, y, 'ro',label=r'concentric')
plt.xlabel(r'$c$',fontsize=20)
plt.ylabel(r'$\frac{2D}{R^3}\bar{T}_1^{(3)(a,c)}$',fontsize
   =20)
plt.xlim([0,1])
plt.xticks([0,0.5,1], [r'0',r'0.5',r'1'],fontsize=14)
plt.yticks([0,0.15,0.3], [r'0',r'0.15',r'0.3'],fontsize=14)
plt.legend(loc=3,fontsize=15,frameon=False)
plt.tight_layout()
plt.savefig('3DMeanTimeUDContinuedFraction.pdf')
plt.show()
```

G.6.2.2 Mean round-trip time in a circular domain

```
"""Plot of the round trip mean time from the nuclear
   surface to the cellular
surface and back"""
import numpy as np
from mpmath import *
import matplotlib.pyplot as plt
import math
from scipy.stats import poisson
from scipy.misc import factorial
import scipy.special
import itertools
"""We define the radius of the cell, the radius of the
   nucleus and the
diffusion coefficient"""
b=1
a=0.1
D=0.5
"""We change the python plot such that it does not have
   upper or rightward
border"""
fig = plt.figure(frameon=False)
ax = plt.subplot(111)
ax.spines['top'].set_visible(False)
ax.spines['right'].set_visible(False)
ax.yaxis.set_ticks_position('left')
ax.xaxis.set_ticks_position('bottom')
"""We define the convolution function that gives the mean
   time from the
cellular surface starting with a non-uniform initial
   distribution given by the
hitting density"""
def averagebipolarmeantimenonuniform(c,N):
    d = 1/c*(0.25*(b**2+a**2-c**2)**2-a**2*b**2)**0.5
    tau2 = np.log(d/b+(1+(d/b)**2)**0.5)
```

```
tau1 = np.log(d/a+(1+(d/a)**2)**0.5)
"""We transform the hitting density into a complex
   Fourier series in
complex form"""
B = np.ones(2*N+1)
for n in range(0,N+1):
    B[N+n] = 1/(2*np.pi)*(2*np.cosh(tau2)*np.exp(-n*
       tau1)/(d*np.cosh(n*(tau1-tau2)))-1/d*(np.exp(-(n
       -1)*tau1)/(np.cosh((n-1)*(tau1-tau2)))+np.exp(-(
       n+1)*tau1)/(np.cosh((n+1)*(tau1-tau2)))))/2
    B[N-n] = 1/(2*np.pi)*(2*np.cosh(tau2)*np.exp(-n*
       tau1)/(d*np.cosh(n*(tau1-tau2)))-1/d*(np.exp(-(n
       -1)*tau1)/(np.cosh((n-1)*(tau1-tau2)))+np.exp(-(
       n+1)*tau1)/(np.cosh((n+1)*(tau1-tau2)))))/2
B[N] = 1/(2*np.pi)*(np.cosh(tau2)/d-np.exp(-tau1)/(d*np
   .cosh(tau1-tau2)))
m = int((len(B)-1)/2)
F = np.zeros(2*m+1)
"""We transform the mean time T_2 into a Fourier series
    in complex form"""
for n in range(0,m+1):
    F[m+n] = -((2*d)/(D*n*np.exp(n*tau2)))*(d*c*n/(1+np
       .exp(2*n*(tau1-tau2)))-1/(2)*tanh(n*(tau1-tau2))
       )/2
    F[m-n] = -((2*d)/(D*n*np.exp(n*tau2)))*(d*c*n/(1+np
       .exp(2*n*(tau1-tau2)))-1/(2)*tanh(n*(tau1-tau2))
       )/2
F[m] = (d/(2*D))*((tau1-tau2)-c*d)
"""We convolute the two complex Fourier series"""
G = np.convolve(B,F)
al = np.ones((len(G)+1)/2)
m = int((len(G)+1)/2)
l = int((len(G)-1)/2)
"""We transform the complex Fourier series back into
   normal form"""
for i in range(m):
```

```
        al[i] = G[l+i] + G[l-i]
    al[0] = al[0]/2
    ret = 0
    az=[]
    """We determine the mean time from the cellular surface
        starting with a
    non-uniform initial distribution given by the hitting
       density """
    for i in range(len(al)):
        Ai = 2*np.pi*np.exp(-i*tau2)/np.sinh(tau2)
        az.append(Ai)
        ret += al[i]*Ai
    return ret
"""We upload the numerical simulations for the round trip
   mean time"""
txt=str("2Dt2Simulation.txt")
text_file = open(txt, "r")
lines = text_file.read().split(" ")
g=[]
M=[]
B=[]
for i in range(len(lines)-1):
    if i%3==0:
        g.append(float(lines[i]))
    if i%3==1:
        M.append(float(lines[i]))
    if i%3==2:
        B.append(float(lines[i]))
"""We plot the numerical simulations for the round trip
   mean time"""
plt.errorbar(g, M, B, fmt='o',label='numerical')
NRPRT=np.linspace(0,1-a-0.01,500)
"""We define the average mean time for a Brownian particle
   starting uniformly
of the nuclear surface to the reach the cellular surface"""
def T1AVG(c,N):
```

```
    d = (1/c)*(0.25*(b**2+a**2-c**2)**2-a**2*b**2)**0.5
    tau2 = np.log(d/b+(1+(d/b)**2)**0.5)
    tau1 = np.log(d/a+(1+(d/a)**2)**0.5)
    ret = 0
    for n in range(1,N):
        ret += 2*np.exp(-2*n*tau1)/D*(-tanh(n*(tau1-tau2))*
           a**2/(2*n)+d*c/(1+np.exp(-2*n*(tau1-tau2))))
    ret += (a**2/(2*D))*(tau2-tau1)+d*c/(2*D)
    return ret
h=[averagebipolarmeantimenonuniform(x,20) for x in NRPRT]
h1=[T1AVG(x,20) for x in NRPRT]
"""We obtain the analytic round trip mean time"""
h2=[x+y for x,y in zip(h,h1)]
ax.plot(NRPRT,h2,label=r'exact',linewidth=1.25)
"""We plot the round trip mean time for the concentric case
   """
x=0
y1=-(b**2-a**2)/(4*D)+b**2/(2*D)*np.log(b/a)
y2=(b**2-a**2)/(4*D)-a**2/(2*D)*np.log(b/a)
ax.plot(x, y1+y2, 'ro',label=r'concentric')
plt.xlabel(r'$c$',fontsize=20)
plt.ylabel(r'$\frac{2D}{R^2}\left(\bar{T}_1^{(2)}+\bar{T}_2
   ^{\varepsilon,2}\right)(a,c)$',fontsize=20)
plt.xticks([0,0.5,1], [r'0.0',r'0.5',r'1'],fontsize=14)
plt.yticks([0,1,2], [r'0',r'1',r'2'],fontsize=14)
plt.xlim([0,1])
plt.ylim([0,2.4])
plt.legend(loc=3,fontsize=15,frameon=False)
plt.tight_layout()
plt.savefig('TavgTotal.pdf')
plt.show()
```

G.6.2.3 Combined subplot of $\bar{T}_1^{(2)}(a,c)$ and $\bar{T}_2^{(2)}(a,c)$

```
"""We plot the average mean times \bar{T}_1^{(2)} and \bar{
   T}_2^{(2)} as
```

```
functions of the nuclear displacement"""
import numpy as np
from scipy.spatial.distance import pdist, squareform
import matplotlib.pyplot as plt
import math
import scipy.special as sp
from mpmath import *
"""We change the python plot such that it does not have
   upper or rightward
border"""
fig = plt.figure(frameon=False,figsize=(6, 6))
ax=plt.subplot(2, 1, 1)
ax.spines['top'].set_visible(False)
ax.spines['right'].set_visible(False)
ax.yaxis.set_ticks_position('left')
ax.xaxis.set_ticks_position('bottom')
"""We define the radius of the cell, the radius of the
   nucleus and the
diffusion coefficient"""
b=1
a=0.1
D=0.5
"""We upload the numerical simulations for average mean
   time \bar{T}_1^{(2)}
and plot them"""
txt=str("barT1.txt")
text_file = open(txt, "r")
lines = text_file.read().split(" ")
C=[]
A=[]
B=[]
for i in range(len(lines)-1):
    if i%3==0:
        C.append(float(lines[i]))
    if i%3==1:
        A.append(float(lines[i]))
```

```
    if i%3==2:
        B.append(float(lines[i]))
"""We plot the approximate average mean time \bar{T}_1^{(2)}
   }"""
ax.errorbar(C, A,B, fmt='o',label='numerical')
"""We convert the Cartesian coordinates into bipolar
   coordinates"""
def bipolar(x,y,c):
    d = (1/c)*(0.25*(b**2+a**2-c**2)**2-a**2*b**2)**0.5
    A = (b**2+d**2)**0.5
    x = x+A
    tau = 0.5*np.log(((x+d)**2+y**2)/((x-d)**2+y**2))
    return tau
"""We define the average mean time \bar{T}_1^{(2)}"""
def averagebipolarmeantime3(c,N):
    d = (1/c)*(0.25*(b**2+a**2-c**2)**2-a**2*b**2)**0.5
    tau2 = np.log(d/b+(1+(d/b)**2)**0.5)
    tau1 = np.log(d/a+(1+(d/a)**2)**0.5)
    ret = 0
    for n in range(1,N):
        ret += 2*np.exp(-2*n*tau1)/D*(-tanh(n*(tau1-tau2))*
           a**2/(2*n)+d*c/(1+np.exp(-2*n*(tau1-tau2))))
    ret += (a**2/(2*D))*(tau2-tau1)+d*c/(2*D)
    return ret
"""We define the average mean time \bar{T}_2^{(2)}"""
def averagebipolarmeantime4(c,N):
    d = (1/c)*(0.25*(b**2+a**2-c**2)**2-a**2*b**2)**0.5
    tau2 = np.log(d/b+(1+(d/b)**2)**0.5)
    tau1 = np.log(d/a+(1+(d/a)**2)**0.5)
    ret = 0
    for n in range(1,N):
        ret += (2*np.exp(-2*n*tau2)/D)*(np.tanh(n*(tau1-
           tau2))/(2*n)-d*c/(1+np.exp(2*n*(tau1-tau2))))
    ret += (tau1-tau2)/(2*D)-d*c/(2*D)
    return ret
NRPRT=np.linspace(0,1-a-0.0001,400)
```

```
h=[averagebipolarmeantime3(x,150) for x in NRPRT]
"""We plot the exact average mean time \bar{T}_1^{(2)}"""
ax.plot(NRPRT,h,label=r'exact',linewidth=1.25)
"""We define the approximation of \bar{T}_1^{(2)}"""
def RemusApprox(c):
    return (1-c**2)/(4*D)-a**2/(2*D)*np.log(1/a)-a**2/(2*D)
       *(np.log(1-c**2)+(1-3*c**2)/(2*(1-c**2)))
"""We define the approximation of \bar{T}_2^{(2)}"""
def Remus_approx5(c):
    return 1/(4*D)*(c**2-1)+1/(2*D)*np.log(1/a)+a**2/(4*D)
       *(1-4*c**2+c**4)/(1-c**2)**2-1/(2*D)*np.log(1-c**2)
"""We define the approximation of \bar{T}_2^{(2)} derived
   by Condamin et al."""
def Remus_approx6(c):
    return 1/(4*D)*(c**2-1)+1/(2*D)*np.log(1/a)-1/(2*D)*np.
       log(1-c**2)
ax.plot(NRPRT,RemusApprox(NRPRT),label=r'approximation',
   linewidth=1.25)
plt.ylabel(r'$\frac{2D}{R^2}\bar{T}_1^{(2)}(a,c)$',fontsize
   =20)
plt.xticks([0,0.5,1], [r'0',r'0.5',r'1'],fontsize=14)
plt.yticks([0,0.2,0.4], [r'0.0',r'0.2',r'0.4'],fontsize=14)
plt.xlim([0,1])
plt.legend(loc=3,fontsize=13,frameon=False)
ax = plt.subplot(212)
"""We upload the numerical simulations for average mean
   time \bar{T}_1^{(2)}
and plot them"""
txt=str("barT2.txt")
text_file = open(txt, "r")
lines = text_file.read().split(" ")
C=[]
A=[]
B=[]
for i in range(len(lines)-1):
    if i%3==0:
```

```
            C.append(float(lines[i]))
        if i%3==1:
            A.append(float(lines[i]))
        if i%3==2:
            B.append(float(lines[i]))
ax.errorbar(C, A,B, fmt='o',label='numerical')
NRPRT=np.linspace(0,1-a-0.001,500)
h=[averagebipolarmeantime4(x,100) for x in NRPRT]
"""We plot the exact average mean time \bar{T}_2^{(2)}"""
ax.plot(NRPRT,h,label=r'exact',linewidth=1.25)
"""We plot the approximate average mean time \bar{T}_2^{(2)
    }"""
ax.plot(NRPRT,Remus_approx5(NRPRT),color='red',label=r'
    approximation',linewidth=1.25)
"""We plot the approximation derived by Condamin et al. to
    the average mean
time \bar{T}_2^{(2)}"""
plt.plot(NRPRT,Remus_approx6(NRPRT),'--',color='olive',
    label=r'Condamin et al.',linewidth=1.25)
ax.spines['top'].set_visible(False)
ax.spines['right'].set_visible(False)
ax.yaxis.set_ticks_position('left')
ax.xaxis.set_ticks_position('bottom')
plt.xlim([0,1])
plt.xticks([0,0.5,1.0], [r'0',r'0.5',r'1'],fontsize=14)
plt.yticks([0,2,4], [r'0',r'2',r'4'],fontsize=14)
plt.xlabel(r'$c$',fontsize=18)
plt.ylabel(r'$\frac{2D}{R^2}\bar{T}_2^{(2)}(a,c)$',fontsize
    =18)
plt.legend(loc=4,fontsize=13,frameon=False)
plt.tight_layout()
plt.savefig('CombinedSubplot.pdf',bbox_inches='tight')
plt.show()
```

G.7 Hitting density

G.7.1 No target in a circular domain

G.7.1.1 Numerical simulation

```
"""We simulate Brownian motion inside a disk and record the
    end point on the
disk boundary"""
import numpy as np
from scipy.spatial.distance import pdist, squareform
import matplotlib.pyplot as plt
import matplotlib.animation as animation
import math
import sys
class ParticleBox:
    """
    init_state is an [N x 2] array, where N is the number
       of particles:
       [[x1, y1],
        [x2, y2],
        ...               ]
    bounds is the size of the box: [xmin, xmax, ymin, ymax]
    """
    def __init__(self,
                 init_state = [[1, 0],
                               [-0.5, 0.5],
                               [-0.5, -0.5]],
                 bounds = [-10, 10, -10, 10],
                 size = 0.04,
                 M = 0.05,
                 G = 9.8):
        self.init_state = np.asarray(init_state, dtype=
           float)
        self.M = M * np.ones(self.init_state.shape[0])
        self.size = size
        self.state = self.init_state.copy()
```

```
        self.time_elapsed = 0
        self.bounds = bounds
        self.G = G
    def step(self, dt):
        """We define the number of particles, radius of
           disk, initial position
        of particles and the diffusion coefficient"""
        global  nrprt, b, c,D
        """step once by dt seconds"""
        time_step=np.random.exponential(scale=dt,size=None)
        self.time_elapsed += time_step
        """We create a copy of the position vector of the
           Brownian particles"""
        state_backup_2=self.state.copy()
        """We update the position of the Brownian particles
           """
        self.state[:,0] += np.random.normal(0,np.sqrt(2*D*
           time_step),len(self.state[:,0]))
        self.state[:,1] += np.random.normal(0,np.sqrt(2*D*
           time_step),len(self.state[:,1]))
        """We determine which particles crossed the disk
           boundary and delete
        them"""
        r1=[math.sqrt(x**2+y**2) for x,y in zip(self.state
           [:,0],self.state[:,1])]
        r2=[math.sqrt(x**2+y**2) for x,y in zip(
           state_backup_2[:,0],state_backup_2[:,1])]
        C=[math.exp(-(b-R1)*(b-R2)/(D*dt)) for R1,R2 in zip
           (r1,r2)]
        u=np.random.uniform(0,1,len(self.state[:,0]))
        Dist=np.where(C>u)
        for i in Dist[0]:
            theta=np.arctan2(self.state[i,1], self.state[i
               ,0])
            """We record the position of the particles on
               the boundary"""
```

```
            file.write(str(theta)+"  ")
        self.state=np.delete(self.state, Dist, axis=0)
        nrprt=len(self.state[:,0])
        if nrprt==0:
            file.close()
            sys.exit()
"Diffusion coefficient"
D=0.5
"Outer radius"
b=1
"Initial position"
c=0.89
txt=str("gpDatafileHP_c=0.89")+str(".txt")
file = open(txt, "w")
time=0
"Number of particles"
nrprt=500000
np.random.seed()
zr = np.zeros(nrprt)
os = np.ones(nrprt)
x=c*os
y=zr
"Position vector of particles"
init_state=np.c_[x, y]
print(init_state)
box = ParticleBox(init_state, size=0.001)
"Time step"
dt = 0.0001
""" set up figure and animation """
fig = plt.figure()
fig.subplots_adjust(left=0, right=1, bottom=0, top=1)
ax = fig.add_subplot(111, aspect='equal', autoscale_on=
   False,
                     xlim=(-1.1, 1.1), ylim=(-1.1, 1.1))
""" particles holds the locations of the particles """
particles, = ax.plot([], [], 'ro', ms=6)
```

```
""" rect is the box edge """
rect = plt.Rectangle(box.bounds[::2],
                     box.bounds[1] - box.bounds[0],
                     box.bounds[3] - box.bounds[2],
                     ec='none', lw=2, fc='none')
circle_1=plt.Circle((0,0),b,color='b',fill=False)
ax.add_patch(rect)
ax.add_patch(circle_1)
def init():
    """initialize animation"""
    global box, rect
    particles.set_data([], [])
    rect.set_edgecolor('none')
    return particles, rect
def animate(i):
    """perform animation step"""
    global box, rect, dt, ax, fig, circle
    box.step(dt)

    ms = int(fig.dpi * 2 * box.size * fig.get_figwidth()
             / np.diff(ax.get_xbound())[0])
    """ update pieces of the animation """
    rect.set_edgecolor('none')
    particles.set_data(box.state[:, 0], box.state[:, 1])
    particles.set_markersize(ms)
    return particles, rect
ani = animation.FuncAnimation(fig, animate, frames=100,
                              interval=10, blit=True,
                                 init_func=init)
plt.show()
```

G.7.1.2 Plot

```
"""We plot the hidding density of Brownian particle
   diffusing inside a circle
"""
```

```
import numpy as np
import matplotlib.pyplot as plt
import math
from scipy.stats import poisson
from scipy.misc import factorial
import scipy.special
import itertools
"""We define the radius of the cell, the radius of the
   nucleus, the number of
Brownian particles used in the simulation and the number of
    bins on the
cellular surface used to calculate the hitting density"""
b=1
a=0.1
M=500000
N=3000
"""We define the hitting density function"""
def hit_prob_in_out(theta,c):
    p=-(1/(4*np.pi*b))*(2/b*(c**4-b**4-b*c**3*np.cos(theta)
       )+2*c*np.cos(theta)*(2*b**2-c**2))/((c**2+b**2-2*b*c
       *np.cos(theta))**2)
    return p
L=2*np.pi/N
NRPRT=np.linspace(-np.pi,np.pi,N)
fig = plt.figure(frameon=False)
ax = plt.subplot(111)
color_vec=['darkblue','darkgreen','darkred']
I=0
"""We plot the numerical simulations"""
for c in [0.25,0.5,0.89]:
    print(c)
    bins=np.zeros(N)
    txt=str("gpDatafileHP_c="+str(c))+str(".txt")
    text_file = open(txt, "r")
    lines = text_file.read().split()
    for i in range(len(lines)-1):
```

```
        bins[int((float(lines[i])-np.pi)/L)-1]+=1/(M*L)
    text_file.close()
    ax.plot(NRPRT,bins,color=color_vec[I])
    I+=1
color_vec=['cornflowerblue','lime','lightcoral']
I=0
"""We plot the hitting density function for values of the
   nuclear displacement
c=0.25, c=0.5 and c=0.89"""
for c in [0.25,0.5,0.89]:
    h=[hit_prob_in_out(x,c) for x in NRPRT]
    ax.plot(NRPRT,h,color=color_vec[I],label=r'$c=$'+str(c)
       ,linewidth=1.25)
    I+=1
"""We change the python plot such that it does not have
   upper or rightward
border"""
ax.spines['top'].set_visible(False)
ax.spines['right'].set_visible(False)
ax.yaxis.set_ticks_position('left')
ax.xaxis.set_ticks_position('bottom')
plt.xticks([-np.pi,-np.pi/2,0,np.pi/2, np.pi], [r'$-\pi$',r
   '$-\frac{\pi}{2}$',0,r'$\frac{\pi}{2}$', r'$\pi$'],
   fontsize=16)
plt.xlim([-np.pi,np.pi])
plt.yticks([0,1.5,3],['0','1.5','3'],fontsize=14)
plt.xlabel(r'$\theta_2$',fontsize=16)
plt.ylabel(r'$\varepsilon_0^{(2)}(\theta_2)$',fontsize=16)
plt.legend(loc=1,fontsize=14,frameon=False)
plt.tight_layout()
plt.savefig('gpHD2019nt.pdf')
plt.show()
```

References

Amitai, A. & Holcman, D. (2017). Polymer physics of nuclear organization and function. *Physics Reports*, **678**, 1–83. 46

Angermann, B.R., Klauschen, F., Garcia, A.D., Prustel, T., Zhang, F., Germain, R.N. & Meier-Schellersheim, M. (2012). Computational modeling of cellular signaling processes embedded into dynamic spatial contexts. *Nature Methods*, **9**, 283. 108

Barkai, E., Garini, Y. & Metzler, R. (2012). Strange kinetics of single molecules in living cells. *Physics Today*, **65**, 29. 46, 108

Barton, G. (1989). *Elements of Green's functions and propagation: potentials, diffusion, and waves*. Oxford University Press. 37, 41, 42, 56, 65, 116, 130, 160, 194, 196, 197, 220

Basnayake, K. & Holcman, D. (2020). Extreme escape from a cusp: When does geometry matter for the fastest brownian particles moving in crowded cellular environments? *The Journal of Chemical Physics*, **152**, 134104. 107, 157

Bénichou, O. & Voituriez, R. (2014). From first-passage times of random walks in confinement to geometry-controlled kinetics. *Physics Reports*, **539**, 225–284. 48, 111

Bénichou, O., Coppey, M., Moreau, M., Suet, P. & Voituriez, R. (2005). Optimal search strategies for hidden targets. *Physical review letters*, **94**, 198101. 29

Bénichou, O., Chevalier, C., Klafter, J., Meyer, B. & Voituriez, R. (2010). Geometry-controlled kinetics. *Nature Chemistry*, **2**, 472. 46

Berezhkovskii, A.M., Makhnovskii, Y.A., Monine, M.I., Zitserman, V.Y. & Shvartsman, S.Y. (2004). Boundary homogenization for trapping by patchy surfaces. *The Journal of chemical physics*, **121**, 11390–11394. 49, 112, 161, 162, 163, 164

Berezhkovskii, A.M., Monine, M.I., Muratov, C.B. & Shvartsman, S.Y. (2006). Homogenization of boundary conditions for surfaces with regular arrays of traps. *The Journal of chemical physics*, **124**, 036103. 162

Berg, H.C. (1993). *Random walks in biology*. Princeton University Press. 1, 2, 4, 6, 8, 164, 166, 167

Berg, H.C. & Purcell, E.M. (1977). Physics of chemoreception. *Biophysical journal*, **20**, 193–219. 162

Bernoff, A.J. & Lindsay, A.E. (2018). Numerical approximation of diffusive capture rates by planar and spherical surfaces with absorbing pores. *SIAM Journal on Applied Mathematics*, **78**, 266–290. 161

Bernoff, A.J., Lindsay, A.E. & Schmidt, D.D. (2018). Boundary homogenization and capture time distributions of semipermeable membranes with periodic patterns of reactive sites. *Multiscale Modeling & Simulation*, **16**, 1411–1447. 161, 162, 189

Bosshart, H. & Heinzelmann, M. (2016). Thp-1 cells as a model for human monocytes. *Annals of translational medicine*, **4**. 158

Bou-Rabee, N. & Holmes-Cerfon, M.C. (2020). Sticky brownian motion and its numerical solution. *SIAM Review*, **62**, 164–195. 160

Brangwynne, C.P., Koenderink, G.H., MacKintosh, F.C. & Weitz, D.A. (2009). Intracellular transport by active diffusion. *Trends in Cell Biology*, **19**, 423–427. 108

Bressloff, P.C. & Newby, J.M. (2013). Stochastic models of intracellular transport. *Reviews of Modern Physics*, **85**, 135. 46, 108

Burrage, K., Cardone, A., D'Ambrosio, R. & Paternoster, B. (2017). Numerical solution of time fractional diffusion systems. *Applied Numerical Mathematics*, **116**, 82–94. 109

Catron, D., Itano, A., Pape, K., Mueller, D. & Jenkins, M. (2004). Visualizing the first 50 hr of the primary immune response to a soluble antigen. *Immunity*, **21**, 341–347. 47

Celli, S., Day, M., Müller, A.J., Molina-Paris, C., Lythe, G. & Bousso, P. (2012). How many dendritic cells are required to initiate a T-cell response? *Blood*, **120**, 3945–3948. 47

Chaumet, P. & Dufour, J. (1998). Electric potential and field between two different spheres. *Journal of electrostatics*, **43**, 145–159. 115, 119

Chen, J.T., Lee, J.W. & Shieh, H.C. (????). A Green's function for the domain bounded by nonconcentric spheres. *Journal of Applied Mechanics*, **80**, 014503. 115, 116, 117, 130, 140

Chevalier, C., Bénichou, O., Meyer, B. & Voituriez, R. (2010). First-passage quantities of brownian motion in a bounded domain with multiple targets: a unified approach. *Journal of Physics A: Mathematical and Theoretical*, **44**, 025002. 48, 111

Cheviakov, A.F. & Ward, M.J. (2011). Optimizing the principal eigenvalue of the Laplacian in a sphere with interior traps. *Mathematical and Computer Modelling*, **53**, 1394–1409. 39, 111

Cheviakov, A.F., Reimer, A.S. & Ward, M.J. (2012). Mathematical modeling and numerical computation of narrow escape problems. *Physical Review E*, **85**, 021131. 48, 112

Condamin, S., Bénichou, O. & Moreau, M. (2007). Random walks and brownian motion: A method of computation for first-passage times and related quantities in confined geometries. *Physical Review E*, **75**, 021111. xii, xxi, xxii, xxiii, 28, 29, 30, 31, 32, 33, 34, 35, 36, 37, 38, 39, 40, 41, 45, 48, 67, 69, 74, 80, 81, 86, 88, 91, 96, 108, 111, 151, 153, 156, 157, 191, 198, 199

Coombs, D., Kalergis, A., Nathenson, S., Wofsy, C. & Goldstein, B. (2002). Activated TCRs remain marked for internalization after dissociation from pMHC. *Nature Immunology*, **3**, 926–931. 46

Coombs, D., Straube, R. & Ward, M. (2009). Diffusion on a sphere with localized traps: mean first passage time, eigenvalue asymptotics, and Fekete points. *SIAM Journal of Applied Math*, **70**, 302–332. 46

Dalton, H.R., Dreier, J., Rink, G., Hecker, A., Janetzko, K., Juhl, D., Bieback, K., Steppat, D., Görg, S., Hennig, H. *et al.* (2014). Coxiella burnetii-pathogenic agent of Q (query) fever. *Transfusion medicine and hemotherapy*, **41**, 60–72. 158, 159

Deaconu, M., Gradinaru, M. & Roche, J.R. (2000). Sojourn time of some reflected Brownian motion in the unit disk. *Probability and Mathematical Statistics*, **20**, 19–38. xxv, 107, 108

Delgado, M.I., Ward, M.J. & Coombs, D. (2015). Conditional mean first passage times to small traps in a 3-D domain with a sticky boundary: Applications to T-cell searching behavior in lymph nodes. *Multiscale Modeling & Simulation*, **13**, 1224–1258. 47, 109, 111

El-Saden, M. (1961). Heat conduction in an eccentrically hollow, infinitely long cylinder with internal heat generation. *Journal of Heat Transfer*, **83**, 510–512. 52, 81

Ellis, E.L. & Delbrück, M. (1939). The growth of bacteriophage. *The Journal of general physiology*, **22**, 365–384. 185

Erban, R. & Chapman, S.J. (2007). Reactive boundary conditions for stochastic simulations of reaction–diffusion processes. *Physical Biology*, **4**, 16. 160, 227

Eun, C. (2018). Theory of curvature-dependent kinetics of diffusion-limited reactions and its application to ligand binding to a sphere with multiple receptors. *The Journal of chemical physics*, **149**, 024102. 162

Eun, C. (2020). Effects of the size, the number, and the spatial arrangement of reactive patches on a sphere on diffusion-limited reaction kinetics: A comprehensive study. *International Journal of Molecular Sciences*, **21**, 997. 189

Garside, P., Ingulli, E., Merica, R., Johnson, J., Noelle, R. & Jenkins, M. (1998). Visualization of Specific B and T Lymphocyte Interactions in the Lymph Node. *Science*, **281**, 96. 47

Godec, A. & Metzler, R. (2016a). First passage time distribution in heterogeneity controlled kinetics: going beyond the mean first passage time. *Scientific reports*, **6**, 20349. 112

Godec, A. & Metzler, R. (2016b). Universal proximity effect in target search kinetics in the few-encounter limit. *Physical Review X*, **6**, 041037. 112

Gradshteyn, I.S. & Ryzhik, I.M. (2014). *Table of integrals, series, and products*. Academic press. 122, 143

Grebenkov, D.S. & Traytak, S.D. (2019). Semi-analytical computation of Laplacian Green functions in three-dimensional domains with disconnected spherical boundaries. *Journal of Computational Physics*, **379**, 91–117. 111

Grebenkov, D.S., Metzler, R. & Oshanin, G. (2017). Effects of the target aspect ratio and intrinsic reactivity onto diffusive search in bounded domains. *New Journal of Physics*, **19**, 103025. 48

Grebenkov, D.S., Metzler, R. & Oshanin, G. (2019). Full distribution of first exit times in the narrow escape problem. *New Journal of Physics*, **21**, 122001. 112

Grebenkov, D.S., Holcman, D. & Metzler, R. (2020). Preface: new trends in first-passage methods and applications in the life sciences and engineering. *Journal of Physics A: Mathematical and Theoretical*, **53**, 190301. 48, 112

Grigoriev, I.V., Makhnovskii, Y.A., Berezhkovskii, A.M. & Zitserman, V.Y. (2002). Kinetics of escape through a small hole. *The Journal of chemical physics*, **116**, 9574–9577. 30

Habib, S., Lindenberg, K., Lythe, G. & Molina-Paris, C. (2001). Diffusion-limited reaction in one dimension: Paired and unpaired nucleation. *The Journal of chemical physics*, **115**, 73–89. 192

Heyda, J.F. (1959). A Green's function solution for the case of laminar incompressible flow between non-concentric circular cylinders. *Journal of the Franklin Institute*, **267**, 25–34. 49, 51, 53, 58, 69

Holcman, D. (2017). *Stochastic processes, multiscale modeling, and numerical methods for computational cellular biology*. Springer. 109

Holcman, D. & Schuss, Z. (2004). Escape through a small opening: receptor trafficking in a synaptic membrane. *Journal of Statistical Physics*, **117**, 975–1014. 48

Holcman, D. & Schuss, Z. (2014). The narrow escape problem. *SIAM Review*, **56**, 213–257. 48, 112

Holcman, D. & Schuss, Z. (2015). Stochastic narrow escape in molecular and cellular biology. *Analysis and Applications. Springer, New York*. 48, 108, 112, 161

Imada, K. & Leonard, W.J. (2000). The JAK-STAT pathway. *Molecular Immunology*, **37**, 1–11. 46, 156

Jansons, K.M. & Lythe, G. (2000). Efficient numerical solution of stochastic differential equations using exponential timestepping. *Journal of Statistical Physics*, **100**, 1097–1109. 189, 193

Jansons, K.M. & Lythe, G.D. (2005). Multidimensional exponential timestepping with boundary test. *SIAM Journal on Scientific Computing*, **27**, 793–808. 189, 193

Jeffery, G.B. (1912). On a form of the solution of Laplace's equation suitable for problems relating to two spheres. *Proceedings of the Royal Society of London. Series A, Containing Papers of a Mathematical and Physical Character*, **87**, 109–120. 220

Katja, L., Ralf, M. & Gleb, O. (2019). *Chemical Kinetics: Beyond the Textbook*. World Scientific. 47

Kerr, I.M., Costa-Pereira, A.P., Lillemeier, B.F. & Strobl, B. (2003). Of JAKs, STATs, blind watchmakers, jeeps and trains. *FEBS letters*, **546**, 1–5. 157

Krummel, M.F., Bartumeus, F. & Gérard, A. (2016). T cell migration, search strategies and mechanisms. *Nature Reviews Immunology*, **16**, 193. 47, 109

Kurella, V., Tzou, J.C., Coombs, D. & Ward, M.J. (2015). Asymptotic analysis of first passage time problems inspired by ecology. *Bulletin of Mathematical Biology*, **77**, 83–125. 47, 49, 51

Lagache, T. & Holcman, D. (2008). Effective motion of a virus trafficking inside a biological cell. *SIAM Journal on Applied Mathematics*, **68**, 1146–1167. 46, 109

Lagache, T., Dauty, E. & Holcman, D. (2009). Quantitative analysis of virus and plasmid trafficking in cells. *Physical Review E*, **79**, 011921. 46, 109

Lauffenburger, D.A. & Linderman, J. (1993). *Receptors: models for binding, trafficking, and signaling*. Oxford University Press. 47, 163

Lawley, S.D. (2020). Universal formula for extreme first passage statistics of diffusion. *Physical Review E*, **101**, 012413. 112

Lawley, S.D. & Madrid, J.B. (2020). A probabilistic approach to extreme statistics of brownian escape times in dimensions 1, 2, and 3. *Journal of Nonlinear Science*, 1–21. 107, 112, 157

Levine, H. (1997). *Partial Differential Equations*. American Mathematical Soc. 19

Liemert, A. (2014). The Green's function of the Poisson equation on the non-concentric annular region. *Journal of Electrostatics*, **72**, 347–351. 51

Lillemeier, B.F., Köster, M. & Kerr, I.M. (2001). STAT1 from the cell membrane to the DNA. *The EMBO Journal*, **20**, 2508–2517. 46

Lindsay, A.E., Spoonmore, R.T. & Tzou, J.C. (2016). Hybrid asymptotic-numerical approach for estimating first-passage-time densities of the two-dimensional narrow capture problem. *Physical Review E*, **94**, 042418. 48

Lindsay, A.E., Bernoff, A.J. & Ward, M.J. (2017). First passage statistics for the capture of a brownian particle by a structured spherical target with multiple surface traps. *Multiscale Modeling & Simulation*, **15**, 74–109. 162

Love, J.D. (1975). Dielectric sphere-sphere and sphere-plane problems in electrostatics. *The Quarterly Journal of Mechanics and Applied Mathematics*, **28**, 449–471. 115, 131, 144, 145

Lythe, G. (2006). Diffusion-limited reaction in one dimension. *Physica D: Nonlinear Phenomena*, **222**, 159–163. 192

Madariaga, M.G., Rezai, K., Trenholme, G.M. & Weinstein, R.A. (2003). Q fever: a biological weapon in your backyard. *The Lancet infectious diseases*, **3**, 709–721. 158

Makhnovskii, Y.A., Berezhkovskii, A.M. & Zitserman, V.Y. (2005). Homogenization of boundary conditions on surfaces randomly covered by patches of different sizes and shapes. *The Journal of chemical physics*, **122**, 236102. 49, 112, 165

Marshall, J. (2016). Analytical solutions for an escape problem in a disc with an arbitrary distribution of exit holes along its boundary. *Journal of Statistical Physics*, **165**, 920–952. 48

Mattos, T.G., Mejía-Monasterio, C., Metzler, R. & Oshanin, G. (2012). First passages in bounded domains: When is the mean first passage time meaningful? *Physical Review E*, **86**, 031143. 107, 157

McGuffee, S.R. & Elcock, A.H. (2010). Diffusion, crowding and protein stability in a dynamic molecular model of the bacterial cytoplasm. *PLoS Computational Biology*, **6**, e1000694. 109

McKenzie, H.W., Lewis, M.A. & Merrill, E.H. (2009). First passage time analysis of animal movement and insights into the functional response. *Bulletin of Mathematical Biology*, **71**, 107–129. 47

Metzler, R. (2019). Brownian motion and beyond: first-passage, power spectrum, non-gaussianity, and anomalous diffusion. *Journal of Statistical Mechanics: Theory and Experiment*, **2019**, 114003. 109

Milne-Thomson, L.M. (2000). *The calculus of finite differences*. American Mathematical Soc. 144, 222

Montroll, E.W. & Weiss, G.H. (1965). Random walks on lattices. II. *Journal of Mathematical Physics*, **6**, 167–181. 47

Morse, P.M. & Feshbach, H. (1954). Methods of theoretical physics. *American Journal of Physics*, **22**, 410–413. 16, 114

Morse, P.M. & Feshbach, H. (2010). *Methods of theoretical physics, Vol. II*. 83, 115

Mullineaux, C.W., Nenninger, A., Ray, N. & Robinson, C. (2006). Diffusion of green fluorescent protein in three cell environments in escherichia coli. *Journal of Bacteriology*, **188**, 3442–3448. 46

Muratov, C.B. & Shvartsman, S.Y. (2008). Boundary homogenization for periodic arrays of absorbers. *Multiscale Modeling & Simulation*, **7**, 44–61. 162

Noh, J.D. & Rieger, H. (2004). Random walks on complex networks. *Physical Review Letters*, **92**, 118701. 29

Pillay, S., Ward, M.J., Peirce, A. & Kolokolnikov, T. (2010). An asymptotic analysis of the mean first passage time for narrow escape problems: Part I: Two-dimensional domains. *Multiscale Modeling & Simulation*, **8**, 803–835. 48

Pinsky, R.G. (2003). Asymptotics of the principal eigenvalue and expected hitting time for positive recurrent elliptic operators in a domain with a small puncture. *Journal of Functional Analysis*, **200**, 177–197. xiv, 30, 198, 199

Prüstel, T. & Meier-Schellersheim, M. (2012). Exact Green's function of the reversible diffusion-influenced reaction for an isolated pair in two dimensions. *Journal of Chemical Physics*, **137**, 054104. 47

Prüstel, T. & Meier-Schellersheim, M. (2013). Theory of reversible diffusion-influenced reactions with non-markovian dissociation in two space dimensions. *Journal of Chemical Physics*, **138**, 104112. 47

Prüstel, T. & Tachiya, M. (2013). Reversible diffusion-influenced reactions of an isolated pair on some two dimensional surfaces. *Journal of Chemical Physics*, **139**, 194103. 47

Redner, S. (2001). *A guide to first-passage processes*. Cambridge University Press. 29, 43, 179, 185

Reingruber, J., Abad, E. & Holcman, D. (2009). Narrow escape time to a structured target located on the boundary of a microdomain. *The Journal of chemical physics*, **130**, 094909. 112

Rice, S.A. (1985). *Diffusion-limited reactions*, vol. 25. Elsevier. 29

Schuss, Z., Singer, A. & Holcman, D. (2007). The narrow escape problem for diffusion in cellular microdomains. *Proceedings of the National Academy of Sciences*, **104**, 16098–16103. 48, 112, 161

Schuss, Z., Basnayake, K. & Holcman, D. (2019). Redundancy principle and the role of extreme statistics in molecular and cellular biology. *Physics of life reviews*, **28**, 52–79. 112

Shabram, P. & Aguilar-Cordova, E. (2000). Multiplicity of infection/multiplicity of confusion. *Molecular therapy*, **2**, 420–421. 185

Shoup, D. & Szabo, A. (1982). Role of diffusion in ligand binding to macromolecules and cell-bound receptors. *Biophysical Journal*, **40**, 33. 163

Singer, A., Schuss, Z. & Holcman, D. (2006a). Narrow escape, part II: The circular disk. *Journal of Statistical Physics*, **122**, 465–489. 48

Singer, A., Schuss, Z., Holcman, D. & Eisenberg, R.S. (2006b). Narrow escape, part i. *Journal of Statistical Physics*, **122**, 437–463. 30, 48, 112, 161

Snyder, W.T. & Goldstein, G.A. (1965). An analysis of fully developed laminar flow in an eccentric annulus. *AIChE Journal*, **11**, 462–467. 52, 81

Speil, J., Baumgart, E., Siebrasse, J.P., Veith, R., Vinkemeier, U. & Kubitscheck, U. (2011). Activated STAT1 transcription factors conduct distinct saltatory movements in the cell nucleus. *Biophysical journal*, **101**, 2592–2600. 157

Stoy, R.D. (1989). Solution procedure for the laplace equation in bispherical coordinates for two spheres in a uniform external field: Parallel orientation. *Journal of applied physics*, **65**, 2611–2615. 115, 125

Textor, J., Henrickson, S.E., Mandl, J.N., von Andrian, U.H., Westermann, J., de Boer, R.J. & Beltman, J.B. (2014). Random migration and signal integration promote rapid and robust T cell recruitment. *PLoS Computational Biology*, **10**, e1003752. 47

Tzou, J.C. & Kolokolnikov, T. (2015). Mean first passage time for a small rotating trap inside a reflective disk. *Multiscale Modeling & Simulation*, **13**, 231–255. 48

Vinkemeier, U. (2004). Getting the message across, STAT! design principles of a molecular signaling circuit. *The Journal of cell biology*, **167**, 197–201. 157

Wosniack, M., Raposo, E., Viswanathan, G. & da Luz, M. (2015). Efficient search of multiple types of targets. *Physical Review E*, **92**, 062135. 46

Zinselmeyer, B.H., Dempster, J., Gurney, A.M., Wokosin, D., Miller, M., Ho, H., Millington, O.R., Smith, K.M., Rush, C.M., Parker, I. *et al.* (2005). In situ characterization of $CD4^+$ T cell behavior in mucosal and systemic lymphoid tissues during the induction of oral priming and tolerance. *Journal of Experimental Medicine*, **201**, 1815–1823. 47

Zwanzig, R. (1990). Diffusion-controlled ligand binding to spheres partially covered by receptors: an effective medium treatment. *Proceedings of the National Academy of Sciences*, **87**, 5856–5857. 163